



**A University of Sussex PhD thesis**

Available online via Sussex Research Online:

<http://sro.sussex.ac.uk/>

This thesis is protected by copyright which belongs to the author.

This thesis cannot be reproduced or quoted extensively from without first obtaining permission in writing from the Author

The content must not be changed in any way or sold commercially in any format or medium without the formal permission of the Author

When referring to this work, full bibliographic details including the author, title, awarding institution and date of the thesis must be given

Please visit Sussex Research Online for more information and further details



# **Synthesis And Supramolecular Chemistry Of $\pi$ -Electron Poor Materials**

Thesis presented for the degree of Doctor of Philosophy

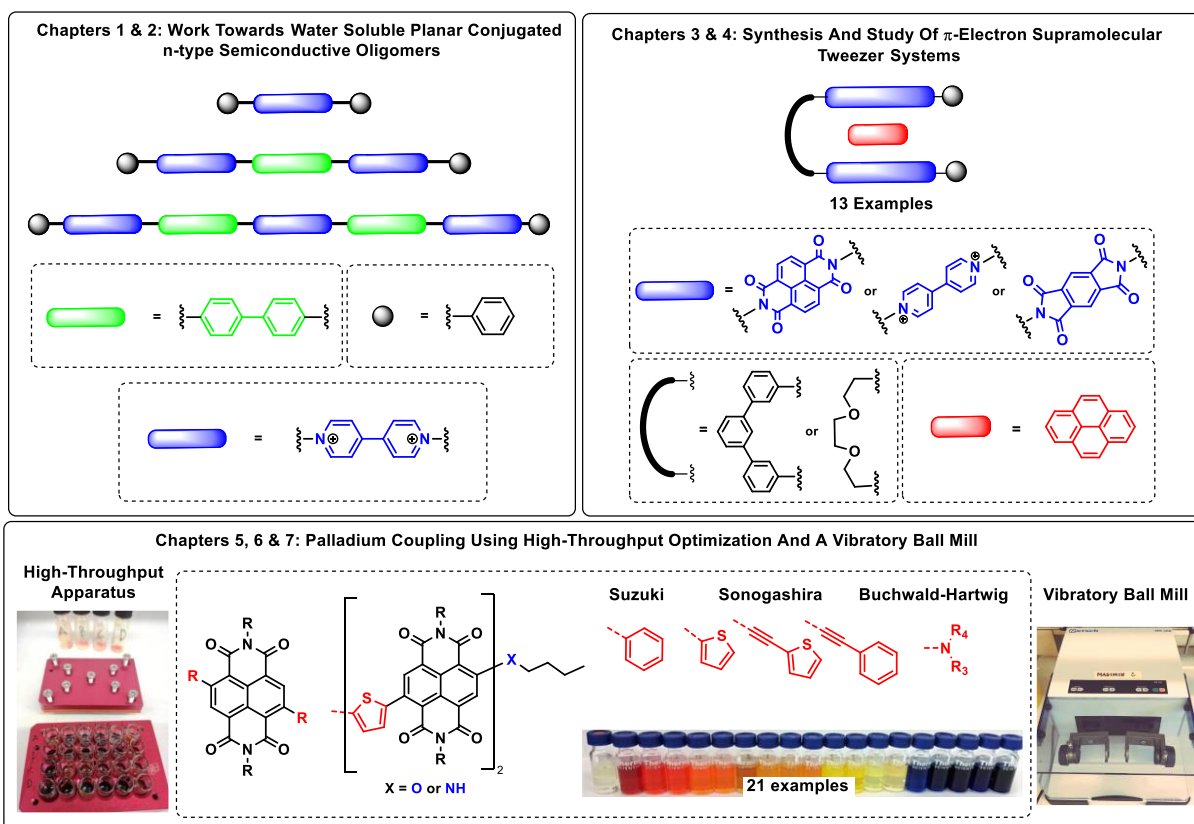
**Lydia Amanda Panther**

University of Sussex, School of Chemistry

Supervised by Dr. Barnaby W. Greenland and Professor John Spencer

October 2022

# Graphical Abstract



# Abstract

$\pi$ -electron poor species occupy a distinct position in the field of polymeric materials and supramolecular chemistry. The work presented in this thesis outlines their use in the production of organic n-type semiconductive materials, the synthesis and supramolecular chemistry of  $\pi$ -electron poor tweezer receptor molecules and the synthesis of small molecule electron acceptors using vibratory ball milling (VBM) protocols. The products of this work are important building blocks in many areas of organic electronics including: organic light emitting diodes (OLEDs), organic field-effect transistors (OFETs) and organic photovoltaic cells (OPVCs) as described sequentially below.

Throughout the experimental and the results and discussion sections, work is focused primarily on structures containing 4,4-bipyridinium (viologen), pyromellitic diimide (PDI), naphthalene diimide (NDI) and core substituted naphthalene diimide (c-NDI) units (Figure 1).

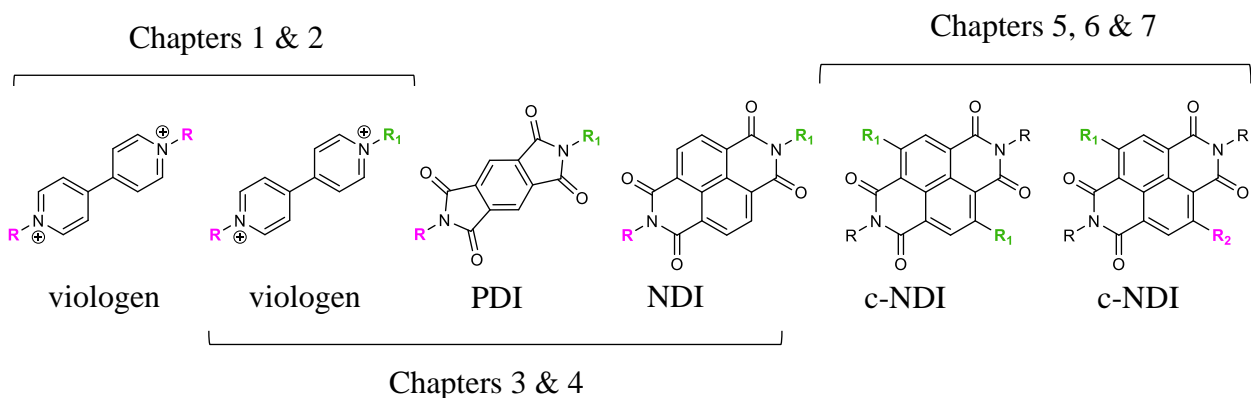


**Figure 1:** Overview of thesis showing the chemical structures that form the basis of each chapter of the thesis

Initially, in the first section (chapters 1 and 2), the use of viologens as n-type semiconductors in molecular wire systems is presented. Chapter one contains the background literature and

motivations that inspired the work. Chapter 2 presents work towards the exploitation of the Zincke reaction to synthesise water soluble 4,4'-bipyridinium containing conjugated planar n-type oligomers. The convergent synthesis route allows rapid synthesis of these oligomers which contain up to 12 aromatic residues.

The following section (Chapters 3 and 4) opens with an overview of the background literature underpinning the supramolecular use of  $\pi$ -electron poor molecules and materials, focussing on those that use molecular tweezer type motifs. Chapter 4 reports the design and realisation of a library of 13 tweezer receptor molecules, each containing two  $\pi$ -electron poor receptor residues, which were either: naphthalene-1,4,5,8-tetracarboxylic diimide (NDI), 4,4'-bipyridinium or benzene-1,2,4,5-tetracarboxylic diimide (PDI). The tweezers differed in the nature of the linking unit, which, was either a flexible 2,2'-(ethylenedioxy)bis(ethylamine) residue or a more conformationally constrained rigid, 3,3''-diamino-*m*-terphenyl unit. A systematic study took place investigating how varying specific structural components of the tweezer-receptors impacts their binding of  $\pi$ -electron rich species. The ability of each tweezer molecule to form supramolecular complexes with  $\pi$ -electron rich residues (1,5-dihydroxynaphthalene and pyrene) was confirmed by UV/Vis and  $^1\text{H}$  NMR spectroscopic studies. The binding stoichiometry of all tweezer type complexes was observed to be 1:1 with respect to host and guest over the concentration ranges studied. The binding constants were determined to be between  $2.3 \times 10^{-5}$  and  $71 \text{ M}^{-1}$  in organic solvents. The water-soluble tweezer compound exhibited association constants approximately one order of magnitude greater in aqueous environments compared to organic solvent systems. It was found that the nature of the linker in conjunction with the steric bulk adjacent to the receptor sites had variable effects on the binding constants for the systems. This demonstrates a complex interplay between minimising entropic losses in the formation of the complex (in systems with rigid linkers) and the ability of the final complex to adopt a more

energetically favourable geometry to maximise supramolecular  $\pi$ - $\pi$  stacking interactions (as is the case for flexible linkers). This chapter showed that the design of tweezer type supramolecular receptors with targeted binding constant values ( $K_a$ ) is non-trivial and still requires structural optimisation supported by detailed binding constant determination studies.

Finally, Chapters 5, 6 and 7 report the core functionalisation of *N,N'*-bis(2-ethylhexyl)-2,6-dibromo-1,4,5,8-naphthalenetetracarboxylic acid (Br<sub>2</sub>-NDI) using Suzuki, Sonogashira and Buchwald-Hartwig coupling reactions through solution state high-throughput Kitalysis<sup>TM</sup> and solid state VBM protocols. VBM was employed to synthesise 21 c-NDI products. The reactions proceed in as little as 1 hour, use commercially available palladium sources (frequently Pd(OAc)<sub>2</sub>) and are tolerant to air and atmospheric moisture. Furthermore, the real-world potential of this green VBM protocol is demonstrated by the double Suzuki coupling of a monobromo(NDI) residue to a bis(thiophene) pinacol ester. The resulting dimeric NDI species has been demonstrated to behave as an electron acceptor in functioning OPVCs.

# Declaration

I confirm that the research described in this thesis is my own work, and that the use of results and materials from other sources has been properly and fully acknowledged.

Signature:

Date:

Lydia Panther

University of Sussex

Falmer

Brighton

East Sussex

BN1 9QJ

October 2022

# Acknowledgments

First and foremost, I would like to give my most heartfelt thanks to my supervisors, Dr. Barny Greenland and Professor John Spencer, for giving me the opportunity to work on this interesting project. To my main supervisor Barny, your support and extremely patient guidance has moulded me into someone with the valuable skillset and talents to tackle my future career confidently. It was a privilege to work under your leadership and thank you for unknowingly showing me how to balance a happy life with a successful career, foundations I will extend into my life and am better in every way for it. Thank you John, for your contagious enthusiasm throughout the PhD but especially the Palladium coupling work. It would not have progressed so far without your suggestions and guidance.

The University of Sussex is thanked for funding this PhD studentship.

My thanks extend to Dr. Lewis Hart at the University of Reading, Dr. Alaa Abdul-Sada at the University of Sussex and Dr. Iain Goodall at the University of Greenwich for Mass Spectrometry measurements that were pivotal to this work. I thank Dr. Mark Roe at the University of Sussex for running the single crystal X-ray studies for the oligomer and tweezer work. Thanks also to EPSRC for the National Crystallography Service at Southampton (Dr. Graham Tizzard and Professor Simon J Cole) that enabled the solving of single crystals in the cNDI work.

At the university of Sussex, my gratitude goes to all the lab members of 301, 248 and 409 including Dr. Andy McGown, for the help in the early years, Yousef, Rachel, Mary, Asma, Tom, Monika and Helena who have helped me academically and personally over my time at Sussex. Thank you to Dr. Dan Guest for setting the initial foundations for the solid-state

optimization work and growing single crystals of cNDI systems later in the project. I would like to offer my sincerest gratitude to my fellow chemist Aemelia, for the proof reading of this thesis and easing my qualms about the project over the last four years.

Thank you to previous members of the Greenland lab group Dr. Tahkur Babra for his patience in showing me some of the earlier synthesis techniques and who suggested I apply for this PhD in the first place and to Dr. Long Chen, for laying the great Zincke groundwork that led to the oligomer work.

Finally, and most importantly, I would like to thank the most important people in my life, my family. To my mum and dad, thank you for the years of continued unwavering support, I would not be where I am today it wasn't for you. Thank you to my sisters Hannah, Heidi and Claudia, and my new Panther family, Gaye, Jonnie and Hollie, who have always been my biggest fans when it comes to the PhD. To my husband and absolute rock, Charlie, thank you for the 10 years (and counting) of continued support and encouragement when it was most needed. Lastly, thank you to my much-missed Uncle Dan for the laughter and fun over the years. We will never forget you and the imprint you have left in our lives.

# Glossary of Terms

MeCN	Acetonitrile
CDCl <sub>3</sub>	Deuterated Chloroform
CV	Cyclic Voltammetry
d	Doublet
DCM	Dichloromethane
δ	Chemical shift
EA	Electron Affinity
HOMO	Highest Occupied Molecular Orbital
IR	Infrared Spectroscopy
IRS	Internal Reference Standard
LUMO	Lowest Unoccupied Molecular Orbital
m	Multiplet
MeOH	Methanol
CD <sub>3</sub> OD	Deuterated Methanol
NEt <sub>3</sub>	Triethylamine
NMR	Nuclear Magnetic Resonance
OFET	Organic Field Effect Transistor
OLED	Organic Light Emitting Diode
OPVC	Organic Photovoltaic Cell

s	Singlet
t	Triplet
TFA	Trifluoroacetic acid
THF	Tetrahydrofuran
UV/vis	Ultraviolet-Visible Spectroscopy
PMHS	Poly(methylhydrosiloxane)

# Contents

<b>GRAPHICAL ABSTRACT.....</b>	<b>I</b>
<b>ABSTRACT .....</b>	<b>II</b>
<b>DECLARATION.....</b>	<b>V</b>
<b>ACKNOWLEDGMENTS .....</b>	<b>VI</b>
<b>CONTENTS .....</b>	<b>X</b>
<b>LIST OF FIGURES .....</b>	<b>XIV</b>
<b>LIST OF SCHEMES.....</b>	<b>XX</b>
<b>LIST OF TABLES .....</b>	<b>XXIII</b>
<b>SECTION 1: LITERATURE AND WORK TOWARDS WATER SOLUBLE PLANAR CONJUGATED N-TYPE SEMICONDUCTIVE OLIGOMERS</b>	<b>1</b>
<b>CHAPTER 1: INTRODUCTION AND PRIOR ART.....</b>	<b>3</b>
1.1 Motivation: bottom-up approaches to electronics.....	3
1.2 Electronic structure of semiconductors.....	4
1.3 Structure of organic light emitting diodes (OLEDs).....	5
1.4 Organic field effect transistors (OFETs).....	7
1.5 Organic photovoltaic cells (OPVCs).....	8
1.6 Types of semiconductors (p and n-types) .....	11
1.6.1 Structure and properties of viologens .....	20
1.6.2 Extended viologen systems .....	21
1.7 Conclusion.....	30
<b>CHAPTER 2: WORK TOWARDS A SERIES OF PLANAR CONJUGATED VILOGEN CONTAINING OLIGOMERS WITH ELECTRONIC APPLICATIONS.....</b>	<b>32</b>
2.1 Synthetic Rationale and Targets .....	32
2.2 Results and discussion .....	34
2.3 Conclusions .....	47
<b>SECTION 2: LITERATURE, SYNTHESIS AND STUDY OF <math>\Pi</math>- ELECTRON SUPRAMOLECULAR TWEEZER SYSTEMS .....</b>	<b>49</b>

## **CHAPTER 3: INTRODUCTION TO SUPRAMOLECULAR CHEMISTRY WITHIN $\pi$ -POOR SYSTEMS ..... 51**

3.1 Supramolecular chemistry and binding constants .....	51
3.2 Different types of non-covalent bonding interactions .....	56
3.3 Viologens in supramolecular systems .....	60
3.3.1 Synthesis of di-viologen containing macrocycles with increased chemical stability using the Zincke reaction .....	65
3.4 Molecular tweezers.....	68
3.4.1 Molecular tweezers containing two viologen species .....	68
3.5 Alternative $\pi$ -electron poor tweezer motifs.....	70
3.6 Conclusion.....	75

## **CHAPTER 4: FLEXIBILITY VERSUS RIGIDITY: STUDY OF HOW CONFORMATIONAL CONSTRAINT IMPACTS BINDING BETWEEN $\pi$ -ELECTRON POOR TWEEZER-TYPE HOSTS AND $\pi$ -ELECTRON RICH GUESTS..... 77**

4.1 Results and Discussion .....	77
4.1.1 Tweezer design and synthesis .....	77
4.1.2 Initial tweezer synthesis attempts: establishing suitable conditions for neutral systems.	80
4.1.3 Synthesis of $\pi$ -electron poor tweezer motifs .....	81
4.1.5 Tweezer-type complexes: Verification of binding through UV-Vis analysis.....	86
4.1.6 Establishing the Stoichiometry of complex formation through the method of continuous variation by $^1\text{H}$ NMR spectroscopic analysis - Job's plot analysis .....	89
4.1.7 Binding constant determination.....	92
4.1.8 Probing applications: switching behaviour.....	97
4.2 Conclusion.....	99

## **SECTION 3: LITERATURE AND WORK TOWARDS PALLADIUM COUPLING REACTIONS USING HIGH THROUGHPUT OPTIMIZATION AND A VIBRATORY BALL MILL..... 101**

## **CHAPTER 5: INTRODUCTION TO THE GREEN SYNTHESIS OF NDI CONTAINING MOLECULES WITH POTENTIAL FOR OPVCS..... 103**

5.1 Green Chemistry.....	103
5.2 Types of greener synthesis .....	104
5.2.1 Controlling selectivity and reactivity of reactions using VBM .....	108
5.3 Types of chemistry carried out in the ball mill.....	110
5.3.1 Early examples of conducting polymers <i>via</i> solid-state synthesis.....	112
5.4 Materials in Organic Photovoltaics .....	114
5.5 Solid state synthesis of NDIs.....	119
5.6 Conclusion.....	120

## **CHAPTER 6: SCOPING CONDITIONS FOR THE SYNTHESIS OF C-NDI CROSS COUPLING REACTIONS ..... 123**

6.1 Results and discussion .....	124
6.1.1 Bulk synthesis of starting reagents .....	124
6.1.2 Sonogashira Cross-Coupling .....	127
6.1.3 Solution State Scoping - Kitalysis™ apparatus .....	136
6.1.4 Sonogashira Coupling Solution High-Throughput Screening .....	138
6.1.5 Introduction to Suzuki Cross-Coupling .....	142
6.1.6 Suzuki solution state high throughput screening .....	143
6.1.7 Suzuki solid state catalyst screening .....	147
6.1.8 Buchwald-Hartwig Amination .....	150
6.1.9 Buchwald-Hartwig Amination Optimization using Kitalysis™ .....	151
6.1.10 Solid State Coupling reactions using Pd(OAc) <sub>2</sub> .....	155
6.2 Conclusion .....	157

## **7 SOLVENT FREE SYNTHESIS OF CORE-FUNCTIONALISED NAPHTHALENE DIIMIDES USING A VIBRATORY BALL MILL: SUZUKI, SONOGASHIRA AND BUCHWALD-HARTWIG REACTIONS. .... 160**

7.1 Introduction .....	160
7.2 Results and Discussion .....	162
7.2.1 Optimization of studies for Suzuki synthesis of c-NDIs .....	162
7.2.2 Substrate scope for the synthesis of c-NDIs by Suzuki coupling .....	164
7.2.3 Suzuki Library Optimizations .....	164
7.2.4 Optimization studies and substrate scope for Sonogashira synthesis of c-NDIs .....	169
7.2.5 Optimization studies and substrate scope for Buchwald-Hartwig amination of c-NDIs .....	172
7.2.6 Impurity analysis after VBM synthesis .....	174
7.2.7 UV/vis Absorption properties of c-NDIs .....	175
7.2.8 Single crystal x-ray analysis .....	179
7.2.9 Applications: Synthesis of c-NDI dimeric systems suitable for OPVC applications ....	180
7.3 Conclusions .....	183

## **8 CONCLUSIONS AND FUTURE WORK ..... 185**

8.1 Review of Results .....	185
8.2 Future Work .....	187

## **9 EXPERIMENTAL DETAILS..... 190**

9.1 Materials .....	190
9.2 Instrumental details .....	190
9.2.1 General instrumental details for this thesis .....	190
9.2.2 Chapter 2 instrument details .....	191
9.2.3 Chapter 4 instrument details .....	191
9.2.4 Chapter 6 & 7 instrument details .....	192

9.3 Detailed synthetic procedures.....	195
9.3.1 Chapter 2 .....	195
9.3.2 Chapter 4 .....	201
8.3.3 Chapter 6 .....	223
8.3.4 Chapter 7 .....	225
<b>10 REFERENCES .....</b>	<b>255</b>

# List of Figures

<b>Figure 1:</b> Overview of thesis showing the chemical structures that form the basis of each chapter of the thesis .....	ii
<b>Figure 2:</b> Energy band diagrams of an intrinsic (left), n-type (middle) and p-type (right) semiconductor.....	5
<b>Figure 3:</b> Schematic representation of an OLED device, the left showing all the individual components and to the right, how light is emitted <i>via</i> the separation of holes and electrons in the semiconductive materials within a device when charge is applied. ....	6
<b>Figure 4:</b> Schematic representation of the typical structure of an organic field effect transistor (OFET) device. ....	7
<b>Figure 5:</b> Schematic representation showing the composition of two types of photoactive layers in OPVCs; (left) a single heterojunction and (right) a bulk ‘all polymer’ heterojunction. ....	8
<b>Figure 6:</b> Schematic representative of a simple bilayer cell in the presence of photons. ....	9
<b>Figure 7:</b> An energy level diagram displaying how electricity is generated in an OPVC in stages. stage 1; cell is irradiated light. stage 2: electron excitation into the LUMO level of the p-type donor. stage 3: subsequent transfer of holes and electrons to the anode and cathode from the p-type donor and n-type acceptor. Stage 4: electricity generated.....	10
<b>Figure 8:</b> Chemical structure of <i>trans</i> -polyacetylene. ....	11
<b>Figure 9:</b> Selected examples of p-type semi conducting molecules and polymers <sup>50,51</sup> .....	13
<b>Figure 10:</b> Selected examples of organic n-type semiconducting molecules and materials <sup>52</sup> .....	14
<b>Figure 11:</b> n-type semiconductors and block co-polymer produced by Swager and co-workers .....	18
<b>Figure 12:</b> Chemical structure of a 4,4-bypyridium (viologen) species. ....	20
<b>Figure 13:</b> Small molecule extended viologen based derivatives produced by Yao, Kato and co-workers in 2020. <sup>104</sup> .....	21
<b>Figure 14:</b> Set of Greenland and colleagues oligomers accessed by utilizing the Zincke reaction. ....	27
<b>Figure 15:</b> Different orientations of the crystal structure <b>1.89</b> : (1) side view of crystal showing the viologens in the plane and other aromatics twisted (2) viewed down the length of the backbone with viologens out of the plane twisting and (3) close up of the dimer with torsion angles displayed and labelled A to E. Solvent molecules were excluded in 1-3 and anions excluded in 2 and 3 for clarity.....	33

<b>Figure 16:</b> Proposed set of viologen containing oligomers containing increasing number of 4,4'-bipyridium residues.....	34
<b>Figure 17:</b> <sup>1</sup> H NMR (600 MHz) Spectra of <b>2.1</b> (CD <sub>3</sub> OD with 1% TFA) recorded at 298K. ...	36
<b>Figure 18:</b> <sup>1</sup> H NMR (600 MHz) of mixture of starting material <b>2.14</b> and desired product <b>2.15</b> following separation techniques. Collected in CD <sub>3</sub> OD and recorded at 298 K. ....	39
<b>Figure 19:</b> <sup>1</sup> H NMR (600 MHz) spectra of <b>2.15</b> recorded in CD <sub>3</sub> OD at 298K. Trace impurities of N-methyl-2-pyrrolidone can be seen between 2-4ppm. ....	40
<b>Figure 20:</b> <sup>1</sup> H NMR (600 MHz) spectra of dimer recorded in CD <sub>3</sub> OD with 1% TFA at 298K. ....	41
<b>Figure 21:</b> <sup>1</sup> H NMR (600 MHz) spectra of intermediate diamine Zincke salt <b>2.16</b> recorded in acetonitrile-d <sub>3</sub> at 298K.....	44
<b>Figure 22:</b> <sup>1</sup> H NMR (600 MHz) spectra of intermediate amine Zincke salt <b>2.17</b> recorded in CD <sub>3</sub> OD at 298K.....	46
<b>Figure 23:</b> Electrospray mass spectrum of trimer <b>2.3</b> .....	47
<b>Figure 24:</b> DNA nucleobases Cytosine, Adenine, Thymine and Guanine and nucleotide with potential non-covalent binding sites labelled. ....	57
<b>Figure 25:</b> Molecular structure of 2-ureido-4[1H]-pyrimidinone (UPy) supramolecular polymer end units. ....	58
<b>Figure 26:</b> Four types of MIAs, left to right; two interlocked rings forming a catenane, a dumbbell containing bulky stoppers looped through a ring to form a rotaxane, a dumbbell without bulky stoppers looped through a ring to form a pseudo rotaxane and an uncapped non-cyclic host with a linear guest species forming a tweezer-type complex.....	58
<b>Figure 27:</b> Schematic taken from Iverson and co-workers work <sup>175</sup> that describes the electrostatic view of aromatic interactions. (top); schematics representing qualitatively aromatic quadrupole moments in electron-rich aromatic rings, such as 1,5-dialkoxynaphthalene (DAN) and benzene (left), as well as electron-deficient aromatics, such as 1,4,5,8-naphthalenetetracarboxylic diimide (NDI) containing strongly electron withdrawing groups (right). (bottom) The various potential modes of stacking, emphasizing locations of electrostatic repulsion or attraction. DFT calculations were used to plot the electrostatic potential surface for each representative aromatic. <sup>175</sup> .....	60
<b>Figure 28:</b> (Top) Structural formula of the bistable [2] rotaxane ( <b>3.12</b> and <b>3.13</b> ) designed by Stoddart and used in the memory crossbar. (Bottom) Schematic representation displaying how	

the device can be switched reconfigurable and recycled repeatedly between ON and OFF states.  
.....62

**Figure 29:** Chemical structures of ExBox<sup>4+</sup> host **3.14** and the eleven different polycyclic aromatic hydrocarbon guest molecules; Coronene (**3.15**), Azulene (**3.16**), Perylene (**3.17**), Phenanthrene (**3.18**), [4]Helicene (**3.19**), Tetracene (**3.20**), Tetraphene (**3.21**), Pyrene (**3.22**), Triphenylene (**3.23**), Chrysene (**3.24**) and Anthracene (**3.25**)..... 63

**Figure 30:** Structures of three macrocyclic diarylbipyridinium salts **3.26-3.28** reported by Stoddart, Greenland and Colquhoun designed to be more chemically stable than methylene containing cyclophanes like blue box and Exbox<sup>4+</sup>.<sup>81</sup> ..... 66

**Figure 31:** (left) Chemical structure of conjugated  $\pi$ -electron poor terphenyl di-viologen tetracationic macrocycle synthesised by the Greenland lab and shown to bind to  $\pi$ -electron rich 1,5-dihydroxynaphthalene derivative **3.30**. (right) Li and co-workers water soluble derivatives **3.31** and **3.32** which were shown to bind to  $\pi$ -electron rich guest species **3.33**. **3.31** was used for the separation of **3.34** and **3.35** from an isomeric mixture. .... 67

**Figure 32:** Cartoon representation of a tweezer receptor undergoing fast encapsulation of electronically complimentary residues that are contained within polymer chains without threading onto the chain itself compared to a slower encapsulation for a macrocycle. Blue represents  $\pi$ -electron poor binding site and red  $\pi$ -electron rich guest species within the polymer chain. .... 68

**Figure 33:** Viologen based tweezer used as a probe to measure  $\pi$ -donor and  $\pi$ -acceptor interactions ..... 69

**Figure 34:** The first example of asymmetric  $\pi$ -electron poor NDI containing tweezer residues (**3.40** and **3.41**) and  $\pi$ -electron rich pyrene containing residues (**3.42** and **3.43**) reported by Colquhoun and co-workers.<sup>226</sup> ..... 71

**Figure 35:** Tweezer residues used by Hayes *at al.* in novel printing inks. (top)  $\pi$ -electron poor NDI containing residue **3.44** and  $\pi$ -electron rich pyrene containing residue **3.45**. (bottom) a schematic representation of the separate ink components and the crosslinking process that takes place in the printing inks. Adapted figure from published work<sup>209</sup> ..... 72

**Figure 36:** Tweezer residues used for selective information sequencing by Colquhoun *et al.*<sup>228</sup> (top) chemical structures of a  $\pi$ -electron poor PDI containing tweezer derivative **3.46** and NDI containing macrocycle **3.48** with complementary  $\pi$ -electron rich pyrenyl containing tweezers **3.47** and **3.49** (bottom) crystal structures of complementary tweezer complex **3.46** and **3.47** (left) and macrocycle **3.48** complexed with tweezer **3.49**..... 73

<b>Figure 37:</b> Cartoon representations of ‘induced-fit’ and ‘lock and key’ models.....	75
<b>Figure 38:</b> Full <sup>1</sup> H NMR (600MHz) spectrum of <b>4.19</b> with shaded proton environments. Recorded in CDCl <sub>3</sub> , reference peak not visible due to masking by product signals. ....	81
<b>Figure 39:</b> Partial <sup>1</sup> H NMR spectrum of Rigid-Vio-Ph recorded in CD <sub>3</sub> OD .....	83
<b>Figure 40:</b> <sup>1</sup> H full spectrum of <b>Rigid-NDI-Hex</b> .....	84
<b>Figure 41:</b> Partial <sup>1</sup> H spectrum of <b>Flexi-PDI-Hex</b> tweezer motif with proton regions shaded. ....	86
<b>Figure 42:</b> (A) Structural representation of complementary, aromatic, $\pi$ - $\pi$ stacked complexes for each binding residue NDI, Vio or PDI with guest species Pyr or DHN (B) Photograph of tweezer complexation in solution between host and guest at a 1:1 ratio (3mM). (C-E) Photophysical data of tweezer complexation between host and guest at a 1:1 ratio observed via UV/vis absorption spectroscopy (3 mM, samples for (C) and (E) recorded in CHCl <sub>3</sub> :trifluoroacetic acid (9:1) and (D) in MeOH).....	88
<b>Figure 43:</b> (top) Structural representation of host-guest complexation between tweezer <b>Flexi-NDI-Bn</b> and <b>Pyr</b> with selected protons labelled. (bottom) Stack of <sup>1</sup> H NMR partial spectra (600 MHz, CDCl <sub>3</sub> : trifluoroacetic acid (9:1)) for varying stoichiometries of <b>Flexi-NDI-Bn</b> with guest species <b>Pyr</b> at a fixed total concentration. * = signal for O-H proton on trifluoroacetic acid. ....	91
<b>Figure 44:</b> <sup>1</sup> H NMR Job plots for host systems <b>Rigid-NDI-Hex</b> , <b>Rigid-Vio-Ph</b> , <b>Rigid-PDI-Hex</b> , <b>Flexi-NDI-Bn</b> , <b>Flexi-Vio-Ph</b> and <b>Flexi-PDI-Bn</b> with guest species <b>Pyr</b> . Neutrally charged tweezers <b>Rigid-NDI-Hex</b> , <b>Rigid-PDI-Hex</b> , <b>Flexi-NDI-Bn</b> and <b>Flexi-PDI-Bn</b> recorded at 10 mg/mL in CDCl <sub>3</sub> :trifluoroacetic acid (9:1) at 298K. Tetracationic systems <b>Rigid-Vio-Ph</b> and <b>Flexi-Vio-Ph</b> recorded at 20 mg/mL in CD <sub>3</sub> OD at 298K. ....	92
<b>Figure 45:</b> (left) partial <sup>1</sup> H NMR (600 MHz) spectral changes induced by titration of 10 mg/mL tweezer molecule <b>Rigid-NDI-Hex</b> with guest species <b>Pyr</b> in CDCl <sub>3</sub> : trifluoroacetic acid (9:1) at 298K. (right) Structural representation of host-guest complexation between tweezer <b>Rigid-NDI-Hex</b> with <b>Pyr</b> . ....	93
<b>Figure 46:</b> (left) Partial <sup>1</sup> H NMR (600 MHz) spectral changes induced by titration of 2 mg/mL tweezer molecule <b>Rigid-Vio-Ph</b> with guest species <b>DHN</b> in D <sub>2</sub> O at 298K. (right) Structural representation of host-guest complexation between tweezer <b>Flexi-Vio-Ph</b> with . ....	97
<b>Figure 47:</b> Partial <sup>1</sup> H NMR (600 MHz) spectra used as a crude switching behaviour experiment. Free guest species <b>DHN</b> (top spectrum), 1:1 host <b>Rigid-Vio-Ph</b> and <b>DHN</b> (middle spectrum)	

and <b>Rigid-Vio-Ph</b> $\supset$ <b>DHN</b> with the addition of triethylamine (bottom spectrum). All spectra recorded in CD <sub>3</sub> OD at 298 K.....	99
<b>Figure 48:</b> types of mechanochemistry; ball milling, planetary mill, extrusion. <sup>240,242</sup> taken from Browne <i>et al.</i> review.....	105
<b>Figure 49 :</b> (left) photograph taken of starting reagents before and after milling within the following chapters in this work, turning from yellow to red; (middle) snapshots of a simulated indentation between spherical clusters of meloxicam (red) and aspirin (blue); (right) the distribution of molecules of meloxicam (red) and aspirin (blue) at stages 1, 2, 3 and 4. Figure adapted from published work by S. James <i>et al.</i> <sup>252</sup> .....	107
<b>Figure 50:</b> Examples of conductive polymers produced using solid-state synthesis techniques; Polyaniline, Poly(3-hexylthiophene), Polythiophene and Poly( <i>o</i> -aminophenol).....	113
<b>Figure 51:</b> Examples of polymers produced in the ball; poly( <i>para</i> -phenylene) <i>via</i> the Suzuki reaction, <sup>297</sup> poly(phenylene vinylene) <sup>296</sup> poly(urethane)s <sup>295</sup> .....	113
<b>Figure 52:</b> Examples of non-fullerene containing fused ring acceptors .....	117
<b>Figure 53:</b> Rylene tetracarboxylic diimides as fullerene alternatives.....	118
<b>Figure 54:</b> Examples of common PyDI and NDI acceptors used in OPVCs.....	119
<b>Figure 55:</b> Solid state synthesis of NDIs .....	120
<b>Figure 56:</b> NDI unit displaying the three main areas of functionalization at the axial, shoulder and core positions. ....	123
<b>Figure 57:</b> Photographs showing the purification of Br <sub>2</sub> -NDI .....	126
<b>Figure 58:</b> Full <sup>1</sup> H NMR (600MHz) of Br <sub>2</sub> -NDI with appropriate proton assignment. Recorded at 298K in CDCl <sub>3</sub> .....	127
<b>Figure 59:</b> Partial <sup>1</sup> H NMR spectra for entry 5 and 6 stacked with starting material spectrum .....	132
<b>Figure 60:</b> Full <sup>1</sup> H NMR spectrum of reaction after ball milling (data correlates to entry 1 in Table 4).....	133
<b>Figure 61:</b> Full <sup>1</sup> H NMR spectrum of reaction after ball milling (data correlates to entry 3 in Table 4).....	134
<b>Figure 62:</b> (left) Photograph of Kitalysis <sup>TM</sup> reaction block and (right) breakdown of reaction wells.....	137
<b>Figure 63:</b> Partial <sup>1</sup> H NMR spectra with catalyst C1-C6 and base K <sub>3</sub> PO <sub>4</sub> .....	140
<b>Figure 64:</b> Photographs showing the work up stages of the reaction vials from the Suzuki cross coupling utilizing the Kitalysis <sup>TM</sup> reaction block. ....	144

<b>Figure 65:</b> Partial $^1\text{H}$ NMR spectra containing $\text{K}_3\text{PO}_4$ , catalyst C1 and solvents A-D (corresponding to column 1 in Table 7 and XPhos Pd G3 is the constant catalyst).....	146
<b>Figure 66:</b> Partial $^1\text{H}$ NMR spectra of solid-state BH reactions to compare against solution state results.....	154
<b>Figure 67:</b> Partial $^1\text{H}$ NMR from solid state BH reaction with palladium acetate catalyst ...	156
<b>Figure 68:</b> Photographs of the interior of the milling jars for the solid state base screen of suzuki coupling reaction of c-NDI.....	163
<b>Figure 69:</b> Stack of the spectra used to determine the conversion of <b>6.5</b> to <b>7.16</b> with and without the addition of LAG agent. $^1\text{H}$ NMR spectra: (1) $^1\text{H}$ NMR spectrum of starting material <b>6.5</b> . (2) $^1\text{H}$ NMR spectrum of the crude reaction mix for <b>6.5</b> to <b>7.16</b> without LAG (conversion 64%). (3) $^1\text{H}$ NMR spectrum of the crude reaction mix for <b>6.5</b> to <b>7.16</b> with LAG (conversion >98%). .....	169
<b>Figure 70:</b> Photograph of 1 mM solutions of the starting material 1b (left) and cross-coupled products <b>7.10</b> – <b>7.30</b> in chloroform under white light. ....	175
<b>Figure 71:</b> Photophysical data of c-NDIs as observed via UV/vis absorption spectroscopy (0.2 mM, $\text{CHCl}_3$ ) for: Suzuki (A and B), Sonogashira (C) and Buchwald-Hartwig (D) coupled products. ....	176
<b>Figure 72:</b> X-ray crystal structures of c-NDI <b>7.16</b> (left) and <b>7.27</b> (right). Minor disorder components and hydrogen atoms are omitted for clarity. Only one independent molecule is shown of <b>7.27</b> . ....	179
<b>Figure 73:</b> Proposed product for the mono-substitution reaction <b>7.34</b> and two isolated alternative products isolated when attempted <b>7.39</b> and <b>7.40</b> .....	181

# List of Schemes

<b>Scheme 1:</b> Mechanism involved in the condensation reaction between a dianhydride and an amine to yield a diimide. ....	15
<b>Scheme 2:</b> Synthesis of Swager water soluble n-type polymers <b>1.19</b> and block co-polymer <b>1.32</b> . ....	19
<b>Scheme 3:</b> Electrochemical interconversion of viologen unit between dicationic $V^{2+}$ , cationic radical $V^{\cdot+}$ and neutral states $V^0$ . ....	20
<b>Scheme 4:</b> Synthetic pathway to small molecule extended viologens produced by Yao, Kato, and co-workers. ....	22
<b>Scheme 5:</b> (left); Poly(viologen) produced by Heinsohn and (right); the Poly(alkanediyl-viologen dibromide) synthesised by Shimomura. ....	23
<b>Scheme 6:</b> Mechanism between pyrilium salts and a primary amine to produce a pyridinium species <sup>108</sup> .....	23
<b>Scheme 7:</b> (top) The synthetic strategy to access polypyridinium homopolymers and (bottom) an example of polymers based on extended viologens in literature, by Harris and co-workers. <sup>114</sup> .....	25
<b>Scheme 8:</b> Formation of a Zincke salt via reaction of pyridine with 2,4-dinitro-chlorobenzene. ....	26
<b>Scheme 9:</b> Synthesis pathway for extended viologen containing oligomers produced by Greenland and co-workers. <sup>82</sup> .....	28
<b>Scheme 10:</b> Structure of dimer by Greenland <i>et al.</i> in cationic state showing twisting as a result of OMe substituents (top) delocalised as the radical upon oxidation (middle) and in the neutral quinoidal form (bottom). ....	29
<b>Scheme 11:</b> Synthesis of a zincke salt from 4,4-bipyridine and 2,4-dinitro-1-chlorobenzene	34
<b>Scheme 12:</b> Reaction scheme to synthesise the unimer <b>2.1</b> . ....	35
<b>Scheme 13:</b> Synthesis of benzidine <b>2.11</b> . ....	36
<b>Scheme 14:</b> Proposed reaction scheme to synthesise mono substituted phenyl viologen <b>2.12</b> . ....	37
<b>Scheme 15:</b> Synthesis of asymmetric mono phenyl viologen <b>2.14</b> . ....	38
<b>Scheme 16:</b> Synthesis of intermediate 7 based on literature <sup>134</sup> .....	38
<b>Scheme 17:</b> Synthesis of <b>2.15</b> using N-methyl-2-pyrrolidone as an alternative solvent .....	40
<b>Scheme 18:</b> Synthesis route for dimer <b>2.2</b> , involving the Zincke reaction. ....	41

<b>Scheme 19:</b> Initial synthesis pathway of conjugated 4,4'-bipyridinium trimer <b>2.3</b> .....	43
<b>Scheme 20:</b> Alternative synthesis route of hexacationic trimer <b>2.3</b> .....	45
<b>Scheme 21:</b> Cyclobis(paraquat- <i>p</i> -phenylene): formed via S <sub>N</sub> 2 reaction between 4,4'-bipyridine derivative <b>3.11</b> and 1,4-bis(bromomethyl) benzene <b>3.10</b> . Commonly coloured blue to depict electron deficiency in publications. ....	61
<b>Scheme 22:</b> Scheme displaying methylene moiety within CBPQT <sup>4+</sup> sensitivity to a nucleophile .....	64
<b>Scheme 23:</b> Synthesis of asymmetric precursors to $\pi$ -electron poor species required for tweezer-receptor synthesis.....	79
<b>Scheme 24:</b> Synthesis and purification of rigid tris-aromatic diamine linker unit <b>4.18</b> . ....	80
<b>Scheme 25:</b> Synthesis of asymmetric NDI species <b>4.19</b> .....	80
<b>Scheme 26:</b> Synthesis of $\pi$ -electron poor tweezer molecules with ridged linker units.....	82
<b>Scheme 27:</b> synthesis of flexible tweeze-type receptors.....	85
<b>Scheme 28:</b> Reaction between anilines and bis(benzotriazolyl)methanethiones in the solution state compared to ball milling techniques where the isolation of intermediates is possible. <sup>258</sup> .....	109
<b>Scheme 29:</b> Reactivity differences for fullerene functionalization in solution vs. ball milling synthesis. <sup>259</sup> .....	110
<b>Scheme 30:</b> Synthesis of PC <sub>61</sub> BM. ODCB = 1,2-dichlorobenzene; .....	115
<b>Scheme 31:</b> Synthesis of NDI-Br <sub>2</sub> <b>6.6</b> from the commercially available NDA <b>6.1</b> .....	125
<b>Scheme 32:</b> Typical conditions for a Sonogashira coupling reaction. ....	127
<b>Scheme 33:</b> Mechanism for the copper facilitated (left) and copper-free (right) Sonogashira cross coupling reaction. Ligands are omitted for clarity. ....	129
<b>Scheme 34:</b> (Top left) Solution state synthesis of c-NDIs. (Top Right) ball mill protocols of aryl acetylenes. (Bottom) our work: initial attempt at ball milling synthesis of c-NDIs. * = yields calculated from <sup>1</sup> H NMR monitoring .....	130
<b>Scheme 35:</b> Initial ball milling Sonogashira conditions .....	135
<b>Scheme 36:</b> Sonogashira coupling Katalysis <sup>TM</sup> optimization conditions.....	138
<b>Scheme 37:</b> Suzuki cross coupling.....	142
<b>Scheme 38:</b> Suzuki cross coupling mechanism. ....	143
<b>Scheme 39:</b> Suzuki-Miyaura conditions for the high-throughput solution state optimization .....	144
<b>Scheme 40:</b> Solid state catalyst optimization for Suzuki coupling .....	148

<b>Scheme 41:</b> General Buchwald-Hartwig amination reaction.....	150
<b>Scheme 42:</b> Mechanism for a general Buchwald-Hartwig amination .....	151
<b>Scheme 43:</b> Buchwald-Hartwig Katalysis <sup>TM</sup> optimization conditions .....	152
<b>Scheme 44:</b> Solid state scheme for coupling reactions using Pd(OAc) <sub>2</sub> as the catalytic source. .....	155
<b>Scheme 45:</b> Coupling reactions using VBM (A) and synthesis of c-NDIs (B-C). A) Contemporary VBM couplings on non-NDI derivatives; B) Traditional solvent-based synthesis of c-NDIs and C) Rapid optimization and VBM synthesis of c-NDIs. 1,5-cod = 1,5-cyclooctadiene carried out in this work.....	161
<b>Scheme 46:</b> Solid state base and catalyst optimization conditions .....	162
<b>Scheme 47:</b> Suzuki coupling of <b>6.5</b> with aryl boronic acids to produce c-NDIs.....	165
<b>Scheme 48:</b> Examples of c-NDI dimer species and synthesis pathways established by Kwon, An, Kim and McNeill groups. ....	180
<b>Scheme 49:</b> Synthesis of the molecular electron acceptor species <b>7.43</b> and <b>7.44</b> .....	182
<b>Scheme 50:</b> Proposed solid state conditions for the synthesis of c-NDI polymers that are known to work as n-type semiconductors in functioning OPVCs. ....	188

# List of Tables

<b>Table 1:</b> Torsion angles in oligomer <b>1.89</b> crystal structure .....	33
<b>Table 2:</b> Bond energies of supramolecular interactions compared to a covalent bond. <sup>142–144</sup> .....	52
<b>Table 3:</b> $K_a$ values for the tweezer compounds studied with specific hosts and in specific solvents. Values are calculated by <i>Bindfit</i> <sup>146,147</sup> using chemical shift data from multiple signals in at least 8 independent <sup>1</sup> H NMR spectra, each containing a fixed concentrated of host and varying concentrations of guest species (See SI for full NMR titration data).....	95
<b>Table 4:</b> Initial ball milling Sonogashira couplings.....	135
<b>Table 5:</b> Chemical structures of pre-loaded catalysts in Kitalysis <sup>TM</sup> reaction block. ....	137
<b>Table 6:</b> Solution state optimization results for Sonogashira coupling .....	141
<b>Table 7:</b> Solution state optimization results for Suzuki coupling.....	147
<b>Table 8:</b> Photograph of jars post reaction for the solid state Suzuki cross coupling catalyst screening.....	148
<b>Table 9:</b> Solid state optimization results for Suzuki coupling .....	149
<b>Table 10:</b> Buchwald-Hartwig high throughput solution state optimization results from <sup>1</sup> H NMR spectra.....	152
<b>Table 11:</b> Solid state using catalyst palladium acetate.....	157
<b>Table 12:</b> Optimization of Suzuki coupling reactions and structures of pre-catalysts. ....	163
<b>Table 13:</b> Optimization of Suzuki coupling; screening choice of catalyst, boronic acids, base and addition of LAG.....	166
<b>Table 14:</b> Scope of c-NDI products 2a-2k synthesised via Suzuki coupling using VBM methods and isolated by flash column chromatography. ....	168
<b>Table 15:</b> Optimization of the Sonogashira coupling between phenylacetylene and 1b in the solid state. 1,5-cyclooctadiene (10 wt%) as LAG agent.....	170
<b>Table 16:</b> Scope c-NDI synthesised via Sonogashira coupling (3a - 3f) using VBM and isolated by flash column chromatography. ....	171
<b>Table 17:</b> Optimization of the Buchwald-Hartwig amination between carbazole and 1b under VBM conditions. ....	173
<b>Table 18:</b> Scope of c-NDI products <b>7.27 – 7.30</b> synthesised via Buchwald-Hartwig amination using VBM methods.....	174
<b>Table 19:</b> UV-Vis absorbance values of <b>6.5</b> and c-NDIs <b>7.10 – 7.30</b> recorded at 0.2 mM in chloroform. (NS – not seen) .....	177

**Section 1: Literature and work  
towards water soluble planar  
conjugated n-type semiconductive  
oligomers**

# **Chapter 1**

## **Introduction to organic conductive materials and their applications**

# Chapter 1: Introduction and Prior Art

## 1.1 Motivation: bottom-up approaches to electronics

Digital storage and Microelectronics has underpinned the progress in many industries. By 2030,<sup>1</sup> the Global Consumer Electronics Market is predicted to be valued at £930 billion, therefore, the electronics industry is being pushed to its limits by the demand for smaller devices. Gordon Moore - the CEO of Intel (between 1975 and 1987), formalised this trend in 1965 when he noticed that every two years, the density of transistors found on a silicon chip doubled. Known as Moore's Law, this empirical trend has been sustained to this day.

This trend of reducing component size has been maintained using fabrication routes and methodologies that are based exclusively on top-down approaches. The silicon chips are fabricated *via* photolithography which produces silicon integrated-circuits that are approaching their lowest theoretical size limit.<sup>2</sup> This is achieved by UV radiation striking a thin layer of polymer through a mask, resulting in cross-linking upon contact with the light, forming an insoluble pattern, which is then etched onto the silicon wafer surface.

However, the physical limitations, space and significant cost are all slowing further advancements. An example of this can be seen in photolithography where the wavelength of incident light is already in the uttermost ultraviolet region which essentially limits the resolution of the top-down fabrication technique for future use. Instead of marking the end for electronic miniaturisation, novel bottom-up approaches are being investigated which could be the overall solution for device miniaturisation where molecular scale building blocks can create structures that are engineered to have self-assembling properties.<sup>3</sup>

The world's current smallest transistor using top-down methods is 1 nm in size, which is about 10 times greater in size than an atomic bond.<sup>4</sup> Carbon based materials for electronic applications are a likely candidate for bottom-up methodologies as they have lower raw material and production costs as well as simpler fabrication techniques into large area devices than silicon. Not only this, but carbon has a lower density at 2.26 g/cc than silicon (2.33 g/cc), enabling the potential for lighter weight electronic materials. Carbon based materials also frequently exhibit excellent physical properties, such as flexibility, and the ability to be fabricated into devices by simple printing techniques, which is hard to achieve for inorganic-based electronics. This disparity of scale, density, cost, and fabrication methods presents considerable potential to solve the size conundrum and develop electronic materials with interesting novel physical characteristics. With technology now vital in our ever-evolving world, the race is on to build novel semiconducting molecules and materials to solve the issue of scale in this exciting field.

## 1.2 Electronic structure of semiconductors

Understanding how semiconductors function is crucial in allowing optimization of systems. Figure 2 shows the energy level diagrams for the three classes of semiconductor: intrinsic, n-type and p-type. In an intrinsic semiconductor, the conduction band, also referred to as the lowest unoccupied molecular orbital (LUMO), is separated by the valence band, or the highest occupied molecular orbital (HOMO), by an energy difference which is termed the band gap. In an n-type inorganic semiconductor, the addition of electron dopants results in the reduction in the energy level of the LUMO.<sup>5</sup> This means that electrons from the valence band can be more easily promoted into the conduction band. In contrast to n-type doping, p-type dopants increase the energy level of the HOMO. This also has the effect of reducing the HOMO-LUMO band gap. The energy levels of semiconductor materials can, therefore, all be tuned by the addition

of dopants. The HOMO and LUMO bands of organic semiconductors are equivalent to the valence and conduction bands in inorganic semiconductors.

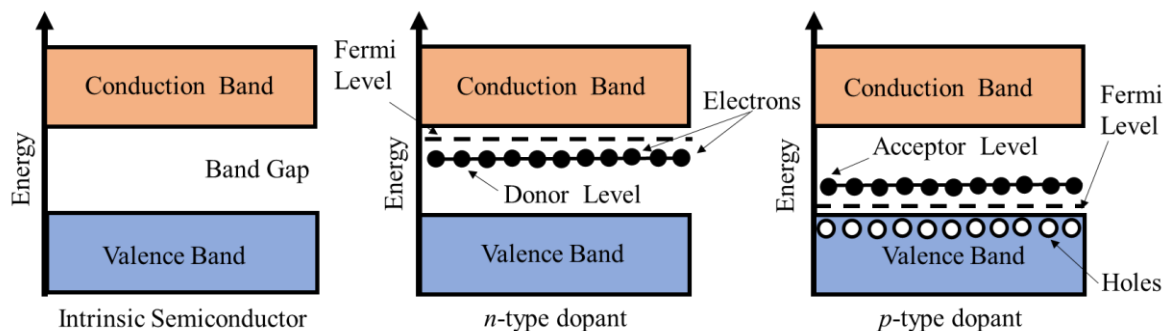


**Figure 2:** Energy band diagrams of an intrinsic (left), n-type (middle) and p-type (right) semiconductor.

With the electronic structure and different types of semiconductors discussed, attention is now turned to the applications of these into working electronic devices. Organic p-type and n-type semiconductors are extensively used in organic light emitting diodes (OLEDs), organic field effect transistors (OFETs) and organic photovoltaic cells (OPVCs). The underlying concepts to how these devices function will now be briefly discussed over the following three sections.

### 1.3 Structure of organic light emitting diodes (OLEDs)

Organic light emitting diodes (OLEDs) produce light when electric current passes in one direction. A typical OLED is comprised of a layer of organic material sandwiched between two electrodes, the cathode and anode, which are deposited onto a substrate. The organic material is composed of two parts; a p-type semiconductor that has a suitable HOMO to easily lose electrons, and an n-type semiconductor which can readily accept electrons (Figure 3). The positive charges that remains in the HOMO is called a hole. The boundary between these two materials is termed the depletion zone. When voltage is applied to the system, free electrons and holes are created. A photon is released, therefore light is generated, by the combination of

the electrons from the n-type semiconductor and the holes from the p-type semiconductor in the depletion zone.

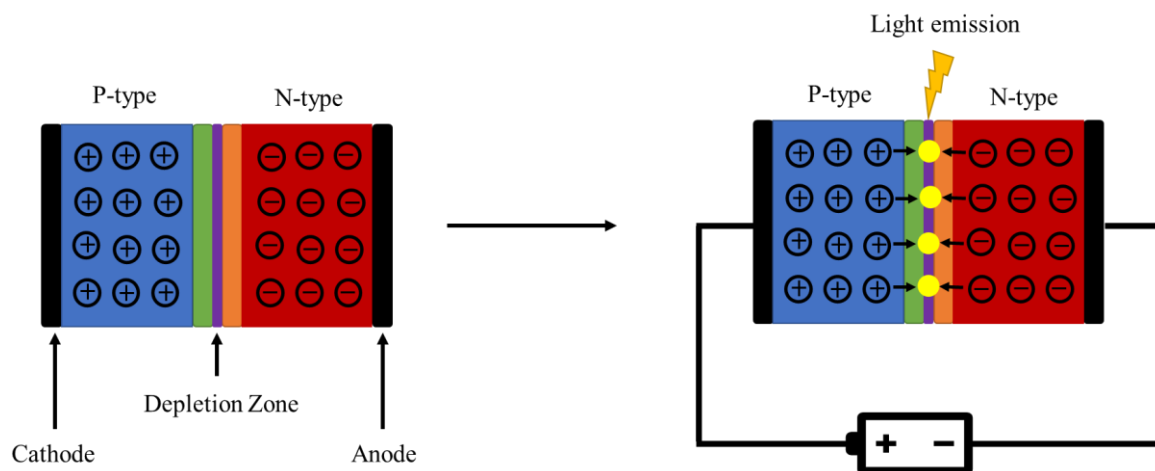


**Figure 3:** Schematic representation of an OLED device, the left showing all the individual components and to the right, how light is emitted *via* the separation of holes and electrons in the semiconductive materials within a device when charge is applied.

The band gap energies of the n/p type semiconductor governs the colour of the emitted light released. Therefore, discovering materials with band gaps that can produce the primary colours on the visible spectrum is extremely valuable in OLED device development.

When assessing the suitability of a molecule or material for a new OLED device, the efficiency of the system is considered by studying the charge carrier (either electron or hole) mobility. The electron mobility characterises how quickly an electron can move through a semiconductive material under the influence of an electric field. The corresponding quantity for holes is known as the hole mobility. The electron affinity can also be assessed, and this is a measure, usually in an n-type material, of the degree to which a molecule or atom, attracts additional electrons. Therefore researchers are aiming for materials with the highest charge mobilities in order to fabricate more efficient devices.

## 1.4 Organic field effect transistors (OFETs)

A transistor is a device composed of a semiconductor that has the ability to regulate voltage and current in electronic circuits. These form the basis of all modern-day processors in electronics, with the computing power directly related to the number of transistors in a given area. An organic field effect transistor (OFET) is a type of transistor containing organic materials which uses an electric field to control the flow of current in a semiconductor (Figure 4). OFETs often function as a capacitor where electrical energy is stored in an electric field. Typically, they have two plates which contain three main components in an OFET: the gate, the source, and the drain.

Between these plates are the semiconducting organic layer and dielectric layer. The first plate is a conducting channel between two ohmic contacts, called the drain and the source contacts. The second plate is called the gate and controls the charges induced into the channel. Charge carriers flow from the organic layer when a charge is applied from the source to the drain. The charge carriers can be electrons for n-type materials, holes for p-type materials or both electrons and holes for a double injection device. The gate controls the charge carrier movement from the source to the drain.

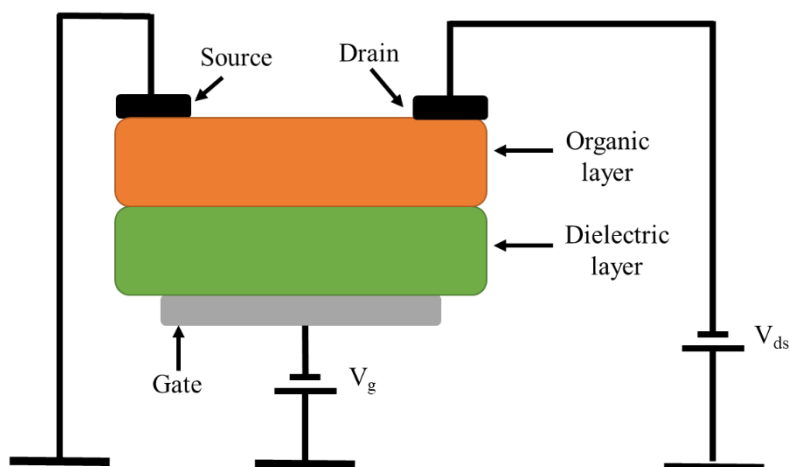


**Figure 4:** Schematic representation of the typical structure of an organic field effect transistor (OFET) device.

The relationship between these three components governs the efficiency of the device. When developing organic semiconductors that efficiently create a charge injection from the electrode, the on/off ratio (difference between the off-state and on-state current) and the characteristic of charge mobility need to be understood and analysed. A higher mobility of charge carriers enables faster switching thus increasing the efficiency of the device.

## 1.5 Organic photovoltaic cells (OPVCs)

A photovoltaic cell (PVC), or solar cell, is an electronic device that produces electricity *via* the photovoltaic effect by converting the energy provided from individual photons. Accordingly, an organic PVC (OPVC) utilizes processes within organic materials to produce electrical charge. In terms of composition, OPVCs are similar to OLEDs (Figure 3), where organic layers are sandwiched between electrodes, the anode and cathode. The organic layer consists of a n-type electron accepting material and p-type electron donating/hole producing material, separated by the depletion zone at the boundary of these two materials. The chemical process which produces electricity in an OPVC takes place at the depletion zone. The way these two organic materials are situated between the electrode has been optimized (Figure 5). They can be two simple layers termed a bilayer cell, or mixed together, known as a bulk heterojunction cell.

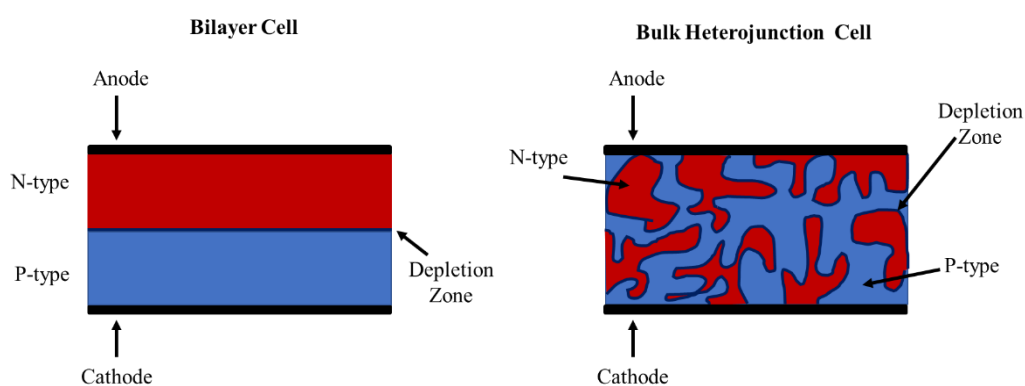


**Figure 5:** Schematic representation showing the composition of two types of photoactive layers in OPVCs; (left) a single heterojunction and (right) a bulk ‘all polymer’ heterojunction.

In the latter, this increases contact between the p-type and n-type material, thus increasing the surface area of the depletion zone, allowing the potential for more electricity to be produced by the device. The distance required for the charge carriers to travel to its respective electrode is also reduced in a bulk heterojunction composition, further increasing efficiency.

When light strikes an OPVC, energy is provided to the cell *via* a photon. The amount of energy provided is dependent on the frequency of light and can be calculated using Equation 1.1

where E is energy, h is Planck's constant and  $\nu$  is frequency.

Equation 1.1 
$$E = h\nu$$

Unlike OLEDs where energy (in the form of light) is produced by the *combination* of electrons and holes, the energy provided (in the form of light) in OPVCs is converted into electrons and holes and the *separation* of these produces electricity (Figure 6).

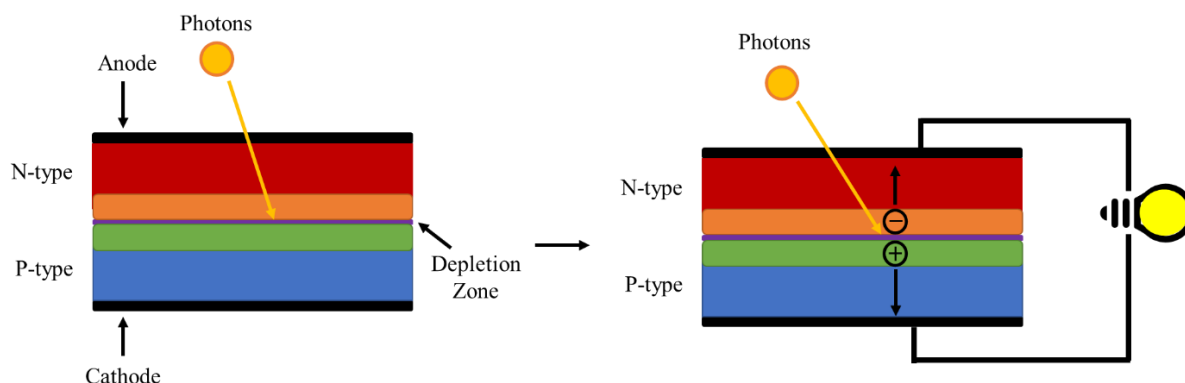


**Figure 6:** Schematic representative of a simple bilayer cell in the presence of photons.

We will now analyse the processes (Stages 1 to 4, Figure 7) taking place at the energy levels of the n-type and p-type materials within the organic layer to understand this further. In stage 1, sunlight strikes the cell, and this injects energy that is absorbed by the HOMOs of the p-type material. The intrinsic structure of the p-type donor means it is favourable for the energy to excite and promote a single electron into the LUMO level, producing a hole in its place. This

is not intrinsically favourable for the n-type material. In stage 2, the single electron in the HOMO of the p-type material is transferred to the electron accepting lower energy LUMO level of the n-type semiconductor by crossing the depletion zone. This can be transported further to the cathode which is lower in energy than the LUMO of the n-type acceptor. Simultaneously, the hole in the p-type donor can be shifted to the anode (stage 3). This separation and movement of electrons produces a current that can be used to power a device, for example illuminate a lightbulb (stage 4).

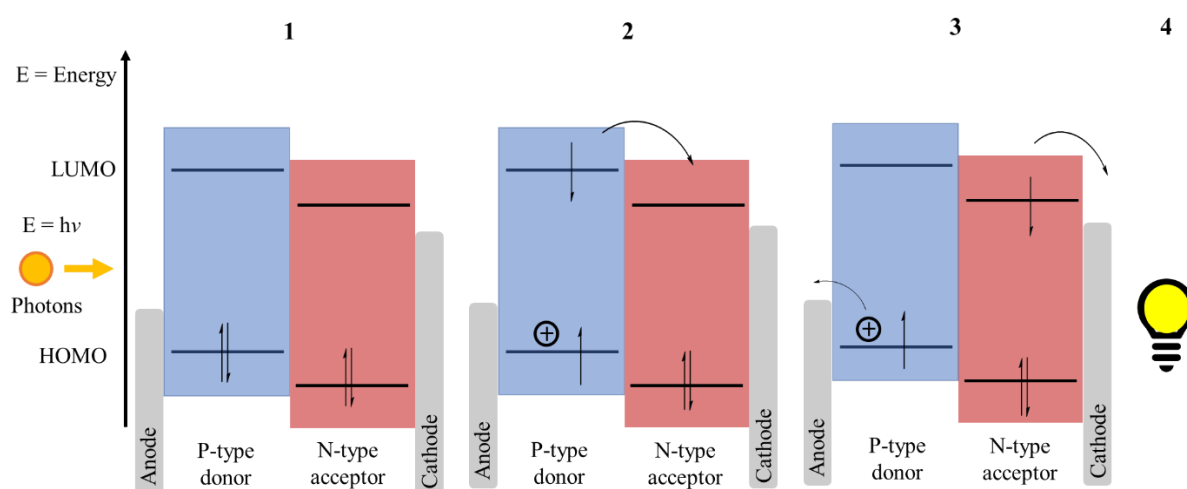


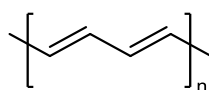
**Figure 7:** An energy level diagram displaying how electricity is generated in an OPVC in stages. stage 1; cell is irradiated light. stage 2: electron excitation into the LUMO level of the p-type donor. stage 3: subsequent transfer of holes and electrons to the anode and cathode from the p-type donor and n-type acceptor. Stage 4: electricity generated.

When studying the effectiveness of OPVCs a value often considered is the power conversion efficiency (PCE). This can be defined as the percentage of light (solar energy) exposed to an OPVC that is converted into usable electricity.

Now that it is understood how devices such as OLEDs, OFETs and OPVCs can function utilising organic semiconductors, the type of molecules used in these devices will now be explored.

## 1.6 Types of semiconductors (p and n-types)

Early examples towards the first organic semiconductors began in the 19<sup>th</sup> century where, in 1862, Henry Letheby obtained a partially conductive material, polyaniline (**1.12** in Figure 9), by anodic oxidation of aniline in sulphuric acid.<sup>6</sup> The field did not gain traction until the mid-1960's when it was realised that certain classes of organic materials, which are typically insulators, become semiconductors when injected with charge carriers from electrodes, which is a form of p-type doping in early examples.<sup>7,8</sup> This discovery led to an influx of research on the development of conductive polymers, with the most significant of these by Alan J. Heeger, Alan MacDiarmid and Hideki Shirakawa in 1977,<sup>9</sup> who observed that conductivity was markedly increased in *trans*-polyacetylene (structure **1.0** shown in Figure 8) when doped with halogen vapours. Along with their future work,<sup>10,11</sup> this pivotal discovery gained these three researchers the Nobel prize in 2001.<sup>12</sup>



**1.0**, *trans*-polyacetylene

**Figure 8:** Chemical structure of *trans*-polyacetylene.

Since then, there are now many examples of organic semiconducting molecules in the literature,<sup>13,14</sup> with almost 40,000 published research papers and *ca.* 3,400 review articles currently in the field.<sup>15</sup> Some of the main families of p and n-type organic semiconductors are shown in Figures 9 and 10.

p-type organic semiconductors behave as electron donors or hole transporters whereas n-type materials are electron accepting or electron transporters. Within the development of organic p-type semiconductors, examples include (Figure 9); commercially available Poly[(9,9-dioctylfluorenyl-2,7-diyl)-co-bithiophene] (F8T2, **1.1**<sup>16-18</sup>) and Poly[2-methoxy-5-(3',7'-

dimethyloctyloxy)-1,4-phenylenevinylene] (MDMO-PPV, **1.2**<sup>19,20</sup>) as well as hydrocarbon based Poly(phenylenevinylene) (PPV, **1.14**<sup>21</sup>) and fused ring pentacene (**1.3**<sup>22,23</sup>). The latter has been studied extensively in organic thin-film effect transistors due to having a hole mobility of up to 5.5 cm<sup>2</sup>/V·s,<sup>24</sup> which exceeds that of amorphous silicon. However, its rapid oxidation in air makes commercialization problematic. Thiophene based derivatives include regioregular Poly(3-hexylthiophene) (P3HT, **1.4**<sup>25-27</sup>), poly-[2,5-thienylene vinylene] (PVT, **1.5**<sup>28,29</sup>),  $\alpha$ -sexithiophene (**1.6**<sup>30,31</sup>),  $\alpha,\omega$ -di-hexyl-hexathienylene, (DH-6T, **1.7**<sup>32-35</sup>) and Thiophene-*N*-methylpyrrole (**1.8**<sup>36,37</sup>). Thiophene units are ubiquitous within organic electronics as the coplanar rigid structures and increased  $\pi$ -conjugation within the polymers, compared to a singular unit of thiophene, promote intermolecular  $\pi$ - $\pi$  stacking in the solid state which generates a higher charge carrier mobility.<sup>38</sup>

Finally, aromatic polymer systems containing one of the most electronegative atoms, nitrogen, exhibit low band gaps and display good charge carrier mobilities from both electrons and holes,<sup>39</sup> making them ideal for electronic applications. Examples include metallophthalocyanines (**1.9**<sup>40-43</sup>), poly triaryl amine (**1.10**<sup>44</sup>), polypyrrole (**1.11**<sup>45,46</sup>), polyaniline (**1.12**<sup>12,47</sup>) and poly[2,7-carbazolylenevinylene] (PCzV, **1.13**<sup>48,49</sup>).

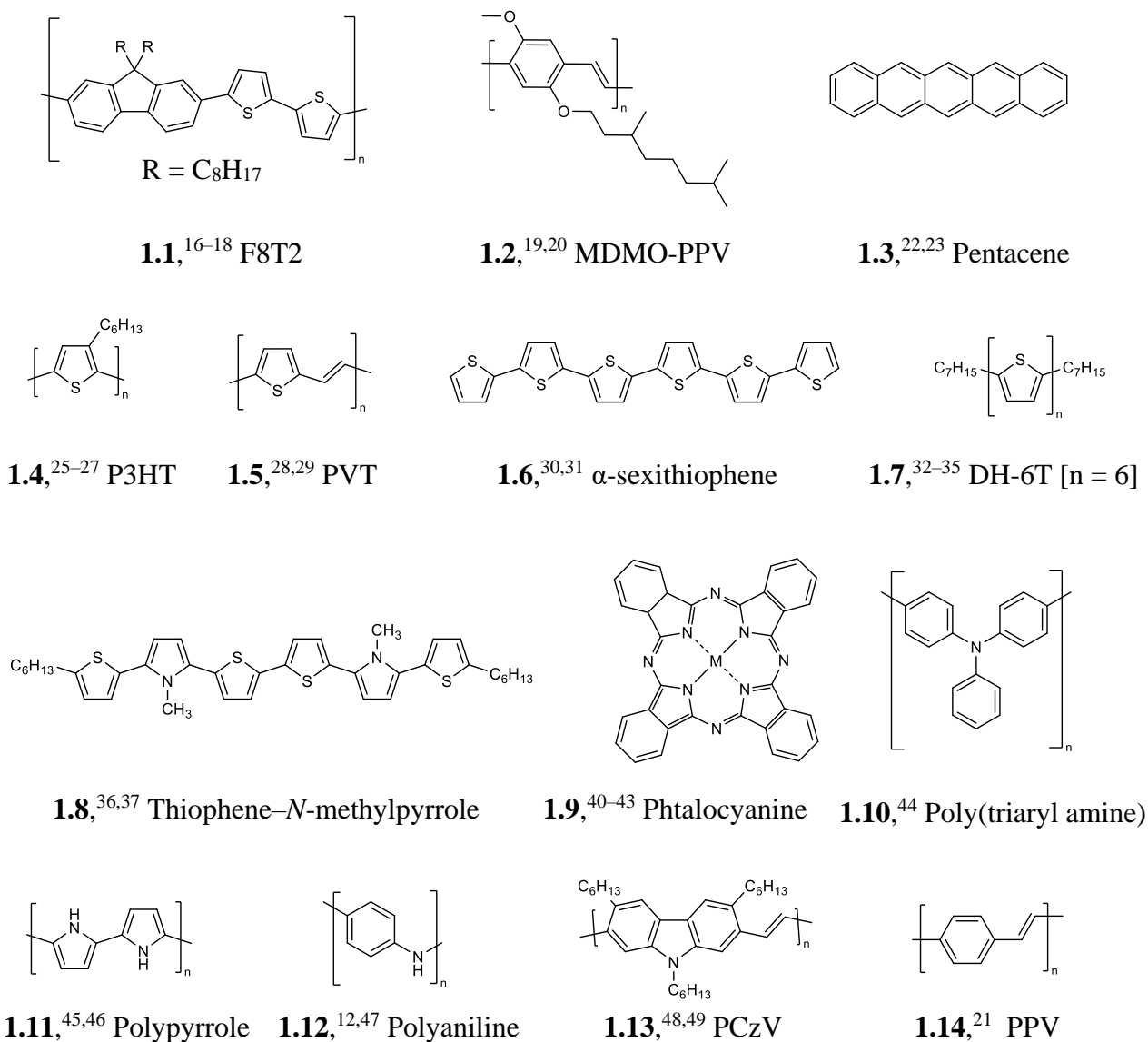


**Figure 9:** Selected examples of p-type semi conducting molecules and polymers <sup>50,51</sup>

Compared to p-type organic semiconductors, there are fewer examples of n-type organic semiconductors in general. This is due to n-type organic materials having complex synthesis routes, sensitivity to oxidation and often poor solubility.

The best way to optimize the charge carrier mobility of n-type organic semiconductors is to decrease the electron density along the  $\pi$ -conjugation in the neutral state. This can be achieved by adding functional groups, usually electron withdrawing, onto the  $\pi$ -conjugated molecules

within the material. For instance, nitrile, amides, fluorides, and imides have frequently been used. This allows access to low-lying HOMO and LUMO energy levels into which electrons can be injected. The LUMO energy level ideally should be lower than  $-3$  eV for efficient electron injection. A selection of seminal examples of predominantly small molecule n-type semiconducting materials are shown below in Figure 10.

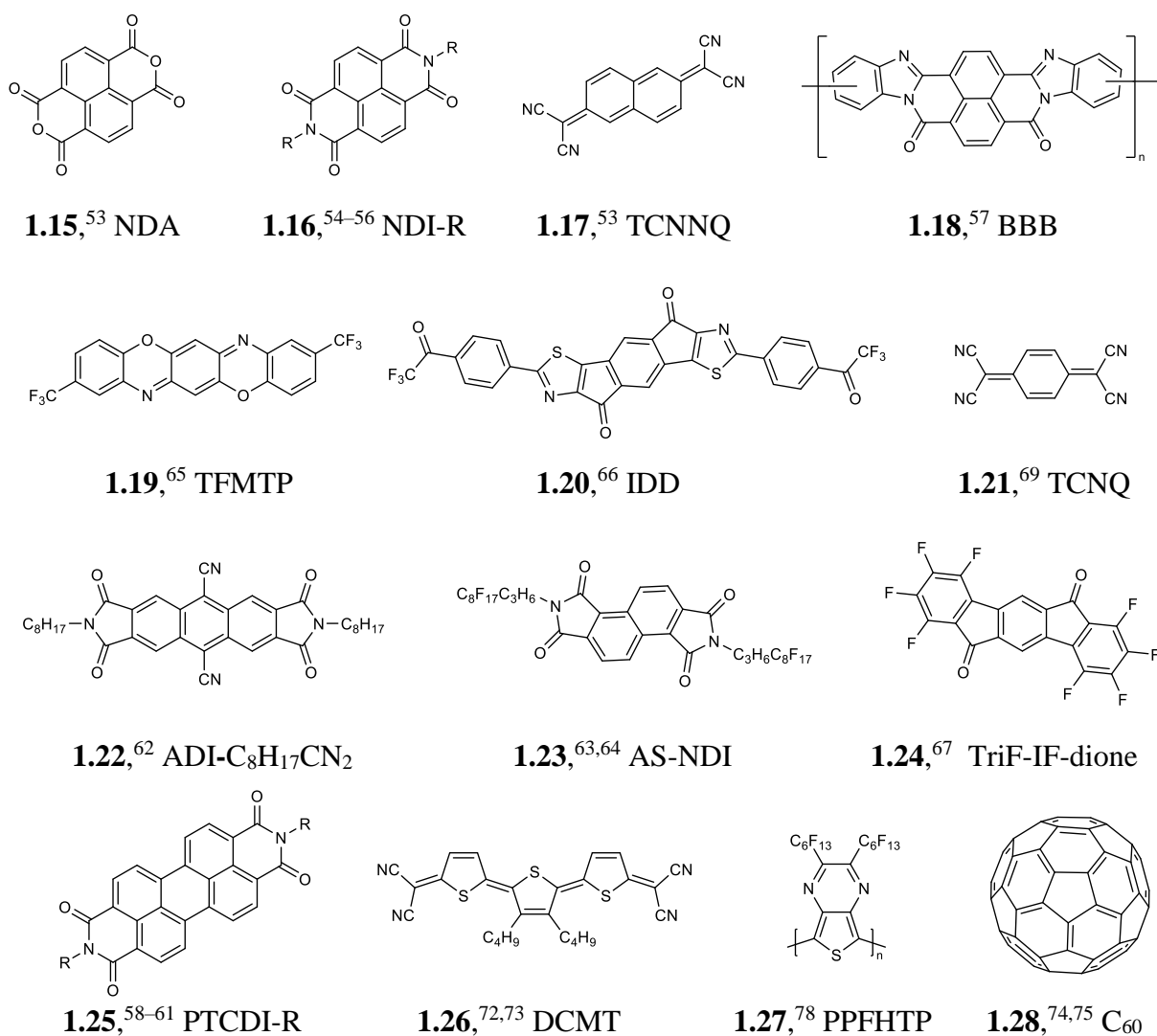
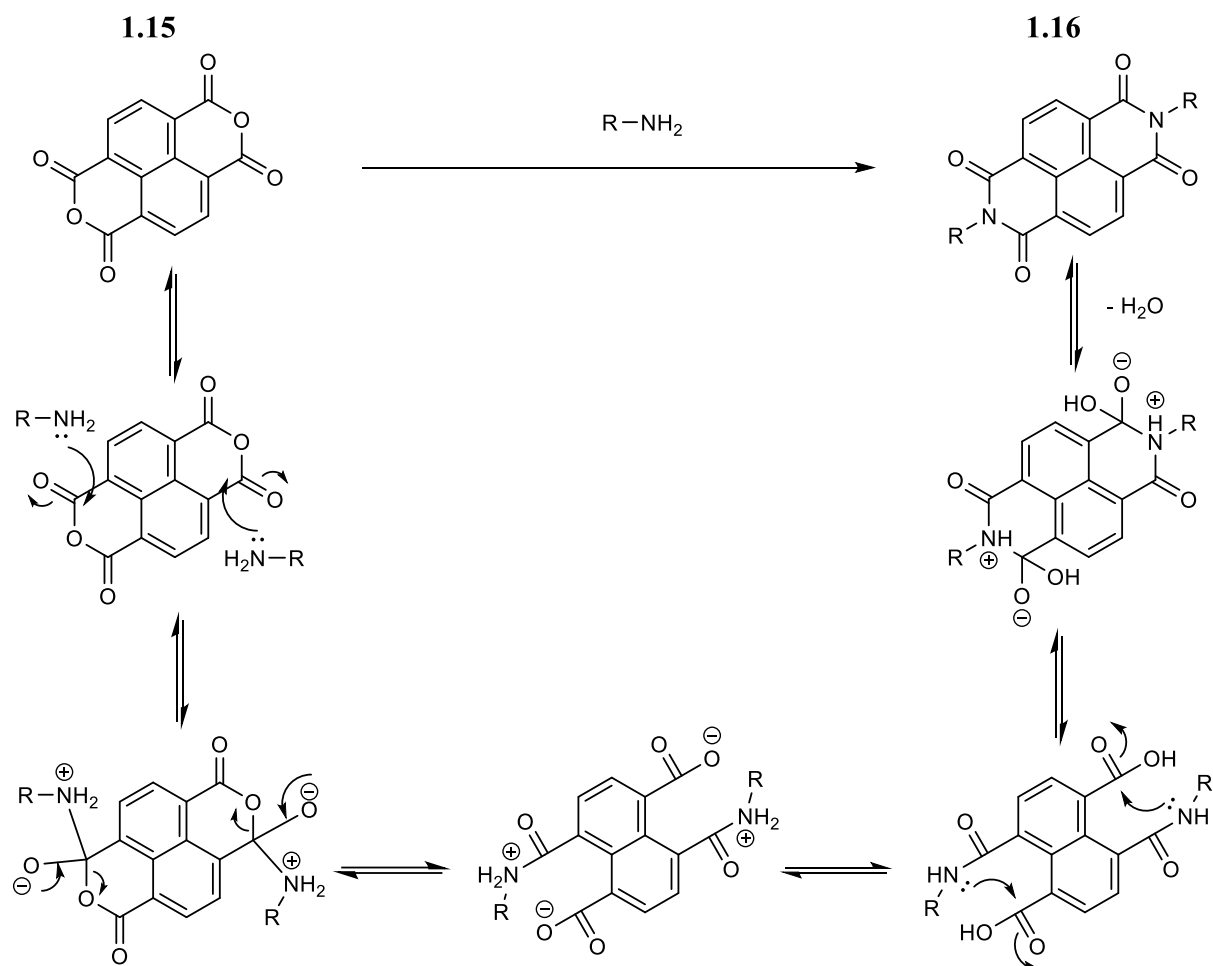


**Figure 10:** Selected examples of organic n-type semiconducting molecules and materials <sup>52</sup>

Organic n-type semiconductors containing naphthalene tetracarboxylic dianhydride (NDA, **1.15**<sup>53</sup>) moieties are amongst the most widely studied partly as a consequence of the inexpensive

nature of the starting material and well developed chemistry. NDA derivatives also show high thermal and photostable stability, high electron affinity and contain a coplanar conjugated structure, all of which are useful in the design of efficient and long lasting organic electronic devices. Additionally, the ease of modification at either the dianhydride units *via* a condensation reaction with an amine shown in Scheme 1 (**1.16**<sup>54-56</sup>, derivatives **1.18**<sup>57</sup> and **1.25**<sup>58-61</sup>), or addition of chosen functional groups at the aromatic core provide the potential to create a range of high-performance solution-processable low-lying LUMO materials. Subsequent analogues based on the above rationale include functionalised anthracene dicarboximide (ADI-C<sub>8</sub>CN<sub>2</sub>, **1.22**<sup>62</sup>) and angular shaped naphthalene tetracarboxylic diimide (AS-NDI, **1.23**<sup>63,64</sup>) systems.



**Scheme 1:** Mechanism involved in the condensation reaction between a dianhydride and an amine to yield a diimide.

Fluorine containing aromatic compounds feature often in n-type organic semiconductors (E.g. Trifluoromethyltriphenodioxazine (TFMTP, **1.19**<sup>65</sup>), 4,9-Dihydro-s-indaceno[1,2-b:5,6-b']dithiazole-4,9-dione (IDD, **1.20**<sup>66</sup>) and fluorinated indenofluorenedione (TriF-IF-dione, **1.24**<sup>67</sup>)) as fluorine is a good electron donating atom due to the lone pair which depresses the LUMO, thus improving the conducting abilities. Furthermore, it is observed that organic semiconductors which are fluorocarbon-based experience a kinetic air barrier mechanism which contributes towards air stability in devices.<sup>68</sup>

Electron withdrawing cyano substituents also prove to be commonplace in n-type organic semiconductor development, once again due to the LUMO lowering ability. 7,7,8,8-Tetracyanoquinodimeth-ane (TCNQ, **1.21**<sup>69</sup>), is a popular choice with a low-lying LUMO energy level of about -4.8 eV and electron affinity (EA) of 4.3 eV.

TCNQ was extensively studied due to its ability to form highly conductive charge transfer salts<sup>70</sup> and was first integrated into OFETs in 1994 by Brown and co-workers.<sup>69</sup> Modification by extension of the aromaticity to a naphthalene unit (tetracyanonaphthaquinodimethane (TCNNQ, **1.17**<sup>53</sup>)) increases the EA to 4.70 eV and doping of the system with fluorine increases it further (EA = 5.24 eV for fluorinated derivative of **1.21** and EA = 5.37 eV for F-doped **1.17**).<sup>71</sup>

In 2002, Chesterfield *et al.* developed dicyano containing terthiophene-based quinoid methane derivatives<sup>72,73</sup> (DCMT, **1.26**) as n-type materials in OFETs with electron mobilities as high as  $0.2 \text{ cm}^2 \text{ V}^{-1} \text{ s}^{-1}$  observed for films under vacuum.

Finally, buckminsterfullerene ( $\text{C}_{60}$ , **1.28**<sup>74,75</sup>) and its functionalized derivatives are one of the most widespread electron accepting materials used in organic electronics because of their high electron affinity. The optical absorption properties match that of the solar spectrum which make them ideal candidates for photovoltaic applications and conversion efficiencies of up to 5.7% have been reported for  $\text{C}_{60}$  based polymer cells.<sup>76</sup>

There are fewer n-type semiconducting polymer examples in the literature, with early research dominated with n-type small molecules, many of which are discussed above. In contrast to small molecules, organic polymer semiconductors can be developed to have improved film-forming properties. This is important in the properties of the final devices, where films can have enhanced morphological robustness with superior stretchability and mechanical flexibility compared to small molecules.<sup>77</sup> The broader potential physical and rheological properties of polymers from the addition of functional groups means the solubility can be altered more easily than small molecules which makes them better suited for solution-based processing techniques, allowing cost-effective high-throughput device fabrication over large areas.

The work of Babel and Jenehke in the early 2000's on the ladder polymers of benzimidazobenzophenanthroline type materials (BBL and BBB, **1.18**<sup>57</sup> in Figure 10) was one of the first intrinsic n-type polymers used in OFETs. Following this, Swager and co-workers developed a fluorinated polymer (poly(2,3-bis(perfluorohexyl)thieno[3,4-b]pyrazine, (PPFHTP, **1.27**<sup>78</sup> in Figure 10) which was shown to display n-type behaviour, exhibit high thermal and air stability, high EA (4.12 eV), low optical bandgap (0.87 eV for thin films) and selected solubility in fluoruous solvents in OFET and OPVC devices.

One of the most noteworthy examples of n-type polymers was disclosed by Swager and colleagues and is of particular importance to the work in this thesis. They produced a series of water-soluble di-pyridinium containing electron accepting n-type conjugated polymers<sup>79</sup> (**1.29-1.31**) shown in Figure 11. Water solubility is a desirable characteristic for large scale processing of electronic devices. These three conjugated polymers show high EA (from 3.90 eV to 4.14eV) which are comparable to C<sub>60</sub> based n-type materials.

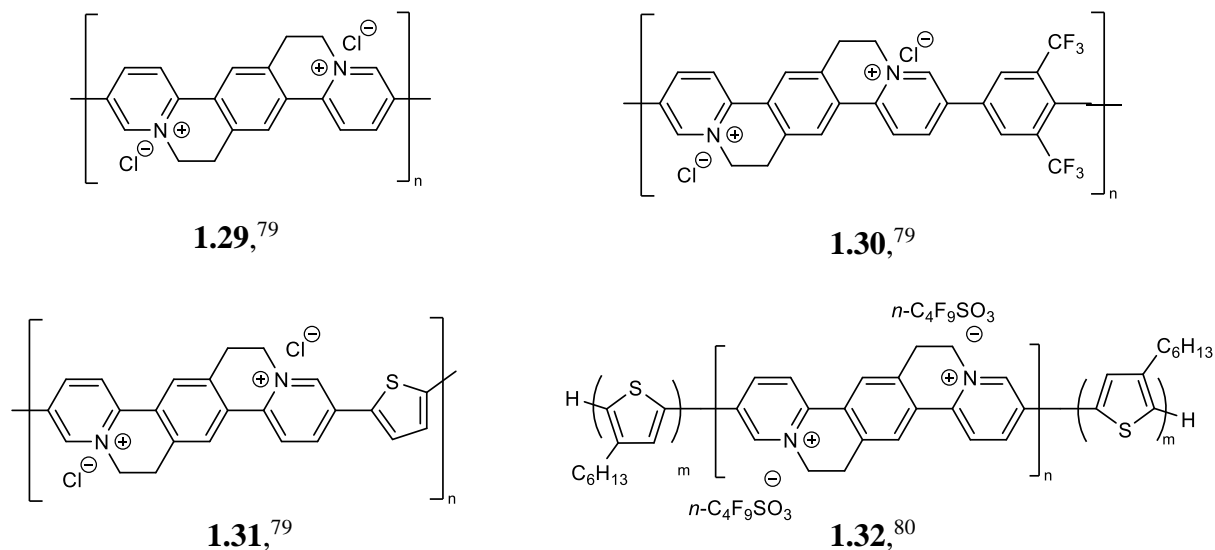


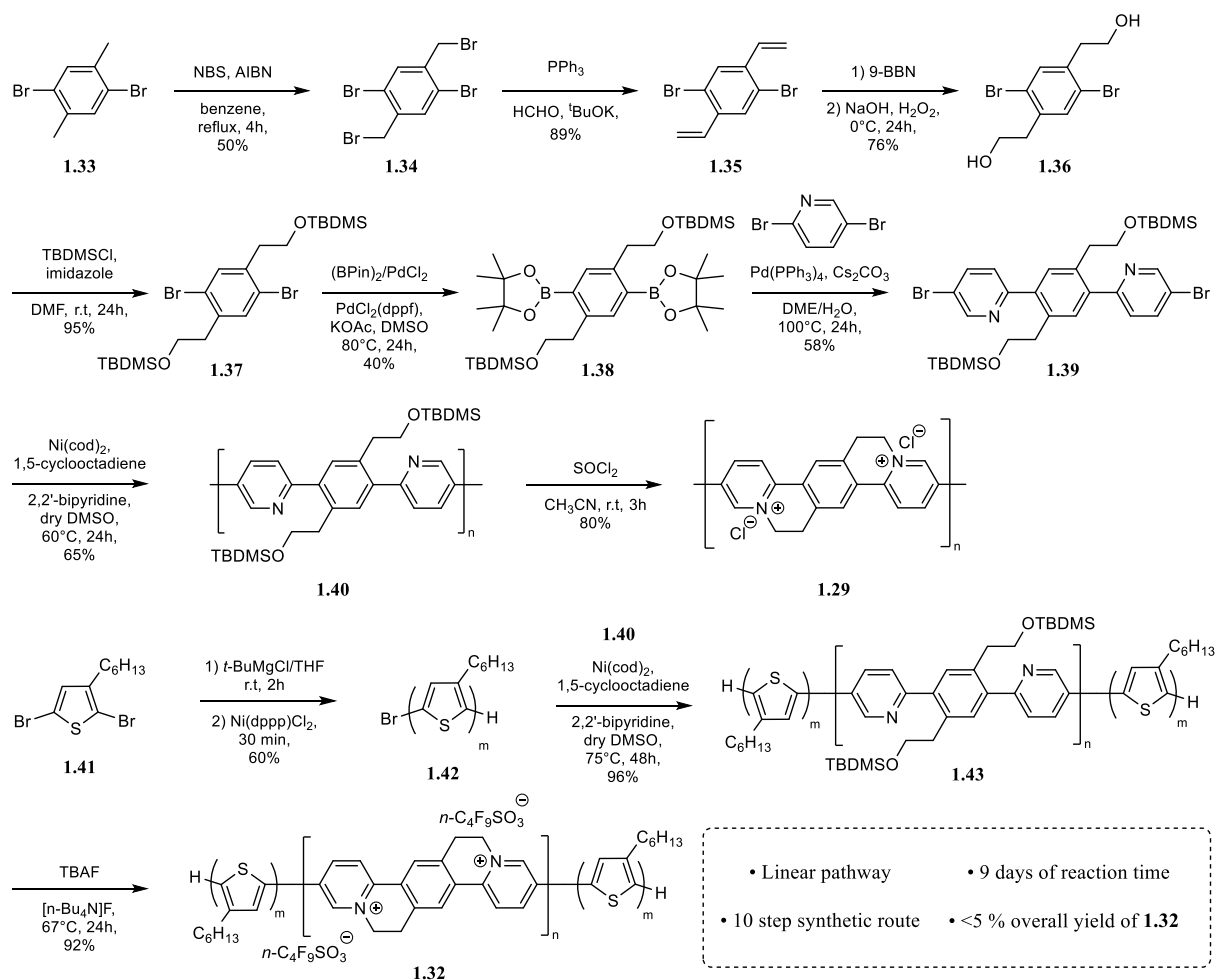
**Figure 11:** n-type semiconductors and block co-polymer produced by Swager and co-workers

The low LUMO energies are as a result of highly electron withdrawing intrinsic pyridinium rings. Swager also showed that the HOMO/LUMO and optical band gap can be modified by producing co-polymers where acceptor residues, such as thiophene (**1.31**) or ortho-substituted trifluoromethyl phenyl (**1.30**), separate the pyridinium units.

Subsequent work by Swager produced a crystalline-crystalline conjugated donor-acceptor block copolymer<sup>80</sup> (**1.32**) based on their previous systems. The block co-polymers contain the n-type conjugated poly(pyridinium phenylene) units as the electron accepting moiety and regioregular poly(3-hexylthiophene) as the p-type electron donor moiety. The block co-polymer exhibited an ionization potential (HOMO energy level) of 5.1 eV and the LUMO energy level

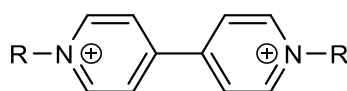
was calculated to be 3.8-4.0 eV *via* cyclic voltammetry. However, it should be noted that these block co-polymers showed solubility in aprotic solvents, such as DMSO and DMF. They are desirable candidates for photovoltaic materials as they displayed broad optical absorption bands that extended close to the near-infrared region, matching the solar spectrum frequency range.

The synthesis route to the block co-polymer **1.32** and pyridinium unit **1.29** is shown in Scheme 2. In summary, it is linear, requires 8 steps to reach the product (10 for the block co-polymer), 9 days of reaction time and is low yielding with an overall yield of <5%. This would make large-scale production of these materials extremely unrealistic unless the reaction was optimized.



**Scheme 2:** Synthesis of Swager water soluble n-type polymers **1.19** and block co-polymer **1.32**.

Despite the lengthy synthesis, the work from the Swager group described above opened the way towards accessing water soluble conjugated pyridinium species with n-type semiconducting properties. Much of the synthetic complexity comes from producing the pyridinium species during the synthesis (e.g., **1.33** to **1.40**, Scheme 2). However, it is well known<sup>81-84</sup> that 4,4'-bipyridinium (viologen) species (below, Figure 12) which contain the preformed targeted pyridinium species in the Swager materials, can be incorporated directly into polymers and therefore may provide access to these class of structures with reduced synthetic effort. The origin, structure, and potential of viologens as n-type semiconductors will be expanded upon below.

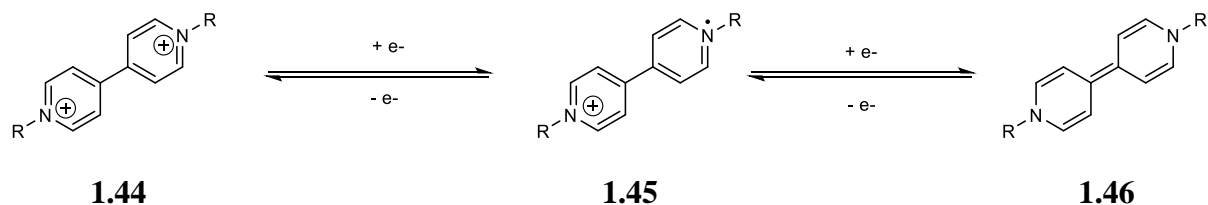


**1.44**

**Figure 12:** Chemical structure of a 4,4'-bipyridinium (viologen) species.

### 1.6.1 Structure and properties of viologens

Viologens (V) are disubstituted 4,4'-bipyridinium ions and can undergo two one-electron transfer reactions consecutively to form firstly a radical cation (**1.45**) and secondly a neutral quinoidal species<sup>85</sup> (**1.46**) from its original di-cationic state (**1.44**) as shown in Scheme 3.



**Scheme 3:** Electrochemical interconversion of viologen unit between dicationic  $V^{2+}$ , cationic radical  $V^{+•}$  and neutral states  $V^0$ .

Viologen containing materials can behave as semi conductive molecules and polymers due to their highly reversible redox properties.<sup>86</sup> This is facilitated by their planar backbone which allows for fast electron transfer with little structural change and their intrinsic  $\pi$ -electron deficiency enables them to be electron accepting materials.<sup>87</sup> Therefore, small molecule containing viologen species behave as n-type semiconductors and have resulted in them being ubiquitous in a wide range of research fields.<sup>88</sup> These include: organic aqueous redox flow batteries<sup>89,90</sup> (OARFBs), energy storage,<sup>91</sup> electron-transfer photosensitisers,<sup>92</sup> electrochromic displays,<sup>93</sup> photovoltaic cells,<sup>94</sup> biosensors,<sup>95</sup> OFET memory storage,<sup>96</sup> OLEDs,<sup>97,98</sup> herbicides,<sup>99</sup> catalytic hydrogen generation<sup>100</sup> and in supramolecular chemistry.<sup>87,101,102</sup> Extended and polymeric viologen structures<sup>103</sup> containing different functional groups or multiple viologens provide increased ability to tune the band gap, and can therefore expand the efficiency of the semiconductor.

### 1.6.2 Extended viologen systems

Recently, Yao, Kato *et al.* produced a set of small molecule ‘extended viologens’, whereby the two pyridinium rings of a viologen unit are separated by an additional aromatic ring, for instance, a phenyl, thiophene, 3,4-ethylenedioxy thiophene or pyridine species (**1.47-1.50**, Figure 13).<sup>104</sup> The n-type semiconductive nature of these small molecule extended viologens were utilized in the application of rechargeable molecular ion batteries.

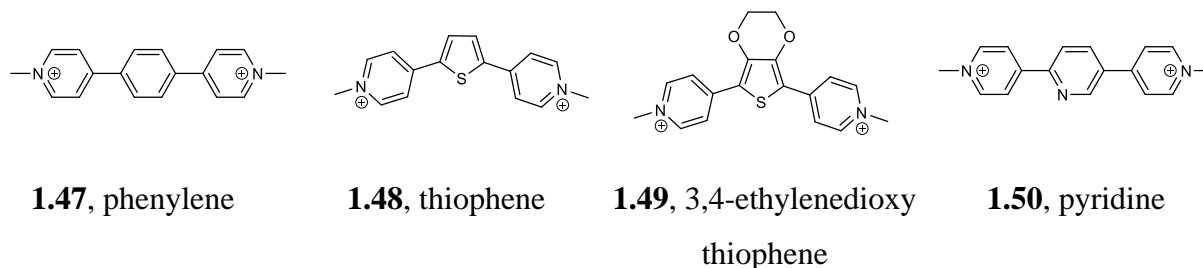
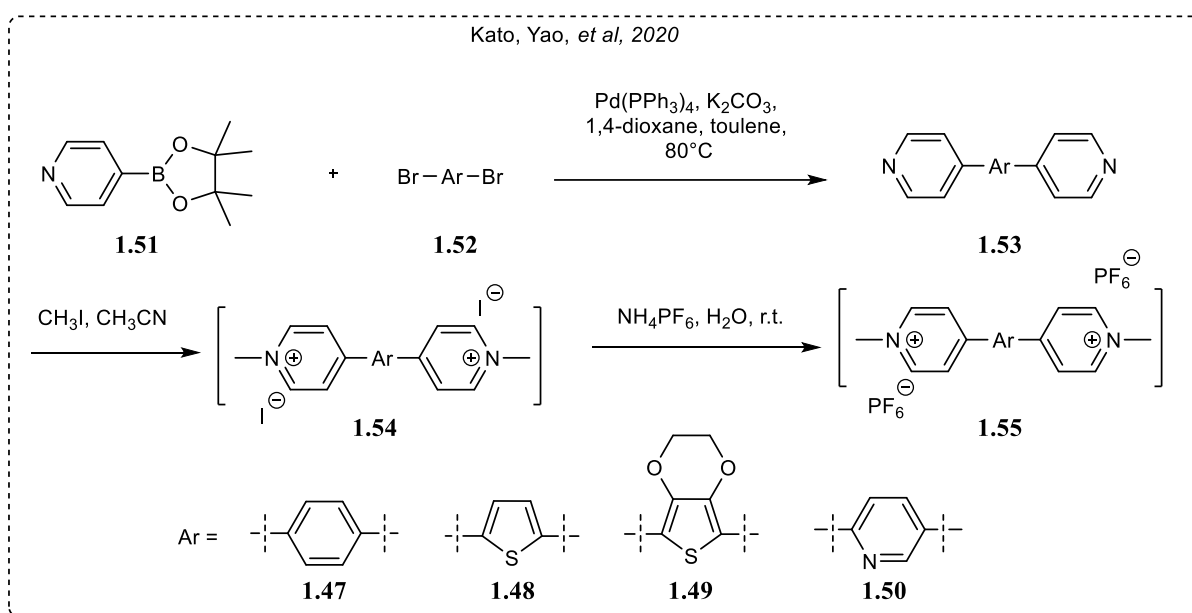


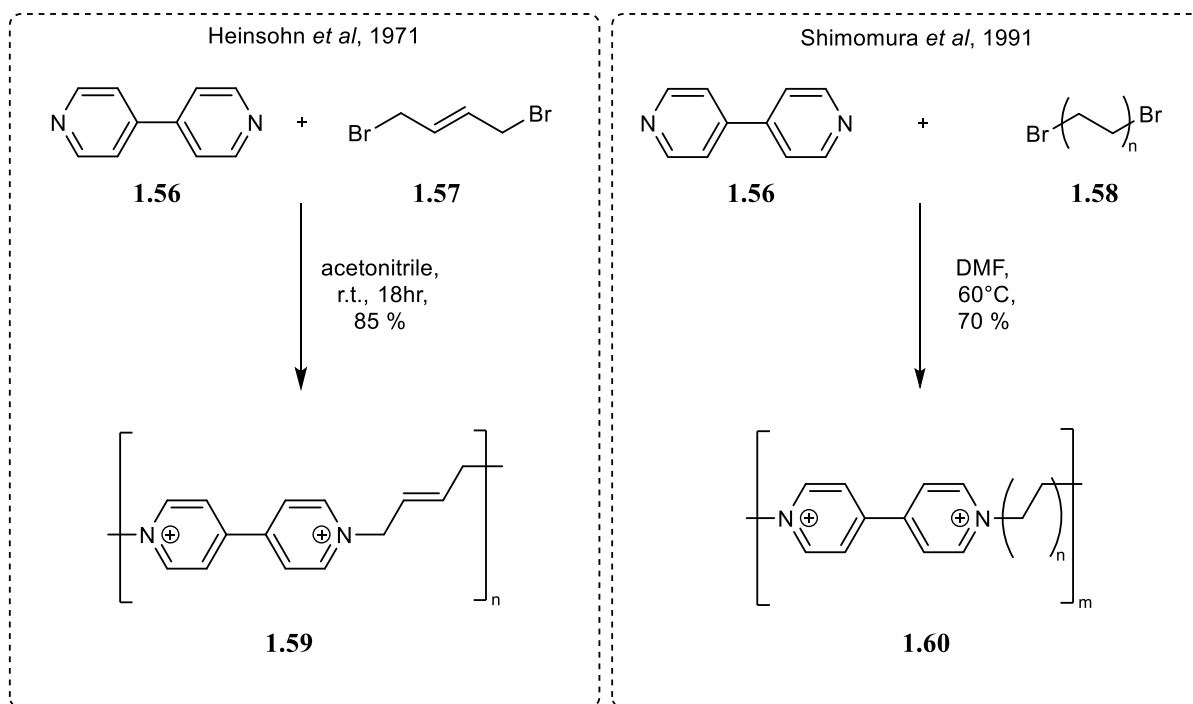
**Figure 13:** Small molecule extended viologen based derivatives produced by Yao, Kato and co-workers in 2020.<sup>104</sup>

Initially, the synthesis of these molecules involved connection of the neutral pyridine unit with an aromatic species, achieved by typical Pd-catalyzed Suzuki-coupling between the di-bromo substituted aromatic species **1.52** and 4-pyridine boronic acid pinacol ester **1.51**. The prepared triad precursor **1.53** was then quaternized using iodomethane to produce the desired extended viologen species **1.54**. Finally, anionic exchange from  $\text{I}^-$  to  $\text{PF}_6^-$  was carried out, using  $\text{NH}_4\text{PF}_6$  in water to isolate the final extended viologen species **1.55** (Scheme 4).



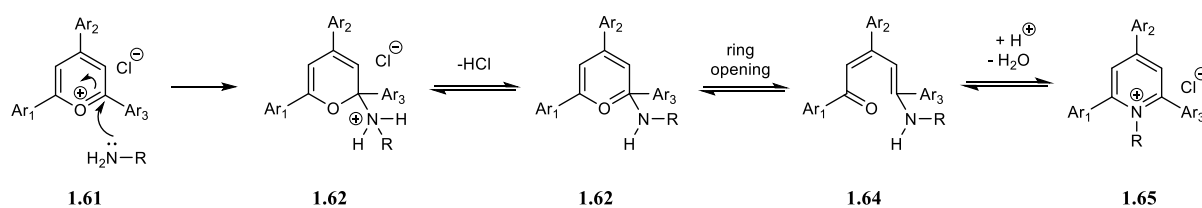
**Scheme 4:** Synthetic pathway to small molecule extended viologens produced by Yao, Kato, and co-workers.

In 1977, Heinsohn and co-workers developed the first known polymer containing a viologen unit.<sup>105</sup> The polymer was synthesised by utilizing the Menshutkin reaction,<sup>106</sup> whereby an equimolar amount of dibromo butene is added to 4,4'-bipyridine (left, Scheme 5). 20 years later, Shimomura and colleague's produced a similar derivative, by addition of 4,4'-bipyridine to the corresponding dibromo alkane, poly(alkanediyl-viologen dibromide).<sup>107</sup> (right, Scheme 5)



**Scheme 5:** (left); Poly(viologen) produced by Heinsohn and (right); the Poly(alkanediyl-viologen dibromide) synthesised by Shimomura.

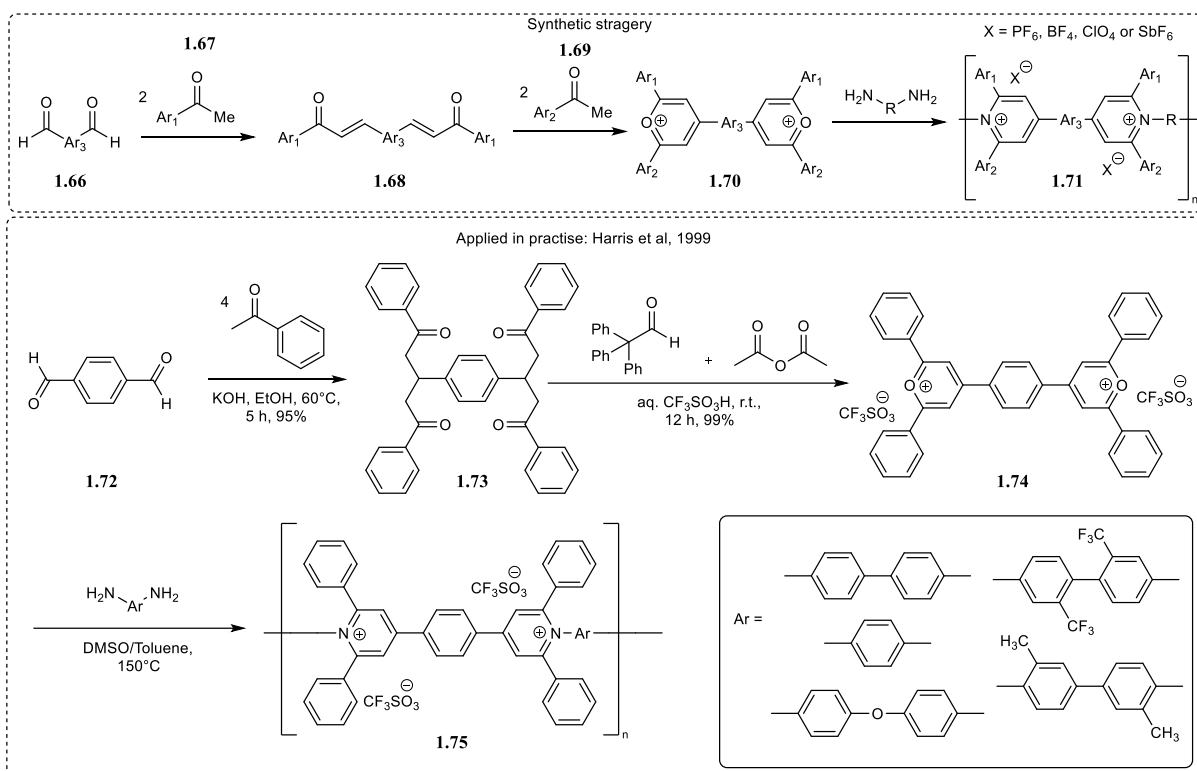
In terms of both of these poly(viologen) systems, the nitrogen situated *within the pyridine ring* acts as a nucleophile for the polymerization reaction. In contrast, there are several synthetic examples where the nitrogen *that forms the pyridinium ring* can behave as the nucleophilic species during the reaction. An example of this is shown in Scheme 6 between primary amines and aromatic substituted pyrylium salts (e.g. **1.61**).<sup>108</sup> Here, **1.61** can be transformed into a ketone by ring opening (**1.64**), which then converts to the pyridinium cation species **1.65** by ring closing and through the expulsion of water.



**Scheme 6:** Mechanism between pyrylium salts and a primary amine to produce a pyridinium species<sup>108</sup>

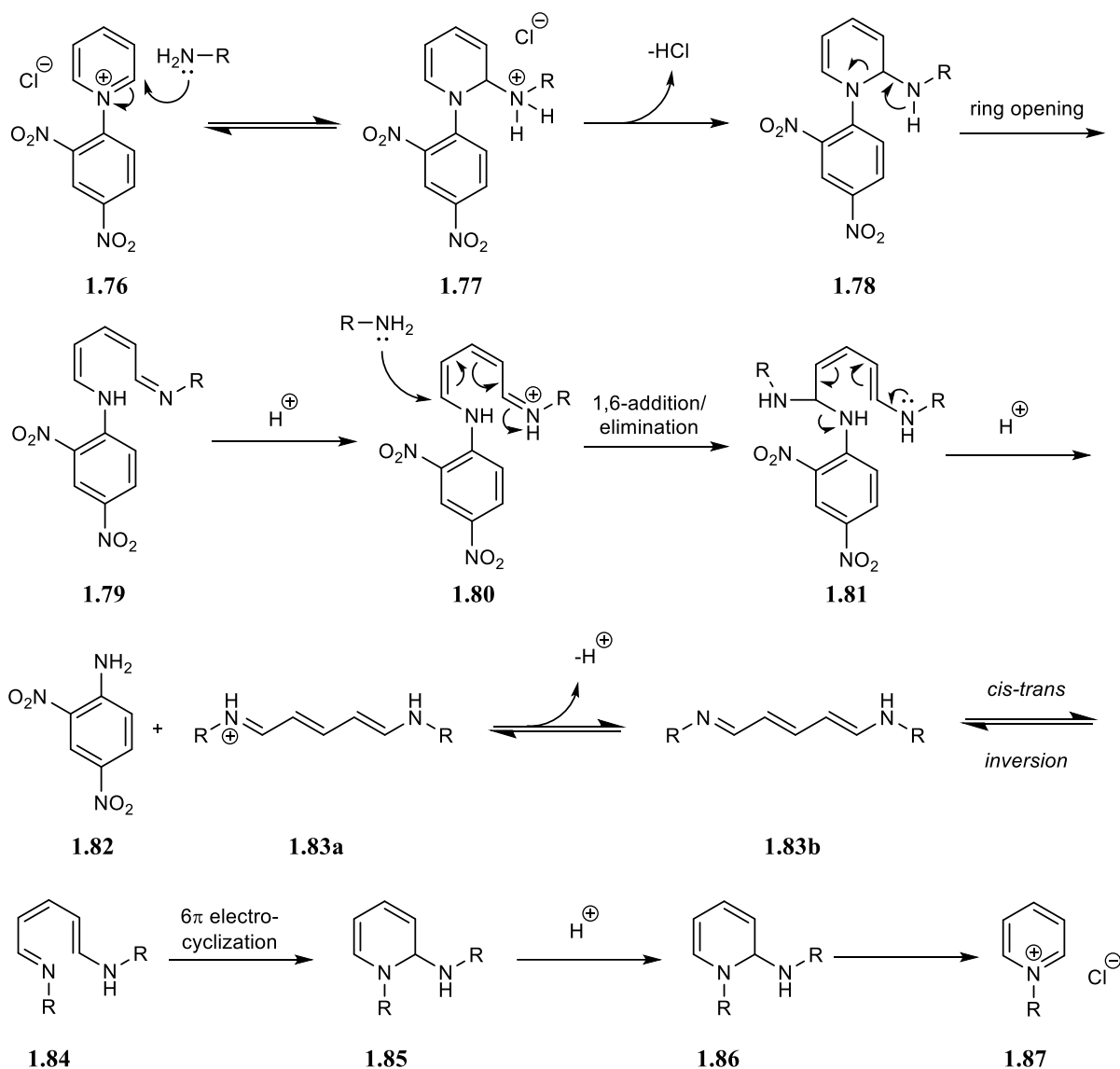
This concept could be applied to an analogue of this system to yield a viologen containing copolymer by reacting a diamine with a bi-pyridinium salt (top of Scheme 6, **1.70** to **1.71**). This can be done to produce polymers which contain extended viologens and the viologen unit can be separated by at least one additional aromatic (**1.71**). It is also worth noting that unlike Heinsohn's and Shimomura's examples where the reaction took place with the already formed aromatic pyridinium ring, aromatic pyridinium salts with aromatic substituents can easily be obtained using the well-established Dilthey synthesis route.<sup>109</sup> This is where a condensation reaction between two equivalents of acetophenone and one equivalent of benzaldehyde (for example an aromatic substituted dibenzaldehyde (**1.67**) e.g. terephthalaldehyde **1.72**) forms the pyridinium salt precursor. An example is shown for the synthesis of bi-pyridinium containing salts (**1.66** to **1.70**, top of Scheme 7).

Several research groups have exploited this to produce polypyridinium species.<sup>110-113</sup> One example includes polymers based on extended viologen units produced by Harris and co-workers (bottom of Scheme 7) in 1999.<sup>114</sup> Briefly, the polymer was synthesised using a novel monomer, *p*-bis[4-(2,6-diphenylpyridinium)]benzene ditriflate **1.74**, prepared by cyclisation of the tetra ketone **1.73** with fluoroboric acid and triphenylmethanol. Based on Dilthey synthesis methodology, the tetraketone was produced by the reaction of terephthalaldehyde **1.72** with four equivalents of acetophenone in the presence of KOH base. This di-cationic activated monomer unit then underwent a condensation polymerization reaction with a diamine to yield the polymer species **1.75** (bottom of Scheme 7). Compared to the Menshutkin reaction (Scheme 5), the pyridinium reaction (Scheme 6) utilizes an activated monomer that experiences nucleophilic attack by the nitrogen containing diamine species. The pyridinium ion forms containing the nitrogen that originated in the nucleophilic diamine species, through the loss of water.



**Scheme 7:** (top) The synthetic strategy to access polypyridinium homopolymers and (bottom) an example of polymers based on extended viologens in literature, by Harris and co-workers.<sup>114</sup>

In a similar manner, the Zincke reaction,<sup>115,116</sup> named after Theodor Zincke in 1904, is a reaction in which a N-(2,4-dinitrophenyl) pyridinium salt can undergo nucleophilic attack of an amine (Scheme 8). The precursor N-(2,4-dinitrophenyl) pyridinium salt can be synthesised by reacting pyridine species with 2,4-dinitro-chlorobenzene. Briefly, the Zincke reaction starts with nucleophilic attack of the N-(2,4-dinitrophenyl) pyridinium salt from the primary amine, which causes ring opening of the pyridinium ring (**1.76** to **1.79**). Intramolecular attack by the nitrogen atom then removes 2,4-dinitroaniline **1.82** whilst concurrently, the König salt<sup>117</sup> (**1.83a** and **1.83b**) is formed. Either **1.83a** or **1.83b** can then undergo a cis-trans inversion followed by 6 $\pi$  electron cyclization to form **1.85**. Finally, proton transfer and amine elimination takes place to yield the desired pyridinium ion species **1.87**.



**Scheme 8:** Formation of a Zincke salt via reaction of pyridine with 2,4-dinitro-chlorobenzene.

This synthesis allows a simple route to extend aromaticity in electron deficient compounds containing a pyridinium species. Despite the fact that this reaction was reported almost 120 years ago, it is still continuing to be relevant and is extensively investigated to develop the reaction yields and substrate scope.<sup>118</sup>

An example of expanding substrate scope is seen in the work by Greenland and colleagues, where various sets of n-type semiconductive oligomeric viologens (Figure 14) were produced.<sup>82,84,119</sup>

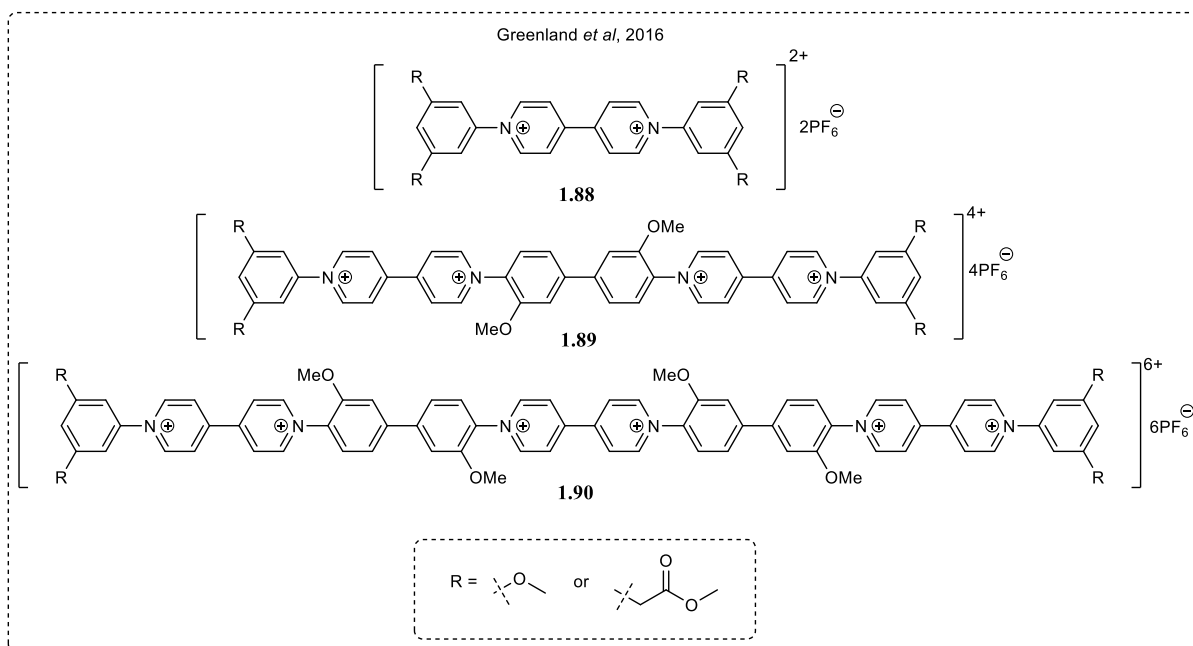
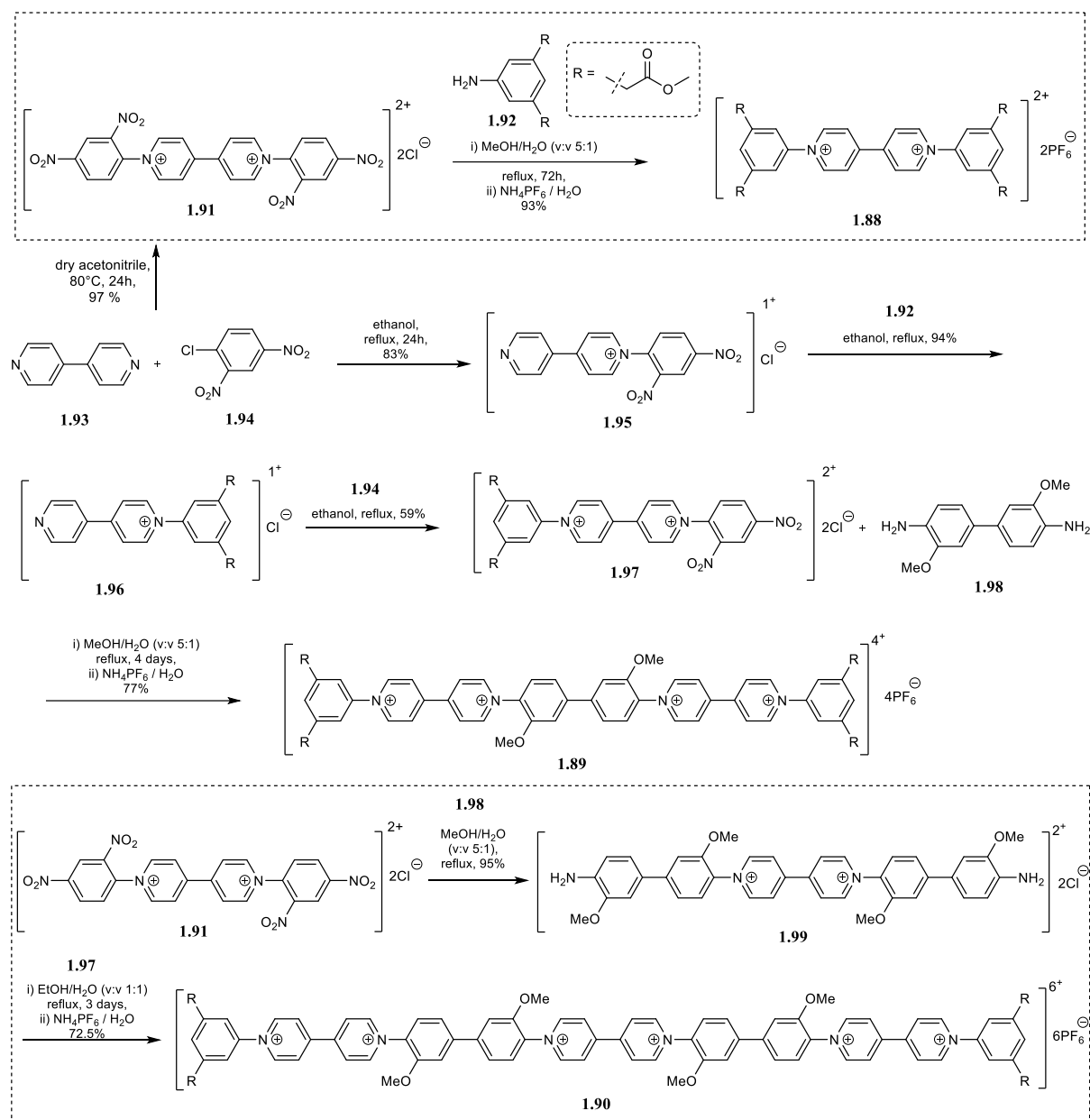


**Figure 14:** Set of Greenland and colleagues oligomers accessed by utilizing the Zincke reaction.

The oligomers, where R is defined as a methoxy functional group, were shown to have semiconductive abilities with n-type behaviour. Conductivity was seen to increase as the aromaticity was extended from the unimer ( $2.20 \times 10^{-11} \text{ S cm}^{-1}$ ), dimer ( $1.54 \times 10^{-10} \text{ S cm}^{-1}$ ) to the trimer ( $6.87 \times 10^{-10} \text{ S cm}^{-1}$ ) and the band gap was observed to be narrower for the trimer (2.3 eV) than the unimer and dimer (both 2.7 eV). To synthesise these oligomers, a synthesis approach was adopted utilizing the Zincke reaction between symmetric or asymmetric Zincke salts and primary anilines. (Scheme 9)

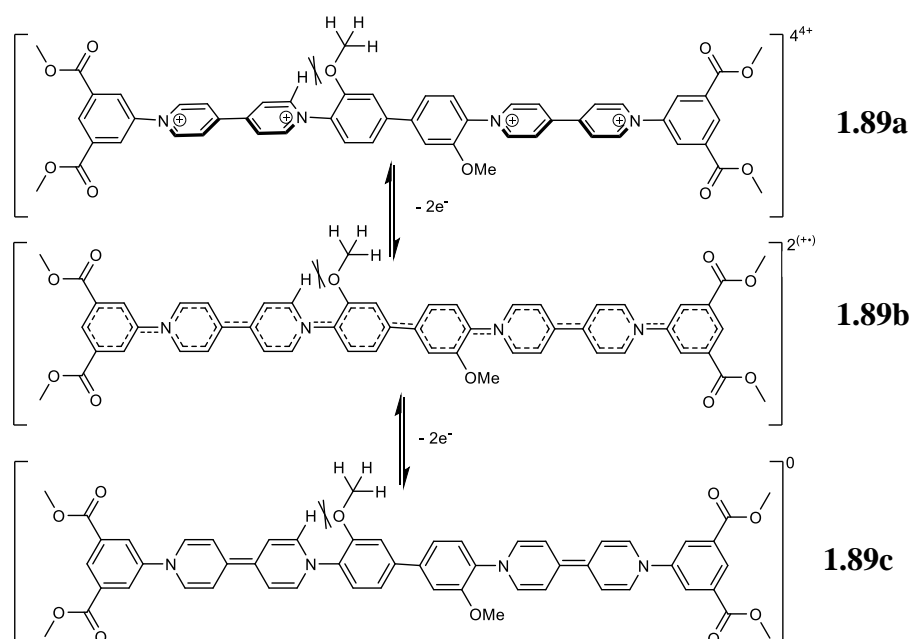


**Scheme 9:** Synthesis pathway for extended viologen containing oligomers produced by Greenland and co-workers.<sup>82</sup>

Compared to Swager's synthesis pathway of n-type pyridinium containing species (Scheme 2), this synthesis route only requires 4 steps to the dimer, or 5 steps to the trimer *via* a convergent route and is higher yielding with an overall yield of 35 % and 24 % for the dimer and trimer respectively. These bipyridinium containing oligomers were not water soluble but it is well

established that the anion can easily be exchanged for a water solubilising anion like chloride ions.

In their initial work, Greenland and co-workers produced structures that contained methoxy substituents along the planar backbone of the viologens. This was speculated to cause twisting of the aromatic backbone with the viologen units in the cationic state **1.89a**, as in Scheme 10. It flattens upon oxidation to the radical state (**1.89b**), however steric clash may further hinder the planar arrangement. To have optimum  $\pi$ -overlap, a planar rod would be advantageous.



**Scheme 10:** Structure of dimer by Greenland *et al.* in cationic state showing twisting as a result of OMe substituents (top) delocalised as the radical upon oxidation (middle) and in the neutral quinoidal form (bottom).

It was originally thought that the methoxy substituents were required to increase the electron density into the aromatic system, thus improving the nucleophilicity of the amine which in turn aided the Zincke reaction. However, further studies<sup>83,120</sup> have shown the methoxy groups are not necessary for the Zincke reaction to proceed.

## 1.7 Conclusion

In conclusion, the brief literature exploration in this chapter has shown that there is capacity for development within the n-type conducting polymers field. The pioneering works by Harris<sup>114</sup> and Swager<sup>78,79</sup> have demonstrated that polymers containing pyridinium species could be successfully synthesised and have applications in opto-electronics. Later, Greenland<sup>82,84,119</sup> reported a robust synthesis route to produce bipyridinium containing oligomers, using the Zincke reaction, which showed good conductivity as n-type materials. However, the scarcity of examples in this area provides much scope for improving and developing these materials. Building on the work produced by Greenland and others,<sup>83</sup> the next chapter contains a series of three water soluble viologen containing oligomers that do not contain any substituents on the aromatic rings and will be a valuable addition to the n-type semiconductor field.<sup>88,121</sup> This could be achieved using the previously discussed high yielding literature established Zincke synthesis route. The proposed structural changes should increase the  $\pi$ - $\pi$  overlap and therefore the efficiency of the redox processes subsequently increasing conductivity.

## **Chapter Two**

**Work towards a series of conjugated  
viologen containing oligomers with  
electronic applications**

# Chapter 2: Work towards a series of planar conjugated viologen containing oligomers with electronic applications

Utilising the Zincke reaction, a series of conjugated viologen oligomers have been synthesised with the potential of semiconductive capabilities.

## 2.1 Synthetic Rationale and Targets

The viologen oligomers synthesised previously in the Greenland group contained methoxy substituents in the backbone (Section 1.6.3 and structure **1.89** below). Data from UV/vis spectroelectrochemistry lead the group to speculate that the presence of the methoxy substituents caused twisting of the aromatic backbone with the viologen units in the cationic state (Section 1.6.2, Scheme 10). This would likely cause a break in the overlap of the  $\pi$ -orbitals along the backbone of the system and therefore, reduce the efficiency of electron transport and consequently conductivity of the systems. During the initial phases of this PhD, I was able to successfully grow crystals suitable for single crystal X-ray analysis of the dimeric viologen synthesised by Dr. Long previously.<sup>82</sup> Crystal growing conditions were inspired by Stoddart *et al.*,<sup>122</sup> *via* vapour diffusion using the solvent:antisolvent system with acetonitrile and diisopropyl ether respectively. The solid-state structure does indeed show the twisting of the backbone in the tetra cationic state as proposed in the original paper on this work (Figure 15). The twisting of the viologen backbone is apparent when viewed from different angles in a ball and stick form (1 in Figure 15) or wire form (2 in Figure 15). The torsion angles labelled A-E in section 3 of Figure 15 and reported in table 1, indicate the most severe twisting of 53°, 68°

and 69° at sights A, C and E respectively, next to the nitrogen sites on the pyridinium rings. Whilst sight B has a lower torsion angle at 26° and D shows negligible twisting with a torsion angle of 0.07°.

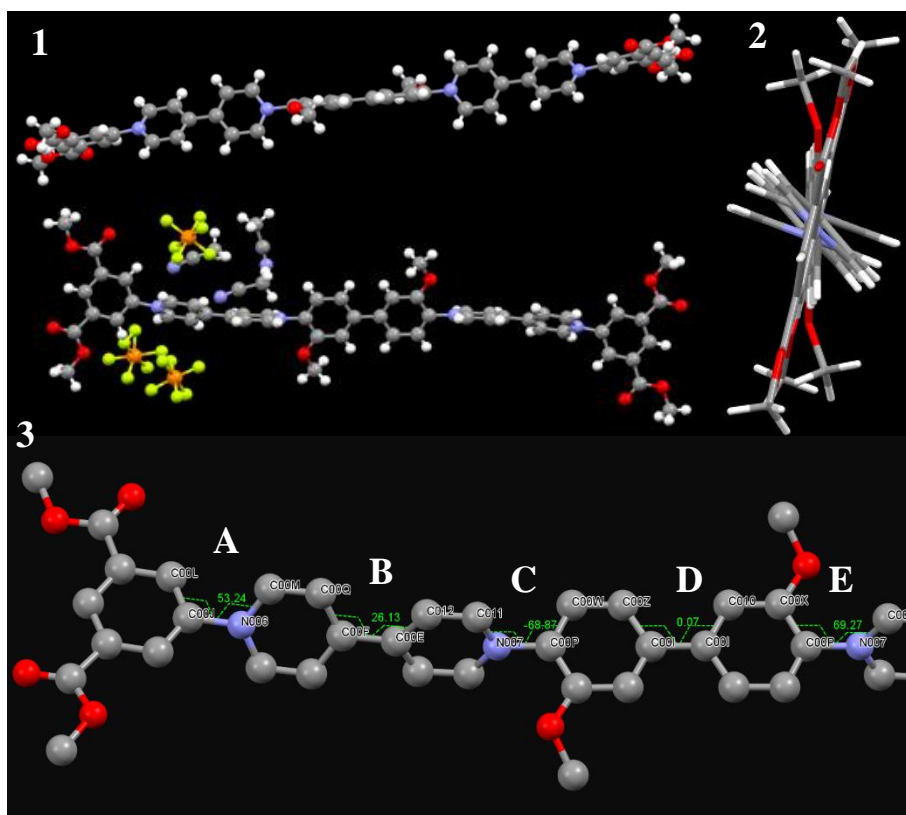


**Figure 15:** Different orientations of the crystal structure **1.89** : (1) side view of crystal showing the viologens in the plane and other aromatics twisted (2) viewed down the length of the backbone with viologens out of the plane twisting and (3) close up of the dimer with torsion angles displayed and labelled A to E. Solvent molecules were excluded in 1-3 and anions excluded in 2 and 3 for clarity.

Label	Atoms	Torsion angle
A	C00L, C00J, N006, C00M	53.24
B	C00Q, C00F, C00E, C012	26.13
C	C011, N007, C00P, C00W	-68.87
D	C00Z, C00I, C00I, C010	0.07
E	C00X, C00P, N007, C00S	69.27

**Table 1:** Torsion angles in oligomer **1.89** crystal structure

With this conclusive data as to the conformation of the oligomeric molecular wires in mind, the first target for this work was to attempt to synthesise a 2<sup>nd</sup> generation of molecular wires that lacked the methoxy group responsible for causing the twist (See Figure 16 – compounds **2.1** to **2.3**).

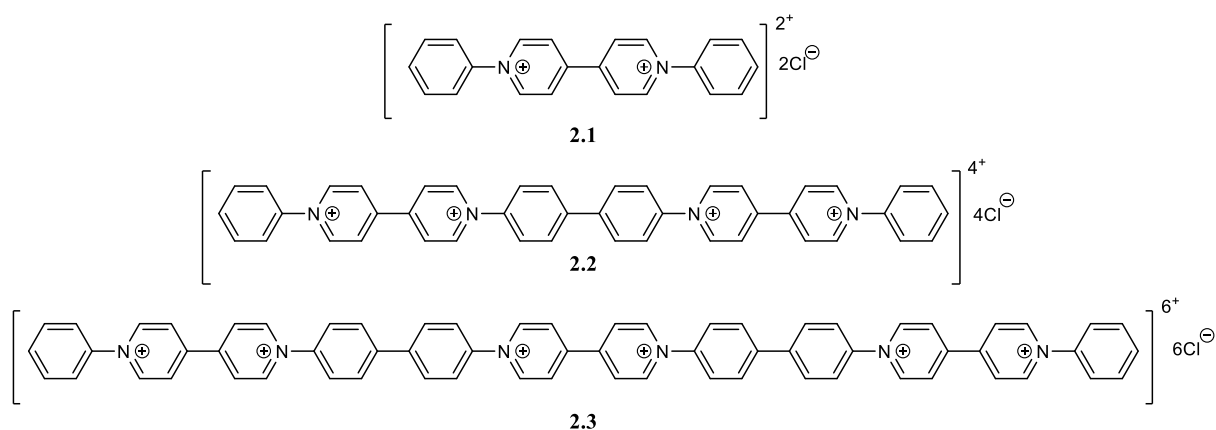
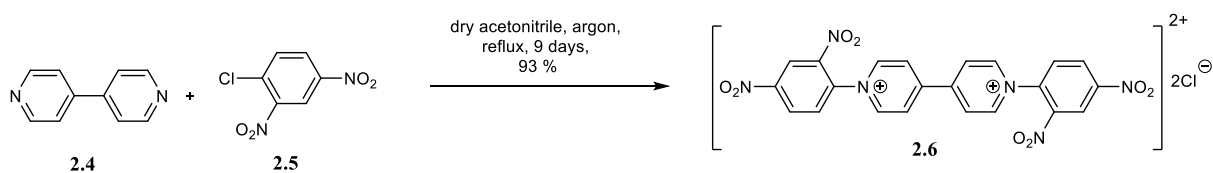


**Figure 16:** Proposed set of viologen containing oligomers containing increasing number of 4,4'-bipyridium residues.

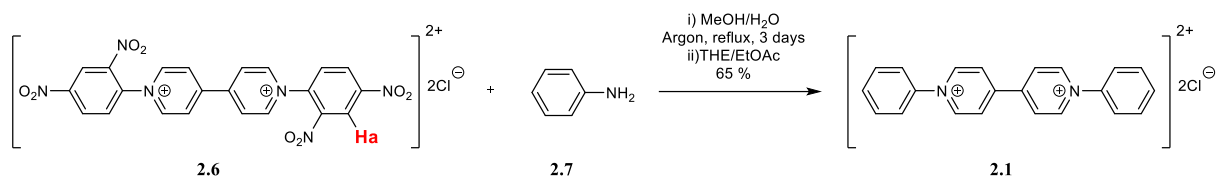
## 2.2 Results and discussion

The synthetic pathway for the oligomers started using the Zincke salt **2.6** that can be synthesised on a multi-gram scale by the addition of an excess of 2,4-dinitrochlorobenzene **2.5** to 4,4'-bipyridium in dry acetonitrile refluxed over nine days (Scheme 11). Although recent literature reports this reaction to be high yielding (95 – 97%) in the same conditions in reaction times between 24-72h,<sup>123–126</sup> we found that we only reached these yields after a prolonged reaction time of nine days.



**Scheme 11:** Synthesis of a zinke salt from 4,4'-bipyridine and 2,4-dinitro-1-chlorobenzene

Initially, the unimer (**2.1**) was synthesised by reaction of **2.6** with aniline **2.7** to produce phenyl viologen **2.1** in 65% yield. The synthesis route followed was adapted from Kamogawa<sup>127</sup> and is shown in Scheme 12, where the chloride salt was isolated, overlooking Kamogawa's final step which involved anionic exchange to the PF<sub>6</sub><sup>-</sup> counter ion. Synthesising oligomers with chloride anions are convenient because they should be soluble in water and protic organic solvents such as methanol and ethanol respectively, which will allow integration into electronic devices using environmentally friendly solvents compared to organic solvents. It also provides a valuable addition to the water-soluble n-type semiconductors which has grown in popularity in recent years due to the greener processing.<sup>128</sup>



**Scheme 12:** Reaction scheme to synthesise the unimer **2.1**.

Success of the reaction could easily be verified with <sup>1</sup>H NMR spectra of **2.1**, where the spectra lacks the singlet resonance peak at 9.46 ppm attributed to a proton found on the 2,4-dinitrobenzyl group and labelled in red as H<sub>a</sub> (Scheme 12) and contains the multiplet between 7.96-7.71 ppm associated with the aromatic protons in aniline. A common problem with these compounds is their tendency to form radical cationic species<sup>82,84,119,129</sup> where the signals in the <sup>1</sup>H NMR spectrum are dramatically broadened. This broadening can be inhibited by adding a drop 2,2,2-trifluoroacetic acid (TFA) to the NMR solvent which consistently produced sharper signals as the acid pushes the equilibrium towards the di-cationic form in solution. The <sup>1</sup>H NMR spectra (Figure 17) showed agreement with Kamogawa's and Porters published spectra.<sup>85,127</sup>

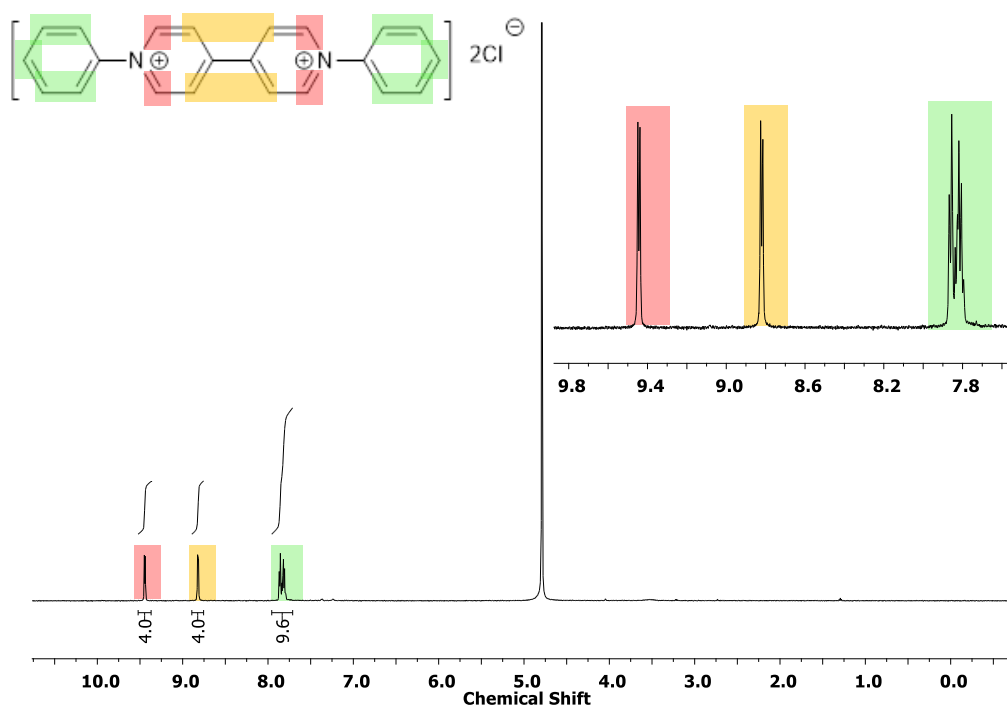
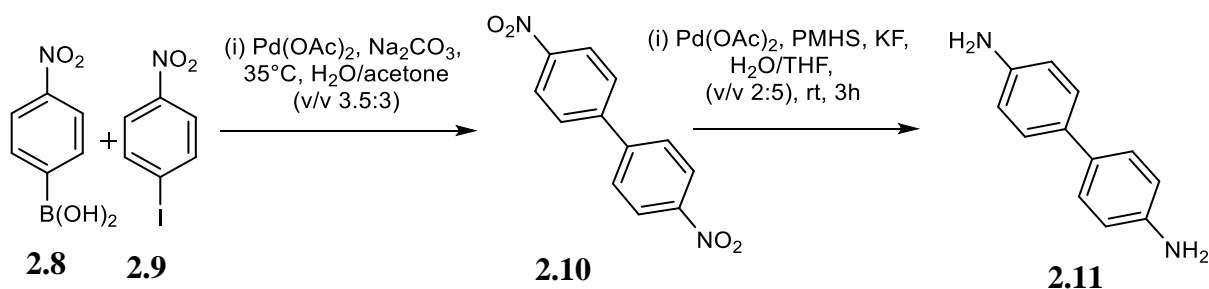


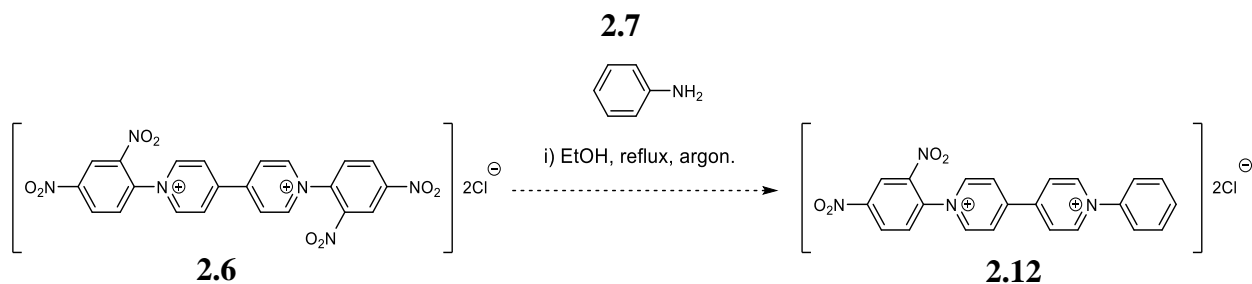
**Figure 17:**  $^1\text{H}$  NMR (600 MHz) Spectra of **2.1** ( $\text{CD}_3\text{OD}$  with 1% TFA) recorded at 298K.

Having prepared the unimer successfully, the next target was synthesis of the dimer **2.2**. The first step of the dimer synthesis involved reacting benzidine **2.11** with Zincke intermediate **2.12**. Benzidine was successfully obtained following a two-step reaction (Scheme 13). Firstly, following typical Suzuki conditions<sup>130</sup> the boronic acid **2.8** was coupled to iodo-benzene **2.9** to produce dinitronaphthalene<sup>131</sup> **2.10**. This was subsequently reduced to the diamine using a palladium acetate and poly(methylhydrosiloxane) (PMHS) as the hydrogen source<sup>132</sup> in nearly quantitative yield as bright orange crystals after column chromatography (v:v EtOH : Hex 1:4).



**Scheme 13:** Synthesis of benzidine **2.11**.

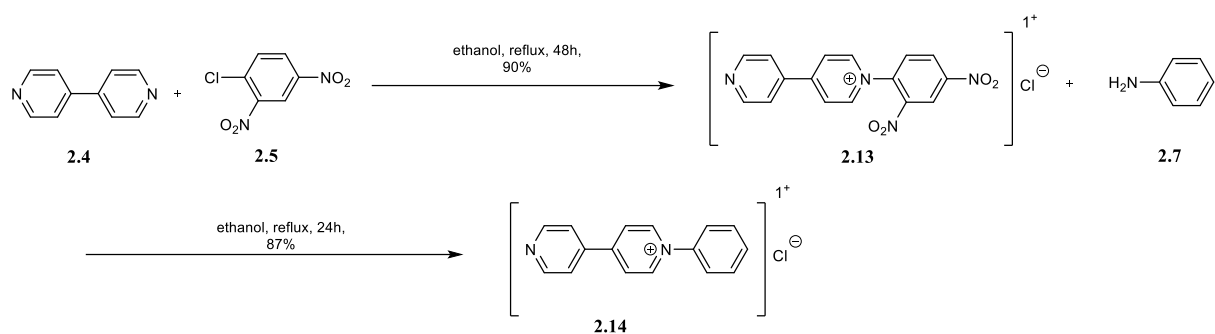
With significant quantities of **2.11** in hand, the next target was mono-Zinck salt **2.12** (Scheme 14). Initial synthesis attempts of **2.12** involved reaction of di-Zincke salt **2.6** with aniline **2.7** in stoichiometric quantities with the hope of producing mono phenyl substituted mono-Zincke salt **2.12**.



**Scheme 14:** Proposed reaction scheme to synthesise mono substituted phenyl viologen **2.12**.

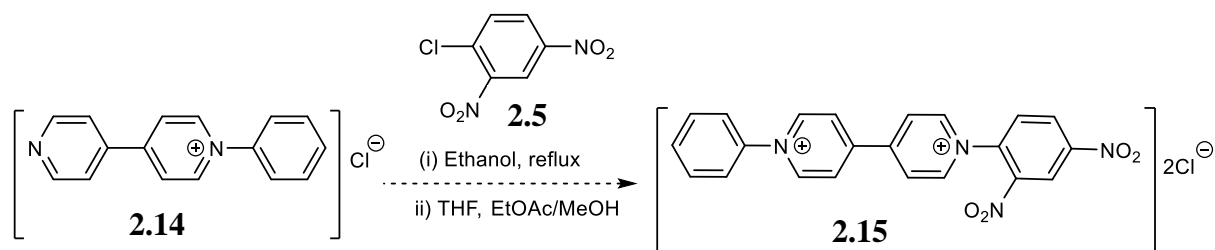
However, the reaction produced a mixture of unreacted di-Zincke salt **2.6** starting material, desired product mono-Zincke monophenyl **2.12** and diphenyl viologen unimer **2.1** that could not be easily separated by precipitation, recrystallization, or reverse phase column chromatography. Therefore, the alternative synthetic pathway outlined in Scheme 12 was designed which has generated high yields of structurally related mono-Zincke salts in our groups previous work.<sup>82,84</sup>

This new method allows greater synthetic control through avoiding undesirable side products by first synthesising mono-Zincke salt **2.13** which can be produced in excellent yield (90%). This simple procedure involves the equimolar addition of bipyridine **2.4** and 1-chloro-2,4-dinitrobenzene **2.5** giving the product as a hydroscopic dark yellow powder.<sup>133</sup> Mono-Zincke salt **2.13** was then reacted with excess aniline **2.7** *via* the Zincke reaction to produce mono-phenyl substituted viologen **2.14** (Scheme 15).



**Scheme 15:** Synthesis of asymmetric mono phenyl viologen **2.14**

This was subsequently reacted with 1-chloro-2,4-dinitrobenzene **2.5** to produce the mono-phenyl mono-Zincke viologen intermediate **2.15**. Initially for conversion of **2.14** to **2.15**, the procedure established by Greenland *et al.* was attempted using ethanol as the solvent, as shown in Scheme 16.



**Scheme 16:** Synthesis of intermediate 7 based on literature<sup>134</sup>

However, a mixture of both starting material (**2.14**) and product (**2.15**) resulted which could not be separated using the original oligomer work up, ii) in Scheme 16, or separation of the chloride salts *via* reverse phase column chromatography. <sup>1</sup>H NMR spectra was recorded of the mixture following separation attempts, shown in Figure 18. Both species resonance peaks can be seen and are coloured appropriately to the corresponding compound.

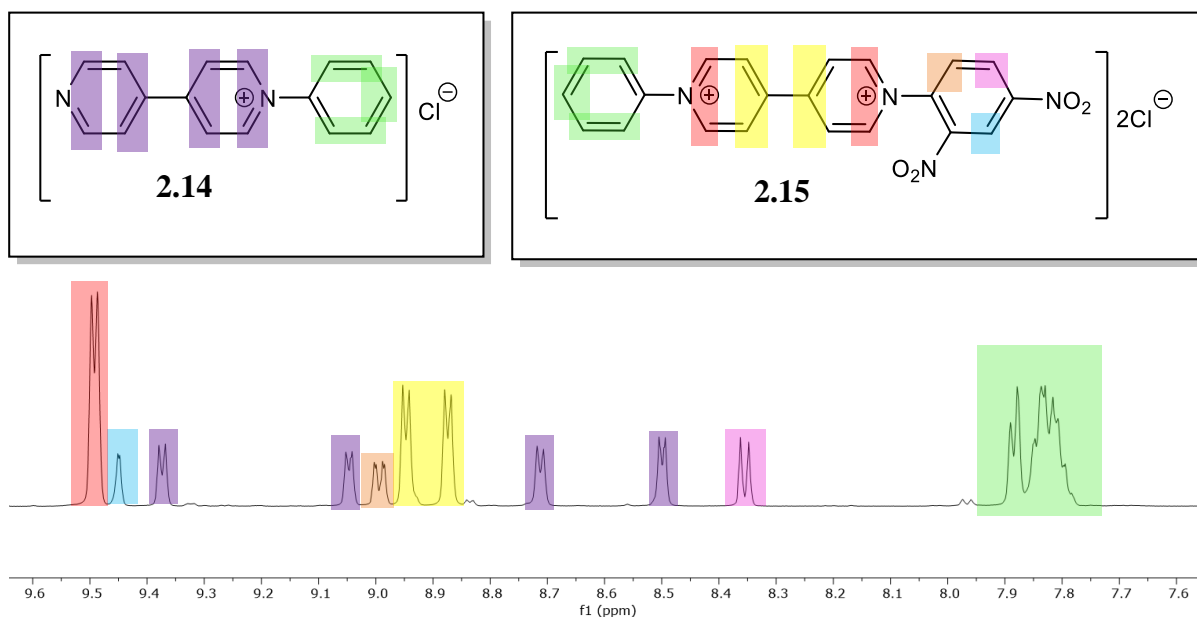
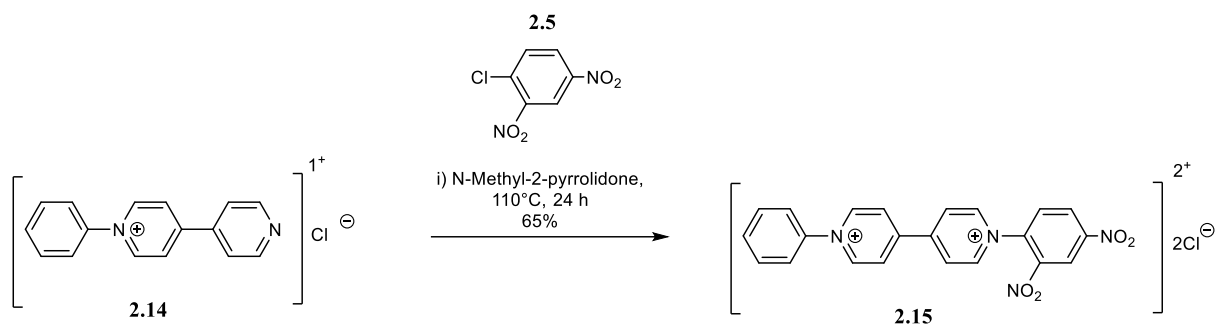


**Figure 18:**  $^1\text{H}$  NMR (600 MHz) of mixture of starting material **2.14** and desired product **2.15** following separation techniques. Collected in  $\text{CD}_3\text{OD}$  and recorded at 298 K.

In a final attempt to isolate **2.15**, anionic exchange of the crude mixture from the  $\text{Cl}^-$  salt to the  $\text{PF}_6^-$  salt followed by column chromatography using 1 %  $\text{NH}_4\text{PF}_6$  in acetonitrile as the solvent was attempted, but a mixture of both compounds as its respective  $\text{PF}_6^-$  derivative was produced. The difficulty in separation suggests that the solubility and properties of **2.14** and **2.15**, even as singly and double charged species, are far more similar than the methoxy containing equivalents in the literature oligomer synthesis. (Section 1.6.2, Scheme 9) Due to this, ideally a solvent that only one compound is soluble in would be beneficial for separation. This was found in the literature to be methyl pyrrolidone, as shown in Scheme 17, where starting material **2.14** was soluble however the product **2.15**, precipitated out as it was produced in synthesis. This was used to isolate **2.15** as a hydroscopic white compound in a respectable 65% yield. A clean  $^1\text{H}$  NMR spectrum (Figure 19), shows isolated **2.15**.



**Scheme 17:** Synthesis of **2.15** using N-methyl-2-pyrrolidone as an alternative solvent

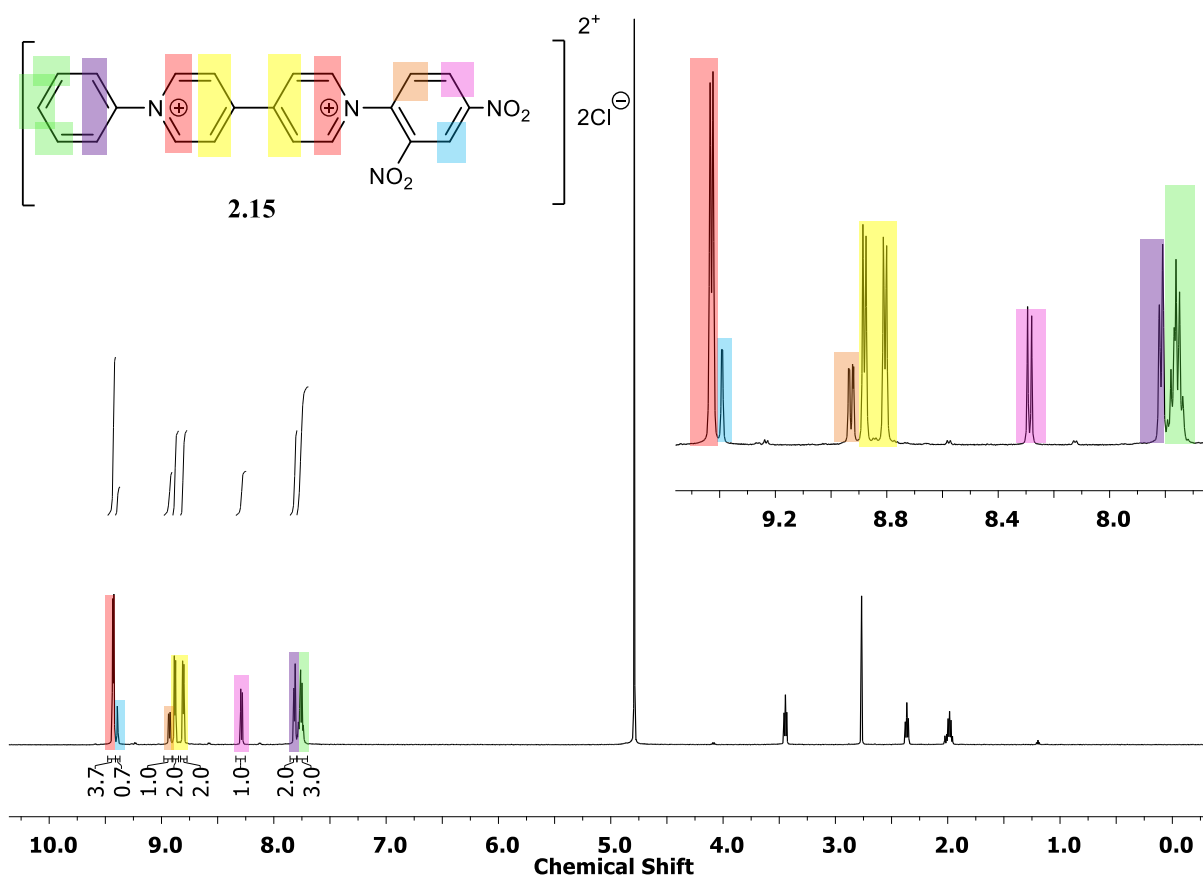
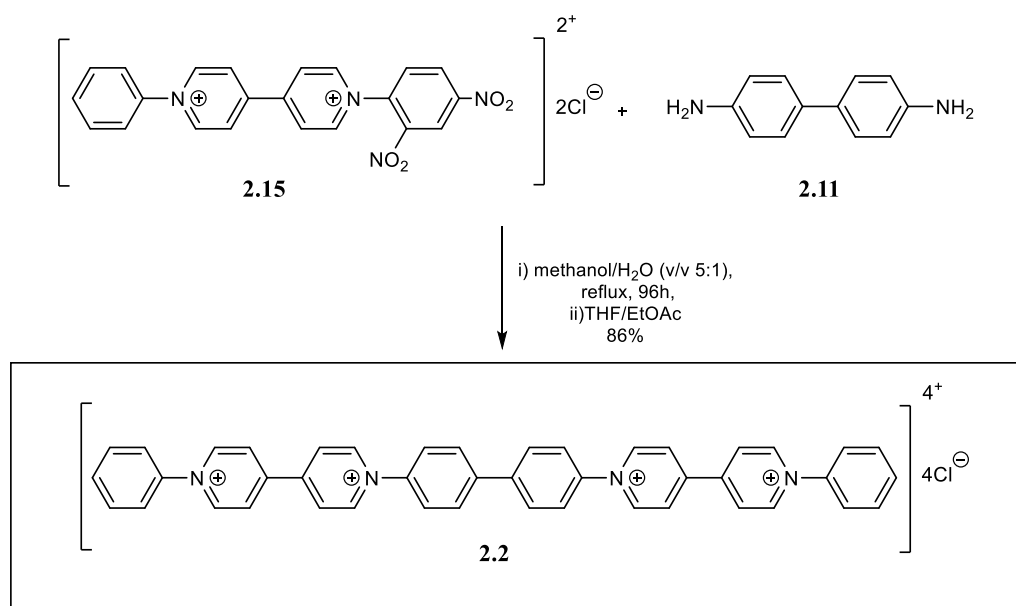


**Figure 19:**  $^1\text{H}$  NMR (600 MHz) spectra of **2.15** recorded in  $\text{CD}_3\text{OD}$  at 298K. Trace impurities of N-methyl-2-pyrrolidone can be seen between 2-4ppm.

With intermediate **2.15** now successfully isolated, efforts moved towards the synthesis of the tetracationic dimer species **2.2**. This involved the Zincke reaction between stoichiometric amounts of previously isolated benzidine **2.11** and **2.15** in a mixture of refluxing methanol and distilled water (v:v MeOH :  $\text{H}_2\text{O}$  5:1). By-product dinitroaniline was then removed by washing the condensed liquor with THF and ethyl acetate (Scheme 18).



**Scheme 18:** Synthesis route for dimer **2.2**, involving the Zincke reaction.

The <sup>1</sup>H NMR spectra of **2.2** is shown below, purified by reverse phase column chromatography (v:v CH<sub>3</sub>CN : MeOH 3:1) (Figure 20).

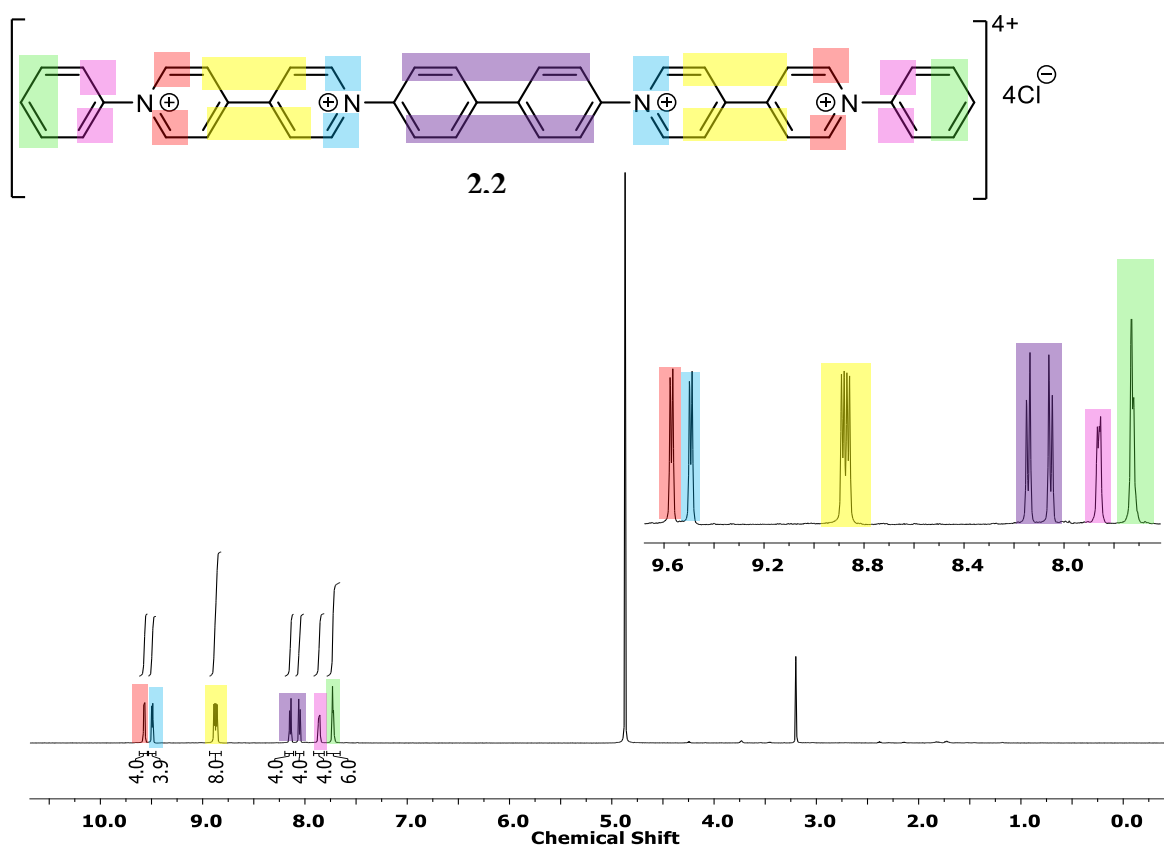


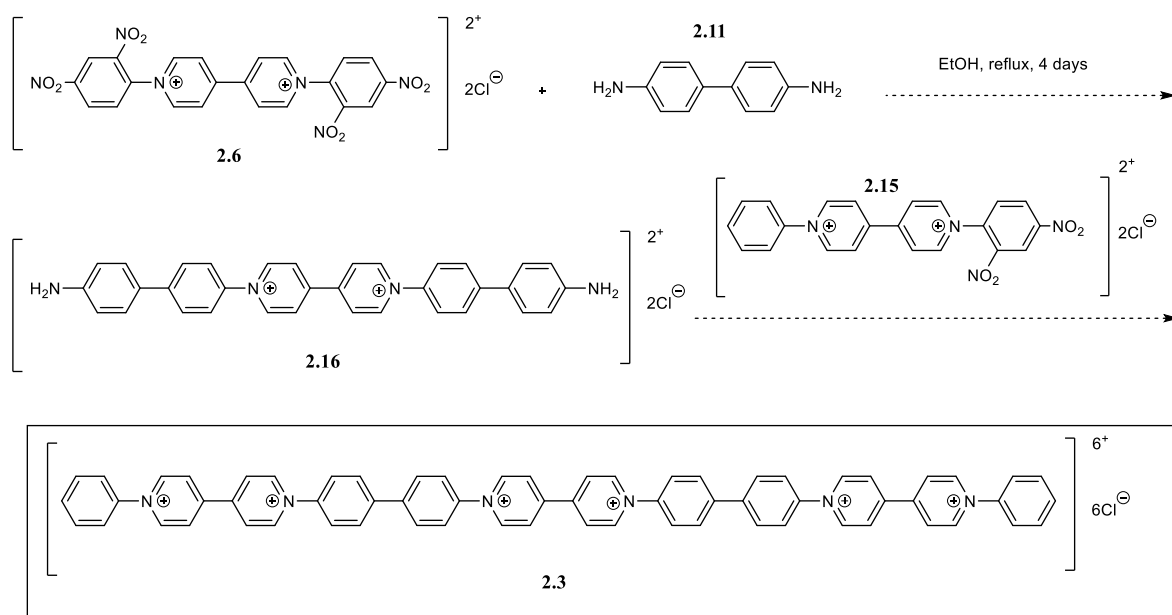
**Figure 20:** <sup>1</sup>H NMR (600 MHz) spectra of dimer recorded in CD<sub>3</sub>OD with 1% TFA at 298K.

The shift downfield in the distinctive 4,4-dipyridinium proton environments to 9.57, 9.49 ppm and 8.87 ppm (red, blue and yellow shaded protons respectively in Figure 20) and separation of the doublet resonance peaks due to asymmetric proton environments, evidences the formation of the dimer. The inclusion of the benzidine unit can be seen by the roofed double doublet resonance peak (shaded in purple in Figure 20) and compared with <sup>1</sup>H NMR spectra of intermediate **2.15** (Figure 19), the spectra lacks the singlet proton resonance at 9.46 ppm attributed to the 2,4-dinitro benzyl group. The integral ratio of the end phenyl group multiplet resonance peak has doubled from 5 to 10 in the dimer spectra (green and pink shaded proton environments), where two phenyl units now reside within the molecule.

In the electrospray mass spectrum of **2.2**, the target species was observed as the quadruply charged ion [(C<sub>44</sub>H<sub>34</sub>N<sub>4</sub>)<sup>4+</sup>] at m/z = 154.5689 Da, in good agreement with the expected value of 154.5690 Da.

Following the successful single crystal growth of dimer **1.89** (Section 2.1, Figure 15) as the PF<sub>6</sub><sup>-</sup> salt, anionic exchange was carried out on a small quantity of dimer **2.2** to convert the chloride anions to PF<sub>6</sub><sup>-</sup>. Vapour diffusion conditions were set up identically to the previous **1.89** but several attempts proved to be unsuccessful, with fine powder not of single crystal quality crashing out.

With the successful synthesis of dimer **2.2** and large quantities of di-Zincke intermediates obtained (**2.6**, **2.11** and **2.15**), synthesis of the hexacationic trimer, **2.3**, was commenced. Initially, di-Zincke salt **2.6** was reacted with excess benzidine **2.11** in an attempt to produce diammine Zincke salt intermediate **2.16** following a literature method,<sup>135</sup> shown in Scheme 19.



**Scheme 19:** Initial synthesis pathway of conjugated 4,4'-bipyridinium trimer **2.3**.

The literature work-up<sup>84,135</sup> of precipitating the cooled down reaction mix (100 mL) into a large quantity of cooled hexane (1 L) resulted in precipitation of both the desired compound **2.16** and the excess diamine **2.11**. Low solubility of the resulting solid meant that the second attempted work up, as described by Greenland for related compounds,<sup>82</sup> involving washing with THF and precipitation from methanol into ethyl acetate proved unsuccessful with a mixture of **2.16** and **2.11** still remaining as observed by <sup>1</sup>H NMR. Flash reverse phase column chromatography (v:v CH<sub>3</sub>CN:MeOH 1:3) of the chloride salt was also ineffective, where the column was contaminated and rendered useless in the process. Compound **2.16** could be isolated as the hexafluorophosphate salt following column chromatography using 1 % NH<sub>4</sub>PF<sub>6</sub> in acetonitrile but in a very low yield of 3 %.

The <sup>1</sup>H NMR spectra of the cleanest sample of **2.16** is shown below in Figure 21. The symmetric molecule shows 6 proton environments and the downfield shift of the distinct 4,4'-bipyridinium to 9.21 and 8.68 ppm (shaded blue and red respectively) evidences the attachment of the benzidine substituents. Inclusion of the unit benzidine can also be seen by the four doublet

resonance peaks between 6.70 and 8.00 ppm (shaded green, orange, yellow and purple in figure 24) split due to the asymmetric influences along the unit.

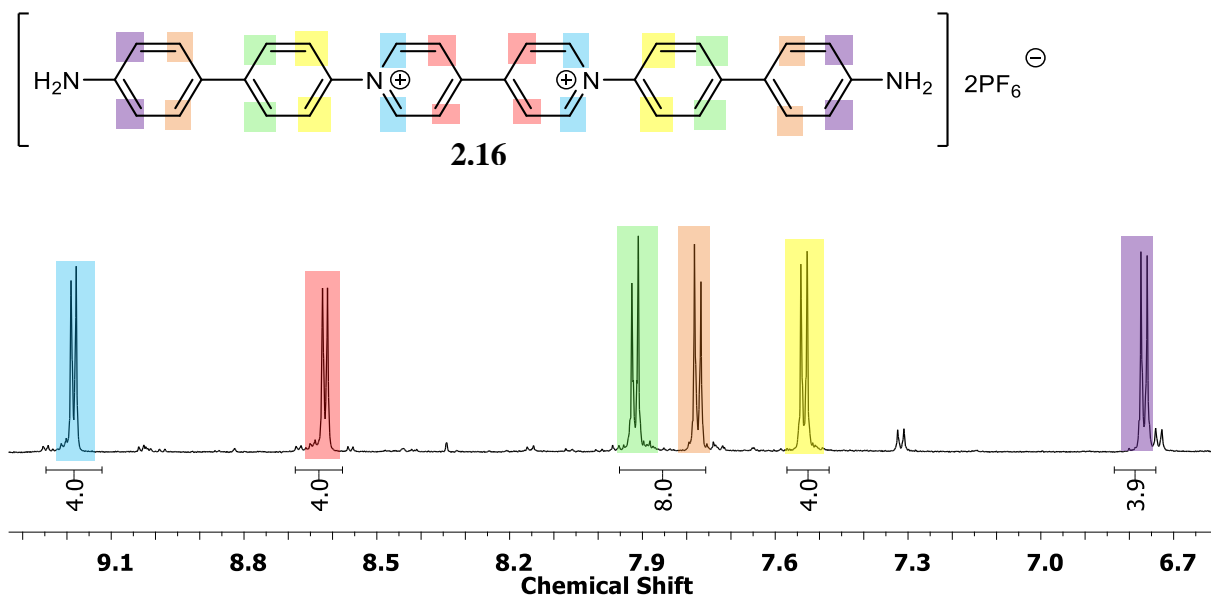


**Figure 21:**  $^1\text{H}$  NMR (600 MHz) spectra of intermediate diamine Zincke salt **2.16** recorded in acetonitrile- $\text{d}_3$  at 298K.

The small quantity of intermediate **2.16** as the hexafluorophosphate salt was then reacted with intermediate **2.15** as the hexafluorophosphate salt in a 1:2 ratio however the resulting  $^1\text{H}$  NMR spectra did not show the expected signals for the trimer and included a host of unexpected signals. Due to the un-reproducibility of resynthesizing and isolating intermediate **2.16** as the hexafluorophosphate salt and the chloride salt being preferable, a different synthetic route was developed. The new route involved reaction and ‘capping’ of di-Zincke salt **2.6** with an asymmetric novel Zincke salt **2.17**, (Scheme 20).



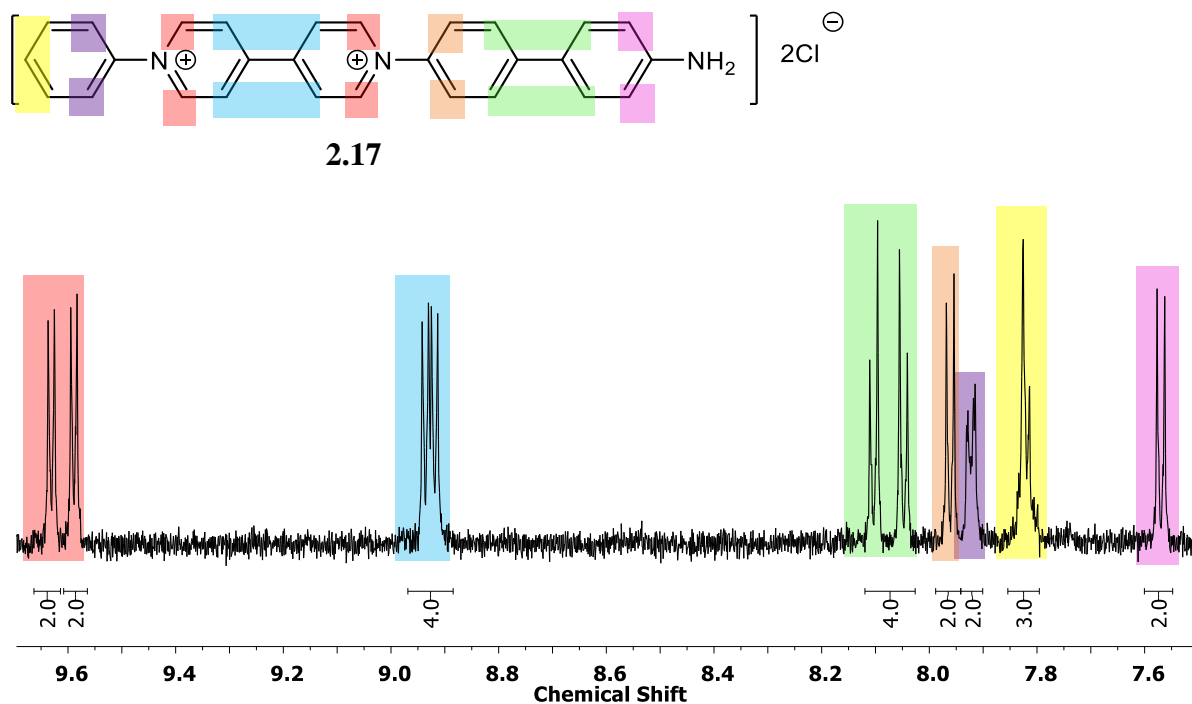
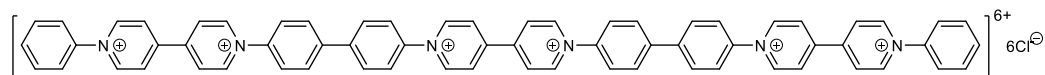


**Figure 22:**  $^1\text{H}$  NMR (600 MHz) spectra of intermediate amine Zincke salt **2.17** recorded in  $\text{CD}_3\text{OD}$  at 298K.

Intermediate **2.17** was then reacted with di-Zincke salt **2.6** in an attempt to generate the trimer. The reaction was carried out with the small quantity of **2.17** synthesised, as a proof of concept reaction before scaling up. The small scale produced too little material to easily column (ca. 14 mg) and recent lab access restrictions has meant a sufficient  $^1\text{H}$  or  $^{13}\text{C}$  NMR spectra has not been obtained. The product can, however, be seen in the electrospray mass spectrum discussed below.

In the electrospray mass spectrum of **2.3**, the target species was observed as the hexa-charged ion  $[(\text{C}_{66}\text{H}_{50}\text{N}_6)^{6+}]$  at  $m/z = 154.4011$  Da, in good agreement with the expected value of 154.4012 Da. Signals for isotopomers of **2.3** can be seen at  $m/6$  values of 154.5684, 154.7354 and 154.9027 each separated by  $1/6$  of a Dalton, as expected. The spectra also shows peaks at  $z = 4$  at 154.8198 (dimer expected mass 154.8199) and  $z = 2$  at 155.0729 and 155.5746 (unimer expected masses 155.0730 and 155.5754) which indicates the presence of tetra charged and di-

charged side products respectively. Although not pure, this spectrum is a proof of concept that the trimer can be synthesised using the proposed Scheme 20 and is now ready to scale up.



Calculated mass : Z = 1, 2 etc.

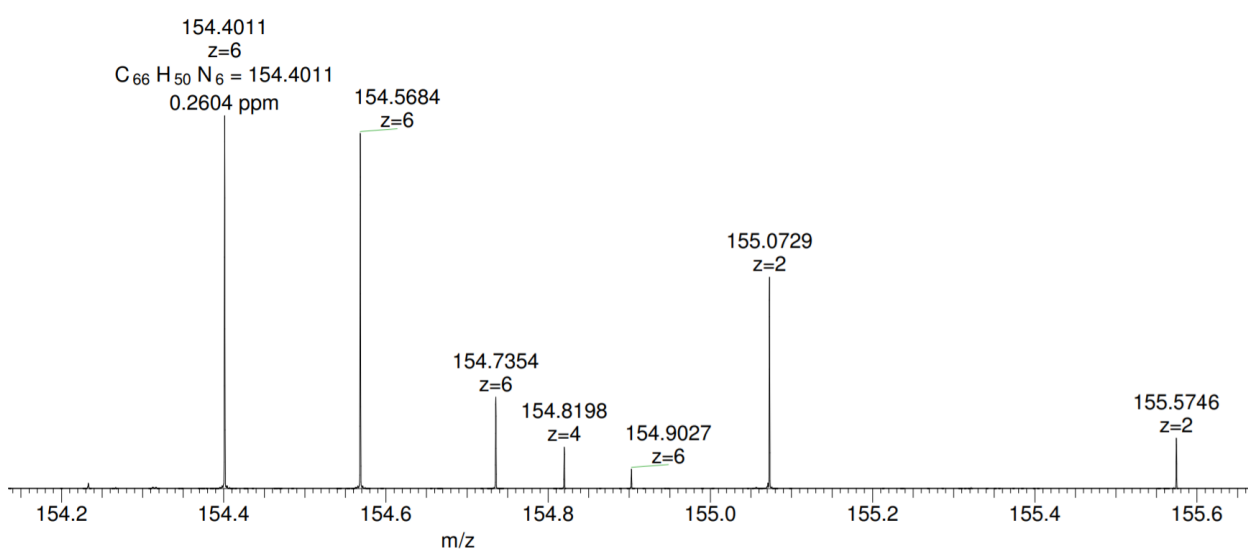


**Figure 23:** Electrospray mass spectrum of trimer **2.3**.

## 2.3 Conclusions

This section has reported the successful high-yielding synthesis of water soluble, conjugated cationic oligomer species unimer **2.1** and dimer **2.2**. These reactions involved two and six steps respectively. The dimer **2.2** synthesis pathway exploits the asymmetric formation of Zincke salts and subsequent Zincke reactions between amines such as aniline or benzidine. Purification of the dimer was also achieved as the chloride salt *via* reverse phase chromatography, allowing rapid synthesis of over 500 mg of clean product. A single crystal of X-ray quality was also

grown of a previously synthesised dimer in the Greenland lab, **1.89**, evidencing the twisting of the backbone in the cationic state. An alternative method to reach trimer **2.3** in contrast to the earlier work reported by Greenland *et al.* was successfully carried out which involved a new route based on the novel intermediate **2.17**. Electrospray mass spectroscopy evidenced the formation of the trimer species **2.3**. Work at this point was halted due to a nine-month lab closure as a result of COVID-19 and the timeline of other projects in the following chapters took precedence. However, this work has shown the robust and reproducibility of the reaction between Zincke salts and aniline. Therefore, provide the background on viologen containing supramolecular systems which forms the basis of the next chapter.

**Section 2:**

**Literature, synthesis and study of  $\pi$ -  
electron supramolecular tweezer  
systems**

## **Chapter 3**

# **Introduction to supramolecular chemistry within $\pi$ -poor systems**

# Chapter 3: Introduction to supramolecular chemistry within $\pi$ -poor systems

## 3.1 Supramolecular chemistry and binding constants

Utilizing non-covalent bonds is a powerful synthetic tool for the preparation of complex molecular architectures. Rather than involving the sharing of pairs of electrons like traditional covalent bonds, non-covalent interactions in supramolecular chemistry was described by Jahn-Marie Lehn as “*chemistry of molecular assemblies and of the intermolecular bond*”.<sup>136,137</sup> One of the specific benefits of non-covalent interactions over covalent bonds is that the strength of the non-covalent bond can be reversibly altered by the application of an external stimulus (e.g. heat / light). This means that they can be incorporated into materials that then exhibit tuneable, responsive properties. These features have resulted in an explosion of research in this field over the last 30 years including several Nobel prizes and over 90,000 articles published to date in supramolecular research.<sup>138,139</sup>

Examples of non-covalent interactions include hydrogen bonding, electrostatic interactions, hydrophobic effects, van der Waals forces, dipole–dipole interactions, ion–ion interactions, ion–dipole interactions, metal–ligand interactions, C–H- $\pi$  and  $\pi$ - $\pi$  interactions.<sup>140,141</sup> Each of these non-covalent interactions display differences in binding kinetics, strength and directionality. The different binding energies of each supramolecular mode is shown below (Table 2). Knowledge of the relative magnitude of each of these allows for the selection of the appropriate supramolecular interaction for the desired purpose.

<b>Supramolecular interaction or bond</b>	<b>Bond energy (kJ mol<sup>-1</sup>)</b>
<b>Hydrogen bond</b>	10 – 65
<b><math>\pi</math> - <math>\pi</math> stacking</b>	0 – 50
<b>Metal-ligand</b>	0 – 400
<b>Electrostatic</b>	250
<b>Covalent bond</b>	100 – 942
<b>Halogen bond</b>	5 – 180

**Table 2:** Bond energies of supramolecular interactions compared to a covalent bond.<sup>142-144</sup>

One of the key parameters in supramolecular interactions is the ability to identify and measure how strong an interaction is in a supramolecular system, which is termed the bonding or association constant ( $K_a$ ). This can be done by characterizing the free energy ( $\Delta G$ ) associated with the interaction. In supramolecular chemistry, the simplest way of measuring this free energy difference is by the equilibrium constant ( $K$ ) of the system, according to equation 3.1, where  $R$  = universal gas constant ( $8.31 \text{ JK}^{-1}\text{mol}^{-1}$ ) and  $T$  = temperature (K):

Equation 3.1 
$$\Delta G = -RT \ln K$$

Binding constants measure the affinity between two or more molecules at equilibrium. In supramolecular chemistry, binding constants for host–host aggregation (for example dimerization) or host–guest complexation are usually studied. This is because the value of the binding constant usually plays an important role in the determination of the functionality of the supramolecular system. This section of the chapter focuses on host-guest complexation, which is important for the experimental work carried out in the following chapter.

When determining binding constants, defining a binding model that relates to the underlying equilibria is required. The binding model is the stoichiometry of the components in the system at equilibrium, and may be for example 1:1, 1:2 or 2:2. The model can then be compared to the data that is recorded for the supramolecular structures (for example *via* titration studies) and if these are in good agreement, data analysis through iterative fitting procedures allows calculation of important values, such as  $K_a$ .

When considering a simple 1:1 host-guest system in solution, the binding model can be seen below, as set out by Pall Thordarson<sup>145-147</sup> (equation 3.2 – 3.4), where H can be defined as the host and the concentration of free host [H], G is the guest and concentration of free guest [G] and finally HG is the complex where the concentration of the complex is [HG].



Equation 3.4 
$$K_a = \frac{[HG]}{[H][G]}$$

The value of at least one quantity [HG], [H] or [G] has to be known to be able to measure  $K_a$  when considering equation 3.4. In practise, these values can be challenging to obtain as the concentrations of un-complexed species in solution cannot be measured directly. However, these can be inferred as the total concentration of host,  $[H]_0$ , and of the guest,  $[G]_0$ , are known as they are determined at the start of each experiment. From these initial values, expressions for [H], [G] and [HG] can be written as shown below in equation 3.5 and 3.6:

Equation 3.5 
$$[H]_0 = [H] + [HG]$$

Equation 3.6 
$$[G]_0 = [G] + [HG]$$

This means that equation 3.4 can be seen to be equivalent to equation 3.7 below and with the expanded formula equation 3.8.

$$\text{Equation 3.7} \quad K_a = \frac{[HG]}{([H]_0 - [HG])([G]_0 - [HG])}$$

$$\text{Equation 3.8} \quad = \frac{[HG]}{[H]_0[G]_0 - [HG]([H]_0 + [G]_0) + [HG]^2}$$

This can be rearranged and expanded to give the quadratic 3.9, which can be rearranged once more to isolate [HG] (Eq. 3.10).

$$\text{Equation 3.9} \quad [HG]^2 - [HG]\left([G]_0 + [H]_0 + \frac{1}{K_a}\right) + [H]_0[G]_0 = 0$$

$$\text{Equation 3.10} \quad [HG] = \frac{1}{2} \left\{ \left( [G]_0 + [H]_0 + \frac{1}{K_a} \right) - \sqrt{\left( [G]_0 + [H]_0 + \frac{1}{K_a} \right)^2 - 4[H]_0[G]_0} \right\}$$

The ability to be able to isolate [HG] is extremely important as the only unknown integer is now the association constant  $K_a$ , the value of interest. Although [HG] cannot be measured directly, it can be measured by monitoring changes to [HG] indirectly. In supramolecular chemistry various titration methods can be used to achieve this as described below.

Each titration technique monitors the changes in a physical property of the system on addition of the guest  $[G]_0$ , while the concentration of the host  $[H]_0$  is kept fixed. The physical property can range from the chemical shift of an NMR resonance ( $\delta$ ) to heat absorbed/released in calorimetry or absorbance change in UV-vis spectroscopy.<sup>147</sup> Less widely used techniques to gain insights into binding constants also include solubility methods,<sup>148</sup> mass spectrometry<sup>149</sup> and potentiometric techniques.<sup>148</sup>

NMR titrations have become one of the most widely used methods to calculate the binding constant. This is as a consequence of the availability of the method and the quality of

information it can provide on the host-guest interaction (for example better insight into the relative orientation of the host and guest in the complex can frequently be inferred from the resonance shifts in the spectra). In addition,  $^1\text{H}$  NMR spectroscopy frequently offers higher sensitivity than other methods (e.g. UV/vis).

There are two ways binding constants can be calculated from NMR experiments and this depends on whether the complexation is slow or fast on the NMR timescale. The most common method and discussed further is the case where complexation/decomplexation is fast on the NMR timescale. In these cases, the chemical shift of the observed NMR resonance ( $\delta$ ) is assumed to be the weighted average of the unbound host [H] and bound species [HG]. This assumption means that equations 3.2-3.10, which depends on the relative mole fraction of the species, can be applied to these systems.

If the NMR resonance of the guest is defined as  $\delta_G$ , the host  $\delta_H$  and the host-guest complex  $\delta_{HG}$ , then we can define change ( $\Delta$ ) in resonance for the host-guest complexation as  $\delta_{\Delta HG} = \delta_{HG} - \delta_H$ . Further, if the NMR resonance of the host before the guest is added is defined as  $\delta_0$ , then the change in physical property (chemical shift of the NMR resonance) is equal to  $\Delta\delta = \delta - \delta_0$ . The NMR version for a simple 1:1 equilibria can now be obtained according to 3.11:

Equation 3.11 
$$\Delta\delta = \delta_{\Delta HG} \left( \frac{[HG]}{[H]_0} \right)$$

This is equivalent to equation 3.9 when [HG] is replaced with the solution shown in equation 3.10 to give equation 3.12:

Eq. 3.12 
$$\Delta\delta = \frac{\delta_{\Delta HG}}{[H]_0} \left( \frac{1}{2} \left\{ \left( [G]_0 + [H]_0 + \frac{1}{K_a} \right) - \sqrt{\left( [G]_0 + [H]_0 + \frac{1}{K_a} \right)^2 - 4[H]_0[G]_0} \right\} \right)$$

Software such as Bindfit<sup>146,147</sup> routinely allows rapid and efficient calculation of binding constants of a system using these equations and the underlying theory discussed above when only  $[H]_0$ ,  $[G]_0$  and  $\Delta\delta$  is known.

The following section of this chapter gives a broad overview into types of non-covalent bonding, examples of functional supramolecular systems and how this motivates the experimental work in Chapter 4.

## 3.2 Different types of non-covalent bonding interactions

Nature is exceptional at using supramolecular chemistry to transmit, store and replicate information with a relatively limited range of structural units.<sup>150</sup> One of the most well studied and widely known non-covalent interactions in supramolecular chemistry is hydrogen bonding, which can be used to generate complex self-assembled systems from small molecules and polymers.

A prominent example of this in nature can be seen in the self-assembled architecture, DNA. The interaction between two DNA strands is facilitated by four nucleobases: thymine (T), adenine (A), cytosine (C) and guanine (G) (**3.1** to **3.4** in Figure 24). The two strands of DNA are held together by C-G and A-T base pairs to form the well-known double helix structure. While the selectivity of these base-pair interactions is controlled mainly by hydrogen bonding, both  $\pi$ - $\pi$  stacking and hydrophobic effects also play a role in stabilizing the resulting structure. The potential hydrogen bonding, metal binding sites,  $\pi$ - $\pi$  stacking and hydrophobic sites have been highlighted in one nucleobase, guanine (**3.4**, Figure 24). Nucleotides, which are attached to nucleobases in the helix structure, also show the potential for hydrogen bonding and electrostatic interactions, labelled in structure **3.5**, Figure 24.<sup>150</sup>

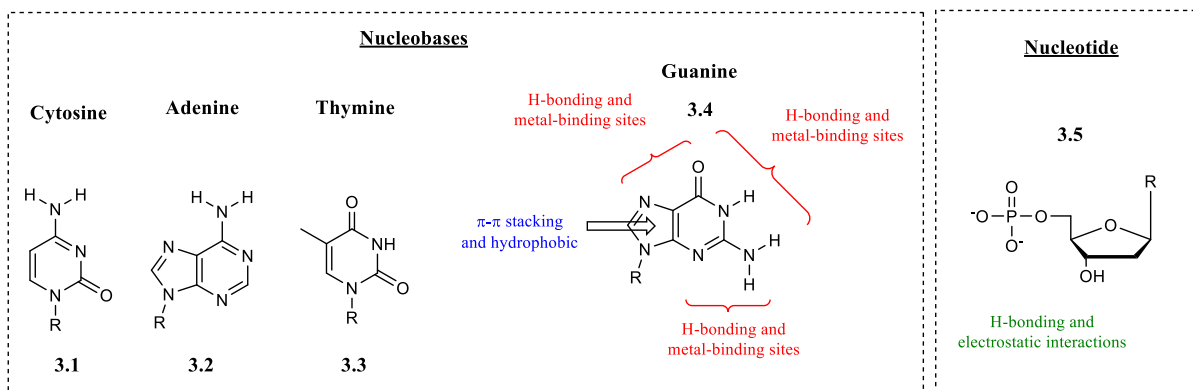
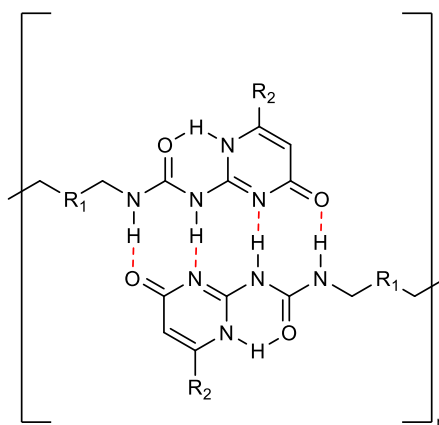


**Figure 24:** DNA nucleobases Cytosine, Adenine, Thymine and Guanine and nucleotide with potential non-covalent binding sites labelled.

Generally, lone hydrogen bonds are relatively weak and are not strong enough to give self-assembled structures that are thermally stable.<sup>151,152</sup> To remedy this, the binding strength can be increased by producing systems with multiple complementary hydrogen bonds. An example of this can be seen with 2-ureido-4[1H]-pyrimidinone (UPy), **3.6** in Figure 25.<sup>153</sup> The Meijer group synthesised UPy in 1997 which contains four complementary hydrogen bonds within the structure and has become one of the most studied supramolecular systems to date.<sup>154</sup> This quadruple hydrogen bonded self-complementary system exhibited a binding energy of 42 kJ mol<sup>-1</sup> meaning that at room temperature in solution, it had the ability to self-associate to form a dimeric system. The environmental and thermal control over bond strength and lifetime makes properties, such as chain length, viscosity, and composition easily tuneable compared to traditional polymers. This has led to UPy based polymer materials being developed to have applications in thermoplastic elastomers,<sup>155</sup> printable supramolecular electrolytes in 3D printing,<sup>156</sup> self-bioscaffolding applications and in healing polymers<sup>157,158</sup> among other applications.



3.6

**Figure 25:** Molecular structure of 2-ureido-4[1H]-pyrimidinone (UPy) supramolecular polymer end units.

Utilizing hydrogen bonding from Pederson's seminal work<sup>159,160</sup> on crown ethers used for recognition of ammonium ions and Villiers<sup>161</sup> and Friedrich Cramer's<sup>162</sup> contribution on cyclodextrins to exploiting  $\pi$ - $\pi$  interactions with complementary systems including calixarene and pyridium ions,<sup>163,164</sup> cucurbituril and viologen units,<sup>120,165</sup> and pillar[5]arene and imidazolium ions<sup>166-169</sup>, a wealth of potential supramolecular binding motifs are available. Such supramolecular interactions have been elegantly used to build up suprastructures with an array of distinct topologies in excellent yields. This is exemplified schematically in the four mechanically interlocked architectures (MIAs) shown below in Figure 26.

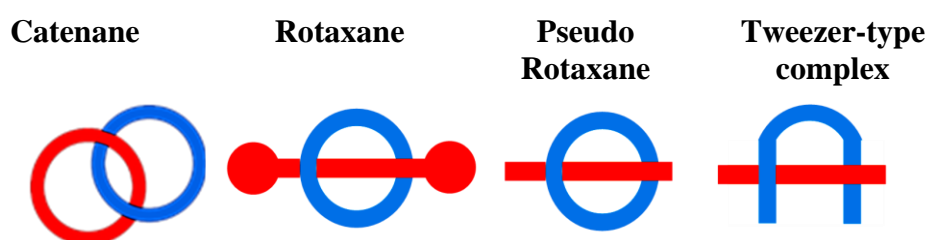


**Figure 26:** Four types of MIAs, left to right; two interlocked rings forming a catenane, a dumbbell containing bulky stoppers looped through a ring to form a rotaxane, a dumbbell without bulky stoppers looped through a ring to form a pseudo rotaxane and an uncapped non-cyclic host with a linear guest species forming a tweezer-type complex.

Catenanes are comprised of two (or more) macrocycles linked together mechanically. The macrocycles are free to move relative to each other, but they cannot be separated unless a covalent bond in one of the macrocycles is broken. Rotaxanes contain a dumbbell shaped unit threaded through a cavity while a pseudo rotaxane lacks the bulky stoppers that fix the macrocycle in place so the two components can dissociate without breaking a covalent bond.<sup>170–173</sup> Similarly, tweezer type complexes, also known as molecular clips, are a subset of macrocyclic receptors that contain an open cavity capable of binding with a guest species but are non-cyclic. They are comprised of two receptor ‘arms’ which are connected at only one end, resulting in a certain flexibility of the receptor sites.<sup>174</sup> A key feature of supramolecular complexes is the reversible interactions, which allows assembly / disassembly without causing deterioration of the molecules that fabricate them. This ability means they can respond to an external stimulus such as light or heat and allows the possibility to modify the properties of the supramolecule or material.

Of particular importance to this work is the  $\pi$ - $\pi$  interaction which occur between aromatic rings where one is electron poor and one electron rich (Figure 27).<sup>142,175</sup> As described in Figure 27 with electrostatic schematics of aromatics, the favourable and non-favourable arrangement between two electron rich aromatics (left) and complementary electron rich and electron poor residues is shown (right), where face-centred stacking is favourable for electronically complementary residues. This arrangement is involved in donor-acceptor  $\pi$ - $\pi$  stacking interactions in supramolecular systems between the host and guest. With respect to this work, systems where the  $\pi$ -electron poor residues is either a viologen, PDI or NDI (**3.9**) are the most important and will be discussed briefly in the next two sections.

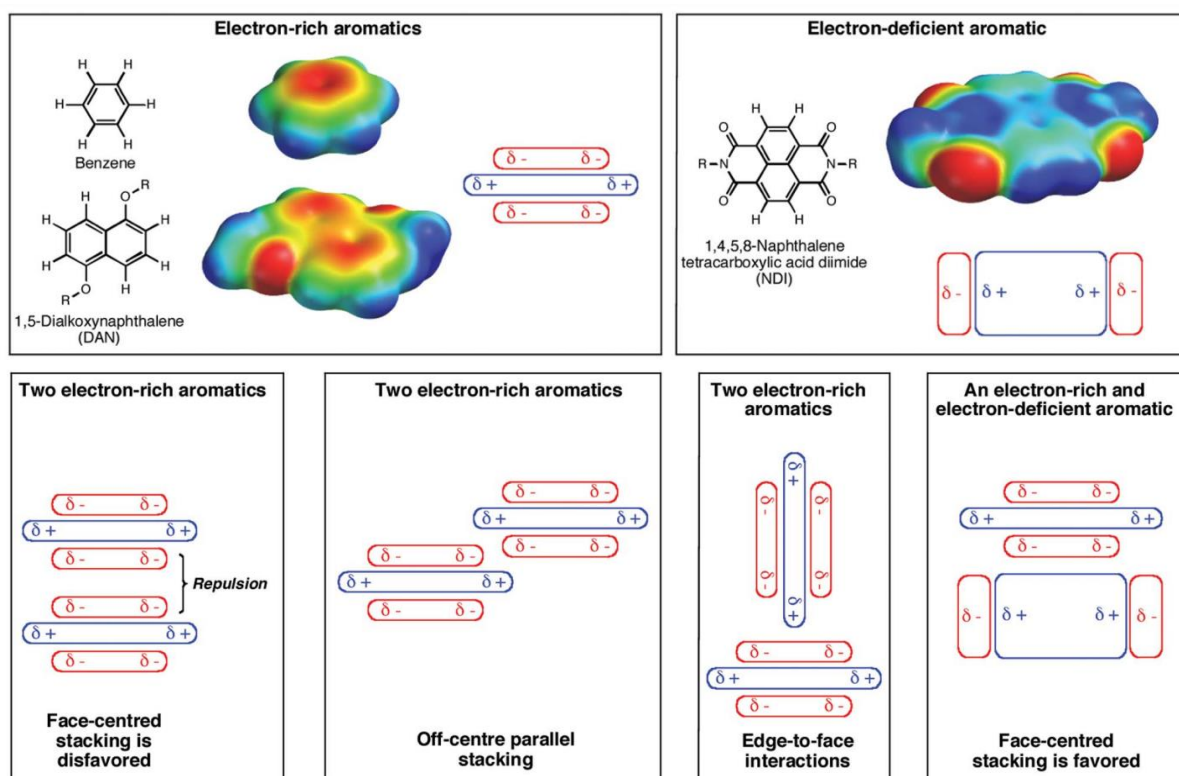


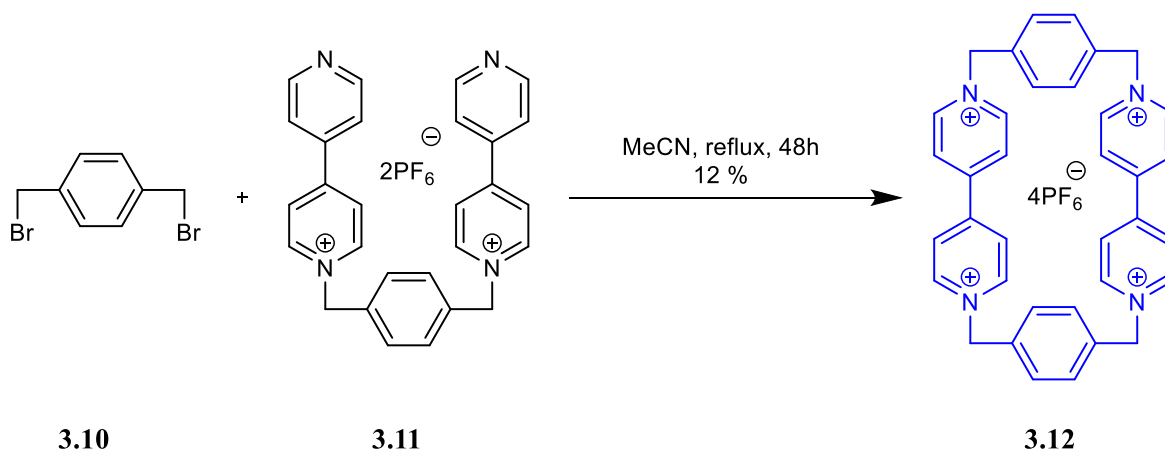
**Figure 27:** Schematic taken from Iverson and co-workers work<sup>175</sup> that describes the electrostatic view of aromatic interactions. (top); schematics representing qualitatively aromatic quadrupole moments in electron-rich aromatic rings, such as 1,5-dialkoxy-naphthalene (DAN) and benzene (left), as well as electron-deficient aromatics, such as 1,4,5,8-naphthalenetetracarboxylic diimide (NDI) containing strongly electron withdrawing groups (right). (bottom) The various potential modes of stacking, emphasizing locations of electrostatic repulsion or attraction. DFT calculations were used to plot the electrostatic potential surface for each representative aromatic.<sup>175</sup>

### 3.3 Viologens in supramolecular systems

In addition to their use in n-type semiconductive materials discussed in chapter 1 and 2, viologen units can also be utilized in supramolecular chemistry as the host or guest species. The strength of these interactions can also be modulated by taking advantage of the fast and reversible oxidation and reduction processes exhibited by viologen species.<sup>97</sup> These interactions can be harnessed to design structures that have the ability to behave as a molecular ‘switch’ in which they can be reversible chemically, photochemically or electrochemically.<sup>176</sup> One of the most well studied examples and with specific interest to this work is the use of

cyclobis(paraquat-*p*-phenylene) (CBPQT<sup>4+</sup>), colloquially known as blue box, in the assembly of these supramolecular systems and will be explored further in this chapter.

Between the 1960s and early 80s, Professor Siegfried Hünig pioneered the synthesis of viologen-containing cyclophanes and developed the redox chemistry associated, for example  $\pi$ -dimerization (also known as pimerization), between these viologen-containing compounds.<sup>87,177–181</sup> These foundations led to the synthesis of the CBPQT<sup>4+</sup> (**3.12**) by Stoddart and co-workers in 1988.<sup>182,183</sup> The utility of which heavily contributed towards the Nobel Prize in 2016,<sup>184</sup> CBPQT<sup>4+</sup> is synthesised by an S<sub>N</sub>2 reaction between 4,4'-bipyridine derivative **3.11** and 1,4-bis(bromomethyl) benzene **3.10** (Scheme 21). Blue box has been incorporated into the structures of charged catenanes<sup>185–187</sup> and rotaxanes<sup>188,189</sup> *via* self-assembly, and in which the resulting systems are capable of rotational motion<sup>190</sup>, controllable switching,<sup>176,191,192</sup> and data storage.<sup>193</sup>



**Scheme 21:** Cyclobis(paraquat-*p*-phenylene): formed via S<sub>N</sub>2 reaction between 4,4'-bipyridine derivative **3.11** and 1,4-bis(bromomethyl) benzene **3.10**. Commonly coloured blue to depict electron deficiency in publications.

An interesting application is the fabrication of a bistable [2] rotaxane that contains a 160-kilobit molecular electronic memory, the ground state conformation is shown below in **3.13** (Figure 28).<sup>193</sup> The MIA is oriented with the (purple) hydrophilic stopper in contact with a silicon

bottom-nanowire electrode and the hydrophobic bulky end group opposite on the right to stop the macrocycle from slipping off. The ground state conformation corresponds to the low-conductance or 0 'OFF' state in the molecular switch. The switching mechanism involved oxidation of the tetrathiafulvalene (green) site to  $TTF^{1+}$  or  $TTF^{2+}$  accompanied by the shift of the blue electron poor CBPQT<sup>4+</sup> cyclophane from the  $TTF^+$  site to the electron rich dioxynaphthalene site (red). The  $TTF^+$  was then reduced back to  $TTF^0$  oxidation state to form the high conductance, metastable co-conformer state 1 or 'ON' state. The metastable state had a relaxation time back to the ground state ( $t_{1/2}$ ) of about an hour. Although the paper revealed that this system has several 'switch defects' it is an excellent utilisation of  $\pi$ - $\pi$  interactions.

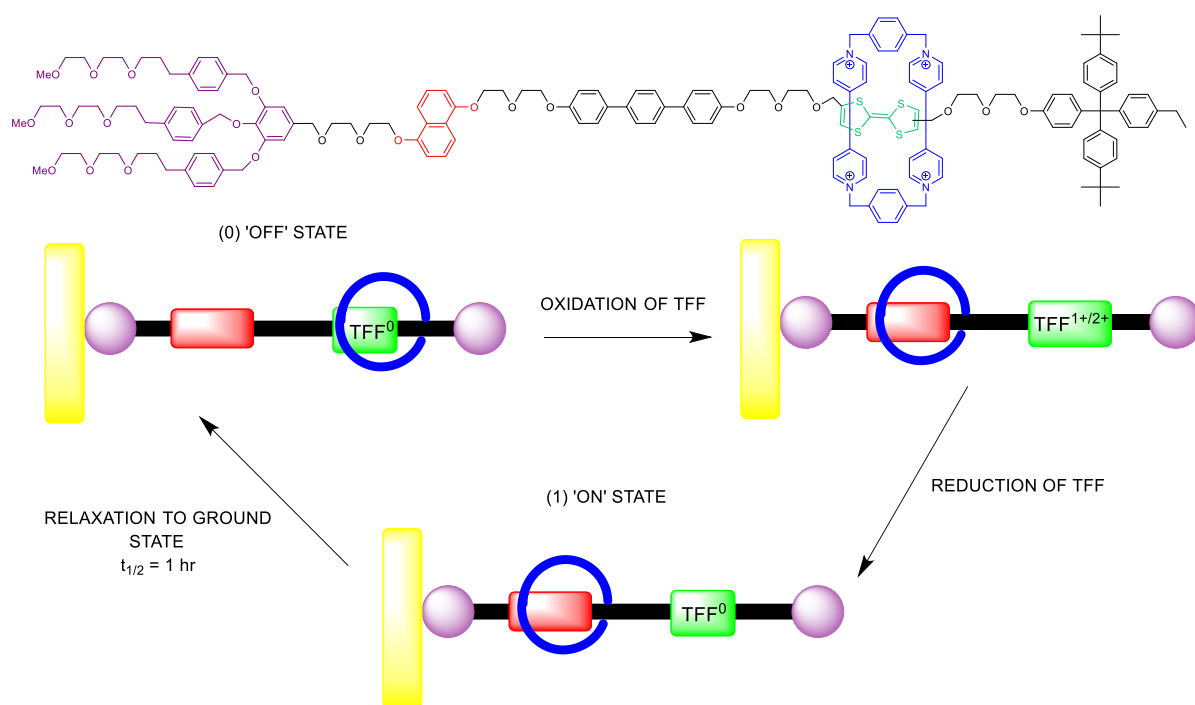


**Figure 28:** (Top) Structural formula of the bistable [2] rotaxane (**3.12** and **3.13**) designed by Stoddart and used in the memory crossbar. (Bottom) Schematic representation displaying how the device can be switched reconfigurable and recycled repeatedly between ON and OFF states.

Stoddart and co-workers have also produced variants of the blue box cyclophane, specifically work using an extended viologen macrocycle (ExBox<sup>4+</sup>, **3.14**) which was shown to act as a polycyclic aromatic hydrocarbon (PAH) ‘scavenger’.<sup>122</sup> The  $\pi$ -electron-poor 1,4-phenylene-bridged (“extended”) bipyridinium units (ExBIPY<sup>2+</sup>) was synthesised by a direct- template protocol and the extended cavity (approximately 3.5 Å in width and 11.2 Å in length when considering the van der Waals radii) was successfully able to bind to a range of  $\pi$ -electron rich small guest molecules to form a series of pseudorotaxanes. The paper displayed crystal structures of 11 different PAHs ranging in size and shape **3.15** – **3.25**, bound with the ExBox<sup>4+</sup>, with pyrene (highlighted in Figure 29) showing strong binding at 7610 M<sup>-1</sup>. ExBox<sup>4+</sup> has also been shown to function as a molecular switch in a [2] catenane containing MIA.<sup>194</sup>

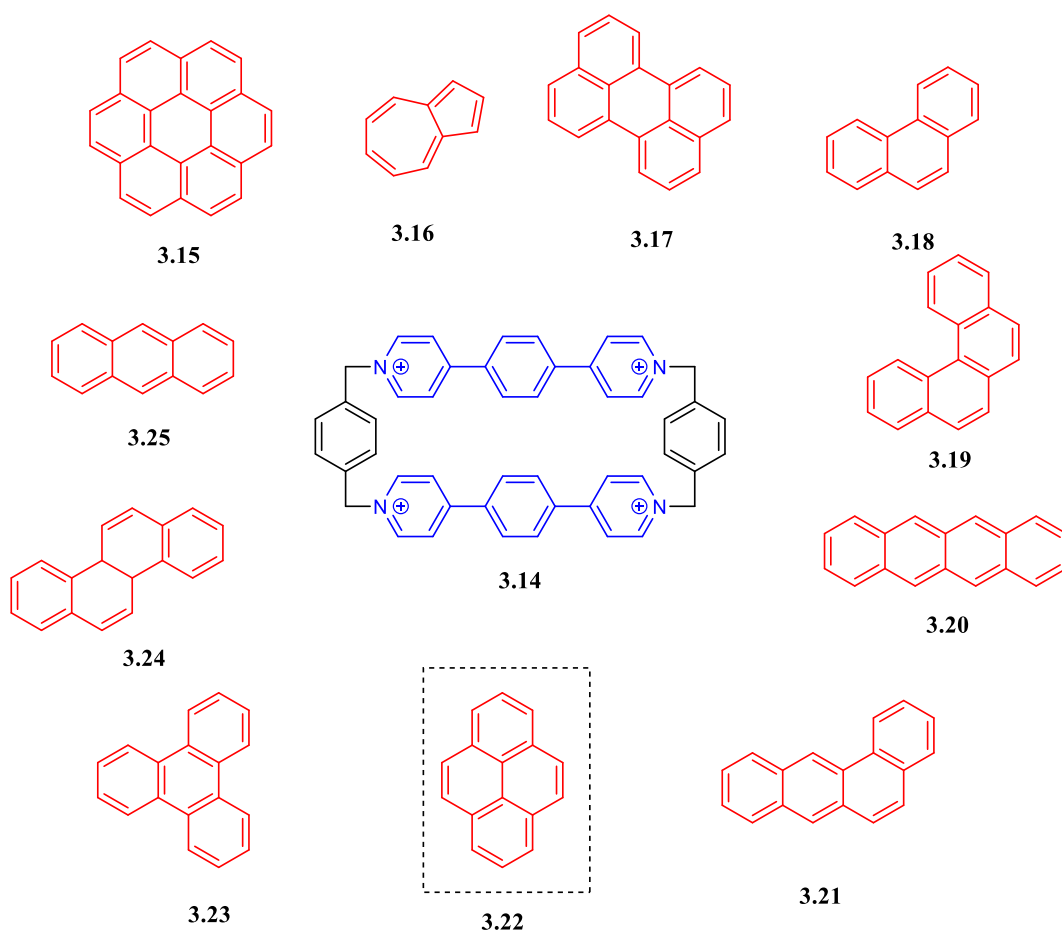
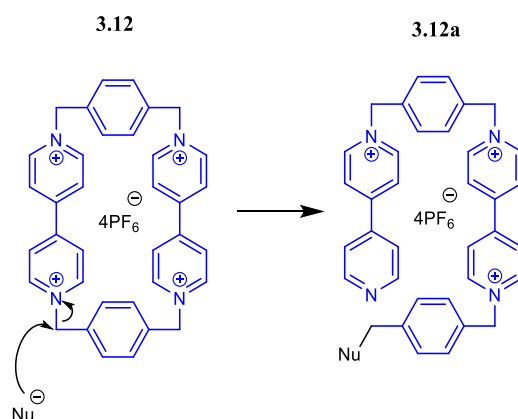


**Figure 29:** Chemical structures of ExBox<sup>4+</sup> host **3.14** and the eleven different polycyclic aromatic hydrocarbon guest molecules; Coronene (**3.15**), Azulene (**3.16**), Perylene (**3.17**), Phenanthrene (**3.18**), [4]Helicene (**3.19**), Tetracene (**3.20**), Traphene (**3.21**), Pyrene (**3.22**), Triphenylene (**3.23**), Chrysene (**3.24**) and Anthracene (**3.25**).

However, the individual components of these molecular machines (e.g. blue box and ExBox<sup>4+</sup>) often include chemically labile groups such as the N-benzylbipyridinium moiety,<sup>184</sup> which is susceptible to cleavage under nucleophilic or basic conditions. For example, in the presence of a multitude of nucleophiles or under basic conditions, nucleophilic attack on, or deprotonation of, the benzylic methylene group leads to a host of ring-opened and rearranged products.<sup>81</sup> Scheme 22 shows a possible non-reversible reaction of a nucleophile attacking the methylene moiety contained within CBPQT<sup>4+</sup>. This hinders the range of chemistries available on MIAs containing CBPQT<sup>4+</sup> or ExBox<sup>4+</sup>, to only four reactions; S<sub>N</sub>2, Olefin Metathesis, Copper Catalysed Alkyne-Azide cycloaddition (CuAAC, also referred to as click chemistry) and Copper-Free Azide-Alkyne cycloaddition (copper free click chemistry) reactions<sup>195</sup>.



**Scheme 22:** Scheme displaying methylene moiety within CBPQT<sup>4+</sup> sensitivity to a nucleophile

To overcome the stability issues associated with these systems, Stoddart,<sup>86</sup> Colquhoun<sup>81</sup> and Greenland<sup>82</sup>, among others,<sup>196</sup> have developed methodologies that utilise the Zincke reaction to place an sp<sup>2</sup> centre next to the ammonium species. This results in structures without the chemically sensitive methylene moiety in the final product and their synthesis and properties are discussed in the next section.

### 3.3.1 Synthesis of di-viologen containing macrocycles with increased chemical stability using the Zincke reaction

Figure 30 displays the endeavours of Stoddart, Colquhoun and Greenland, an example of three viologen containing cyclophanes, each synthesized using the Zincke reaction. These no longer contain the reactive  $sp^3$  hybridised carbon like in  $CBPQT^{4+}$  and have been shown to be stable in a range of nucleophiles including tetra-*N*-butylammonium iodide, tri-phenyl phosphine, sodium methoxide and pyridine.<sup>81</sup>

The sulphonyl containing cyclophane has also been shown to successfully bind to  $\pi$ -electron rich guest species such as 1,5-bis[2- (hydroxyethoxy) ethoxy]naphthalene. Binding between **3.26** and 1,5-bis[2- (hydroxyethoxy) ethoxy]naphthalene was 130 times weaker than  $CBPQT^{4+}$  host with the same guest.<sup>182</sup> This was proposed to be due to the cyclophane only containing one di-viologen within the macrocycle,<sup>81</sup> and having a larger cavity diameter of 8.2 Å compared to  $CBPQT^{4+}$ 's 6.8 Å.<sup>176</sup>

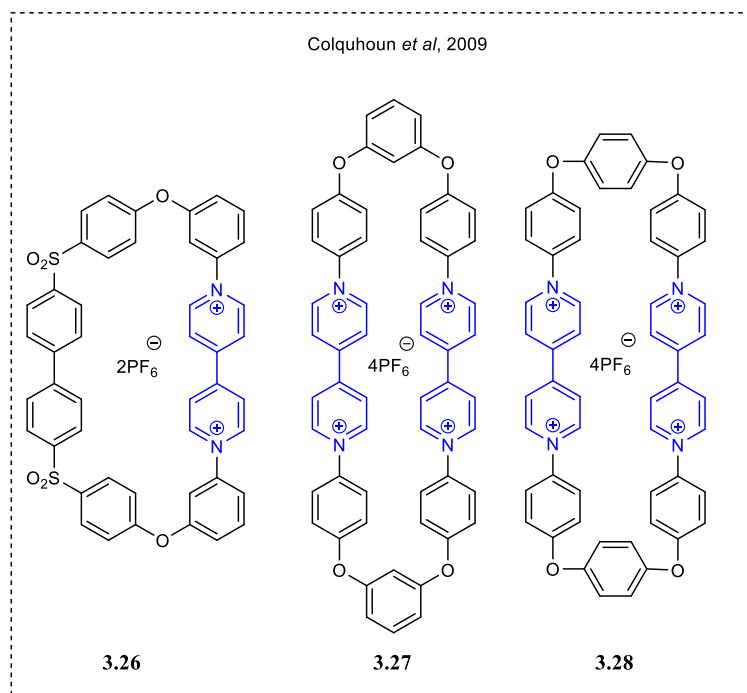


**Figure 30:** Structures of three macrocyclic diarylbipyridinium salts **3.26-3.28** reported by Stoddart, Greenland and Colquhoun designed to be more chemically stable than methylene containing cyclophanes like blue box and Exbox<sup>4+</sup>.<sup>81</sup>

The Greenland lab synthesised a chemically stable tetracationic macrocycle utilising the Zincke reaction that contains two di-viologen species connected by conjugated terphenyl groups,<sup>197</sup> which was shown to bind to a  $\pi$ -electron rich 1,5-dihydroxynaphthalene (**DHN**) derivative (Figure 31). Closely structurally related cyclophanes containing the core structure introduced by Greenland and Colquhoun have more recently been studied by Li *et al.*,<sup>196</sup> who show significantly higher binding in aqueous rather than organic solvents.

However, in both of these systems (**3.29** and **3.31**), the single crystal x-ray structures showed that the cavity of the macrocycles was either larger (over double) than the van der Waals radii, at 7.4 Å in **3.29** or was shorter than twice the efficient  $\pi$ - $\pi$  interaction distance in **3.31** at 5.1 Å. This resulted in weaker binding at 150 M<sup>-1</sup> in **3.29** compared to Stoddart's blue box (**3.12**), which has a cavity of 6.4 Å. The rigidity of the macrocycle hinders the binding potential.

The ability to control which guest can more favourably bind to the host was demonstrated in Li and co-workers work with the rigid tetra cationic macrocycle **3.31** and the separation of isomers

anthracene and phenanthrene (whereby anthracene bound more readily and strongly with the host than phenanthrene).

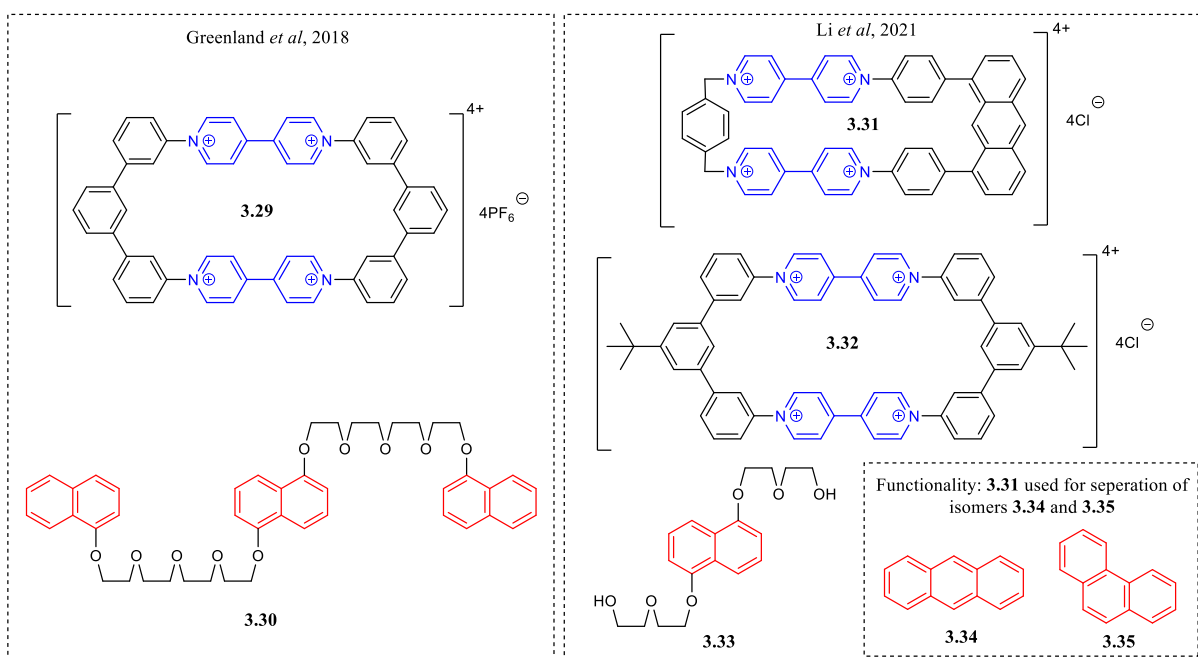


**Figure 31:** (left) Chemical structure of conjugated  $\pi$ -electron poor terphenyl di-viologen tetracationic macrocycle synthesised by the Greenland lab and shown to bind to  $\pi$ -electron rich 1,5-dihydroxynaphthalene derivative **3.30**. (right) Li and co-workers water soluble derivatives **3.31** and **3.32** which were shown to bind to  $\pi$ -electron rich guest species **3.33**. **3.31** was used for the separation of **3.34** and **3.35** from an isomeric mixture.

The chemical stability of the host system and/or the binding strength between a host-guest interaction has the potential to be optimized when considering the linker that connects the two binding sites together. Either a preorganized unit can create a fixed cavity size or a linker with increased structural flexibility can afford the ability for a variable cavity size.

Increasing the flexibility of a cavity through the structural design could see an increase in binding strengths, or expand the range of molecules that could be bound. The host compounds discussed so far are macrocyclic in structure. However, in principle, any arrangement of one or more  $\pi$ -electron poor species in which efficient face to face stacking can occur, could result in complexation with  $\pi$ -electron rich species with appreciable binding constants. Accordingly, the

synthesis and properties of non-macrocyclic, ‘tweezer’-type receptor residues are discussed in the next section.

### 3.4 Molecular tweezers

An intrinsic structural property of cyclophane-type receptors is that in order to interact most strongly with guest species within the main chains of polymers they must thread onto the end of the polymer, a process that is entropically costly, and therefore can take extended periods of time to occur.<sup>198–202</sup> A cartoon representation of this is shown below in Figure 32. In contrast, molecular tweezers are able to encapsulate electronically complementary residues that are contained within polymer chains without threading onto the chain itself. Therefore, such tweezer type residues have found significant use in materials chemistry, in particular, healable polymers,<sup>203–206</sup> molecular level information processing,<sup>207</sup> UV cured polymers for flexible electronic devices,<sup>208</sup> and controlled inkjet deposition.<sup>209</sup>

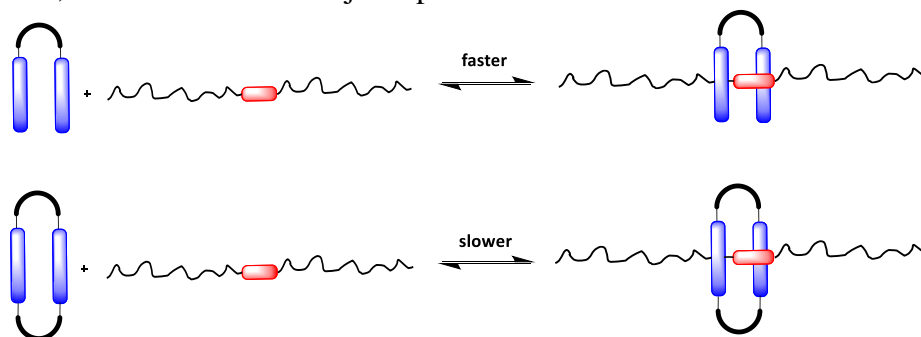


**Figure 32:** Cartoon representation of a tweezer receptor undergoing fast encapsulation of electronically complementary residues that are contained within polymer chains without threading onto the chain itself compared to a slower encapsulation for a macrocycle. Blue represents  $\pi$ -electron poor binding site and red  $\pi$ -electron rich guest species within the polymer chain.

#### 3.4.1 Molecular tweezers containing two viologen species

Sluysmans, Stoddart and co-workers reported a viologen containing tweezer-type probe to determine the mechanical strength of donor-acceptor  $\pi$ -interactions in the solution state (Figure

33).<sup>210</sup> The molecular tweezer **3.36** was capable of encapsulating well known  $\pi$ -donor guest species *via*  $\pi$ -interactions, such as diamionaphthalene, (**3.37**) dimethoxybiphenyl, (**3.38**) and dimethoxynaphthalene (**3.39**).

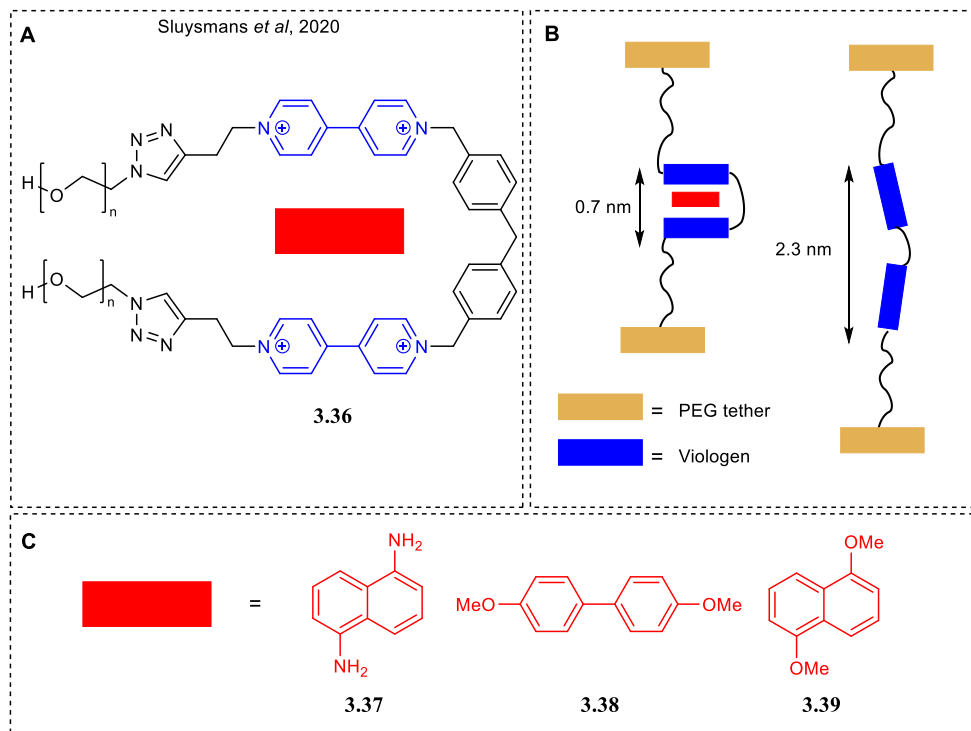


**Figure 33:** Viologen based tweezer used as a probe to measure  $\pi$ -donor and  $\pi$ -acceptor interactions

The system was studied by using single-molecule force spectroscopy where the mechanical breaking of the non-covalent interactions between the  $\pi$ -acceptor viologen units and  $\pi$ -donor guest molecules **3.37** to **3.39** could be monitored. The  $\pi$ -acceptor viologen unit was trapped between a smooth mica substrate and the tip of an atomic force microscope (AFM). The tip was then pulled away from the surface which provided a characteristic force-distance signature applied on the closed (A, left) and open (B, right) arrangement of the tweezer-type system. It was found that an extension from 0.7 nm to 2.3 nm was seen depending on whether a guest species was encapsulated by the viologen receptors. The association constants of the host-guest

complexation between host **3.36** was calculated to be  $6 \times 10^4 \text{ mol}^{-1}$ ,  $1 \times 10^2$  and  $3 \times 10^4$  respectively for guest species **3.37**, **3.38** and **3.39**.

In principle, a range of  $\pi$ -electron poor structures could be used in similar ways to viologen  $\pi$ -electron poor receptors. Amongst the most widely studied are diimide type residues, for example NDI and PDI. These have been incorporated into a range of ‘tweezer’ type supramolecular systems by various groups including Iverson,<sup>211–214</sup> Takahar,<sup>215</sup> Whitlock,<sup>216</sup> Zhao,<sup>217</sup> and Zimmerman.<sup>218,219</sup>

### 3.5 Alternative $\pi$ -electron poor tweezer motifs

The use of NDI<sup>220</sup> and PDI in supramolecular systems is facilitated by their relative ease of synthesis (condensation reaction between a dianhydride and an amine to yield a diimide, see Scheme 1 in section 1.6 for details), thermal stability, accessible reversible oxidation states and large  $\pi$ -electron poor surface area which contributes towards increasing the binding potential.<sup>221–225</sup>

In 2008, Colquhoun and co-workers produced the first examples of asymmetric NDI tweezer type complexes<sup>226</sup> which contained a  $\pi$ -electron poor residue formed of two or more NDI derivatives (**3.40** and **3.41** in Figure 34), connected by triethylenedioxy linking units with ethyl hexyl end groups for increased solubility of the system. This was shown to bind *via*  $\pi$ - $\pi$  stacking interactions with a  $\pi$ -electron rich mono or bis-pyrenyl based residue (**3.42** and **3.43** in Figure 34). These complexes displayed a high tensile modulus and binding constants increased between 300 and 11,000  $\text{M}^{-1}$  as the number of face to face  $\pi$ - $\pi$  stacking NDI and pyrenyl residues were increased, as calculated by UV-vis binding studies, using the dilution method.<sup>227</sup>

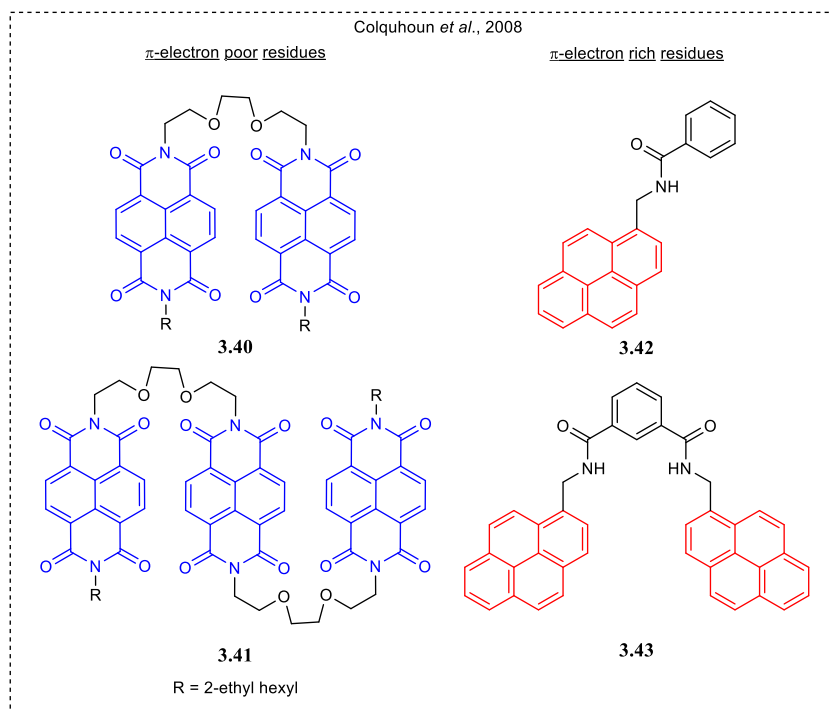


**Figure 34:** The first example of asymmetric  $\pi$ -electron poor NDI containing tweezer residues (**3.40** and **3.41**) and  $\pi$ -electron rich pyrene containing residues (**3.42** and **3.43**) reported by Colquhoun and co-workers.<sup>226</sup>

The fundamental ‘tweezing’ component in this structure has been harnessed in a range of supramolecular materials, for example those that undergo healing at elevated temperatures.<sup>203,206</sup> A particularly notable example of an application of this type of supramolecular interaction was disclosed by the Hayes lab during the production of novel printing inks.<sup>209</sup> They synthesised a double component ink system, where an electron rich based species containing pyrenyl (**3.45**) or perylene end-groups and a chain folding NDI based  $\pi$ -electron poor species (**3.44**), could interact utilizing  $\pi$ - $\pi$  stacking interactions and this supramolecular cross linking interaction between these two components produced colours (Figure 35).<sup>209</sup>

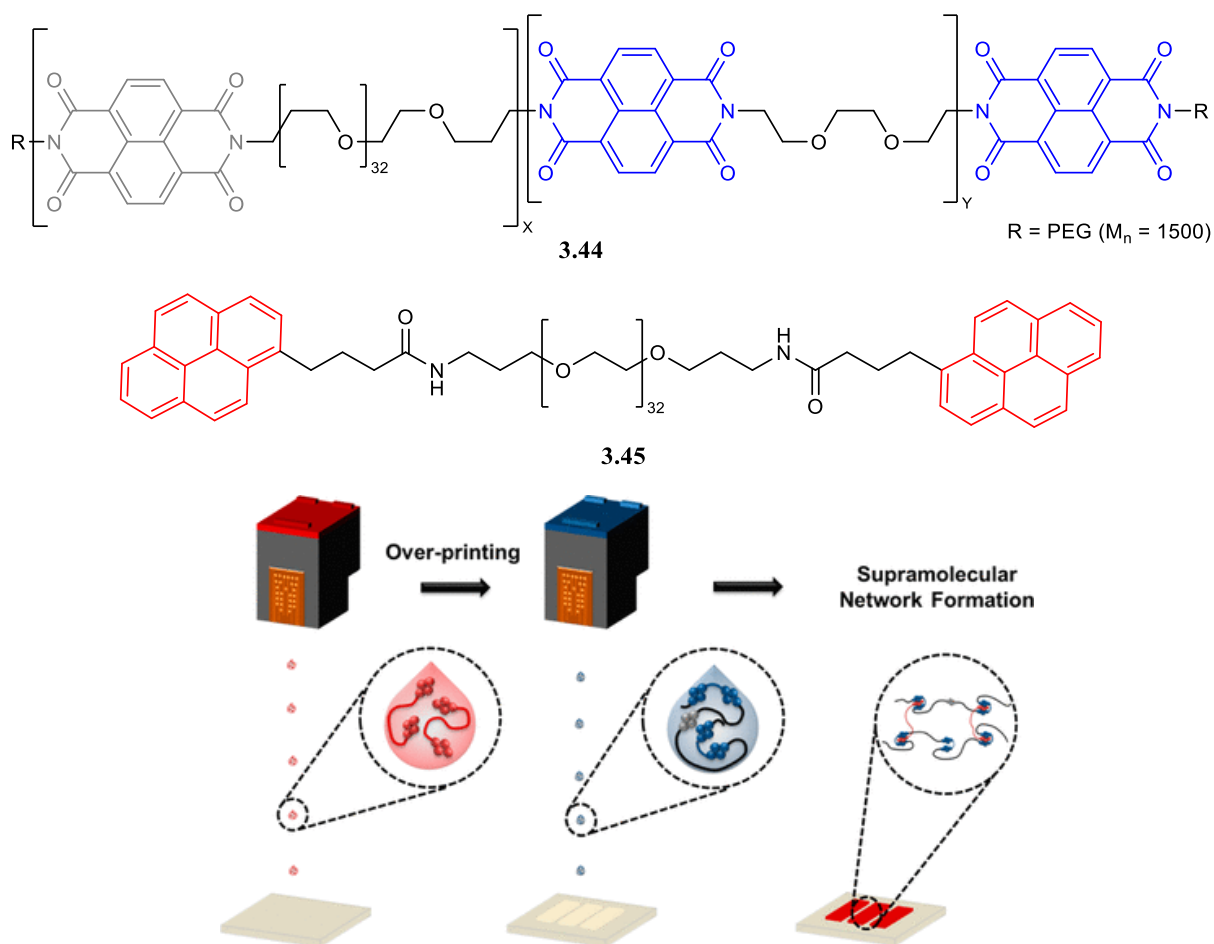


**Figure 35:** Tweezer residues used by Hayes *at al.* in novel printing inks. (top)  $\pi$ -electron poor NDI containing residue **3.44** and  $\pi$ -electron rich pyrene containing residue **3.45**. (bottom) a schematic representation of the separate ink components and the crosslinking process that takes place in the printing inks. Adapted figure from published work<sup>209</sup>

The instantaneous supramolecular cross-linking interaction, where a charge-transfer complex was formed between the pyrenyl tweezer **3.45** or perylene tweezer and naphthalene diimide tweezer **3.44**, resulted in red and green printed images respectively if **3.45** or perylene containing residue was complexed with **3.44**. The combined ink components were able to be deposited onto a range of substrates for example steel, glass and polycarbonate films. They displayed excellent mechanical properties such as toughness and durability. In this work, oligomers with low molecular weights were selected which reduced the risk of blockages in the inkjet nozzle.

In a similar vein, Colquhoun and co-workers<sup>228</sup> synthesised a collection of complexes between tweezer molecules and diimide oligomers, linear (**3.46**) and macrocyclic (**3.48**) (Figure 36). Solid state structures of the complex displayed polyimide chain folding of **3.46** when complexed with a  $\pi$ -electron rich pyrene-based tweezer **3.47** and  $\pi$ - $\pi$  interactions between **3.48** and **3.49** revealed a mechanism for sequence recognition. The crystal structure of **3.48** and **3.49** displayed the ability of one particular tweezer molecule, **3.49**, to detect long-range sequence information in chain-folding aromatic copolyimides with extraordinarily high sensitivity by favouring binding with the NDI residue rather than the biphenyl residue in the macrocycle.<sup>228</sup>

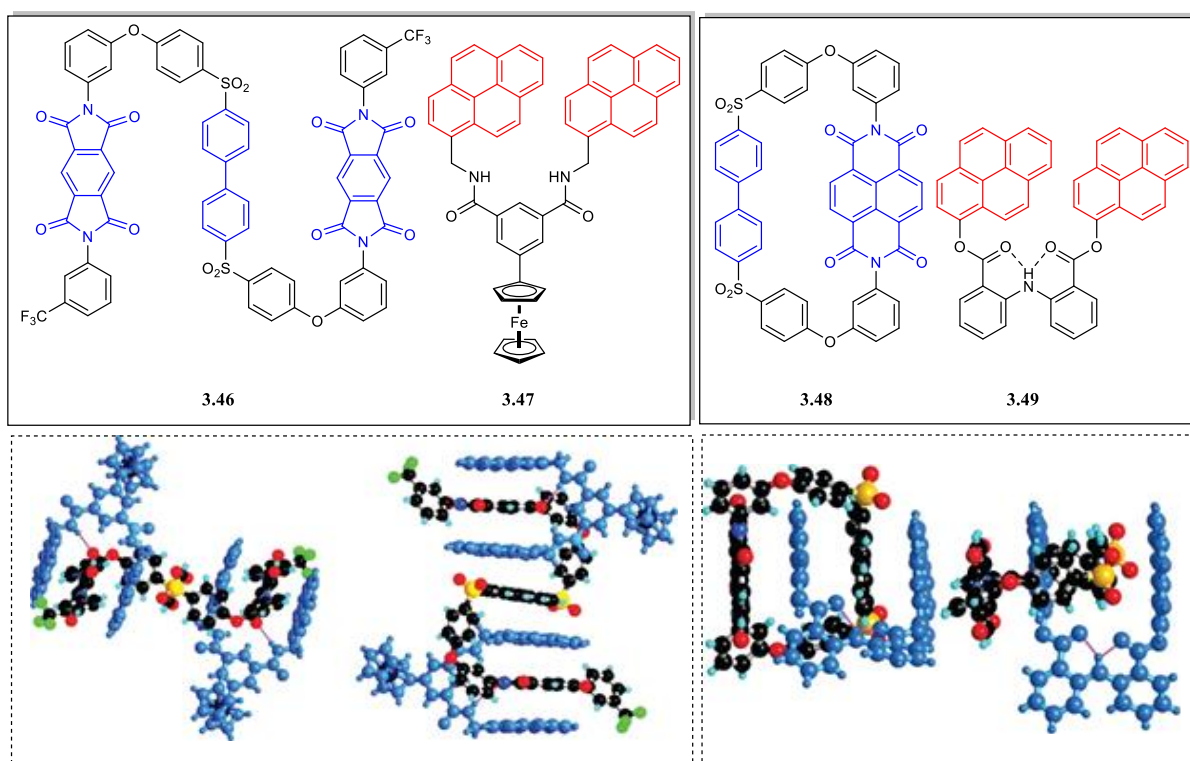


**Figure 36:** Tweezer residues used for selective information sequencing by Colquhoun *et al.*<sup>228</sup> (top) chemical structures of a  $\pi$ -electron poor PDI containing tweezer derivative **3.46** and NDI containing macrocycle **3.48** with complementary  $\pi$ -electron rich pyrenyl containing tweezers **3.47** and **3.49** (bottom) crystal structures of complementary tweezer complex **3.46** and **3.47** (left) and macrocycle **3.48** complexed with tweezer **3.49**

NDI derivatives including the  $\pi$ -electron poor residues mentioned above have also been shown to have application in information processing. Colquhoun and colleagues produced a binary copolymer composed of a linear sequence of  $\pi$ -poor residue containing NDI, aromatic and

aliphatic residues (4,4'-Bis[4-(3-aminophenoxy)benzenesulfonyl]-1,1'-biphenyl and 2,2'-(ethylenedioxy)bisethyl units), and sequence selective intercalation of a pyrene based tweezer residue formed a binary sequence co-polymer that underpins the concept of digital information storage.<sup>207</sup> The inclusion of the pyrene tweezer-based  $\pi$ -rich residue was observed by <sup>1</sup>H NMR and interestingly the <sup>1</sup>H NMR resonances reflected an underlying mathematical fractal, specifically a fourth-quarter cantor set.

The Iverson group, and others, have utilised the  $\pi$ - $\pi$  stacking behaviour of naphthalene diimide based oligomers with  $\pi$ -electron rich 1,5-dialkoxynaphthalene units by incorporating the units as DNA base surrogate phosphoramidites which are capable of intercalation between the DNA double helix.<sup>212,229–233</sup> This provides the ability to sequence-specifically bind and manipulate DNA, which is a valuable therapeutic target for chemists.

During the design and synthesis of molecular tweezers the nature of the linker, which connects the two receptor residues, is a key determinate of the chemical stability and binding properties of the final system. For example, it can be flexible or rigid and this will govern the binding model to either an 'induced fit' or 'lock and key' type model (Figure 37).<sup>174</sup> Understanding the effect, if any, the linker connecting the tweezer binding sites has on the  $\pi$ - $\pi$  stacking interactions within supramolecular networks will allow greater control and future design of optimised systems. As shown in the examples above (section 3.7), the nature of the binding sites and the structure of the linker can govern the application of the complex (e.g. from printing inks to data storage).

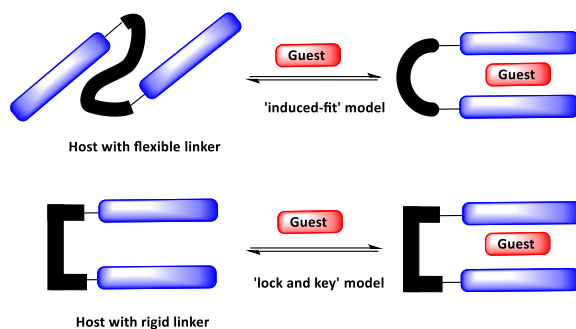


**Figure 37:** Cartoon representations of 'induced-fit' and 'lock and key' models.

### 3.6 Conclusion

In conclusion, this brief literature exploration has detailed the utility of supramolecular interactions, specifically those involving  $\pi$ - $\pi$  stacking interactions. Selected examples, such as those from Iverson, Colquhoun<sup>228</sup> and Hayes,<sup>209</sup> have been used to demonstrate how supramolecular interactions can be built into functional materials. Of specific interest to this work is the supramolecular tweezer type complex where two  $\pi$ -electron deficient species (viologen, PDI and NDI) are separated by a linker unit, which has been exploited in such diverse applications as healable materials, printing inks, molecular probes, information sequencing and primitive flash memory.

Herein we report the design, synthesis, and binding analyses of a series of redox-active supramolecular tweezer molecules, four neutral and two tetra-cationic systems. It is hoped that insight into the conformational constraint will be seen from structural changes in the connecting termini of the tweezer (flexible or rigid) and to see if the end group has an effect, if any, on the binding ability of the  $\pi$ -poor compound with a  $\pi$ -rich guest species.

## Chapter Four

# **Flexibility vs. Rigidity: A study of how conformational constraint impacts binding between $\pi$ -electron poor tweezer-type hosts and $\pi$ -electron rich guests.**

This information in this chapter refers to our publication<sup>234</sup> whereby author contributions are listed below: B.W.G. conceived and supervised the work assisted by J.S. The synthesis, photophysical, crystal growth and binding studies were carried out by L.A.P. for all the reported compounds unless stated otherwise. M.S. carried out synthesis and purification of **Flexi-NDI-Hex**. B.W.G. and L.A.P. drafted the manuscript through discussion with all the authors who approved the final version of the manuscript.

# Chapter 4: Flexibility versus Rigidity: Study of how Conformational Constraint Impacts Binding between $\pi$ -electron poor tweezer-type hosts and $\pi$ -electron rich guests.

Highlights:

- 11 tweezer type host receptor molecules each containing two NDI, PDI or viologen  $\pi$ -electron poor residues
- Each tweezer host contains two  $\pi$ -electron poor residues connected by either a flexible or rigid linker unit
- Binding stoichiometry was found to be 1:1 with  $\pi$ -electron rich guests for all systems studied
- For analogous pairs of tweezers with rigid and flexible linkers, binding strength was not always determined by the nature of the linker
- Binding was significantly increased for water soluble tweezers compared to the same systems in organic solvents.

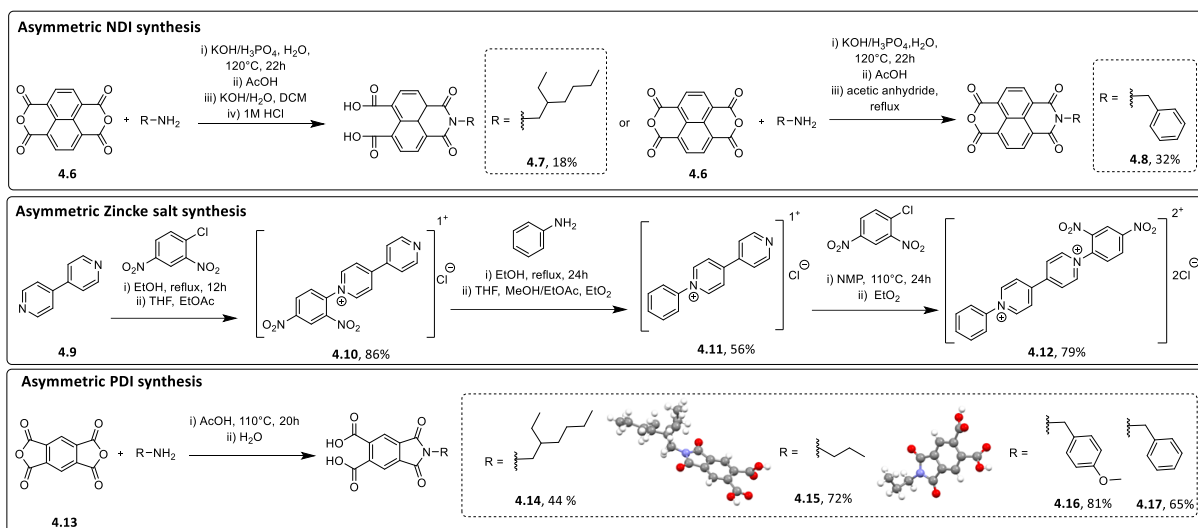
## 4.1 Results and Discussion

### 4.1.1 Tweezer design and synthesis

Our strategy for the synthesis of the tweezer molecules was to use a convergent pathway where two equivalents of the  $\pi$ -electron poor receptor species were added to either the rigid or flexible

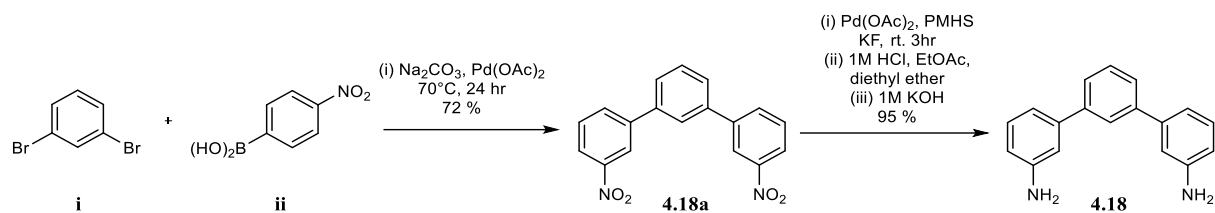
linker unit. To reduce the chance of unintended oligomerisation occurring, a series of desymmetrised  $\pi$ -electron poor species were synthesised (Scheme 23). These  $\pi$ -electron poor species were functionalised at one terminus with an amine or aniline, but the other end were able to react with the linker to produce the targeted tweezer receptors. Ultimately, it was found that to produce pairs of rigid and flexible naphthalene diimide (NDI), pyromellitic diimide (PDI) and viologen tweezers where both members of the pair were soluble in the same solvent, a small library of these desymmetrised  $\pi$ -electron poor precursor species had to be made (Scheme 23).

Briefly, mono-substituted imide residues were produced in moderate yields (**4.7** = 18 % and **4.8** = 32%) by pH controlled imide formation in water between one equivalent of an amine and NDI, as described by Buncel *et al.*<sup>235</sup> The targeted bipyridinium component (**4.12**) was achieved using a three-step procedure starting with the synthesis of the mono-Zincke salt (**4.10**) from 4-4 bipyridine (**4.9**). This species underwent a Zincke reaction with aniline to produce (**4.11**), which was subsequently converted to the mono-Zincke salt **4.12** in 38% overall yield. Mono-functionalised PDI components were produced in varying yields (44-81%) by heating equimolar quantities of PDA and an amine in water with acetic acid.<sup>236</sup> The chemical structures of PDA derivatives containing branched and straight chain amine residues (**4.14** and **4.15**) were confirmed by X-ray crystallographic analysis, which showed conclusively that the products contained two acid groups rather than an anhydride.



**Scheme 23:** Synthesis of asymmetric precursors to  $\pi$ -electron poor species required for tweezer-receptor synthesis.

The synthetic pathway for the rigid tweezer molecules required the key intermediate tris-aromatic diamine **4.18**. This was synthesised from the dinitro terphenyl molecule **4.18** using 1,3- dibromobenzene (**i**) and 3-nitro-phenyl boronic acid (**ii**) (Scheme 24). The reaction was carried out under typical Suzuki conditions to produce tris-aromatic dinitro **4.18a** in good yield as a fine grey powder. The nitro substituents were then converted to amine groups using a palladium acetate catalyst and poly(methylhydrosiloxane) (PMHS) as the hydrogen source. The product was previously isolated by column chromatography on a 1 g scale.<sup>197</sup> Unfortunately, during scale-up to multi grams of materials as required for this section of work, it became apparent that column chromatography would not be suitable to purify this product because the residual PMHS blocked the column. Therefore, a new isolation procedure was developed whereby diamine **4.18** was dissolved in 1M HCl, washed with Et<sub>2</sub>O to remove the PMHS and then the aqueous layer basified by pouring into 1M KOH to furnish up to 12g (*c.* 95 % yield) of pure **4.18** in one simple operation.

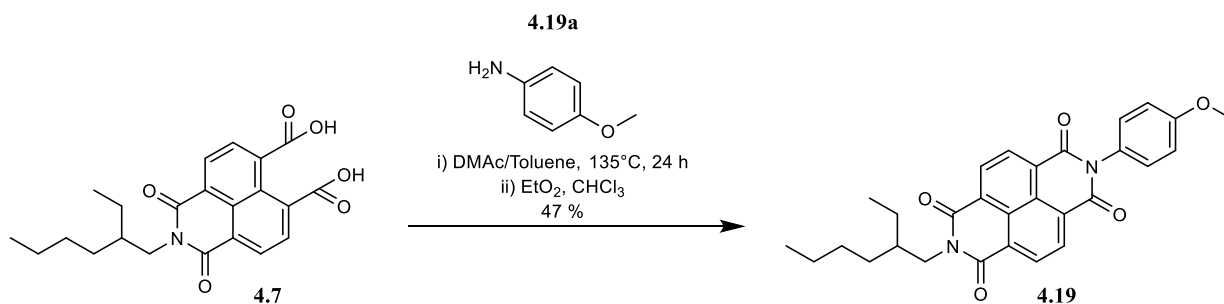


**Scheme 24:** Synthesis and purification of rigid tris-aromatic diamine linker unit **4.18**.

With these components in hand, attention turned to the synthesis of the targeted tweezer molecules with rigid linker groups.

#### 4.1.2 Initial tweezer synthesis attempts: establishing suitable conditions for neutral systems.

As a model reaction to ascertain suitable imide formation reaction conditions between anilines and diacid species such as **4.7** it was decided to synthesise mono aryl mono aromatic NDI (**4.19**) (Scheme 25). Thus **4.7** and 4-methoxyaniline (**4.19a**)<sup>226</sup> were heated in degassed toluene and DMAc overnight to give **4.19**, which could be isolated without using column chromatography.



**Scheme 25:** Synthesis of asymmetric NDI species **4.19**.

The <sup>1</sup>H NMR spectrum of the isolated product **4.19** displays the proton environments that correspond to the aromatic (7.0 – 7.5 ppm) and aryl (0.7 – 1.5 ppm) regions of the end groups in the spectrum (Figure 38).

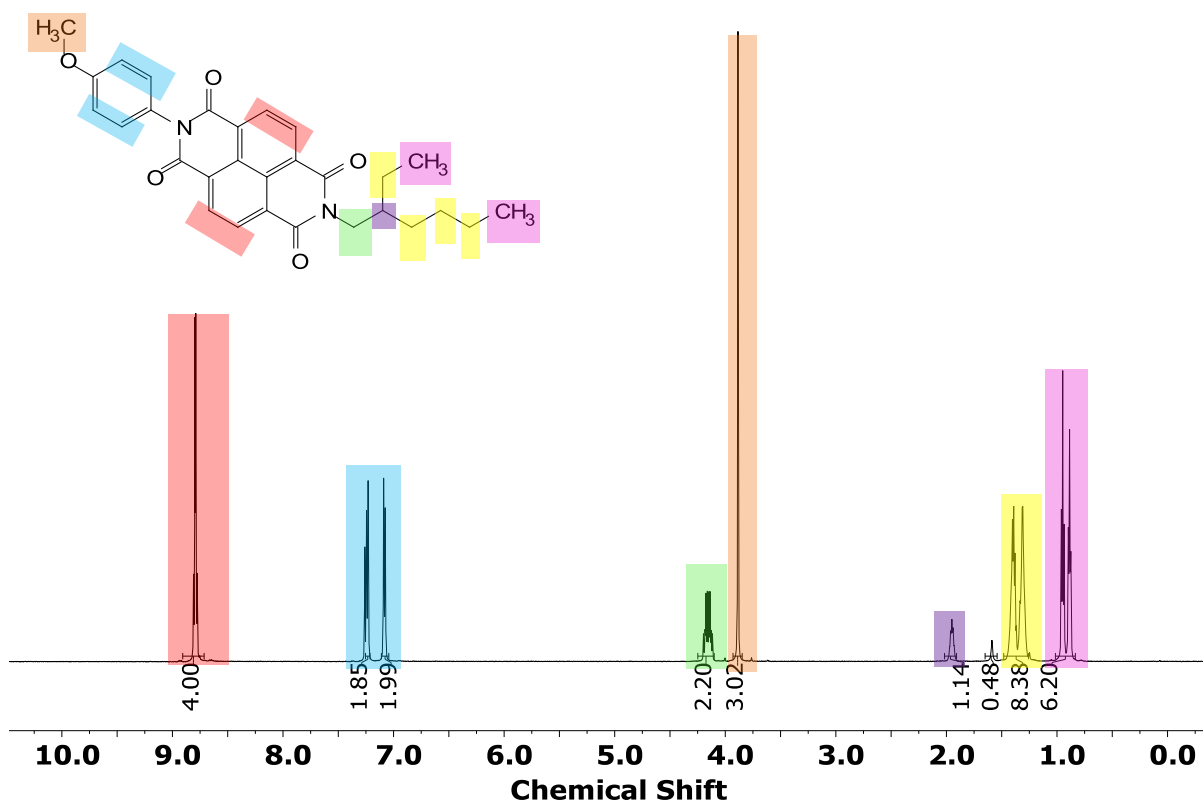
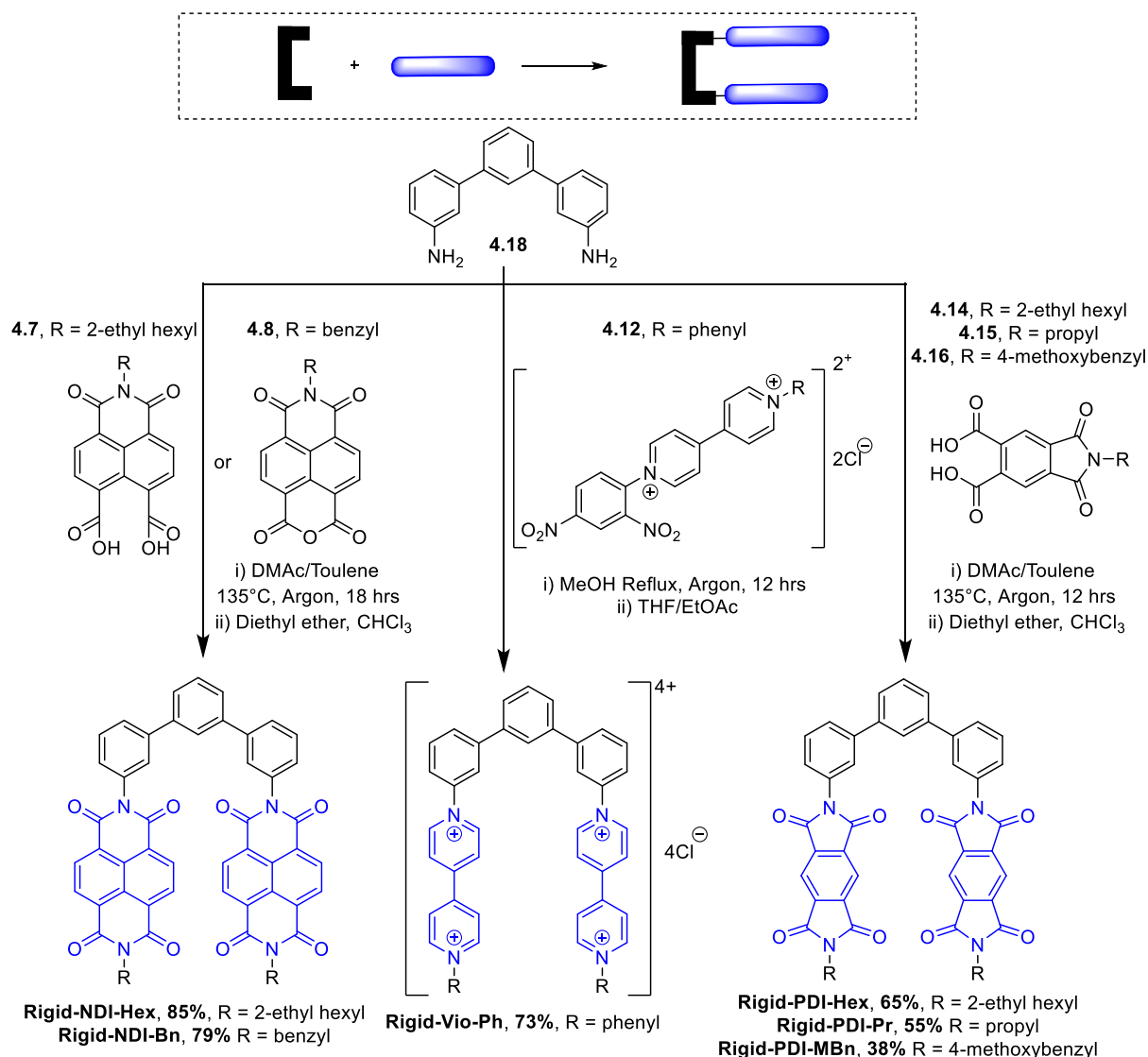


**Figure 38:** Full  $^1\text{H}$  NMR (600MHz) spectrum of **4.19** with shaded proton environments. Recorded in  $\text{CDCl}_3$ , reference peak not visible due to masking by product signals.

### 4.1.3 Synthesis of $\pi$ -electron poor tweezer motifs

The neutral tweezer systems containing NDI and PDI, were synthesised by diimide formation between tris-aromatic diamine **4.18**<sup>197</sup> and the requisite anhydride (**4.8**) or diacid (**4.7**, **4.14**, **4.15**, **4.16** or **4.17**) outlined in Scheme 26 below. The tweezers are referred using the following nomenclature where each name contains three sections in the form: *AA-BB-CC*. *AA* defines the linker used, flexible (**flexi**) or **rigid**; *BB* is the binding residue: **NDI**, viologen (**Vio**) or **PDI**; and *CC* defines the end group': 2-ethyl hexyl (**Hex**), benzyl (**Bn**), phenyl (**Ph**), Propyl (**Pr**) or para substituted methoxy benzyl (**MBn**).

The tetracationic tweezer (**Rigid-Vio-Ph**) with the rigid tris-aromatic linker (**4.18**) was produced *via* the Zincke reaction, inspired by similar work from our group and others<sup>196</sup> during synthesis of linear<sup>82,84,101,119</sup> and macrocyclic viologen containing species<sup>197</sup> (Scheme 26).



**Scheme 26:** Synthesis of  $\pi$ -electron poor tweezer molecules with ridged linker units.

The <sup>1</sup>H NMR spectrum of the isolated **Rigid-Vio-Ph** can be seen below, with assigned proton environments shaded appropriately (Figure 39). The protons that correspond to the tris-aromatic component within the tweezer molecule showed good agreement to the splitting and positions

seen for similarly structured published tetracationic macrocycles.<sup>197</sup> The protons that correspond to the viologen core (shaded red, grey and yellow in Figure 39) will be the most influenced upon future binding studies with a  $\pi$ -electron guest species, so distinct separation from the tris-aromatic proton region is an advantage.

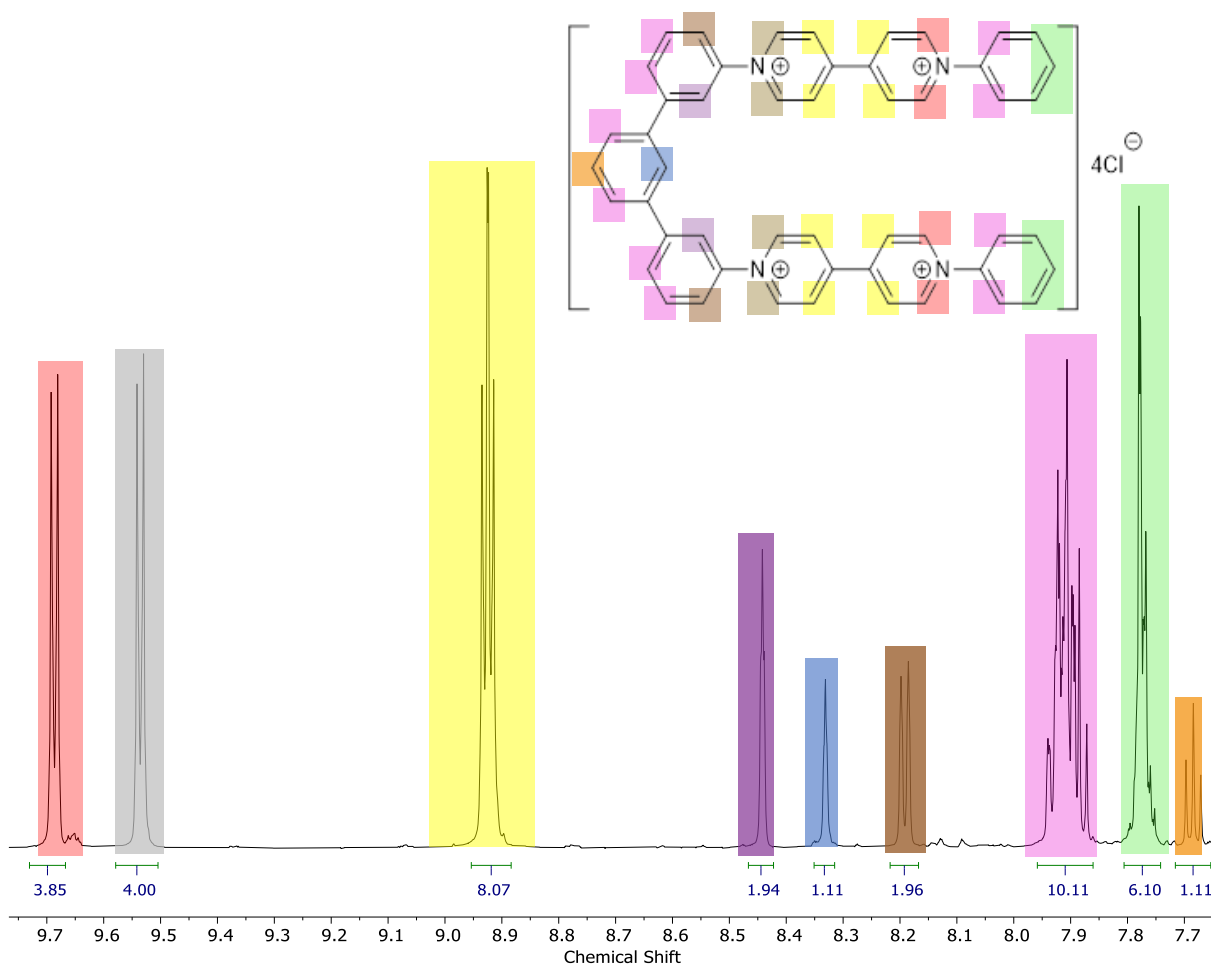


**Figure 39:** Partial  $^1\text{H}$  NMR spectrum of Rigid-Vio-Ph recorded in  $\text{CD}_3\text{OD}$

Initial synthesis of neutral rigid tweezers made it apparent that the correct stoichiometry was extremely important. When stoichiometric quantities were slightly skewed in the reaction attempt from a 1:2 ratio of linker to appropriate terminal end species, a mixture of desired tweezer and undesired mono substituted linker were produced, which was difficult to separate. The separation of excess of terminal end species in the reaction also proved difficult. For example, usual purification techniques were unavailable to remove the excess NDI terminal

end groups as they were only soluble in solvents that the tweezers were not (e.g. **4.7** was readily soluble in water/KOH) and a common solvent system for both (CHCl<sub>3</sub>:TFA 9:1) was unsuitable for silica column chromatography. TLC monitoring was difficult to interpret and sometimes did not show two distinct spots for the monosubstituted species or desired tweezer. Therefore, <sup>1</sup>H NMR monitoring was employed each time to confirm the stoichiometry at T = 0 and once again to confirm the formation and completion of the reaction. The <sup>1</sup>H NMR spectra of isolated tweezer **Rigid-NDI-Hex** with appropriate proton environments shaded can be seen below (Figure 40).

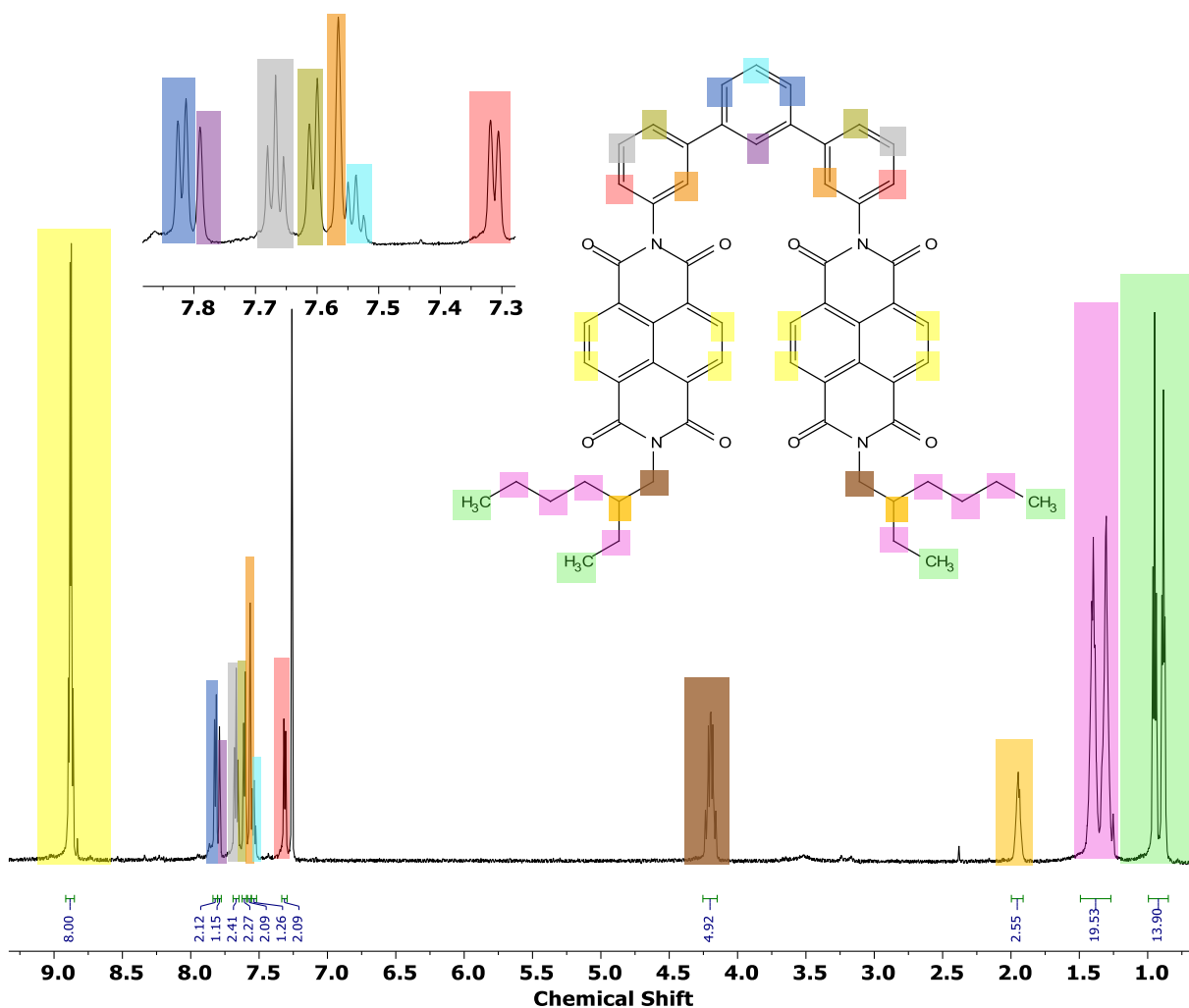
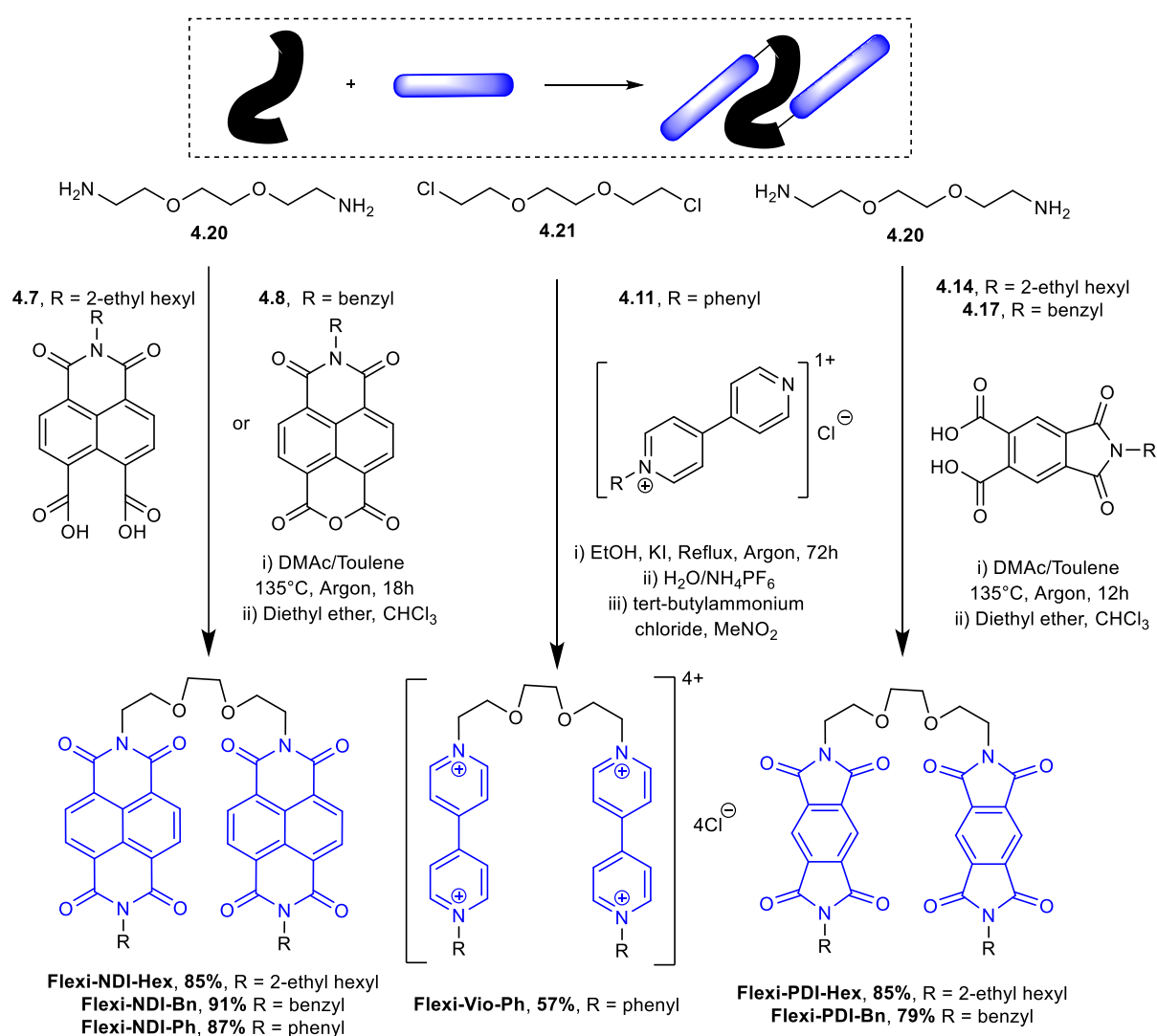


**Figure 40:** <sup>1</sup>H full spectrum of **Rigid-NDI-Hex**

The neutral tweezer receptor compounds containing a flexible linker were produced by addition of diamine **4.20** to the appropriate imide species (**4.7**, **4.8**, **4.14**, or **4.17**) shown in Scheme 27. We were unable to synthesise the di-viologen tweezer **Flexi-Vio-Ph** using aliphatic diamine **4.20** and Zincke salt **4.12**, and therefore had to modify our synthetic strategy. Gratifyingly we found that addition of the pyridine species **4.11** (an intermediate in the synthesis of **Rigid-Vio-Ph**, see Scheme 23) to the dichloride **4.21**, *via* employment of the Finkelstein reaction, furnished our target tweezer **Flexi-Vio-Ph** in respectable yields (57%).



**Scheme 27:** synthesis of flexible tweezer-type receptors.

The  $^1\text{H}$  NMR of the isolated tweezer-type receptor **Flexi-PDI-Hex** (Figure 41) displays the characteristic peaks of the flexible linker unit between 3.6 and 4.0 ppm (shaded blue, green and brown).

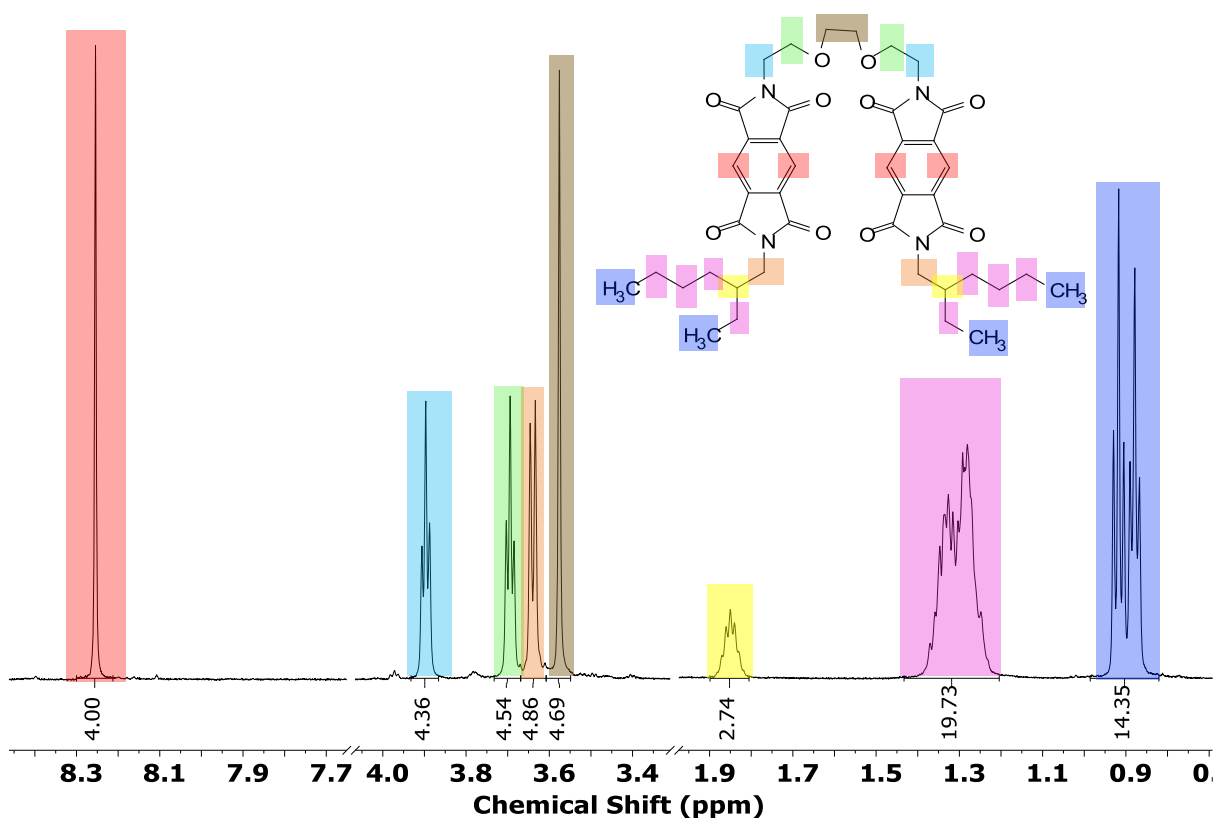


**Figure 41:** Partial  $^1\text{H}$  spectrum of **Flexi-PDI-Hex** tweezer motif with proton regions shaded.

#### 4.1.5 Tweezer-type complexes: Verification of binding through UV-Vis analysis.

Mixtures of  $\pi$ -electron poor and  $\pi$ -electron rich species are well known to produce coloured solutions,<sup>209</sup> which provides a rapid initial verification that supramolecular complexation is occurring. Addition of equimolar quantities of a colourless solution of pyrene (**Pyr**) to either of the pale-yellow solutions of the NDI based tweezer molecules (**Rigid-NDI-Hex** or **Flexi-NDI-Hex**, 3mM,  $\text{CHCl}_3$ : TFA (9:1)) afforded a deep red solution (left in Figure 42). This colour is

as a consequence of the formation of an intense charge-transfer band with  $\lambda_{\max}$  at 538 (**Rigid-NDI-Hex**  $\supset$  **Pyr**) or 545 nm (**Flexi-NDI-Hex**  $\supset$  **Pyr**).

Absorption bands between 480 and 550 nanometres are indicative of charge transfer from the HOMO of  $\pi$ -electron-rich pyrene (**Pyr**) to the LUMO of the  $\pi$ -electron-poor, chain-folding diimide (**Rigid-NDI-Hex** or **Flexi-NDI-Hex**). This demonstrates the formation of a complementary, aromatic,  $\pi$ - $\pi$  stacked complex. For the case of the addition of a solution of **Pyr** to either of the PDI-based tweezers **Rigid-PDI-Hex** and **Flexi-PDI-Hex** (right in Figure 42), the colour change was less pronounced but still visible by eye ( $\lambda_{\max}$  at 500 nm (**Rigid-PDI-Hex**  $\supset$  **Pyr**) or 481 nm (**Flexi-PDI-Hex**  $\supset$  **Pyr**)). Finally, addition of **Pyr** to a solution of either di-viologen tweezers **Rigid-Vio-Ph** or **Flexi-Vio-Ph** gave no appreciable colour change (see Supporting Information). However, changing the nature of the  $\pi$ -electron rich species to 1,5 dihydroxynaphthalene (**DHN**) did result in the appearance of new absorbance bands in the visible region of the spectrum ( $\lambda_{\max}$  at 531 (**Rigid-Vio-Ph**  $\supset$  **DHN**) or 535 nm (**Flexi-Vio-Ph**  $\supset$  **DHN**)) (middle in Figure 42).

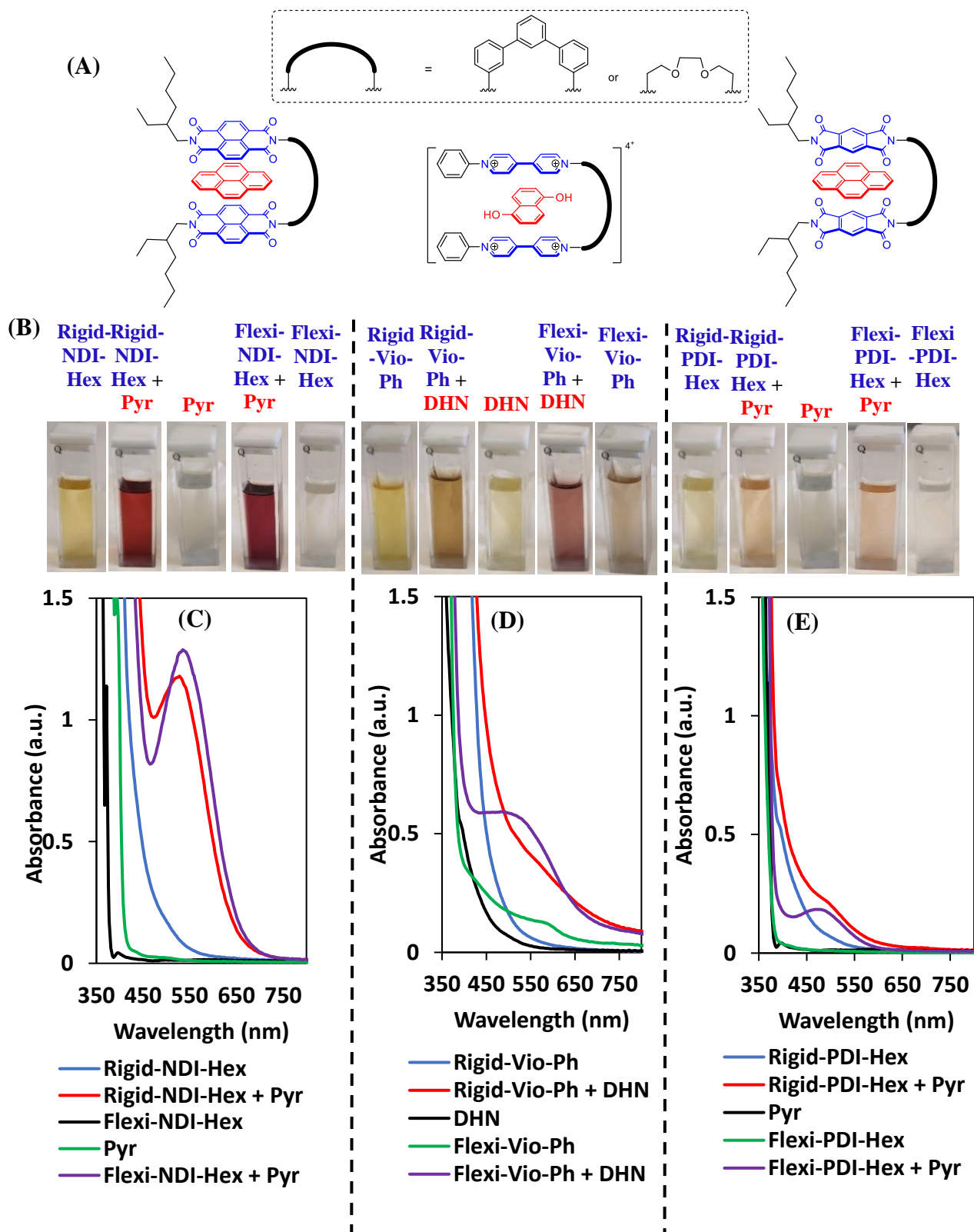


**Figure 42:** (A) Structural representation of complementary, aromatic,  $\pi$ - $\pi$  stacked complexes for each binding residue NDI, Vio or PDI with guest species Pyr or DHN (B) Photograph of tweezer complexation in solution between host and guest at a 1:1 ratio (3mM). (C-E) Photophysical data of tweezer complexation between host and guest at a 1:1 ratio observed via

UV/vis absorption spectroscopy (3 mM, samples for (C) and (E) recorded in CHCl<sub>3</sub>:trifluoroacetic acid (9:1) and (D) in MeOH)

#### 4.1.6 Establishing the Stoichiometry of complex formation through the method of continuous variation by <sup>1</sup>H NMR spectroscopic analysis - Job's plot analysis

The formation of supramolecular complexes in solution was further investigated by <sup>1</sup>H NMR spectroscopy. Figure 43 shows a stack of <sup>1</sup>H NMR spectra for solutions containing **Flexi-NDI-Bn** in isolation (bottom spectrum) and then with increasing molar proportions of guest species **Pyr** at a fixed total concentration of host and guest (for <sup>1</sup>H NMR data for all systems see Supporting Information). Association and dissociation are fast on the NMR timescales as average chemical shift resonance frequencies are observed in all the spectra, rather than changing proportions of signals at two distinct chemical shift values which would be an indication of complexes and un-complexed species.

In this example, large complexation induced upfield shifts ( $\Delta\delta$  up to 0.9 ppm) were observed for the signals of the aromatic diimide residues ( $H_a$  and  $H_b$ ). This can be attributed to mutual ring-current shielding caused by the intercalating pyrene (**Pyr**) on the bis-diimide, confirming the presence of complementary  $\pi$ - $\pi$  stacking supramolecular interactions in solution.

The signals for the two environments on the aromatic diimide **Flexi-NDI-Bn** ( $H_a$  and  $H_b$ ) are resolved as two doublets in the absence of **Pyr**, (bottom spectrum, 0 equiv. of **Pyr**) and when there is a significant excess of **Pyr** (e.g. 90%). However, at 30% mole fraction of **Pyr** the signals  $H_a$  and  $H_b$  coalesce forming a singlet. This suggests orientation of the pyrene in the tweezer

system results in an inequivalent shielding effect on the protons H<sub>a</sub> and H<sub>b</sub>. Aliphatic protons H<sub>e</sub> and H<sub>f</sub> which are in the plane of the diimide species in the complex, also progressively shift upfield as the mole fraction of **Pyr** increases, but to a lesser extent than for H<sub>a</sub> and H<sub>b</sub> ( $\Delta\delta$  up to 0.19 ppm). This is presumably due to the relative proximity of these aromatic and aliphatic protons to **Pyr** in the complex. Conversely, *downfield* complexation shifts ( $\Delta\delta$  ca. 0.15 ppm) were observed for the signals associated with protons H<sub>c</sub> and H<sub>d</sub> (at the midpoint on the flexible linker) as the relative concentration of **Pyr** increases. This indicates that these protons lie in the plane of the pyrene in the complex which is in the *deshielding* zone of **Pyr**. These data are in complete agreement with the geometry of the proposed tweezer-type complexation, shown in Figure 43.

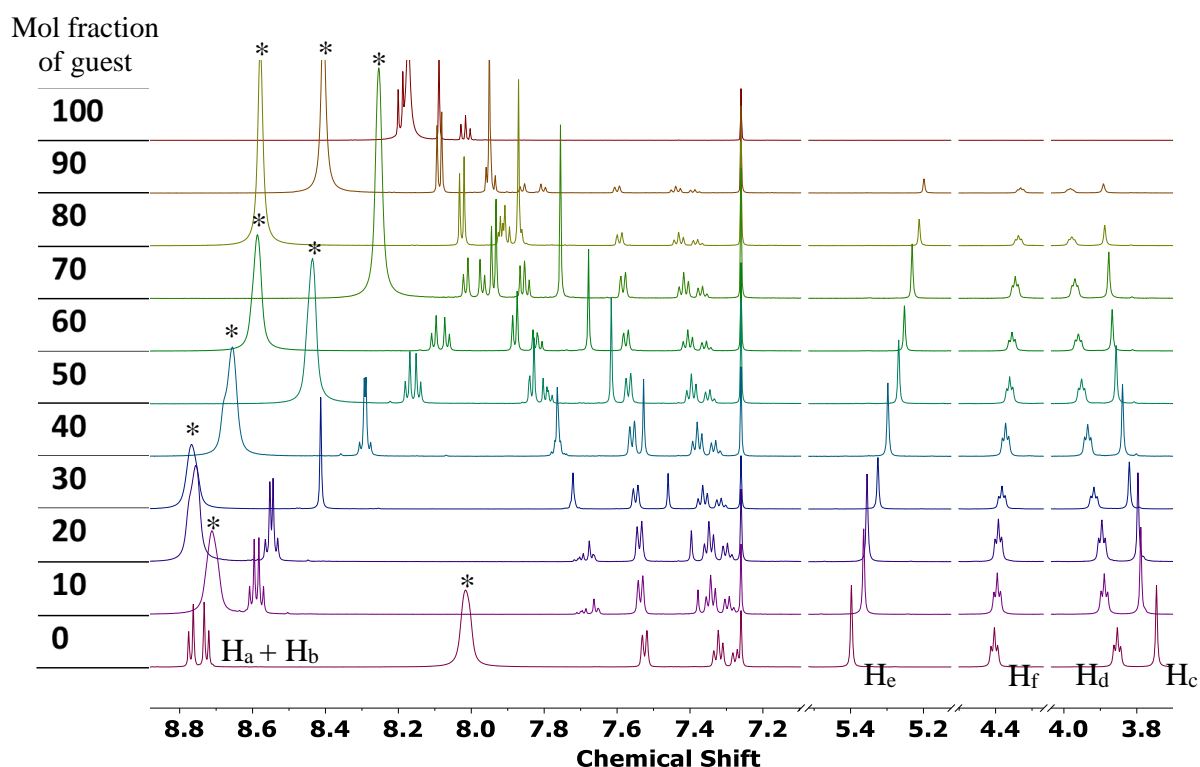
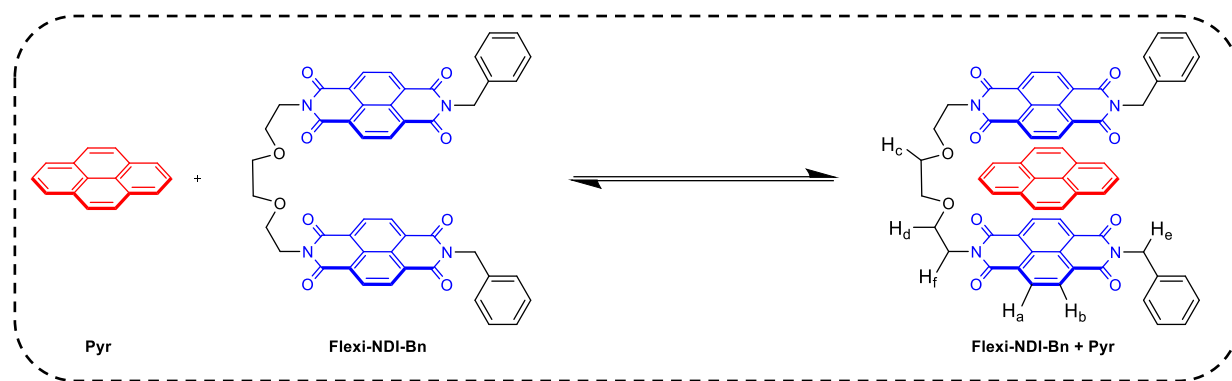


**Figure 43:** (top) Structural representation of host-guest complexation between tweezer **Flexi-NDI-Bn** and **Pyr** with selected protons labelled. (bottom) Stack of  $^1\text{H}$  NMR partial spectra (600 MHz,  $\text{CDCl}_3$ : trifluoroacetic acid (9:1)) for varying stoichiometries of **Flexi-NDI-Bn** with guest species **Pyr** at a fixed total concentration. \* = signal for O-H proton on trifluoroacetic acid.

A Job plot can be used as additional positive confirmation of a binding model to complement titration studies.<sup>146</sup> Job's plots using data from analogous  $^1\text{H}$  NMR spectroscopy studies for six members of the tweezer library can be constructed (Figure 44). In each case the plot maxima is positioned at 0.5 mole fraction, which demonstrates that the stoichiometry of binding in each

complex over the concentration range studied was 1:1, as expected for the complexation mode proposed.

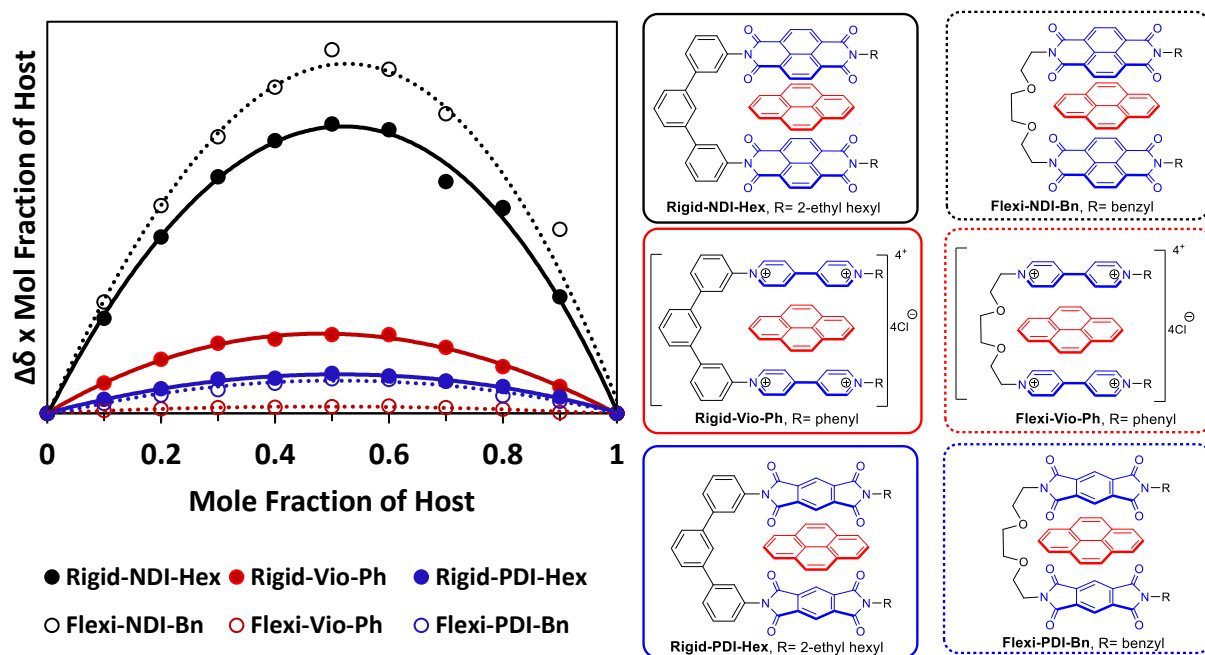


**Figure 44:**  $^1\text{H}$  NMR Job plots for host systems **Rigid-NDI-Hex**, **Rigid-Vio-Ph**, **Rigid-PDI-Hex**, **Flexi-NDI-Bn**, **Flexi-Vio-Ph** and **Flexi-PDI-Bn** with guest species **Pyr**. Neutrally charged tweezers **Rigid-NDI-Hex**, **Rigid-PDI-Hex**, **Flexi-NDI-Bn** and **Flexi-PDI-Bn** recorded at 10 mg/mL in  $\text{CDCl}_3$ :trifluoroacetic acid (9:1) at 298K. Tetracationic systems **Rigid-Vio-Ph** and **Flexi-Vio-Ph** recorded at 20 mg/mL in  $\text{CD}_3\text{OD}$  at 298K.

#### 4.1.7 Binding constant determination

With the binding stoichiometry of the complexes established, it is possible to determine the binding constant ( $K$ ) for each system. This is calculated using  $^1\text{H}$  NMR spectroscopic data from a titration experiment whereby increasing quantities of the guest species are added to a fixed concentration of the host as exemplified for **Rigid-NDI-Hex**  $\supset$  **Pyr** in Figure 45.

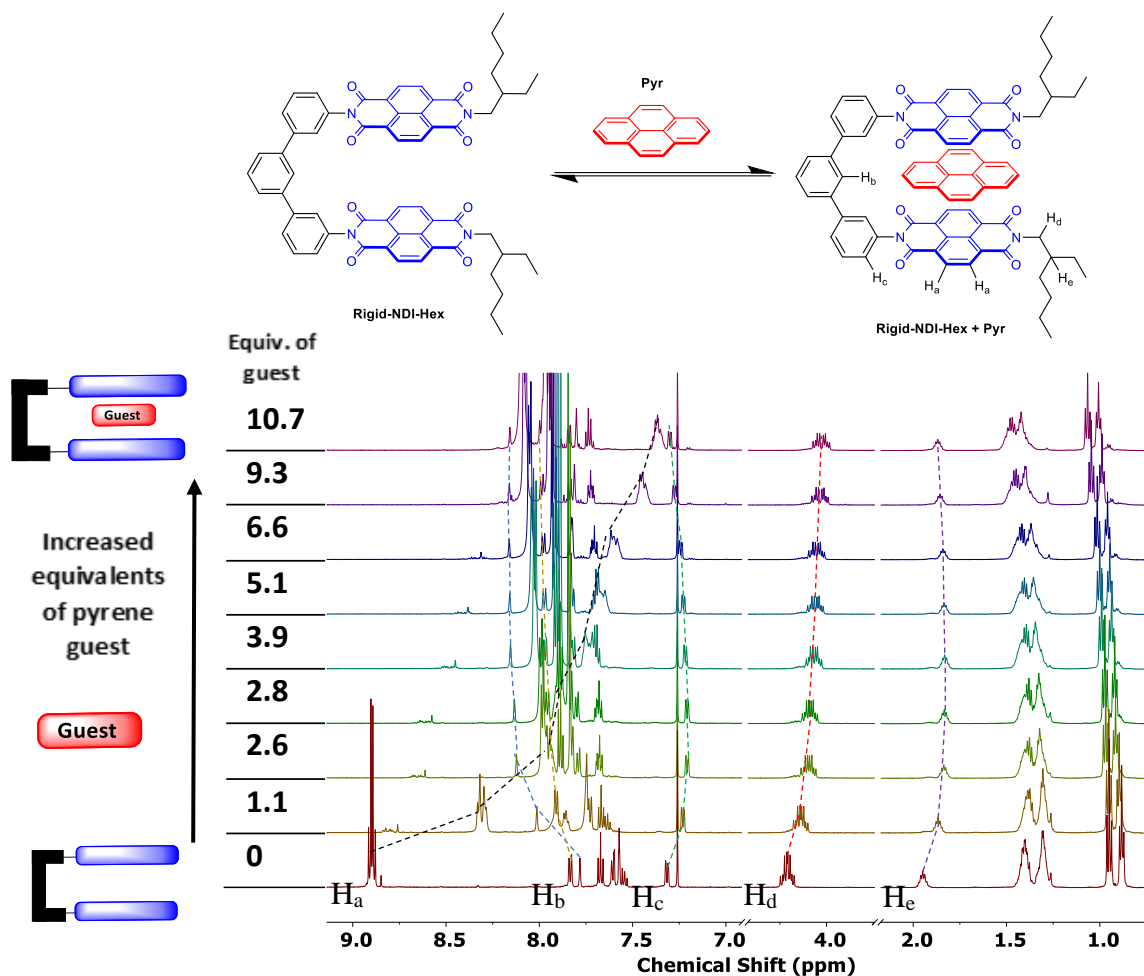
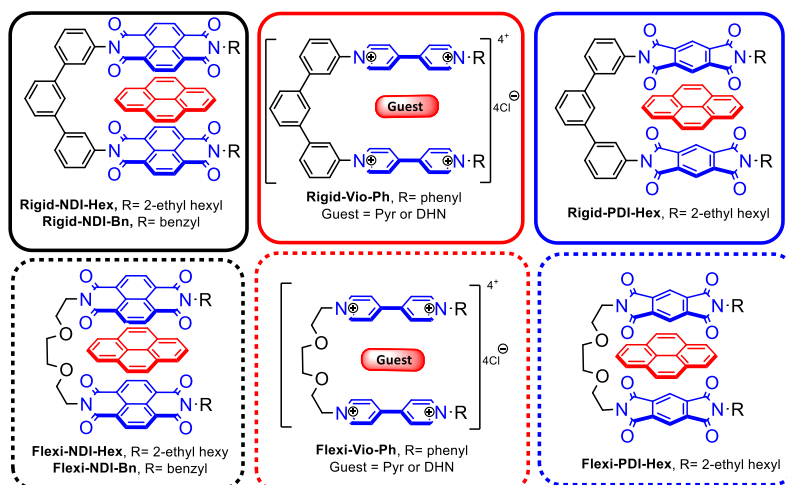


**Figure 45:** (bottom) partial <sup>1</sup>H NMR (600 MHz) spectral changes induced by titration of 10 mg/mL tweezer molecule **Rigid-NDI-Hex** with guest species **Pyr** in CDCl<sub>3</sub>: trifluoroacetic acid (9:1) at 298K. (top) Structural representation of host-guest complexation between tweezer **Rigid-NDI-Hex** with **Pyr**.

It can be seen that similar trends are observed for the change in chemical shifts for protons in the complex (**Rigid-NDI-Hex** ⊃ **Pyr**) as were observed for (**Flexi-NDI-Bn** ⊃ **Pyr**) during the Job's plot analysis presented above (Figure 44). Large complexation induced upfield shifts ( $\Delta\delta$  up to 1.5 ppm) were observed for the signals of the aromatic diimide residues (H<sub>a</sub> and H<sub>b</sub>). In contrast, as more pyrene was added to a fixed concentration of **Rigid-NDI-Hex**, the signal for the H<sub>c</sub> protons, which, are in plane of the pyrene in a tweezer type complex shifts upfield ( $\Delta\delta$  ca. 0.3 ppm). Again, these data are in complete agreement with the proposed tweezer-type

complexation. The binding constant, calculated using Bindfit,<sup>146,147</sup> for (**Rigid-NDI-Hex** ⊃ **Pyr**) was determined to be 71 M<sup>-1</sup> and equivalent data for all species are presented in Table 3.



Entry	Key	Host	Guest	Solvent	Conc of host (mM)	K	Errors (±%)
1	—	<b>Rigid-NDI-Hex</b>	<b>Pyr</b>	CDCl <sub>3</sub> /TFA (9:1)	10.4	71.1	7.0
2	—	<b>Rigid-NDI-Bn</b>	<b>Pyr</b>	CDCl <sub>3</sub> /TFA (9:1)	5.1	18.9	3.2
3	- - -	<b>Flexi-NDI-Hex</b>	<b>Pyr</b>	CDCl <sub>3</sub> /TFA (9:1)	10.0	45	2.3
4	- - -	<b>Flexi-NDI-Bn</b>	<b>Pyr</b>	CDCl <sub>3</sub> /TFA (9:1)	13.2	66.3	2.8
5	- - -	<b>Flexi-NDI-Ph</b>	<b>Pyr</b>	CDCl <sub>3</sub> /TFA (9:1)	13	53.0	2.1
6	—	<b>Rigid-Vio-Ph</b>	<b>Pyr</b>	CD <sub>3</sub> OD /1% TFA	15.4	2.6	0.6
7	- - -	<b>Flexi-Vio-Ph</b>	<b>Pyr</b>	CD <sub>3</sub> OD /1% TFA	7.0	2.3x10 <sup>-5</sup>	0.18
8	—	<b>Rigid-Vio-Ph</b>	<b>DHN</b>	CD <sub>3</sub> OD /1% TFA	23.9	5.5	2.6
9	- - -	<b>Flexi-Vio-Ph</b>	<b>DHN</b>	CD <sub>3</sub> OD /1% TFA	7.0	1.4	4.7
10	- - -	<b>Flexi-Vio-Ph</b>	<b>Pyr</b>	CD <sub>3</sub> CN	9	2.8x10 <sup>-2</sup>	0.29
11	—	<b>Rigid-PDI-Hex</b>	<b>Pyr</b>	CDCl <sub>3</sub>	10.3	10.8	0.76
12	—	<b>Rigid-PDI-Pr</b>	<b>Pyr</b>	CDCl <sub>3</sub> /TFA (9:1)	9	25	2.5

<b>13</b>	<b>—</b>	<b>Rigid-PDI-MBn</b>	<b>Pyr</b>	CDCl <sub>3</sub> /TFA (9:1)	4	22.5	4.5
<b>14</b>	<b>- - -</b>	<b>Flexi-PDI-Hex</b>	<b>Pyr</b>	CDCl <sub>3</sub>	10.3	7.2	1.2
<b>15</b>	<b>- - -</b>	<b>Flexi-PDI-Bn</b>	<b>Pyr</b>	CDCl <sub>3</sub>	14	6.5	3.5

Solvent choice and concentration of host dictated by solubility/nature of host system.

**Table 3:**  $K_a$  values for the tweezer compounds studied with specific hosts and in specific solvents. Values are calculated by *Bindfit*<sup>146,147</sup> using chemical shift data from multiple signals in at least 8 independent <sup>1</sup>H NMR spectra, each containing a fixed concentration of host and varying concentrations of guest species (See SI for full NMR titration data).

When comparing binding constants (Table 3) for NDI tweezers which only vary structurally by the nature of the linker, the rigid tweezer **Rigid-NDI-Hex** shows the greater binding with **Pyr** ( $71 \text{ M}^{-1}$ , entry 1), compared to that measured for the flexible NDI tweezer in the complex **Flexi-NDI-Hex**  $\supset$  **Pyr** ( $45 \text{ M}^{-1}$ , entry 3). Conversely, when the end group is a benzyl or phenyl group, the flexible NDI tweezer (**Flexi-NDI-Bn**  $\supset$  **Pyr**) and (**Flexi-NDI-Ph**  $\supset$  **Pyr**) exhibited binding constants of  $66 \text{ M}^{-1}$  and  $53 \text{ M}^{-1}$  respectively, greater than that observed for the rigid analogue **Rigid-NDI-Bn**  $\supset$  **Pyr** ( $19 \text{ M}^{-1}$ , entry 4). This would suggest that the strength of binding in the NDI systems is governed by both the rigidity of the linker (likely to be entropic effects) and the nature of the R group, presumably due to steric effects.

When examining the di-viologen containing systems (**Rigid-Vio-Ph** and **Flexi-Vio-Ph**, entries 6-10) binding can be seen to be lower in each case for the flexible di-viologen tweezer species when compared to the rigid analogue, regardless of the guest (**Pyr** or **DHN**). For this structural pair therefore, we propose that pre-organization of the host facilitated by the rigid linker minimizes the entropy of conformational change required to produce the tweezer type binding geometry, resulting in higher binding. Exchanging the anion from chloride to

hexafluorophosphate (**Flexi-Vio-Ph**  $\supset$  **Pyr**) increased binding to  $2.8 \times 10^{-2} \text{ M}^{-1}$  from  $2.3 \times 10^{-5} \text{ M}^{-1}$  (entries 7 and 10 respectively).

Finally, when comparing PDI containing systems, binding was seen to be similarly low in flexible and rigid systems, with favour of the rigid systems **Rigid-PDI-Hex**  $\supset$  **Pyr** ( $K = 10.8 \text{ M}^{-1}$ , entry 11), **Rigid-PDI-Pr**  $\supset$  **Pyr** ( $K = 25 \text{ M}^{-1}$ , entry 12) and **Rigid-PDI-MBn**  $\supset$  **Pyr** ( $K = 22.5 \text{ M}^{-1}$ , entry 13) when compared to flexible systems **Flexi-PDI-Hex**  $\supset$  **Pyr** ( $K = 7.2 \text{ M}^{-1}$ , entry 14) and **Flexi-PDI-Bn**  $\supset$  **Pyr** ( $K = 6.5 \text{ M}^{-1}$ , entry 15).

Recently, Zeng, Li *et al.* produced di-viologen containing macrocycles (**3.31** and **3.32**) structurally similar to the cyclophane **3.29** that we studied previously (Section 3.4 in Chapter 3).<sup>196</sup> In contrast to the tetra  $\text{PF}_6$  salt in our work they used the tetra chloride salt, resulting in a water soluble system. The macrocycle showed significant binding to a range of polyaromatic hydrocarbons in water. Inspired by their work, and related supramolecular molecular systems which show that expulsion of high energy water from the cavity of macrocyclic species can enhance binding affinities,<sup>237</sup> we were interested to see if this was the case for our tweezer system.

Accordingly,  $^1\text{H}$  NMR titration studies were carried on  $\text{D}_2\text{O}$  with 1% trifluoroacetic acid (TFA) added to determine the binding constants for **Rigid-Vio-Ph** and **Flexi-Vio-Ph** with **DHN** (Figure 46). Addition of TFA was found to enhance the resolution of the signals in the host compound.<sup>82,197,238</sup>

As concentration of guest species **DHN** increased, significant upfield shifts (<1ppm) are observed for bipyridinium units ( $H_a$  and  $H_b$ ). The binding constants for **Rigid-Vio-Ph** and **Flexi-Vio-Ph** with **DHN** were determined to be 15 and 204  $M^{-1}$  in  $D_2O/TFA$ , which is an order of magnitude greater than observed for the same host guests pair in  $MeOH/TFA$  (1.4 and 5.5  $M^{-1}$  entries 7 and 8, Table 3).

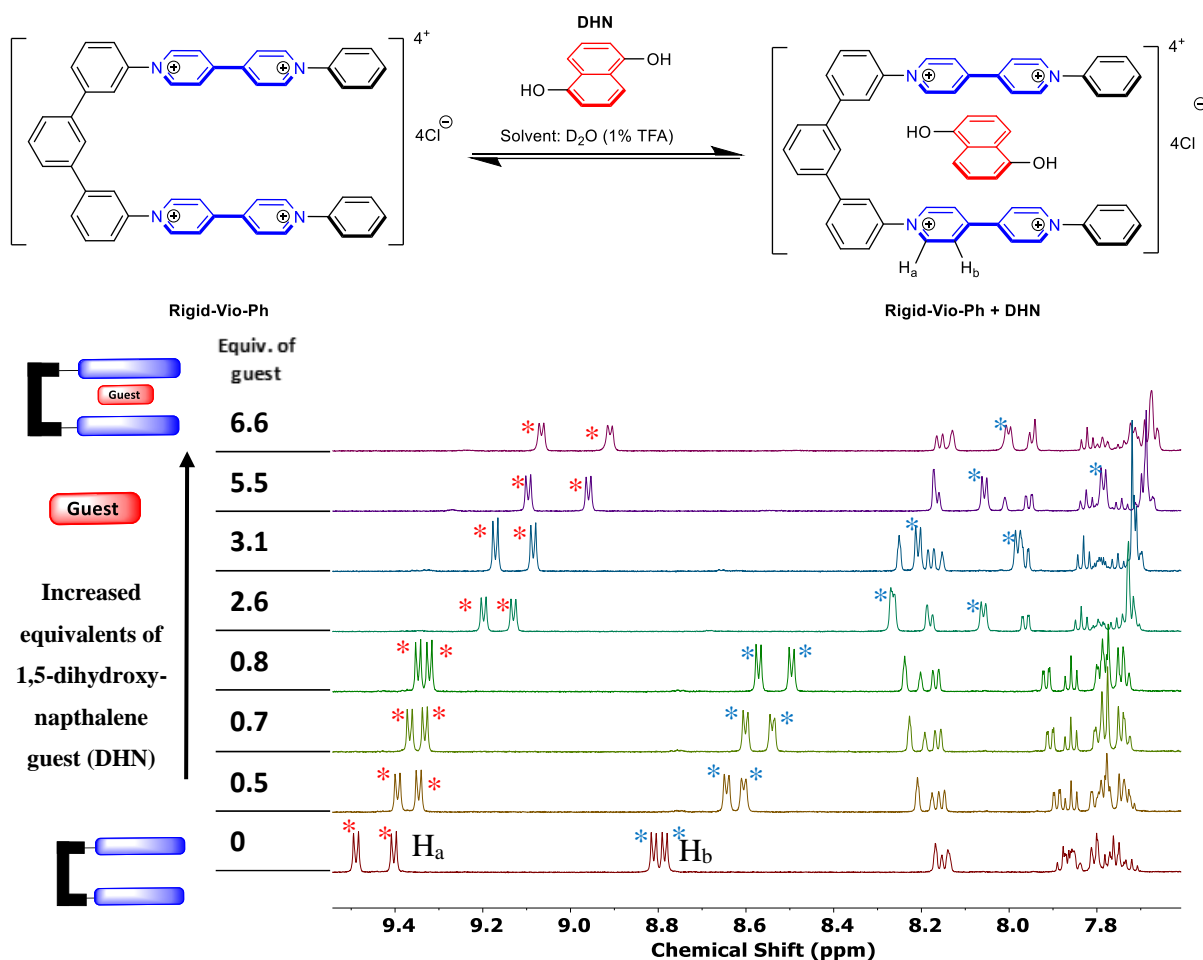


**Figure 46:** (bottom) Partial  $^1H$  NMR (600 MHz) spectral changes induced by titration of 2 mg/mL tweezer molecule **Rigid-Vio-Ph** with guest species **DHN** in  $D_2O$  at 298K. (top) Structural representation of host-guest complexation between tweezer **Flexi-Vio-Ph** with **DHN**.

#### 4.1.8 Probing applications: switching behaviour

The ‘real world’ application of tweezer-type receptors has been shown to be in healing materials, printing inks and potentially nano-scale memory (see Section 3.5). In all these systems introducing the ability of the tweezer receptor to complex and uncomplex from the

guest species on command would be an exciting feature. Viologens are known to display distinct redox processes which can be accessed by addition of base (such as triethylamine) to reduce the viologen cationic species to a radical species (see Chapter 1). Conceptually, the change in electronics between cationic and radical cationic species means it is no longer favourable to bind to a  $\pi$ -rich guest species and the tweezer complexation should uncomplex. Here we assessed the ability of switching behaviour between **Rigid-Vio-Ph** with **DHN** guest with a crude  $^1\text{H}$  NMR probing experiment (Figure 47).

Initially, the  $^1\text{H}$  NMR spectrum of guest species **DHN** was recorded (top spectrum), then one equivalent of host species Rigid-Vio-Ph was added, and the spectrum was re-recorded, displaying the shift in proton peaks of the guest ( $\Delta\delta = 0.12$  ppm compared to protons which correspond to **DHN** in top spectrum) upon complexation (middle spectrum). Then, a drop of triethylamine was added to the system and the  $^1\text{H}$  NMR recorded once again (bottom spectrum). The proton peaks that correspond to the tweezer motif become NMR silent when the species is reduced to the diradical dicationic form, and the resonances that correspond to the guest species essentially return to the chemical shift values observed in the uncomplexed species ( $\Delta\delta = 0.01$  ppm compared to protons which correspond to **DHN** in top spectrum) (top spectrum). This initial study confirms that this tweezer motif can be controllably un-complexed through the addition of a chemical stimuli, in this instance addition of base.

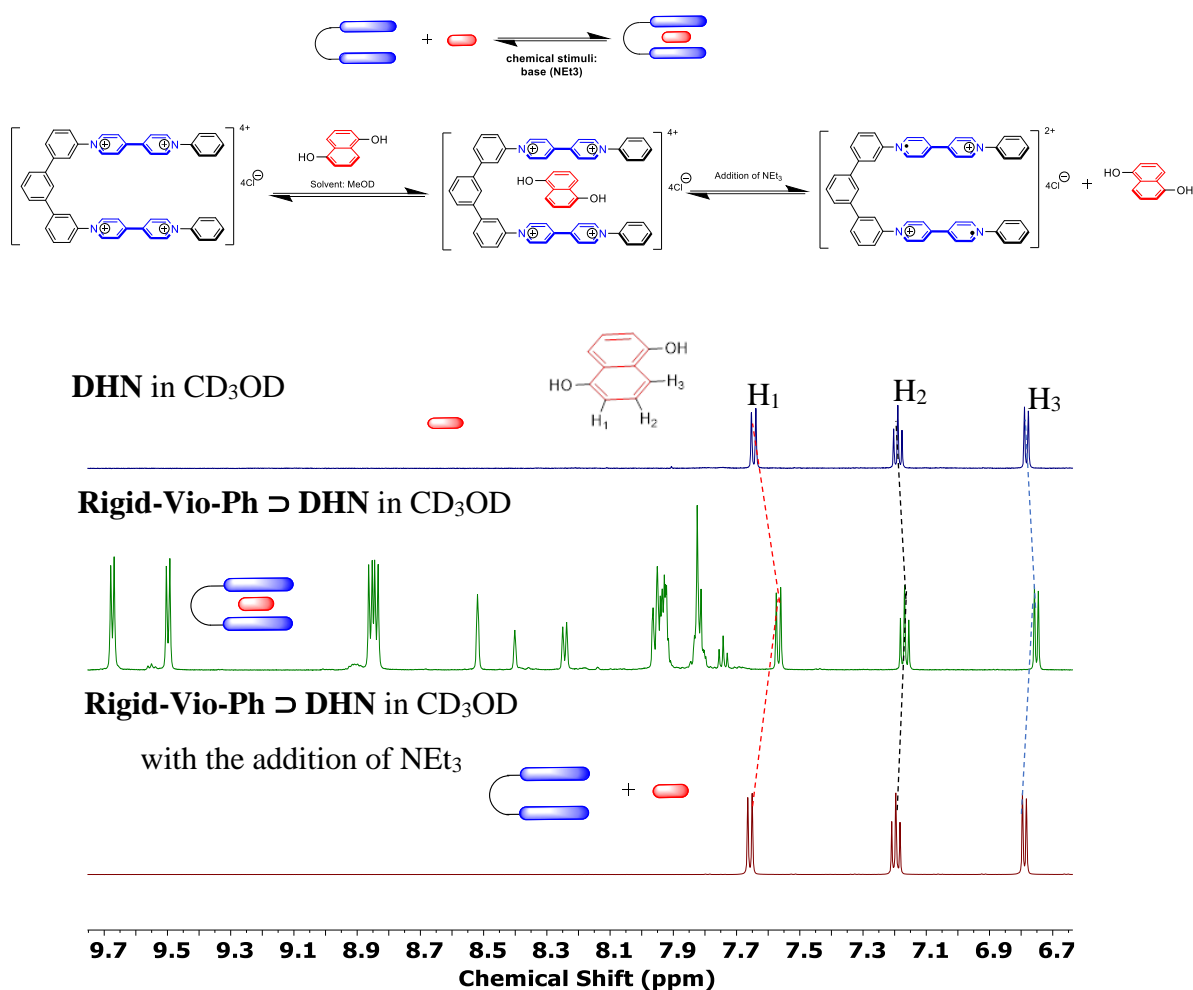


**Figure 47:** Partial  $^1\text{H}$  NMR (600 MHz) spectra used as a crude switching behaviour experiment. Free guest species **DHN** (top spectrum), 1:1 host **Rigid-Vio-Ph** and **DHN** (middle spectrum) and **Rigid-Vio-Ph**  $\supset$  **DHN** with the addition of triethylamine (bottom spectrum). All spectra recorded in  $\text{CD}_3\text{OD}$  at 298 K.

## 4.2 Conclusion

In this study we report an efficient synthesis of a range of six novel tweezer systems, each containing two,  $\pi$ -electron poor receptor sites. The molecular tweezers varied by the nature of the receptor side (viologen, PDI or NDI), linker residue (flexible or rigid) and steric size of the end group. All tweezers were found to form  $\pi$ - $\pi$  stacked complexes with  $\pi$ -electron rich guest species in a 1:1 stoichiometry over the concentration range studied. Analysis of the changes in

chemical shift of protons at different positions in the tweezer molecules between the complexed and un-complexed systems showed conclusively that the guest molecules were positioned in the cavity of the tweezer, with two face to face  $\pi$  -  $\pi$  stacking interactions. For tweezer compounds that contained the same  $\pi$ -electron poor species but varied by the nature of the linker (rigid vs flexible) or nature of the 'R' group, there was no consistent trend as to which system produced the complex with the highest binding constant. These results demonstrate the subtle interplay between pre-organisation facilitating complex formation over greater flexibility enabling the complex to achieve a more energetically favourable binding geometry. Lastly, we observe significant increases in binding constants for tweezer systems in aqueous solvent systems compared to the same components in organic solvents (e.g. **Rigid-Vio-Ph** $\supset$ **DHN**  $K_a = 204 \text{ M}^{-1}$  in  $\text{D}_2\text{O/TFA}$  and  $5.5 \text{ M}^{-1}$  in  $\text{MeOH/TFA}$ ).

All the chemistry in this chapter focuses on the synthesis and application of  $\pi$ -poor species with axial substitution, however there are a range of molecules with core substitution of the  $\pi$ -poor residue that has many valuable uses. Examples of these are given in the following chapter.

## **Section 3:**

**Literature and work towards  
palladium coupling reactions using  
high throughput optimization  
techniques and a vibratory ball mill.**

## **Chapter 5**

# **Introduction to the green synthesis of NDI containing molecules with potential for OPVCs**

# Chapter 5: Introduction to the green synthesis of NDI containing molecules with potential for OPVCs

This final section of the thesis (Chapters 5 to 7) describes the work towards the optimization of a new environmentally friendly solid-state synthesis of core functionalized NDI molecules which have potential applications in OPVCs. To place this in context, this chapter briefly describes the aims of green chemistry and types of green synthesis, with a particular focus of mechanochemistry, especially ball milling protocols. The benefits of ball milling are explored and the different available chemistries in the ball mill are looked into, specifically focussing on advances in palladium cross-coupling reactions and materials chemistry. A brief history of materials used in OPVCs is explored and why NDI is an attractive candidate within materials chemistry for OPVCs applications.

## 5.1 Green Chemistry

*Green Chemistry* as a concept was introduced to the scientific community in 1991 and can be defined as the “*design of chemical products and processes to reduce or eliminate the use and generation of hazardous substances.*”<sup>239</sup> It is clear that any chemical substance has the potential to possess hazardous properties, for example: toxicity (cause of cancer, mortal or other illnesses), physical hazards (explosive properties or flammability for example) or global hazards (climate change, overheating, decrease in ozone layer, etc)<sup>240</sup> and this concept aims to mitigate these. The 12 principles of green chemistry were developed by Paul Anastas and John

Warner in 1998 and outlines a framework for making a greener chemical, process, or product.<sup>241–243</sup> They include:

1. Prevention of waste
2. Atom economy
3. Less hazardous chemical syntheses
4. Design of safer chemicals
5. Safer solvents and auxiliaries
6. Design for energy efficiency
7. Promotion of the use of renewable raw materials
8. Design for degradation at the end of life
9. Use of selective catalysis
10. Reduce Derivatives
11. Real-time analysis for pollution prevention
12. Inherently safer chemistry

Moving away from traditional solvent-based chemistry processes is essential as these can use large volumes of solvents, many of which are by-products from the oil and gas industry, and have hazards such as low flash points, high flammability, toxicity, and atmospheric pollution.

## 5.2 Types of greener synthesis

Greener synthesis methods than solvent based synthesis methods that often require heating include mechanochemistry, microwave irradiation, photocatalysis, hydro(solvo)thermal, ultrasound-assisted (sonochemical) and magnet field-assisted synthesis.<sup>244,245</sup> This chapter will focus on mechanochemistry as a technique to reach synthetically valuable materials.

The origins of mechanochemistry began with the simple pestle and mortar, but the reaction success was dependant on the physical strength and endurance of the operator which led to reproducibility and scalability issues.<sup>244</sup> Nowadays mechanochemistry, which can be carried out using either a vibratory ball mill (VBM) or a planetary ball mill (PBM), is a powerful strategy for the rapid, clean, and environmentally friendly synthesis of compounds (Figure 48).

These are both batch techniques where the output of the reaction is produced in set quantities by a reaction which starts and stops. In contrast, extrusion techniques offer the possibility to produce materials in non-batch conditions, where the product can be continuously produced provided there's a continuous feed of starting reagents. The continuous variation of mechanochemistry is chemical extrusion. Chemical extrusion was identified by IUPAC as one of 10 world-changing technologies in 2019.<sup>246</sup>

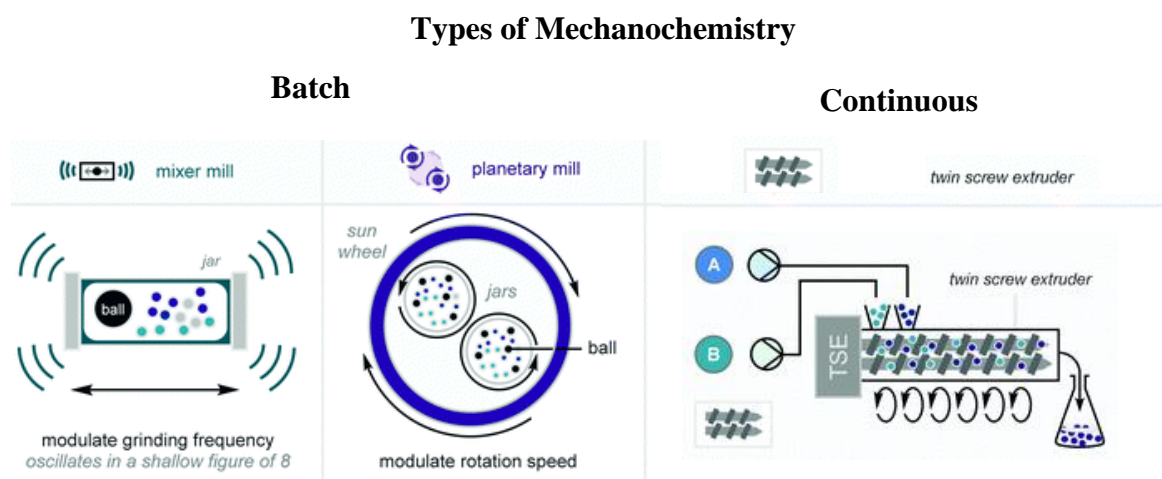


**Figure 48:** types of mechanochemistry; ball milling, planetary mill, extrusion.<sup>245,247</sup> taken from Browne *et al.* review

Ball milling is suited for smaller scale reactions (between a few milligrams to a few hundred milligrams) and functions by oscillating horizontally (in a shallow figure of 8 shape), two mass balanced milling jars at a chosen frequency. On the other hand, PBM is better suited for scales up to a few grams and operates by rotating around an orbit at the centre at a modulated rotation speed.<sup>248,249</sup> Drawbacks of ball-milling methods include the limited ability to control temperature and the difficulty in scaling up the technique. These can be negated by the mechanochemical technique: twin screw extrusion, which allows continuous solvent-less

milling in a temperature-controlled environment. Extruders involve solid reactants being added to a grinding chamber through a feeder (or feeders) and the material is blended until the product is formed *via* reactive extrusion (right in Figure 48).

In terms of molecular organic synthesis, extrusion techniques are still in their infancy, with the first example as recent as 2017 by Crawford and James.<sup>250</sup> The technique is more mature in the field of pharmaceutical formulation (though not synthesis) however, as exemplified by Nokhodchi's work with hot melt extrusion.<sup>251-254</sup>

Within VBM and PBM, the physical composition of the jar and grinding balls, among other parameters, can result in different type of particle fragmentation of the starting materials. These have been categorised into three types of fragmentation: abrasion, cleavage or fracture.<sup>255,256</sup> In ball milling, the material of the balls used as the grinding media, as well as the vessel, can be selected accordingly, dependent on the nature of the chemicals in the reaction. For example, if they are inorganic materials or acidic in nature.<sup>244</sup>

The James group have investigated how materials behave when they are mixed through computational studies to investigate the distribution of molecules when two different molecules are mixed together (For example, meloxicam and aspirin, red and blue particles respectively in Figure 49).<sup>257-259</sup> As the stages progress from 1 to 4, where 1 represents both molecules before collision, and stage 4 represents post-collision, the degree of mixing can visibly be seen in the simulation and particle distribution graph by the adhesion of particles on the surface of the opposite molecule. Stage 2 sees the molecules collide and upon separation in stage 3, residue of the opposite molecules can be seen on the opposite molecule. This simulation shows the process of mixing while the distribution graphs (left) displays the number of molecules combining upon collision.

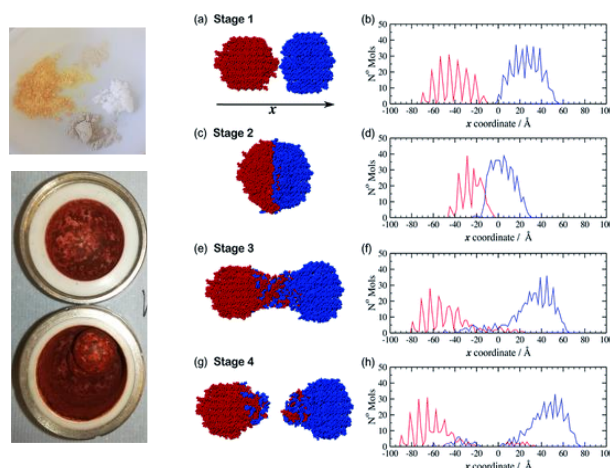


**Figure 49** : (left) photograph taken of starting reagents before and after milling within the following chapters in this work, turning from yellow to red; (middle) snapshots of a simulated indentation between spherical clusters of meloxicam (red) and aspirin (blue); (right) the distribution of molecules of meloxicam (red) and aspirin (blue) at stages 1, 2, 3 and 4. Figure adapted from published work by S. James *et al.*<sup>257</sup>

When designing a synthesis protocol using ball milling techniques there are a range of factors that can influence the reaction:

- i) The grinding media, composition, volume, density, or mass of the grinding balls.
- ii) The quantity of balls selected which governs the free volume in the vessel.
- iii) The volume of starting materials which affects the free volume.
- iv) The frequency of vibration.
- v) The addition of a grinding auxiliary/agent or a wetting agent (also known as a liquid assisted grinding (LAG)) to enhance and/or control reactivity.

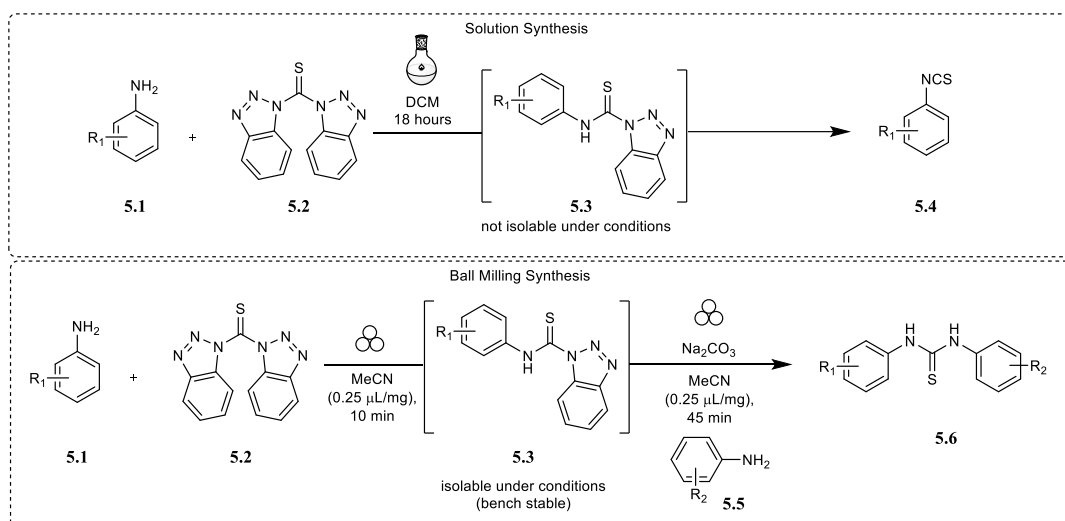
Each of these five factors affects the energy created during each collision. For example, a higher milling load means the vessel is more filled with material, this leads to less thermal energy in the systems due to dampening of the impact between the inner walls of the vessel and the balls, through absorption of the grinding stock.

As well as the environmental benefits associated with solvent free mechanochemistry, this technique has also been shown to have additional benefits over conventional solution state

techniques. For example mechanochemical promoted reactions have been shown to allow access to different chemical selectivity or chemical reactivities as well as promoting reactions between species that exhibit poor solubility in traditional solvents.<sup>260</sup>

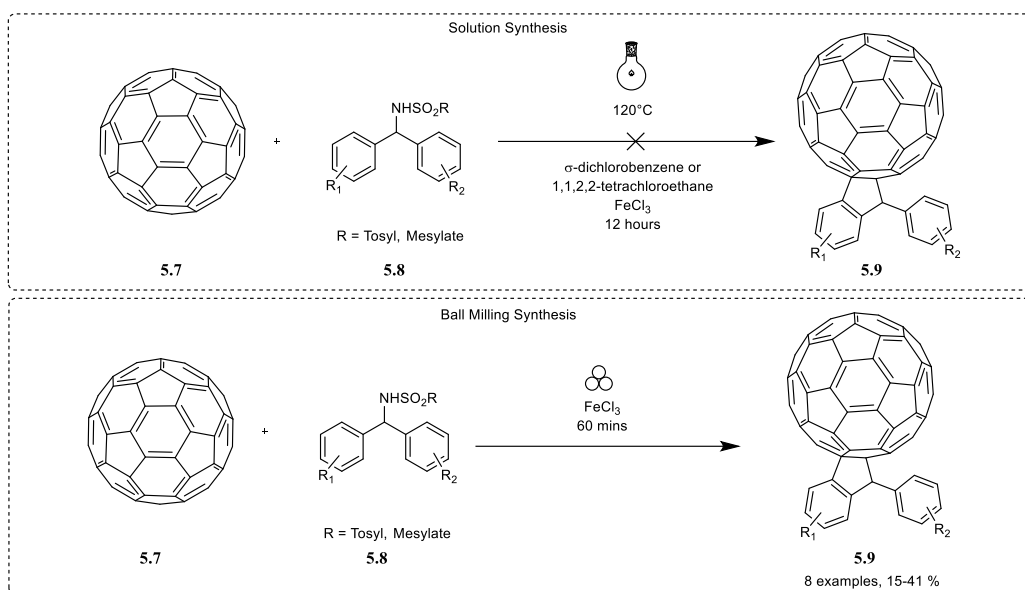
### 5.2.1 Controlling selectivity and reactivity of reactions using VBM

An example of novel chemical selectivity promoted by ball milling can be seen with the reaction of aniline (**5.1**) with bis(benzotriazolyl)methanethiones (**5.2**) (Scheme 28). In solution, **5.1** reacts with **5.2** to form the corresponding isothiocyanates (**5.4**) and benzotriazoles through intermediate N-(thiocarbamoyl) benzotriazoles (**5.3**).<sup>261,262</sup> Due to the high reactivity of **5.3** in solution, it is not isolatable using conventional solution chemistry. In 2015, Frišćić and co-workers reported the first isolation of **5.3** using mechanochemistry.<sup>263</sup> Excellent yields (>97%) of **5.3** were obtained by milling **5.1** with **5.2** within 10 minutes using acetonitrile as a LAG agent. Additionally, the isolated intermediate **5.3** was found to be bench stable in the solid state and could be used for the further synthesis of both symmetrical and non-symmetrical thioureas (**5.6**) with by the addition of anilines with varying structures (**5.5**). This example shows that ball milling can be exploited to isolate reactive intermediates not possible in solution, which can then be used to form different reaction products in the ball mill (thioureas) compared to solution (thioisocyanates) when reacted with a subsequent aniline in shorter reaction times.



**Scheme 28:** Reaction between anilines and bis(benzotriazolyl)methanethiones in the solution state compared to ball milling techniques where the isolation of intermediates is possible.<sup>263</sup>

As well as selectivity in the previous example, different reactivities and chemistries not successful in the solution state can be seen in the ball mill.<sup>244</sup> Also, the elimination of solvents in mechanochemistry means that low solubility reagents are not an issue. Low solubility starting materials and different reactivity compared to solution state is exemplified in this fullerene functionalisation (Scheme 29). Reported in 2013 by Wang and co-workers,<sup>264</sup> C<sub>60</sub>-fused indanes were attempted to be produced in solution using high boiling point solvents ( $\sigma$ -dichlorobenzene or 1,2,2,2-tetrachloroethane) for long reaction times (12 hours), but no reaction took place.<sup>264</sup> However, when attempted in the ball mill without any solvent and for 60 mins, 8 examples of C<sub>60</sub>-fused indanes were able to be synthesised (with yields varying from 15–41%) using ball milling.



**Scheme 29:** Reactivity differences for fullerene functionalization in solution vs. ball milling synthesis.  
264

Now that the parameters and benefits of mechanochemistry have been established above, the types of chemistry that can be carried out in the ball mill will be explored further below.

## 5.3 Types of chemistry carried out in the ball mill

Mechanochemistry is becoming an established methodology for carrying out a range of chemical reactions using little or no solvents; for example, in the synthesis of amino esters,<sup>265–267</sup> hydrazones,<sup>268</sup> peptides<sup>269</sup> and nitrones.<sup>270</sup> More recently, metal catalysed reactions such as 2022 Nobel prize winning<sup>271</sup> click chemistry,<sup>272</sup> activation of acyl azides<sup>273</sup> and couplings which include Suzuki,<sup>274,275</sup> Sonogashira (either containing copper<sup>276</sup> or copper free<sup>277,278</sup>), Negishi,<sup>279</sup> Mizoroki-Heck,<sup>280</sup> C-H coupling<sup>281</sup> and Buchwald-Hartwig aminations<sup>282–284</sup> have all been successfully carried out in a ball mill.

Metal catalysed cross-coupling reactions provide a versatile and reliable technique for the bond-formation between a sp<sup>2</sup>-hybridized aromatic halide (acting as an electrophile) and an

organometallic (nucleophile) using a metal catalyst. This can be used for the formation of a carbon-carbon or carbon-heteroatom bond. The ability to form C-C, C-O, C-P, C-S, C-B and C-N bonds<sup>285</sup> through cross-coupling reactions has resulted in applications through a wide breadth of fields. This includes applications in fields such as agrochemistry,<sup>286</sup> materials chemistry, natural product synthesis<sup>287</sup> and medicinal chemistry,<sup>288</sup> among others, due to the mild conditions associated with the reactions and their tolerance for a wide selection of functional groups.

Researchers Koji Kubota and Hajime Ito have developed a range of Palladium cross-coupling reactions *via* ball milling protocols using widely available bases and catalysts across a wide substrate scope. During optimisation studies, they found that the addition of 1,5-cyclooctadiene (1,5-cod) as a liquid-assisted grinding (LAG) agent led to increased yields in reactions on non-NDI derivatives. They postulated that this increased yield was as a consequence of decreasing the aggregation of the Pd catalyst.<sup>274,282</sup>

In particular, Palladium cross-coupling reactions have played a critical role in medicinal chemistry. The widespread study and success of cross-coupling reactions in medicinal chemistry is mainly due to the reliability and reproducibility of the reactions, which are extremely attractive to chemists in the structure optimisation phase of the process.<sup>288</sup> Within this field palladium catalysed cross coupling reactions become the go-to methodology for medicinal chemistry. As well as the advantages ball milling can offer in terms of greener synthesis, reliability, selectivity, reactivity and short reaction times, among other benefits, has led to a substantial body of research in ball milling within the medicinal chemistry sector.<sup>244,289,290</sup>

The lack of attention on solvent free synthesis for materials chemistry is more surprising as a consequence of the disparate scales of production between fine chemicals and materials such

as polymers. This is surprising because the European polymer demand has been estimated to be 61.8 million metric tonnes in 2018;<sup>291</sup> compared to total imports of pharmaceutical products in 2019 of 5.5 million tonnes.<sup>292</sup>

### 5.3.1 Early examples of conducting polymers *via* solid-state synthesis

The early examples of conductive polymers synthesised in the solid state (Figure 50) utilized manual grinding *via* a pestle and mortar. In 2002, Qu and co-workers<sup>293,294</sup> demonstrated the solid-state synthesis of doped polyaniline (**5.10**) by grinding frozen aniline at -20°C using a pestle and mortar for 30 minutes with inorganic acid H<sub>4</sub>SiW<sub>12</sub>O<sub>40</sub> (known as silicotungstic or tungstosilicic acid). The reaction was relatively simple but obvious drawbacks concerning the manual grinding aspect, reproducibility, scalability and general experiment conditions led to Kaner and *et al.* developing a ball milling protocol for the synthesis of **5.10**.<sup>295</sup> In their work, they studied the effect of other derivatised anilines and dopants on the conductive products and synthesised these using anilinium salts such as anilinium chloride and oxidants such as ammonium peroxydisulphate. Posudievsky and colleagues work followed, which showed that the molecular weight of **5.10** prepared by ball milling was comparable to using solution-based methods.<sup>111</sup>

The solid-state synthesis of other conducting polymers have also been reported. Takahara and co-workers utilized 3-hexylthiophene to synthesise poly(3-hexylthiophene) (P3HT, **5.11**) by manual grinding and subsequent aging for 24 h.<sup>296</sup> Aging polymers is a phenomena that involves molecular-level relaxation with time which effects the macroscopic physical properties, such as volume and enthalpy, of the polymer. Nurulla and colleagues<sup>297</sup> carried out manual grinding of terthiophene and FeCl<sub>3</sub> to yield poly(thiophene) derivatives (**5.12**). Later solid-state syntheses of **5.12** by Kumar *et al.* found that aging at elevated temps (100°C) led to

high molecular-weight polymers, whereas room temperature aging led to low-molecular weight products ( $M_n = 3000$  Da).<sup>298</sup> Finally, Poly(*o*-aminophenol) (**5.13**) has been produced using automated pestle and mortar grinder apparatus by the Zoromba lab group.<sup>299</sup>

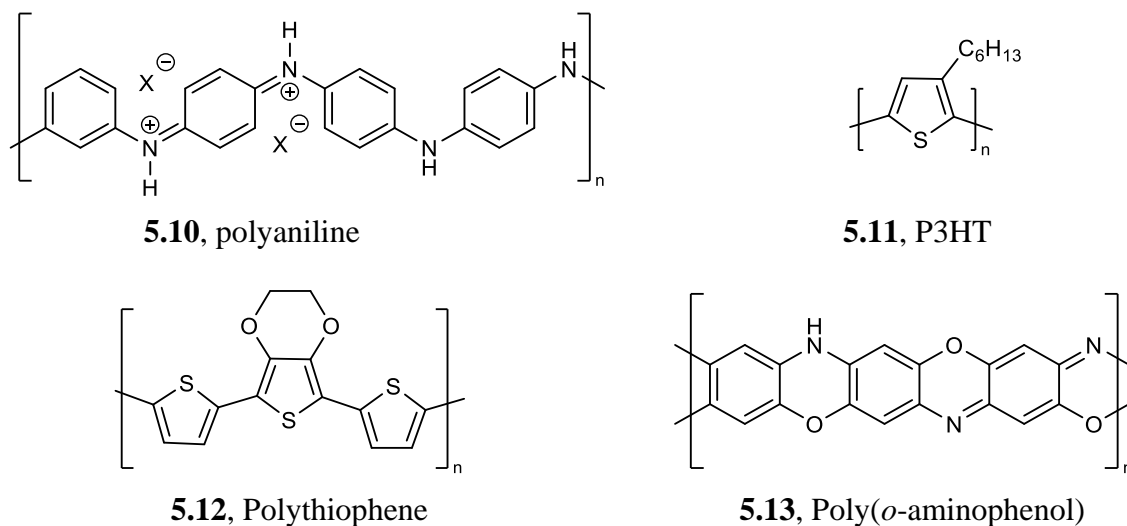


**Figure 50:** Examples of conductive polymers produced using solid-state synthesis techniques; Polyaniline, Poly(3-hexylthiophene), Polythiophene and Poly(*o*-aminophenol)

Selected examples of materials chemistry performed using mechanochemistry include (Figure 51) the VBM synthesis of poly(urethane)s by Wilson and co-workers (**5.16**),<sup>300</sup> in addition to cross-coupling reactions leading to the production of poly(phenylene vinylene)<sup>301</sup> (**5.15**) and poly(*para*-phenylene) polymers (**5.14**) *via* the Suzuki reaction.<sup>302</sup> This latter synthesis is particularly laudable for its use of palladium milling balls to generate the catalytic species *in situ*, rather than the addition of a specific molecular pre-catalyst.

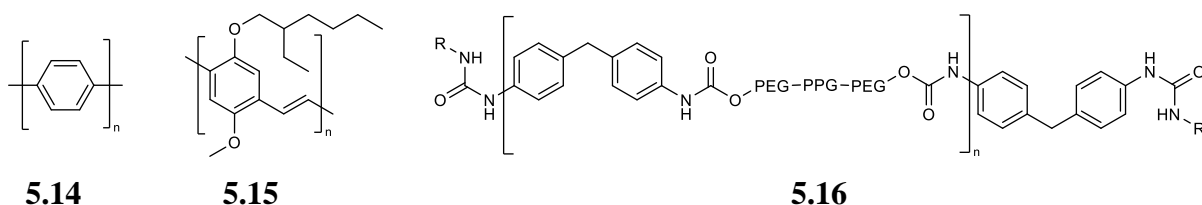


**Figure 51:** Examples of polymers produced in the ball; poly(*para*-phenylene) *via* the Suzuki reaction,<sup>302</sup> poly(phenylene vinylene)<sup>301</sup> poly(urethane)s<sup>300</sup>

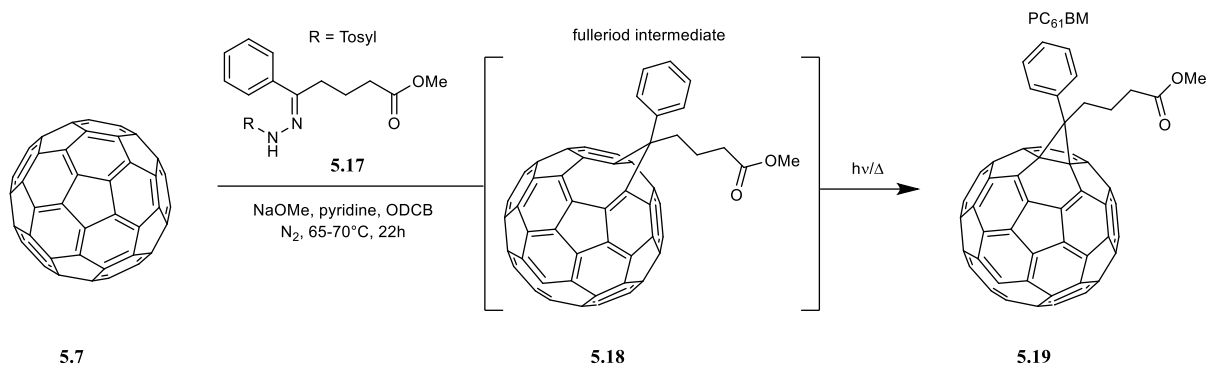
With respect to the materials chemistry, surprisingly, there are not any examples in the literature of photovoltaic materials synthesised using ball milling protocols. Not only are these materials extremely valuable and important in the development of green energy, but the current synthesis routes often frequently require harsh conditions and toxic solvents to be made.<sup>303</sup> The types of materials and synthesis routes of these materials used in organic photovoltaics (OPVCs) will be discussed in the next section.

## 5.4 Materials in Organic Photovoltaics

A description of the different types of solar cells and how they function is described in the introduction of this work (Chapter 1, Section 1.5). This section aims to discuss a few pertinent examples of materials used in OPVCs that are important to this work starting with molecular n-type molecules based on fullerene structures.

Buckminster Fullerene was first postulated in space in the 1970s, isolated at the University of Sussex in 1986 by Kroto and co-workers,<sup>304</sup> and their discovery leading to the Nobel Prize to Professors Richard E. Smalley, Robert F. Curl, Jr. and Sir Harry Kroto in 1996.<sup>305</sup>

Amongst their many useful properties, fullerenes were the first electron acceptor small molecules shown to have application in OPVCs.<sup>304</sup> Nowadays, bulk heterojunction fullerene-based OPVCs have been extensively researched, with fullerene derivatives of [6,6]-phenyl-C<sub>61</sub> (or C<sub>71</sub>)-butyric acid methyl ester (PC<sub>61</sub>BM<sup>306</sup> or PC<sub>71</sub>BM<sup>307</sup>) the most prolifically used acceptor materials. The general synthesis of PCBMs consists of two steps: firstly [2+1] cycloaddition to prepare the fulleroid **5.18** from C<sub>60</sub> **5.7** and 4-benzoylbutyrate *p*-tosylhydrazone **5.17**, followed by isomerization of **5.18** to PC<sub>61</sub>BM (**5.19**), under a nitrogen atmosphere (Scheme 30).<sup>306,308</sup>



**Scheme 30:** Synthesis of PC<sub>61</sub>BM. ODCB = 1,2-dichlorobenzene;

Fullerene-based electron acceptors were considered to be the best candidates in OPVCs because of their integral high electron mobilities and their ability to be incorporated into blended networks with donors, which is favourable for charge transport and separation.<sup>309</sup> The highest power conversion efficiency (PCEs) reached for these devices, under optimized conditions, were >8% for small molecule solar cells and as high as 11% for polymer solar cells.<sup>310–317</sup>

However, fullerene-based OPVCs actually have several drawbacks. These include limited energy-level tunability,<sup>318</sup> low access to functionalisation due to the fullerene structure, limited light-absorption properties<sup>319</sup> and photochemical instability.<sup>320</sup> Another issue that can occur derives from the synthesis of fullerene based OPVCs, which relies on the modifications of the fullerene structure. The modification is based on an addition reaction which causes a break in conjugation between the fullerene core and the attached aromatic unit which limits the red-shift of absorption approaching more to the visible/near infrared region. This, in turn causes the increase of energy levels of the highest occupied molecular orbital (HOMO) and decrease of the lowest unoccupied molecular orbital (LUMO), widening the energy gap of the n-type semiconductive material which leads to lower efficiency OPVCs.<sup>321</sup>

Furthermore, high purities are required for materials used in OPVCs, meaning that fullerene-based materials require purification using techniques such as silica gel chromatography (sometimes required multiple times) and HPLC.<sup>321</sup> This increases the processing time, price of

the materials, limits the output, and overall restricts the practical applications of these materials in large scale production of OPVCs.<sup>321</sup>

Due to these reasons, work towards non-fullerene acceptor containing organic small molecule and polymer electron acceptors has been developed. In contrast, small molecule and polymer-based materials offer the ability to be easily chemically modified and the HOMO-LUMO gap can be easily fine-tuned through the modification of the backbone or aromatic side-groups. The purification of organic small molecules can easily be carried out using traditional column chromatography on silica gel and can be done on a large scale, at low cost. Moreover, a crucial advantage in non-fullerene acceptor materials like organic small molecules and polymers is the increased control of the solution viscosity. This is an important factor for the solution processing of large scale OPVCs.<sup>322,323</sup>

The need for non-fullerene based small molecules and polymers as electron acceptors to replace fullerene derivatives in OPVCs is great. There are two main types that are most widely studied in the literature; rylene tetracarboxylic diimide and fused-ring acceptors.<sup>324</sup>

Fused ring acceptors are composed of a planar  $\pi$  bridge containing fused rings that are substituted with aryl or alkyl side chains that are orientated above or below the plane, between two strongly  $\pi$ -electron-withdrawing moieties.<sup>325</sup> They exhibit similar long-wavelength absorptions and comparable electron affinities to fullerene-based acceptors.

An indacenodithiophene (**5.20** in Figure 52) core is the most popular choice and modification of this fused ring core can be used to alter the electron affinity, ionization energy and absorption wavelength of the system. This can be achieved by addition of electron donating groups to the core. Select examples of modified cores (Figure 52) include thieno[3,2-*b*]-thiophene containing (**5.21**), expanded core through insertion of thiophene units (**5.22**) and star-shaped with a benzo[1,2-*b*:3,4-*b'*:5,6-*b''*]trithiophene-based core (**5.23**). Electron withdrawing 3-(1,1-Dicyanomethylene)-1-indanone (**24b**) is a typical end group in fused-ring acceptor-based materials.

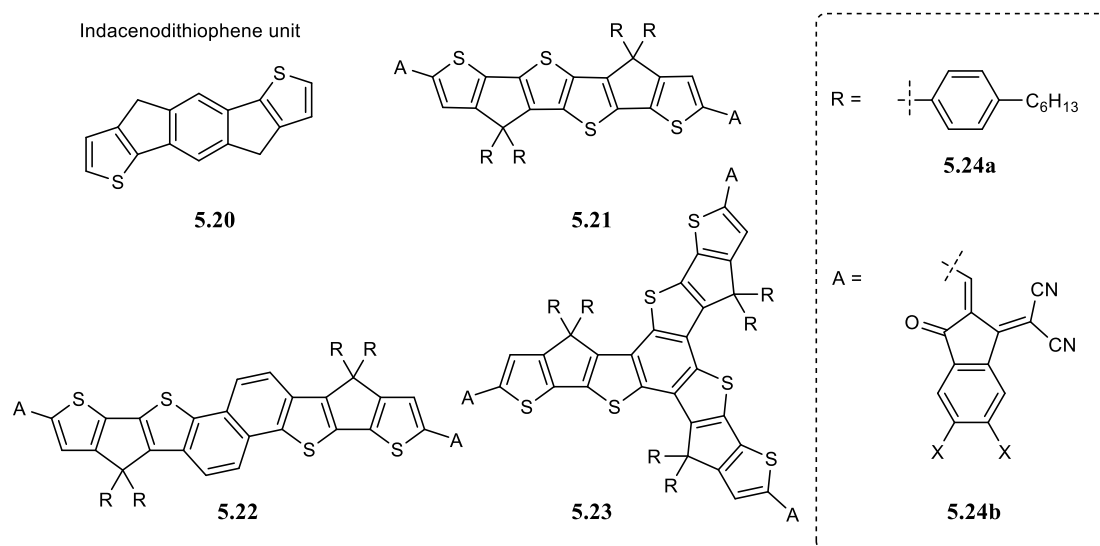


**Figure 52:** Examples of non-fullerene containing fused ring acceptors

The second type of non-fullerene containing acceptor small-based molecules are rylene tetracarboxylic diimides. These are composed of an aromatic core with two electron withdrawing dicarboxylic imide end groups. The typical structures researched in this class of compound are shown in Figure 53 and include Pyromellitic (**5.25**), 1,4,5,8-Naphthalene (NDI, **5.26**), 1,2,5,6-Naphthalene (**5.27**), Perylene (PyDI, **5.28**) and Coronene (**5.29**) diimide derivatives. NDI and PyDI species are the most commonly researched owing to their increased electron deficient core compared to **5.25** as well as more established synthesis and modification of the core routes compared to **5.27** and **5.29**. They are promising candidates due to their

relatively high charge carrier mobilities and electron affinities, self-assembling properties and excellent thermal, photochemical, and chemical stabilities.<sup>326,327</sup>

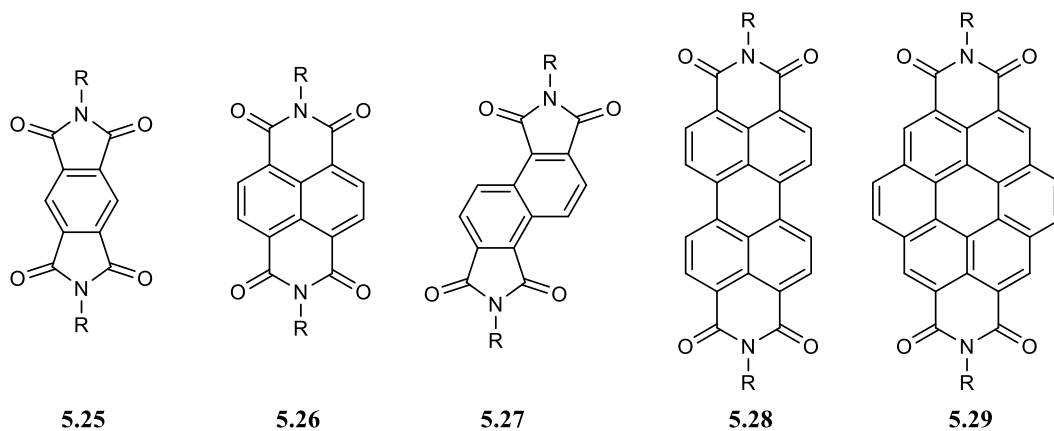


**Figure 53:** Rylene tetracarboxylic diimides as fullerene alternatives

PyDI examples are shown in Figure 54 and include: Small molecule core functionalized PyDI **5.32**, PyDI dimer (**5.30**) and PyDI containing polymer along the axial backbone (**5.31**). Small molecule acceptor dimer species which contain NDI acceptor (A) and thiophene derivatives donor (D) units arranged in an A-D-A composition (**5.34** and **5.35**) have been shown to have application in OPVCs.<sup>328,329</sup> Further, PyDI and NDI co-polymers (**5.33** and **5.36**), containing functional groups such as carbazoles<sup>330,331</sup> or thiophene derivatives<sup>332</sup> respectively have been employed in organic electronics as acceptor materials. OPVCs based on such NDI polymer acceptors exhibit some of the highest known PCE values for all-polymer solar cells.<sup>333</sup>

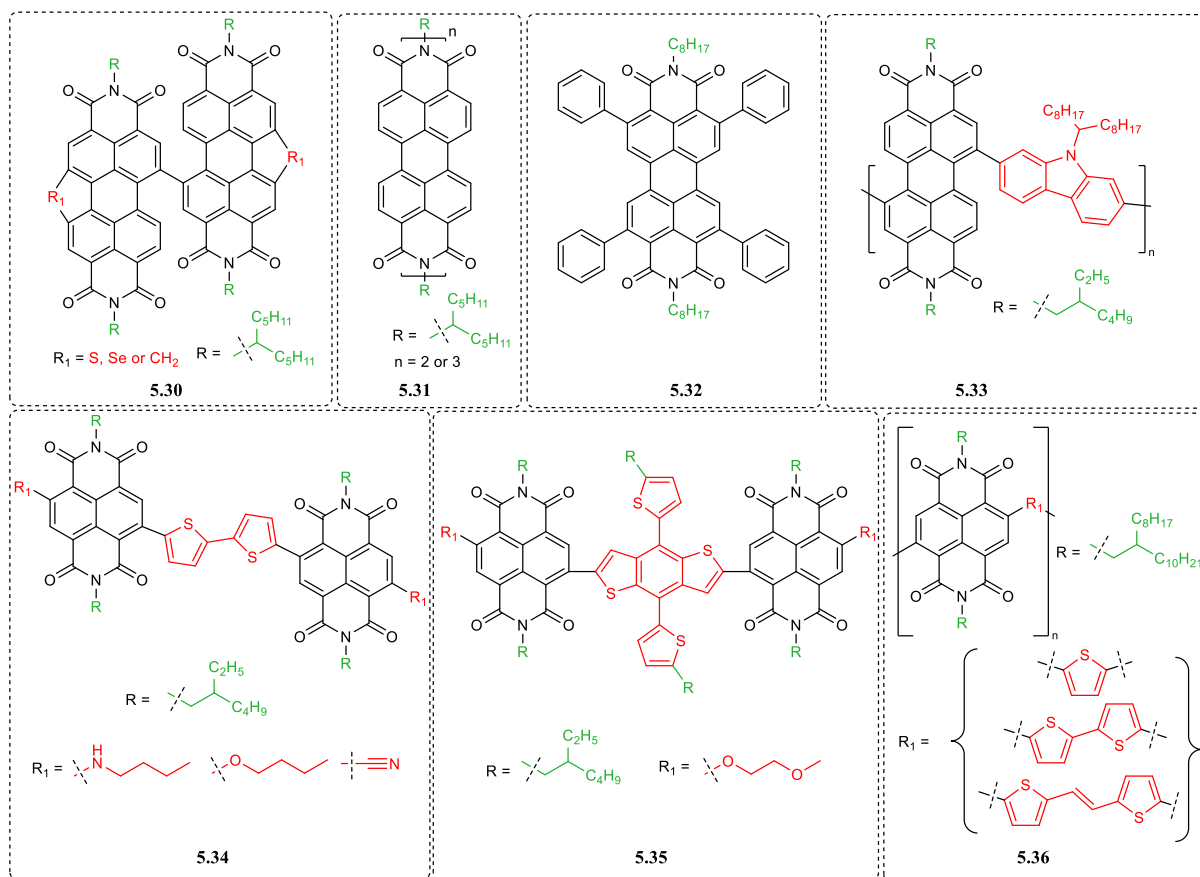


**Figure 54:** Examples of common PyDI and NDI acceptors used in OPVCs.

The strategies to prepare core substituted NDIs described above involve either Stille coupling (5.34, 5.35 and 5.36) between thiophene derivative containing tin based reagents, Suzuki coupling with carbazole derivative containing pinacol boronic acids (5.33) or aromatic boronic acid (5.32), with halogen substituted the respective rylene diimide core.

## 5.5 Solid state synthesis of NDIs

To date, only Kumar and Mukhopadhyay have produced functionalized NDIs using mechanochemical means.<sup>334</sup> However, their VBM synthesis generated C-P bonds to give di-phosphonium substituted radical ions  $[\text{NDI}(\text{PR}_3)_2]^+\text{Br}^-$ , rather than producing new C-C bonds at the core of the NDI species (left in Figure 55). James and co-workers, have examined the

axial (not core) functionalisation of mono naphthalene anhydrides and perylene dianhydride via VBM and extrusion techniques (right in Figure 55).

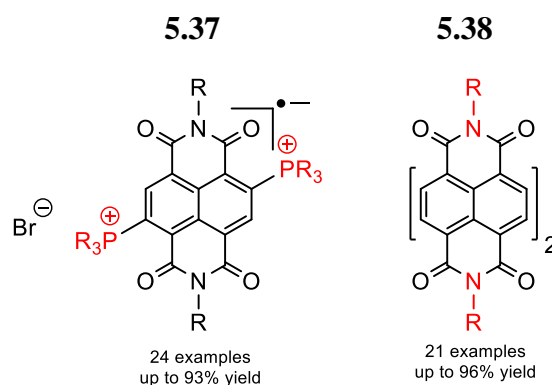


**Figure 55:** Solid state synthesis of NDIs

## 5.6 Conclusion

In conclusion this brief literature exploration has highlighted how green chemistry, particularly ball milling protocols are becoming an established method for the synthesis of cross coupled small molecules, with a large volume of published work focussed on small molecules within the medicinal sector. However, this synthesis methodology has great potential in materials chemistry, as shown by seminal examples of polymer synthesis by Swager<sup>301</sup> and Wilson.<sup>300</sup> Due to the intrinsic issues associated with fullerene based acceptors, Rylene diimides, specifically NDIs, have been shown to be a promising solution as small molecule n-type semiconductive materials in OPVCs. The potential to incorporate NDIs into polymers also provides exciting pathways to electron accepting materials with increased EA in OPVCs.

Robust solution state methodologies of core functionalisation of NDIs are documented in the literature and gives a good starting point for initial conditions to attempt. The synthesis of c-NDIs is reported in solution-based chemistry using Suzuki,<sup>335</sup> copper facilitated Sonogashira<sup>336–338</sup> and Buchwald-Hartwig<sup>339–341</sup> couplings. These processes often necessitate long reaction

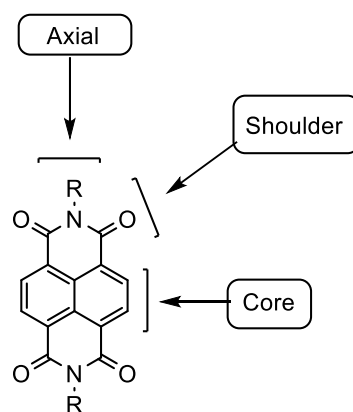
times (e.g. 18 hours),<sup>335</sup> high temperatures (typically solvents at reflux, particularly toxic chlorinated or flammable aromatic solvents), strict anaerobic conditions, employing glove boxes and Schlenk line techniques. Sometimes, they also require light to be excluded.<sup>335</sup> This provides further scope to optimize cross-coupling reactions on cNDIs and the potential to incorporate green synthesis techniques, like ball milling, into the production of these materials.

## **Chapter 6**

# **Scoping conditions for the synthesis of c-NDI coupling reactions**

# Chapter 6: Scoping conditions for the synthesis of c-NDI cross coupling reactions

There are three ways to functionalize an NDI unit, by modification at the axial, shoulder, or core positions (Figure 56).



R = H, alkyl or aryl group

**Figure 56:** NDI unit displaying the three main areas of functionalization at the axial, shoulder and core positions.

Here, we have initiated a research programme to synthesise core-functionalised naphthalene diimide species (c-NDIs) which have well established applications in organic electronics,<sup>326</sup> organic rechargeable batteries,<sup>342</sup> solar cell technology<sup>343</sup> and artificial photosynthesis.<sup>344</sup> In each of these applications, core functionalization<sup>345</sup> is the key synthetic step in order to tune the electronic properties of the resulting molecules, by the manipulation of the energy levels of the conjugated system. This is especially important because unsubstituted NDIs show relatively limited absorption in the visible region, which make them unattractive candidates for use in organic electronics.

The synthesis of c-NDIs is reported in solution-based chemistry using Suzuki,<sup>335</sup> copper facilitated Sonogashira<sup>336–338</sup> and Buchwald-Hartwig<sup>339–341</sup> couplings. These processes often necessitate long reaction times (e.g. 18 hours), high temperatures (typically solvents at reflux, particularly toxic chlorinated or flammable aromatic solvents), strict anaerobic conditions, employing glove boxes and Schlenk line techniques. Sometimes, they also require light to be excluded.<sup>335</sup> This chapter will focus on the optimization of the synthesis of c-NDIs in the solution state, specifically using high-throughput techniques to screen a range of variables, and explore if these conditions can be transferred into the solid state.

## 6.1 Results and discussion

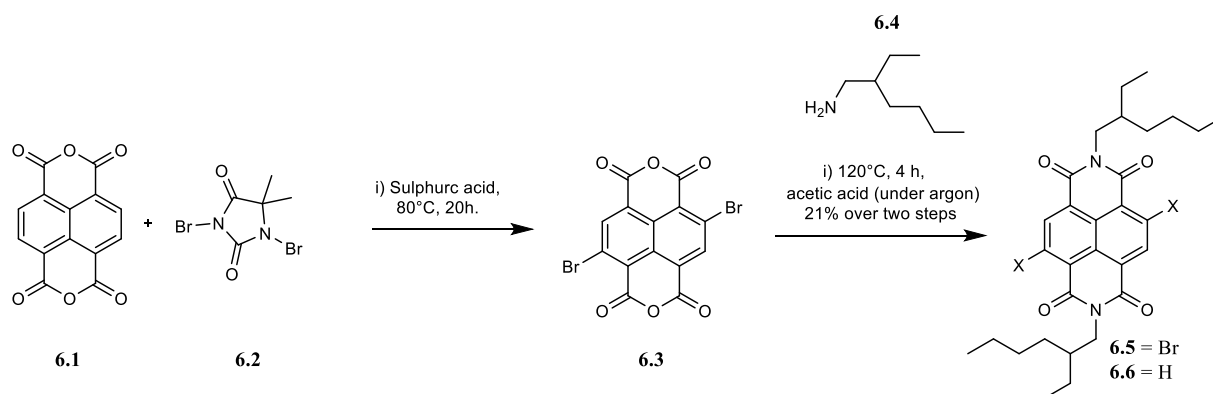
### 6.1.1 Bulk synthesis of starting reagents

Extension of the aromaticity within the NDI core is the simplest method to tune the energy levels of the molecule. This can be achieved by the reaction of halogenated NDI species, with appropriate coupling partners in the presence of a base and palladium catalyst. Therefore, a bulk quantity of di-brominated NDI was required to commence this project, which could be accessed using conditions that are well known in the literature (Scheme 31).<sup>346,347</sup>

Briefly, the synthesis of N,N'-bis(2-ethylhexyl)-2,6-dibromo-1,4,5,8-naphthalene tetracarboxylic acid, (Br<sub>2</sub>-NDI, **6.6**) was achieved over two steps. Firstly, 2,6-dibromo-1,4,5,8-naphthalene tetracarboxylic acid (Br<sub>2</sub>-NDA, **6.3**) was synthesised by following a modified literature procedure<sup>346</sup> by bromination of commercially available naphthalenetetracarboxylic acid (NDA, **6.1**) by 5,5-dimethyl-1,3-dibromohydantoin (**6.2**) in gently heated sulphuric acid to yield crude Br<sub>2</sub>-NDA **6.3**. After a simple work up of precipitation on ice and collection on a fine frit under vacuum, a mixture of NDA-Br<sub>2</sub> **6.3** and NDA starting material **6.1** in a 32:68

ratio was observed (calculated from  $^1\text{H}$  NMR data by integration of the signals at  $\delta = 8.79$  ppm : 8.71 ppm<sup>346,347</sup>). The crude product was used in the next step of synthesis without purification due to its poor solubility.

Imidization<sup>347</sup> was achieved by heating **6.3** with primary amine **6.4** at high temperatures in acetic acid.



**Scheme 31:** Synthesis of NDI-Br<sub>2</sub> **6.6** from the commercially available NDA **6.1**.

In contrast to using the time consuming and relatively unscalable purification of column chromatography described in the literature, samples of **6.5** pure enough for further reactions were readily isolated by washing procedures outlined in Figure 57. Initially, the crude orange solid from the reaction to form **6.3** which contained a mixture of diimides was washed on a fine sinter with water (300 mL), MeOH (500 mL) where red washings were observed, and finally hexane (1 L) where orange washings were observed. Photographs below show the washing process on the bulk synthesis. The crude product was then precipitated by dissolving in the minimum volume of hot  $\text{CHCl}_3$  and slowly pouring into hexane at  $0^\circ\text{C}$  – right in Figure 57. This yielded 25 g of 90:10 ratio of **6.5:6.6** (measured *via*  $^1\text{H}$  NMR). This was purified further by a recrystallization over two weeks in DCM, where it was transferred to the fridge after one week, to yield pure product suitable for cross coupling reactions as a yellow fluffy needle-like crystalline solid (15 g).

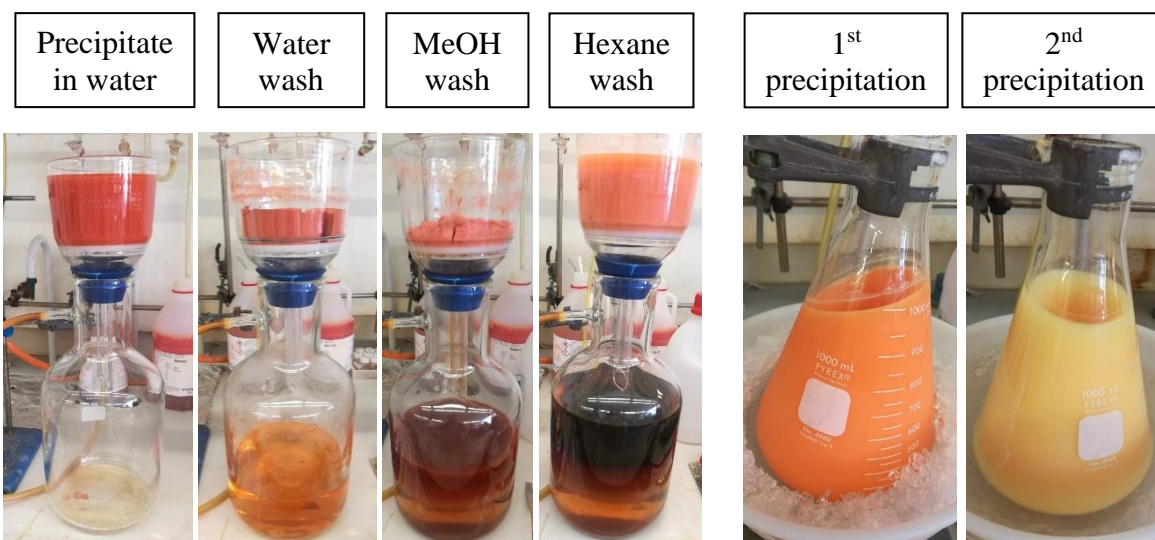


**Figure 57:** Photographs showing the purification of Br<sub>2</sub>-NDI

The <sup>1</sup>H NMR spectrum of the pure Br<sub>2</sub>-NDI **6.5** is shown below with appropriate proton environments assigned (Figure 58). The addition of ethyl hexyl axial functional groups resulted in increased solubility of the compound compared to the intermediate **6.3**, where the <sup>1</sup>H NMR could now be recorded in common deuterated solvents (e.g. CDCl<sub>3</sub>). The product is confirmed by the signals consistent with both the CH<sub>2</sub> next to the imide and alkyl proton environments at 4.15 ppm and between 1-2 ppm respectively. The integration of the aromatic NDI protons at 9.00 ppm is halved to two compared to un-brominated variants without substitution at the core.

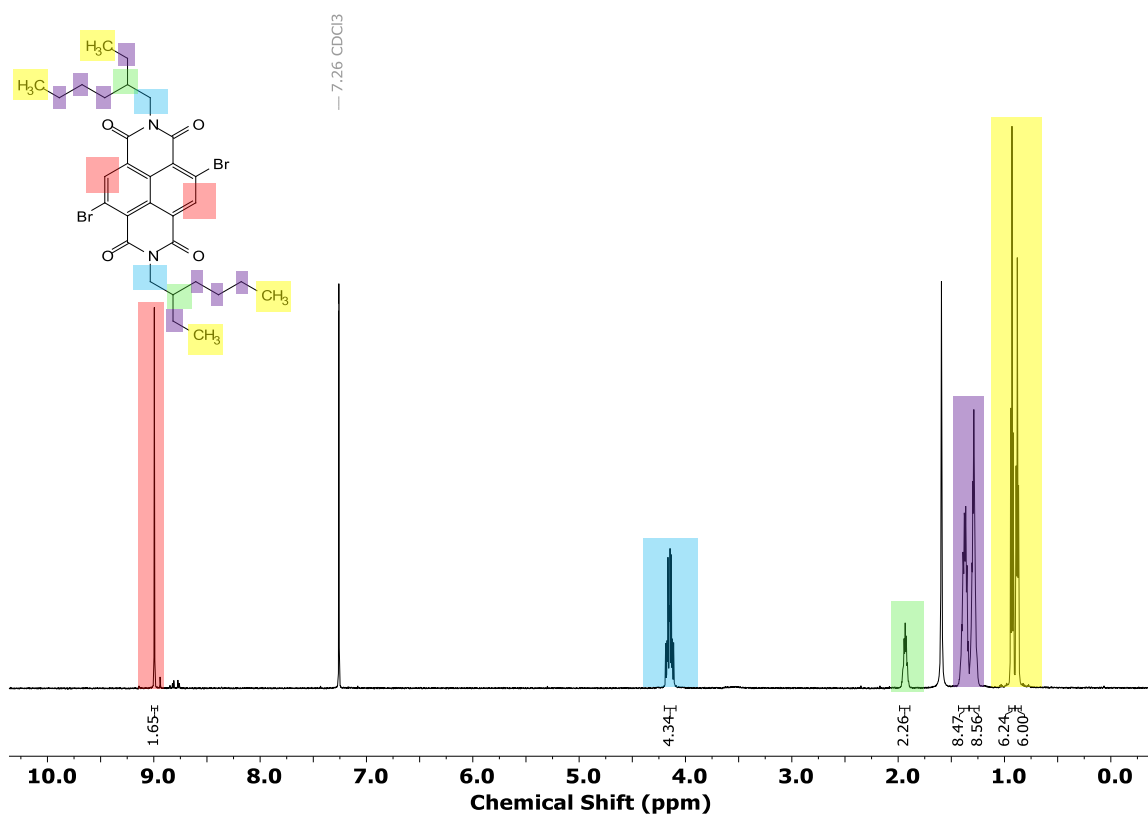
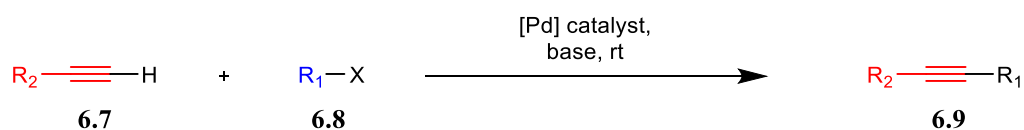


**Figure 58:** Full  $^1\text{H}$  NMR (600MHz) of  $\text{Br}_2\text{-NDI}$  with appropriate proton assignment. Recorded at 298K in  $\text{CDCl}_3$ .

With a large quantity of pure dibrominated starting reagent synthesised, work could now focus on the cross-coupling chemistries available. The following sections in this chapter discuss the initial solid-state attempts and solution state optimization of Sonogashira and Suzuki cross couplings, as well as Buchwald-Hartwig amination reactions involving **6.5**.

### 6.1.2 Sonogashira Cross-Coupling

$\text{C}(\text{sp}^2)\text{-C}(\text{sp})$  bonds (**6.9**) can be formed *via* the Sonogashira coupling of terminal acetylenes (**6.7**) and aryl halides (**6.8**) (Scheme 32), in the presence of a palladium catalyst, a base and sometimes a copper co-catalyst.



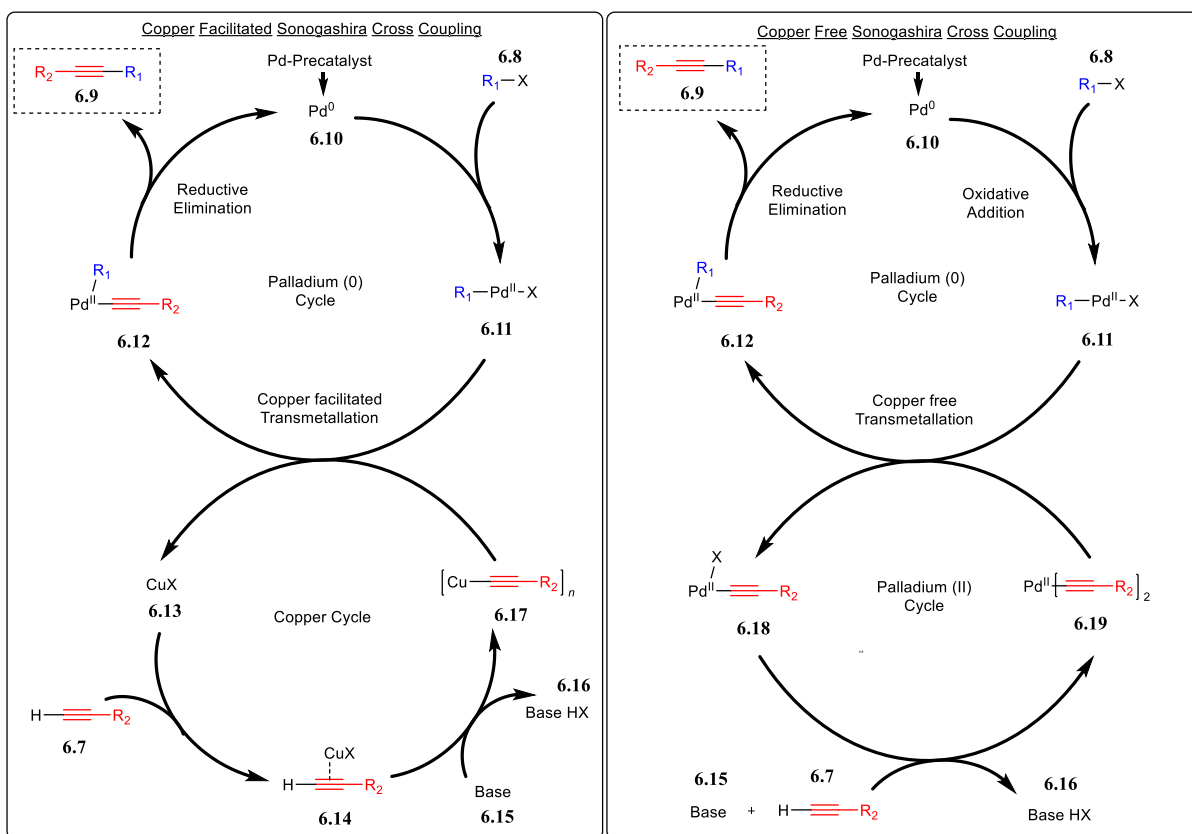
**Scheme 32:** Typical conditions for a Sonogashira coupling reaction.

There are two types of Sonogashira cross coupling; copper facilitated<sup>348</sup> and copper free.<sup>349,350</sup> The mechanisms of how these both proceed are detailed below (Scheme 33). Briefly, for both catalytic cycles the palladium pre-catalyst species is activated to form the reactive Pd(0) species **6.10**. The reactive Pd(0) species then facilitates an oxidative addition reaction with an aryl halide (in our case **6.8** is equivalent to Br<sub>2</sub>-NDI) to produce Pd(II) species **6.11**. The orientation of **6.11** is dependent on the substrates involved and this is thought to be the rate limiting step in the reaction.

In the copper facilitated coupling, **6.11** then reacts with copper acetylide species **6.17**, generated from the copper cycle (steps **6.13** to **6.17**), in the transmetallation step, yielding **6.12** and subsequently regenerating the copper catalyst in the process. On the other hand, in the copper free coupling variation of the Sonogashira coupling, the acetylene is activated through an additional Pd cycle. It has been shown<sup>349</sup> that both Pd monoacetylide species **6.18** and Pd bisacetylide species **6.19** are formed but only the activated species **6.19** facilitates the transmetallation step, forming **6.12** and regenerating **6.18**.

Both copper facilitated and copper free Sonogashira coupling reactions then undergo a reductive elimination reaction of **6.12** to form the desired disubstituted alkyne product **6.7**, regenerating the Pd(0) species in the process. This step is dependent on the cis-orientation of R<sub>1</sub> and R<sub>2</sub> in **6.12**.

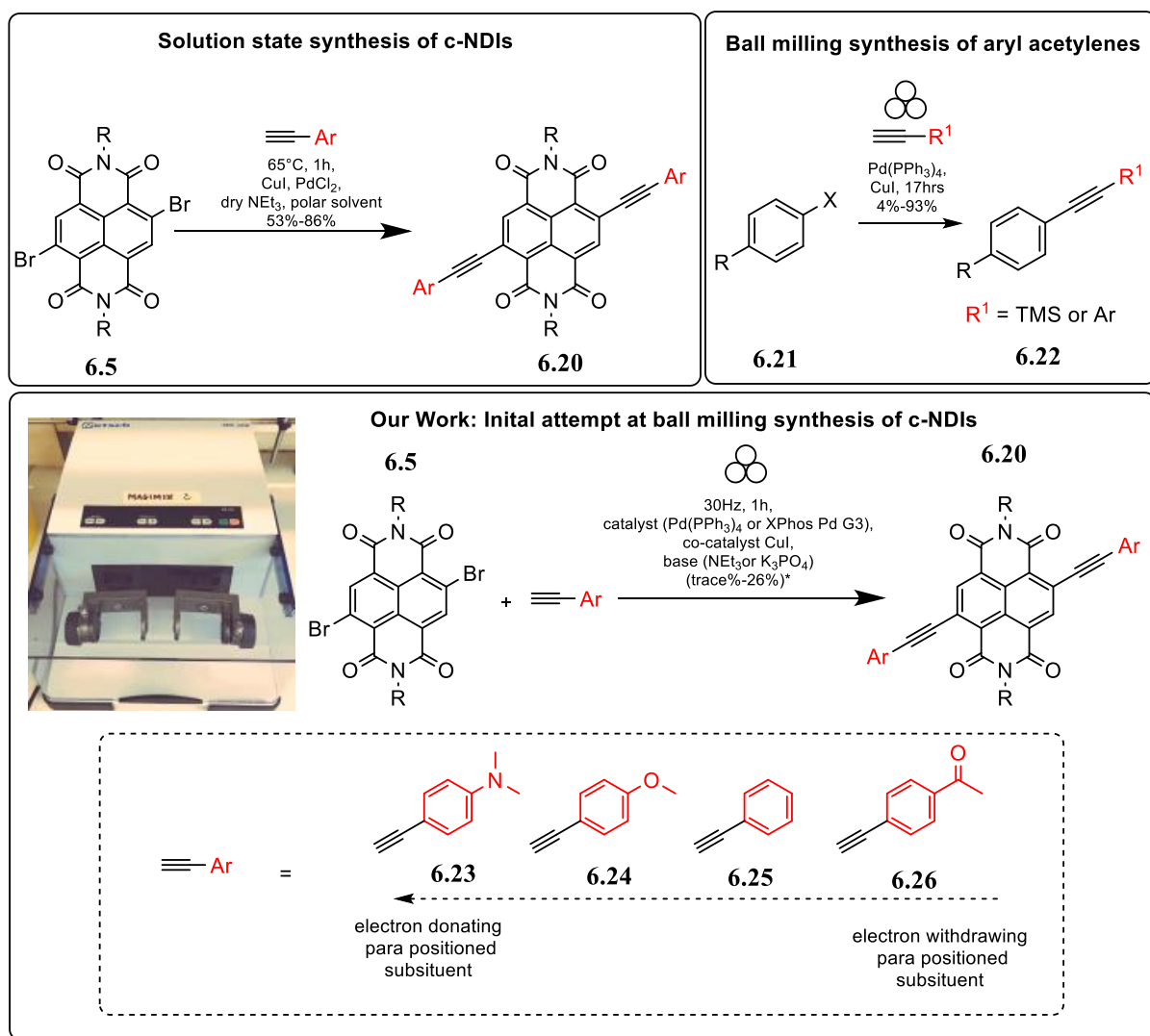
Inert reaction conditions are usually required in Sonogashira coupling reactions as the Pd(0) species is unstable in air.<sup>348</sup> Further, the presence of oxygen in the reaction promotes the formation of unwanted by-products, namely homocoupled acetylene species.



**Scheme 33:** Mechanism for the copper facilitated (left) and copper-free (right) Sonogashira cross coupling reaction. Ligands are omitted for clarity.

We were seeking to find a robust green synthesis route to produce *c*-NDIs *via* Sonogashira coupling which would be tolerant to a range of aryl acetylenes. Therefore, we selected suitable conditions based on solution state synthesis conditions for *c*-NDIs<sup>351</sup> and ball milling protocols of general aryl acetylenes<sup>276</sup> (Scheme 34). For literature ball mill Sonogashira coupling, an iodine containing halide (iodo-benzene **6.21**) with higher reactivity than other aryl halides was used (top right in Scheme 34).

Initial scoping work in our group carried by Dr. Guest ascertained that  $K_3PO_4$  and XPhos Pd G3 worked for the Suzuki coupling of *c*-NDIs in the ball mill as the base and catalyst respectively (top left in Scheme 34), so become the initial choice in this Sonogashira coupling. (bottom in Scheme 34).



**Scheme 34:** (Top left) Solution state synthesis of c-NDIs. (Top Right) ball mill protocols of aryl acetylenes. (Bottom) our work: initial attempt at ball milling synthesis of c-NDIs. \* = yields calculated from  $^1\text{H}$  NMR monitoring

We selected four aryl acetylenes which varied by the electron donating/withdrawing ability of the para substituent with select examples including phenyl, para substituted methoxy, acetyl, and dimethyl N containing acetylenes (**6.23** to **6.26** in Scheme 34). All reactions were carried out at room temperature under bench-top conditions (i.e. without the exclusion of air or moisture).

Further, all ball milling reactions in this thesis were carried out with identical composition of the grinding jar and quantity of balls; zirconium oxide jars and two 15 mm  $\text{ZrO}_2$  milling balls

respectively. The ball milling was operated at 30 Hz for 1 hour with the following reagents per reaction: Br<sub>2</sub>-NDI (100 mg), aryl acetylene of choice (3 equiv.) catalyst (10 mol %), co-catalyst (5 mol %) and base (4 equiv.). Work up involved recording the crude <sup>1</sup>H NMR in CDCl<sub>3</sub> upon completion of milling to assess whether any reaction had occurred.

For example, the reaction between Br<sub>2</sub>-NDI and phenyl acetylene with catalyst and base choice of XPhos Pd G3 and K<sub>3</sub>PO<sub>4</sub> respectively, displayed only a low conversion to desired c-NDI **6.28** (21%, calculated by integration of aromatic protons within the starting material compared to product, shown in partial <sup>1</sup>H NMR spectra, Figure 59 below). Interestingly, Sonogashira coupling with para *N,N*-dimethyl substituent resulted in what appeared to be exclusively the mono substituted c-NDI **6.27**, albeit still in a moderate yield (42%, shown by the two inequivalent signals in the aromatic region of the spectrum, middle spectra in Figure 59). The presence of any remaining NDI-Br<sub>2</sub> starting material **6.5** can be seen clearly in the aromatic proton region (9.00 ppm) when crude reaction NMR spectra are stacked against the starting reagent spectra (Figure 59).

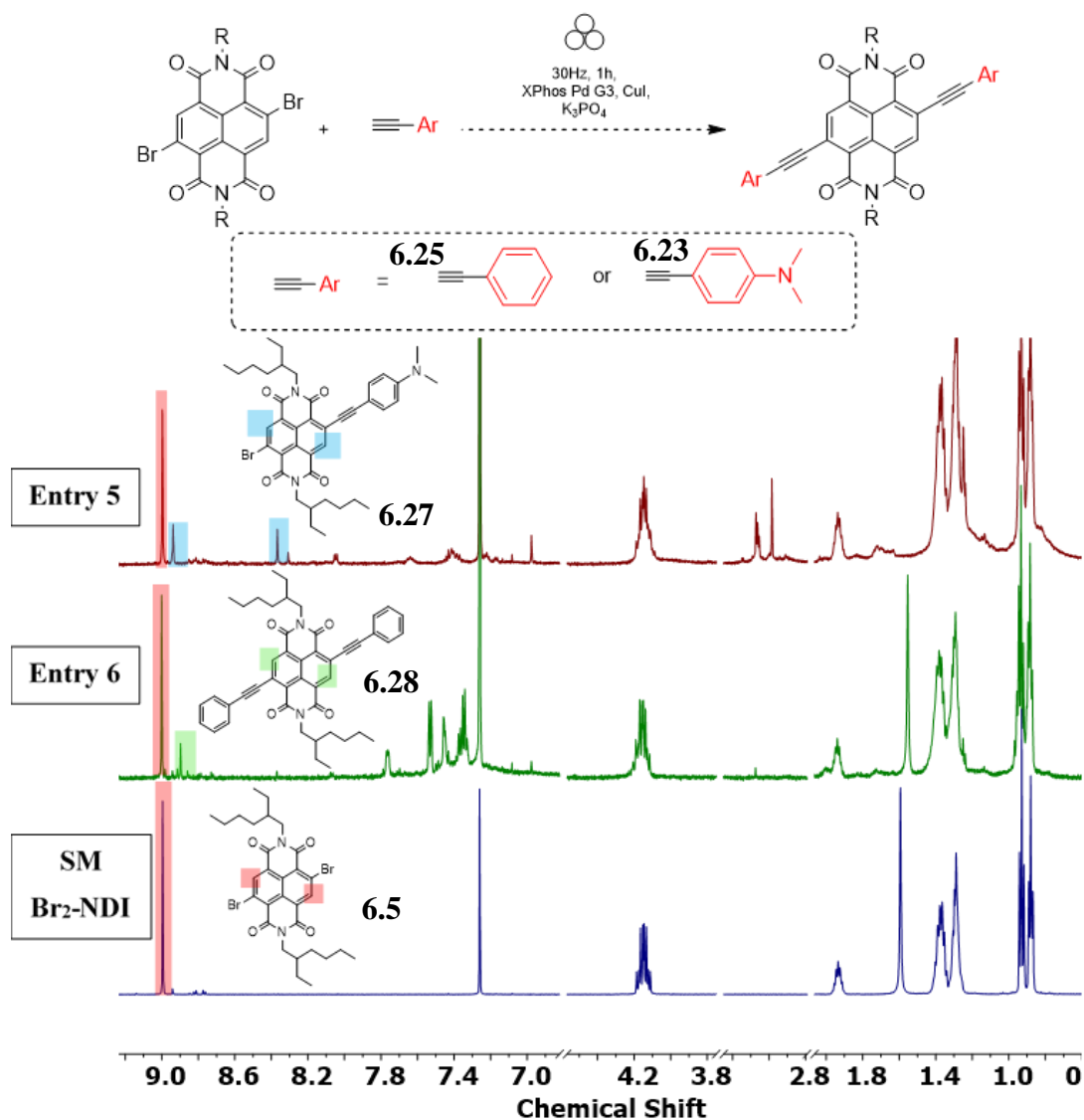


**Figure 59:** Partial <sup>1</sup>H NMR spectra for entry 5 and 6 stacked with starting material spectrum

*Para* substituted methoxy and acetyl acetylene also yielded low conversions to desired c-NDI with these conditions (3 % and 7 % respectively). In an attempt to increase conversion, a stronger liquid base, triethylamine, and a more active catalyst (Pd(PPh<sub>3</sub>)<sub>4</sub>) were selected and attempted with these two low yielding reactions. For *para* substituted methoxy, the conversion to c-NDI **6.30** did increase to 26% however the major product observed in the NMR appeared to correspond to the mono substituted c-NDI **6.29**, with the two aromatic protons from the asymmetric compound highlighted in blue (Figure 60).

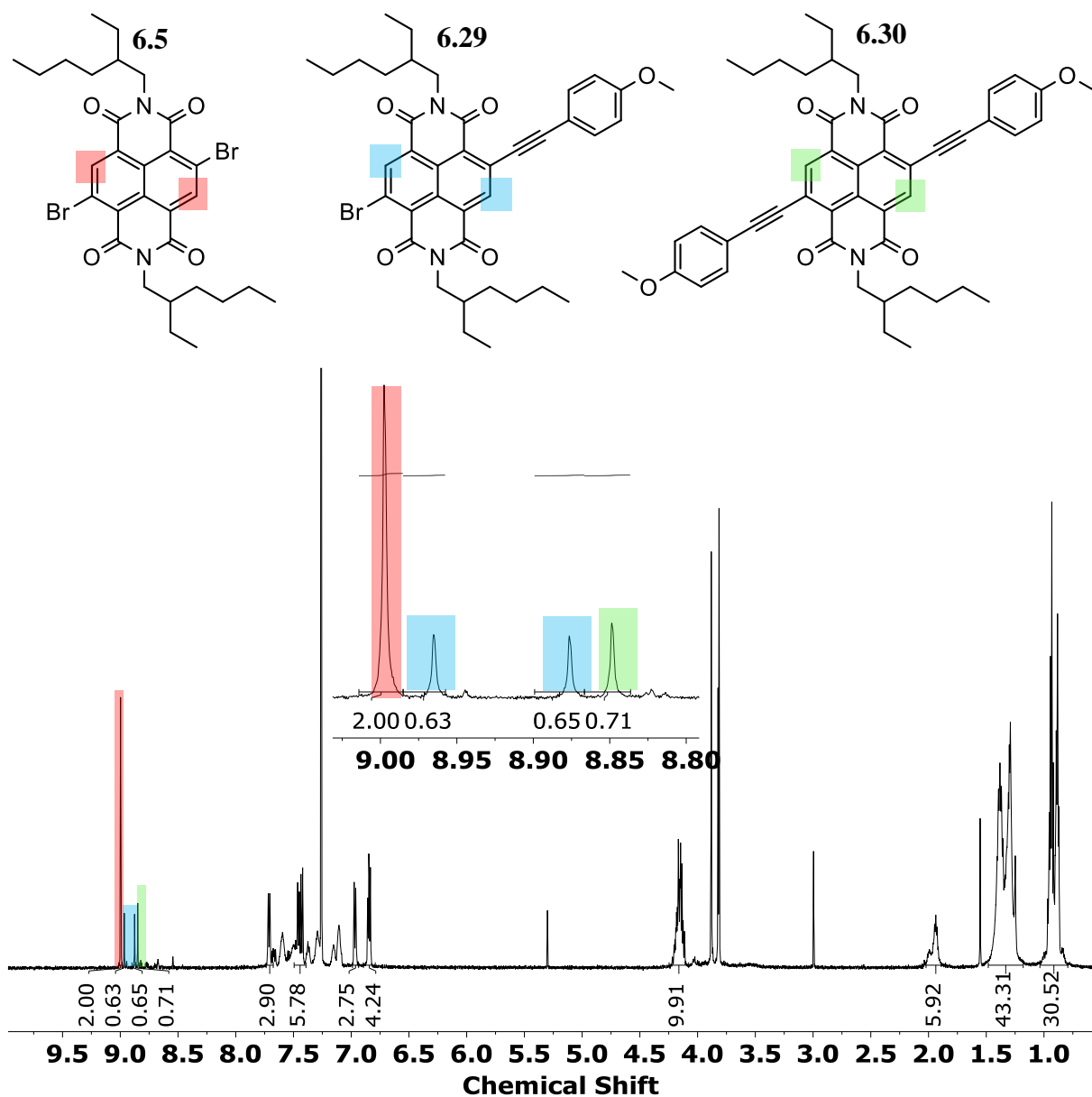


**Figure 60:** Full  $^1\text{H}$  NMR spectrum of reaction after ball milling (data correlates to entry 1 in Table 4)

A similar situation can be seen when the Sonogashira coupling was attempted with para acetyl acetylene, with the proposed asymmetric mono-substituted acetylene **6.31** becoming the major product at 48 % and only 23% of the desired c-NDI **6.32** produced, shown below in Figure 61.

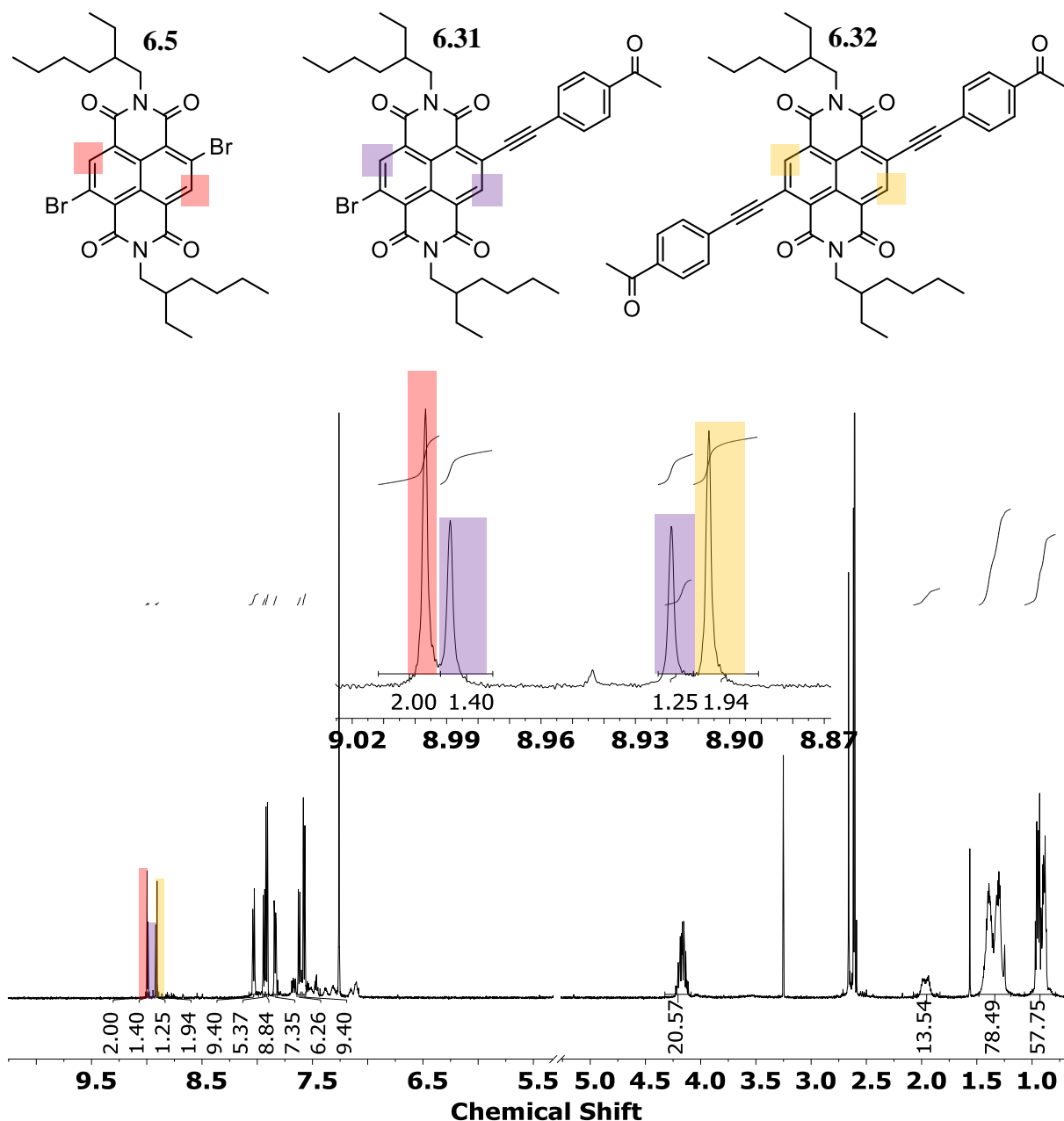
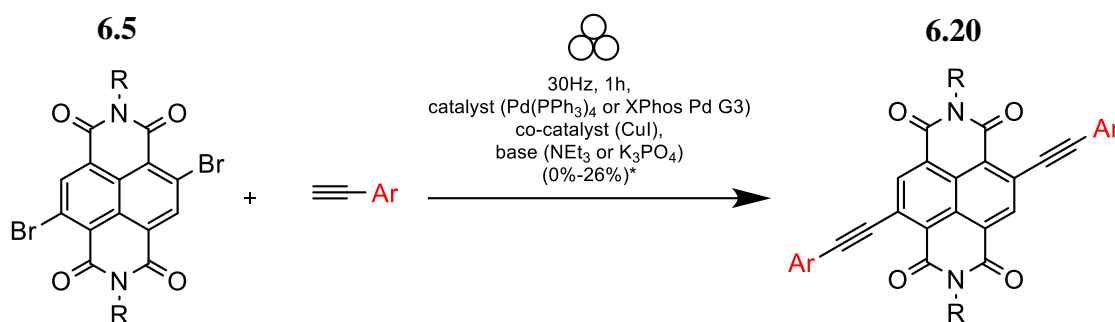


**Figure 61:** Full  $^1\text{H}$  NMR spectrum of reaction after ball milling (data correlates to entry 3 in Table 4)

A summary of the optimisation for the ball milling Sonogashira coupling can be seen in Table 4. Changing the catalyst and base to  $\text{Pd}(\text{PPh}_3)_4$  and  $\text{NEt}_3$  (entry 1 and 3) did increase reaction rate. This conforms with expectations as not only is  $\text{NEt}_3$  a stronger base, which is known to increase rates in Sonogashira couplings,<sup>352</sup> but is also a liquid at room temperature, which is known to affect the reaction kinetics<sup>244</sup> in balling milling processes. However, undesirable side

intermediates seemed to dominant with this pairing of reagents. Due to the difficulty in purifying these types of compounds, complete conversion is desirable.

It seems that the low yields of these reactions may be due to the non-optimal choice of reagents such as the base or catalyst. For example, when  $K_3PO_4$  and XPhosPdG3 (entry 2, 4, 5 and 6) were used there was a general trend of a reduction in yield of disubstituted c-NDI for all c-NDI couplings, when compared to organic amine bases ( $NEt_3$ ) or a different catalyst ( $Pd(PPh_3)_4$ ).



**Scheme 35:** Initial ball milling Sonogashira conditions

No.	SM (3 Equiv.)	Base (4 Equiv.)	Catalyst (10 mol %)	Co-catalyst	LAG ( $\mu$ L)	Time (mins)	$^1H$ NMR conversion %			
							Name	Name	Name	SM
	Aryl Acetylene	Name	Name	Name	Equiv. (mol %)					
1		$NEt_3$	$Pd(PPh_3)_4$	CuI	15	No	60	30	44	26
2		$K_3PO_4$	X Phos Pd G3	CuI	2	No	90	90	7	3
3		$NEt_3$	$Pd(PPh_3)_4$	CuI	15	No	60	28	49	23
4		$K_3PO_4$	X Phos Pd G3	CuI	2	No	90	87	6	7
5		$K_3PO_4$	X Phos Pd G3	CuI	2	No	60	79	0	21
6		$K_3PO_4$	X Phos Pd G3	CuI	2	No	60	68	42	0

The ratio of the mass of reagents to the volume of grinding jars was *ca.*  $20 \text{ mg.cm}^{-3}$ . Reactions were carried out for 1 h at room temperature and a pre-catalyst loading of 10 mol%. Conversions were determined by  $^1H$  NMR spectroscopy in  $CDCl_3$  by comparing the loss of starting material vs gain of product. When used, the LAG is *ca.* 10 wt% of the total reaction mass.

**Table 4:** Initial ball milling Sonogashira couplings

Whilst it seemed that the nature of the substituent on the aryl acetylene did affect the reaction it was observed that all yields were low (28 %).

Due the number of variables that can influence Sonogashira coupling and the range of conditions that can also be modified in our ball milling reaction (i.e. coupling choice which include the choice of base, catalyst, co-catalyst, acetylene as well as ball milling variables such as milling time, addition of LAG, quantity of milling balls, ball size etc.) it soon became apparent that solid state optimization may not be practical. Ball milling reactions have a duration of 1 hour each, only two could be carried out at a time, and used 100 mg of starting reagent **6.5** in each milling jar. With the number of potential variables that could be changed briefly discussed above, this could lead to wasted reagents and be extremely time consuming. Therefore, we looked into high throughput solution state optimization techniques of the coupling reaction to scope the reaction and save time as well as materials before attempting in the ball mill. The results of these will be discussed below.

### 6.1.3 Solution State Scoping - Kitalysis™ apparatus

Kitalysis™ apparatus is a commercially available high throughput technique where 24 microscale reactions can take place simultaneously in a reaction block (Figure 62). The cross-coupling kit contains; 6 x 4 pre-weighed catalysts (Table 5) in glass vials loaded with stir bars and topped with a cap mat, ampules of degassed solvents, aq. 1.5 M K<sub>3</sub>PO<sub>4</sub> base, 4 substrate reaction vials with stir bars and 1 internal reference standard (durene). Pre-loaded catalyst structures (1 – 6 in reaction block, right in Figure 62) are defined as XPhosPd G3 (C1, **6.33**), SPhosPd G2 (C2, **6.34**), cataCXium® APd G2 (C3, **6.35**), APhosPd G3 (C4, **6.36**), P(Cy<sub>3</sub>)Pd G3 (C5, **6.37**) and PEPSI™-IPent (C6, **6.38**) are shown below in Table 5.

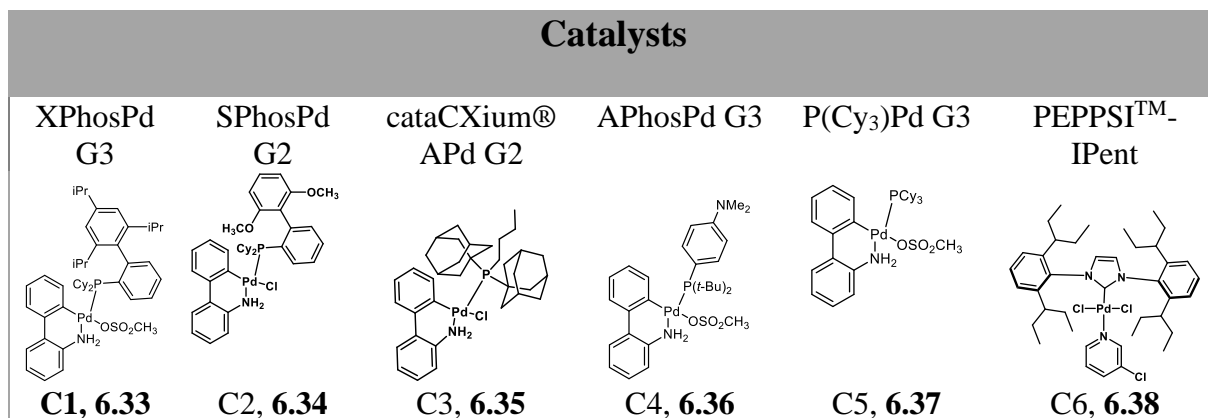


**Table 5:** Chemical structures of pre-loaded catalysts in Kitalysis™ reaction block.

The four variables (A-D, Figure 62) can be changed depending on the desired coupling reaction and can either be the choice of base (20  $\mu$ L, 1.5 M), solvent (100  $\mu$ L) or both.

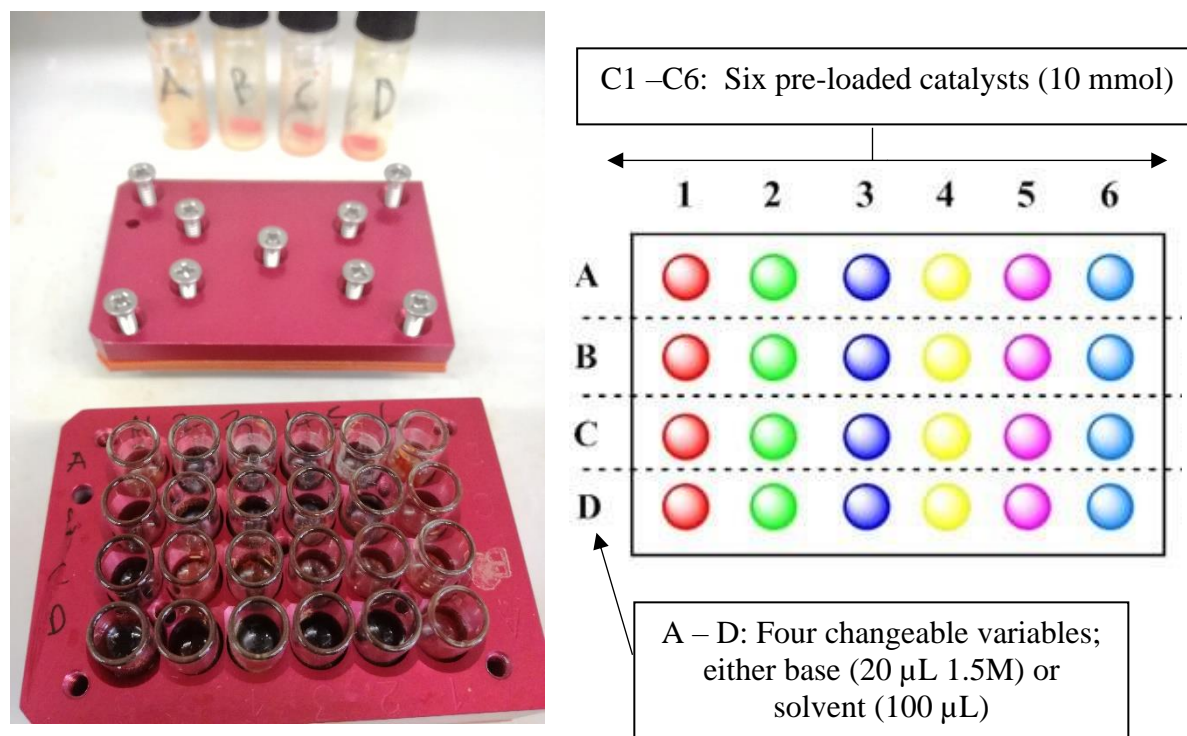


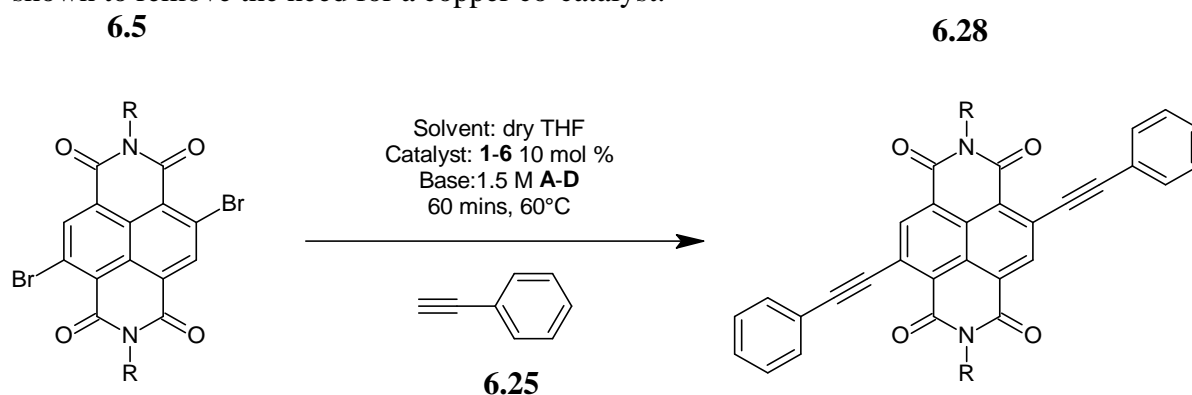
**Figure 62:** (left) Photograph of Kitalysis™ reaction block and (right) breakdown of reaction wells.

The advantages of this technique over the attempted ball milling optimisation methodology include the potential to run 24-microscale reactions in parallel with identical external conditions

i.e. temperature, short reaction times and only small quantities of starting materials are required (i.e. a total of 0.240 g of Br<sub>2</sub>-NDI used in 24 distinct 100 μmol reactions). It gives the ability to compare four bases or solvents against six catalysts. The cross coupling starting reagents (aryl halide **6.5** and acetylene) can be prepared at a desired concentration and injected into the reaction vials containing the defined catalysts, bases and solvent for the cross-coupling reaction. Optimisation using the Kitalysis™ apparatus for the Sonogashira cross coupling of c-NDIs will now be discussed.

### 6.1.4 Sonogashira Coupling Solution High-Throughput Screening

The Kitalysis™ apparatus was set up with the following conditions and each reaction vial contained: Br<sub>2</sub>-NDI (10 μmol per vial), phenyl acetylene (0.013 g total, 30 μmol per vial), catalyst C1 to C6 (10 mol %), co-catalyst CuI (15 mol %), base (20 μL, 1.5 M) and solvent (100 μL) stirring at 300 rpm, 60°C for 1 hour (Scheme 36). Commonly used solution state conditions for Sonogashira coupling were adopted,<sup>348</sup> with dry THF as the solvent and the bases being either K<sub>3</sub>PO<sub>4</sub>, 1,4-diazabicyclo[2.2.2]octane (DABCO), triethylamine (NEt<sub>3</sub>) and KO<sup>t</sup>-Bu were selected. The base is usually responsible for neutralizing the hydrogen halide by-product produced in the coupling (**6.16** in mechanism Scheme 33) but DABCO has also been shown to remove the need for a copper co-catalyst.<sup>277,278</sup>



**Scheme 36:** Sonogashira coupling Kitalysis™ optimization conditions

Upon reaction completion, the work up involved; the addition of a quenching solution (2 % AcOH solution in MeCN) to each reaction vial (500  $\mu$ L) followed extraction of organics with dichloromethane (DCM, 5 mL), washing the organic layer with water (2 x 1 mL) and separation of the organic layer which was then passed through celite to remove palladium impurities. This solution was then dried using MgSO<sub>4</sub> and evaporated to dryness. The solids varied from brown to orange in the 24 reaction vials, with row D displaying a rich pink colour for the Sonogashira coupling reaction. The <sup>1</sup>H NMR was then recorded for each vial by dissolving the solid in 0.5 mL of deuterated solvent (CDCl<sub>3</sub>) containing durene as an internal reference standard (IRS) (6.90 ppm).

The partial <sup>1</sup>H NMR spectra for vials of six of these reaction is shown below (Figure 63), corresponding to row C of the reaction block which includes base K<sub>3</sub>PO<sub>4</sub> in all vials where the changing variable is the catalyst (**6.33** to **6.39**). <sup>1</sup>H NMR spectra of data corresponding to row A, B and D can be seen in the supplementary information (Section S1) that accompanies this thesis. Similarly to the initial solid state reaction general trend (Table 4, entry 1, 2, 3, 4 and 6), a mixture of starting material **6.5**, disubstituted c-NDI **6.28** and monosubstituted c-NDI **6.39** can be seen for catalyst C1, C2 and C3. When comparing identical solid-state conditions (entry 5 Table 4, phenyl acetylene and C1 XPhosPdG3), the solid-state reaction displayed ratios of a mixture of only starting material and disubstituted c-NDI. Whereas the solution state with these identical conditions of phenyl acetylene and C1 XPhosPdG3 (spectra 1, Figure 63) also yielded monosubstituted c-NDI species (appropriate aromatic protons shaded yellow in the <sup>1</sup>H NMR spectra). Catalyst C4, C5 and C6 behaved the most alike to the solid state conditions (where phenyl acetylene was the substrate, entry 5, Table 4) and resulted in only disubstituted c-NDI **6.28** and starting reagent **6.5**. Catalyst C2 and C4 (spectra 2 and 4 in Figure 63) displayed the highest % formation of desired **6.28** at 41 and 50 % respectively, whilst the most poorly

performing catalyst was C3 at 11 % (spectra 3 in Figure 63). Overall, due to the high percentages of undesired **6.5** or **6.39** and low yields of disubstituted c-NDI,  $K_3PO_4$  is not an optimum base for the Sonogashira coupling reaction of c-NDIs in the solid or solution state.

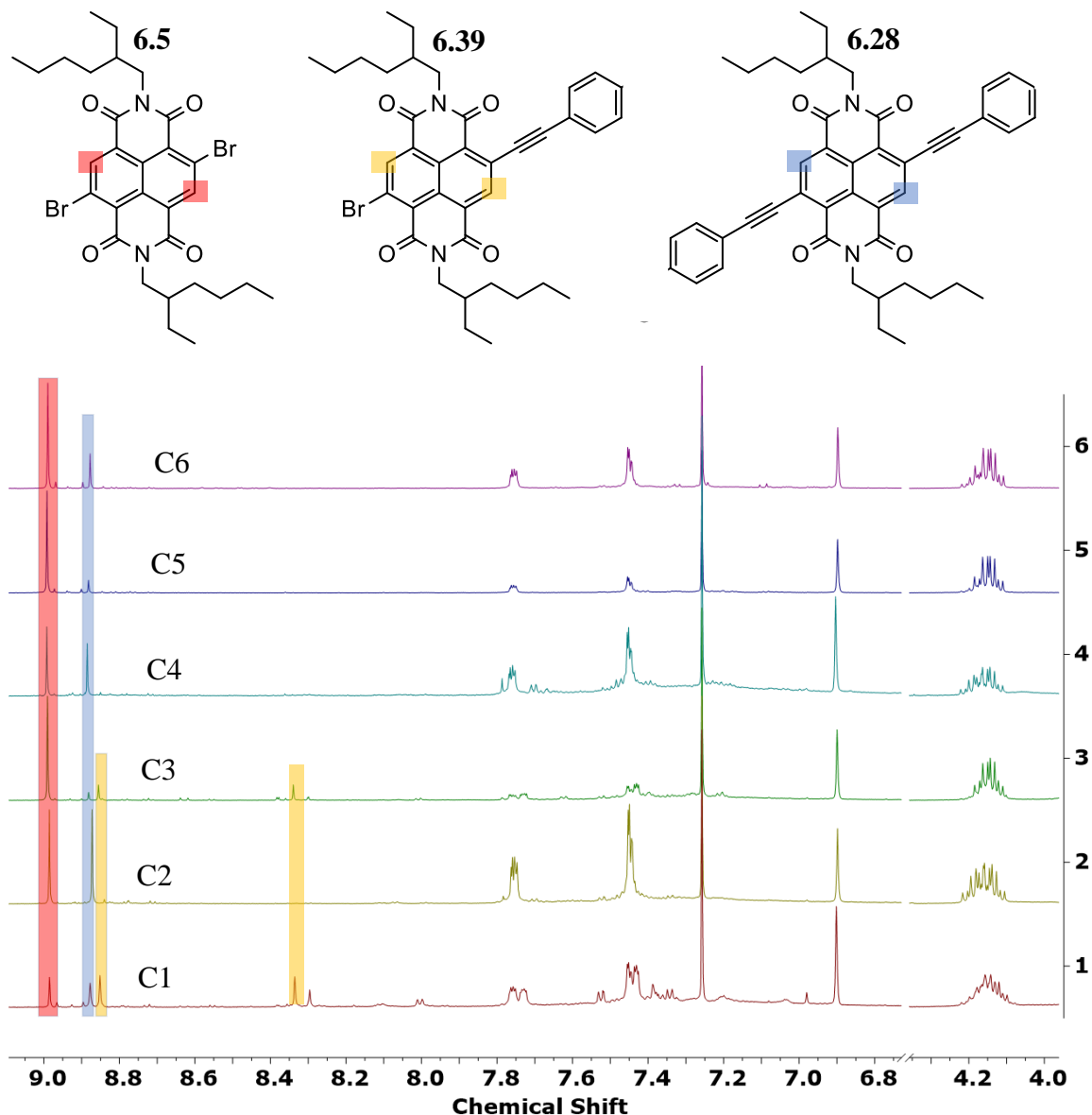


**Figure 63:** Partial  $^1H$  NMR spectra with catalyst C1-C6 and base  $K_3PO_4$

It was soon realised that comparison of 24  $^1H$  NMR spectra by varying the stacking spectra depending on the condition desired to be compared was impractical and led to endless NMR stacks. An alternative presentation style, inspired by Leitch and co-workers cross coupling optimization studies,<sup>353</sup> where a colour coded table was assembled containing the various

conditions and the entries colour coded based on the varying success of reaction was adopted (Table 6). The values in the table correspond to the % conversion to desired product calculated from the integration values of core NDI protons in the  $^1\text{H}$  NMR spectra and are colour coded within 20 % boundaries. Catalyst 1-6 are placed along the x-axis and the bases A-D along the y-axis of the table.

Base	Catalyst					
	X Phos Pd G3	S Phos Pd G2	cataCXium® A Pd G2	APhos Pd G3	P (Cy3) Pd G3	Pd-PEPPSI™-IPent
	1	2	3	4	5	6
A: KOt-Bu	0	31	60	67	34	0
B: NEt <sub>3</sub>	66	100	100	85	100	100
C: K <sub>3</sub> PO <sub>4</sub>	26	50	11	49	13	24
D: DABCO	60	100	83	100	89	0

**Table 6:** Solution state optimization results for Sonogashira coupling

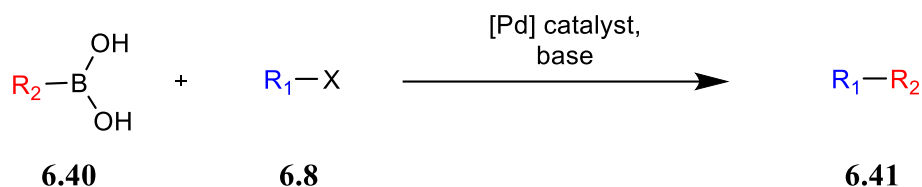
It can be seen from Table 6 that DABCO and NEt<sub>3</sub> are optimum conditions as these bases led to high conversions (mostly complete conversion) to the disubstituted c-NDI **6.28**, regardless of the catalyst used (entry D2-D5 and C2-C5 respectively in Table 6). The observation that the use of DABCO negates the requirement to use copper as a co-catalyst and is also a solid base compared to NEt<sub>3</sub> which is a liquid at room temp, makes it an attractive reagent in green chemistry.

To investigate the use of DABCO in the solid state, the conditions used in entry 2B (catalyst SPhosPd G2 C2 and base DABCO) was replicated in the ball mill at 30 Hz for 1 hour and complete conversion to the disubstituted acetylene c-NDI **6.28** was achieved, demonstrating that this example of conditions also work in a solid-state setting. This shows that high throughput screening methods can quickly yield information on a range of conditions and in this example identified a set of conditions that worked in the ball mill.

With conditions for Sonogashira coupling reactions in the solid state established, using the Kitalysis™ method to probe other cross coupling reaction will now be explored.

### 6.1.5 Introduction to Suzuki Cross-Coupling

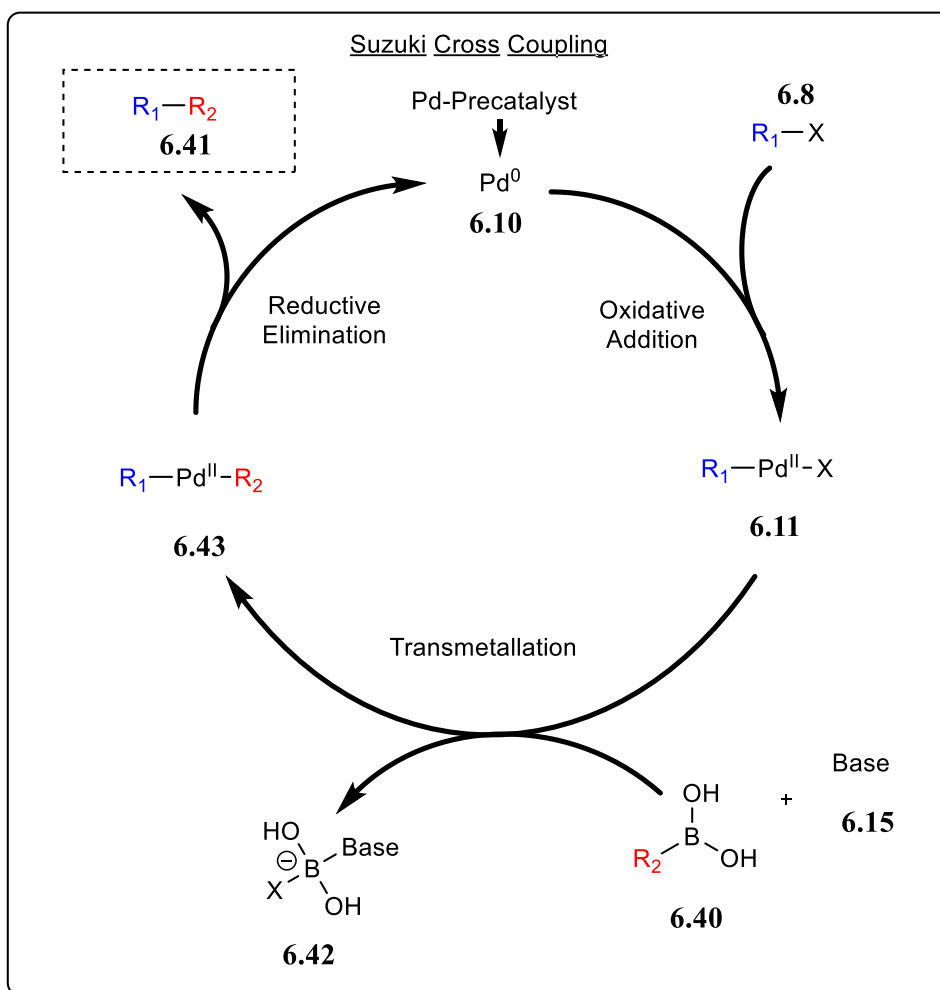
First published in 1979 by Suzuki *et al.*,<sup>354</sup> the Suzuki cross-coupling reaction is an organic reaction where a sp<sup>3</sup> hybridized C-C single bond can be formed by the reaction between an organoboron compound (commonly boronic acid, **6.40** in Scheme 37) and organohalide (**6.8**) coupling partners in the presence of a palladium catalyst and a base (Scheme 37).



**Scheme 37:** Suzuki cross coupling

Initially, the mechanism (Scheme 38) proceeds similarly to the Sonogashira coupling where a palladium pre-catalyst is activated to the palladium (0) species **6.10**. This is then involved in the rate limiting oxidative addition step, where the aryl-halide **6.8** is coupled to the palladium species to form **6.11**. **6.11** forms initially as the *cis*-palladium complex but rapidly isomerizes to the predominant *trans*-configuration.<sup>355</sup> **6.11** then undergoes transmetallation with the boronic acid activated species **6.42** to form **6.43**. The intricacies of this step are not fully understood but it cannot take place without the presence of a base and the base is believed to be responsible for the activation of the boronic acid.<sup>356,357</sup>

Finally, reductive elimination of **6.43** leads to the formation of the desired C-C bonded product **6.41** and the palladium (0) species is regenerated in the process.



**Scheme 38:** Suzuki cross coupling mechanism.

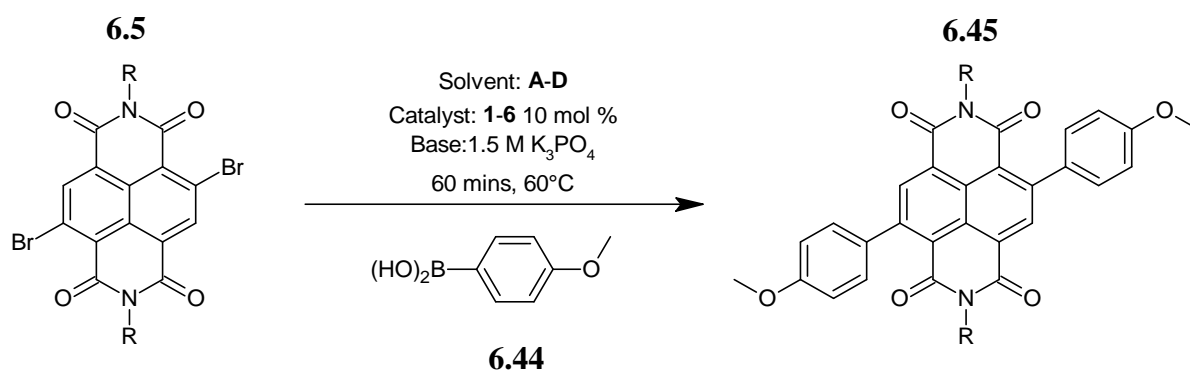
High-throughput screening Kitalysis<sup>TM</sup> apparatus was applied to the Suzuki coupling of *c*-NDIs and the results are discussed below.

### 6.1.6 Suzuki solution state high throughput screening

The starting conditions for the high throughput optimisation for Suzuki coupling reactions were chosen to be K<sub>3</sub>PO<sub>4</sub> (see section 5.1.4) with each of the six preloaded catalysts C1 to C6 and four different solvents. The solvents were selected based on pre-existing Suzuki synthesis of *c*-NDIs in solution<sup>335</sup> and included A-D as dimethylacetamide (DMAc), tetrahydrofuran (THF), toluene and *n*-butanol.

The Kitalysis™ apparatus was set up with the following conditions and each reaction vial contained: Br<sub>2</sub>-NDI (10 μmol per vial), 4-Methoxyphenylboronic acid (30 μmol per vial), catalyst C1 to C6 (10 mol %), 1.5 M K<sub>3</sub>PO<sub>4</sub> (20 μL) and solvent of choice (100 μL) stirring at 300 rpm, 60°C for 1 hour (Scheme 39).

Upon reaction completion, the work up was identical to the Sonogashira coupling and photographs taken throughout the work up are displayed below (Figure 64). This included a water wash (left in Figure 64), separation of the organic layer (middle in Figure 64) and evaporation to crude reaction mixtures for <sup>1</sup>H NMR studies (right in Figure 64).



**Scheme 39:** Suzuki-Miyaura conditions for the high-throughput solution state optimization



**Figure 64:** Photographs showing the work up stages of the reaction vials from the Suzuki cross coupling utilizing the Kitalysis™ reaction block.

The <sup>1</sup>H NMR of each vial was then recorded in deuterated CDCl<sub>3</sub> containing durene IRS. The partial <sup>1</sup>H NMR spectra for vials of four of these reaction is shown below (Figure 65), corresponding to column 1 of the reaction block which includes base K<sub>3</sub>PO<sub>4</sub>, catalyst C1 and

varying solvent A-D.  $^1\text{H}$  NMR spectra of data corresponding to catalyst C2, C3, C4, C5 and C6 can be seen in the supplementary information (Section S1) that accompanies this thesis.  $^1\text{H}$  NMR spectra of the crude reaction mixtures (spectra 2-5 in Figure 65) were stacked against clean starting material **6.5** (spectra 1 in Figure 65) and isolated disubstituted c-NDI **6.45** (spectra 6 in Figure 65). The reactivity (i.e. the % ratio of starting material remaining) and the selectivity (i.e. the % ratio of desired disubstituted cNDI compared to unwanted side products) can be compared by observing specific integrals for the starting materials and products in  $^1\text{H}$  NMR stack shown in Figure 65. The need for both of these parameters is because conversion from starting material can be due to the formation of side products (typically the monosubstituted species).

This situation was observed for the reactions carried out in THF and toluene. In these cases, the complete lack of evidence for the aromatic protons from the starting material (**6.5**) (red shading) shows that THF and toluene displayed the highest reactivity in conjunction with catalyst C1 but delivered the lowest yields of desired c-NDI **6.45** cases (38 % and 53 % respectively). This is due to the presence of unwanted side products present, displayed in the  $^1\text{H}$  NMR spectra by a host of peaks in the aromatic proton region (shaded yellow).

Formation of product **6.45** was seen for all four solvent systems (spectra 2-5 in Figure 65) with DMAc resulting in the highest yield of disubstituted product at 57 %. Two distinct imide proton environments corresponding to the imide protons present in **6.5** and **6.45** (shaded purple and green respectively) can be seen in all four crude  $^1\text{H}$  NMR spectra, suggesting that regardless of solvent, catalyst C1 in combination with  $\text{K}_3\text{PO}_4$ , may not be optimum conditions for this coupling reaction.

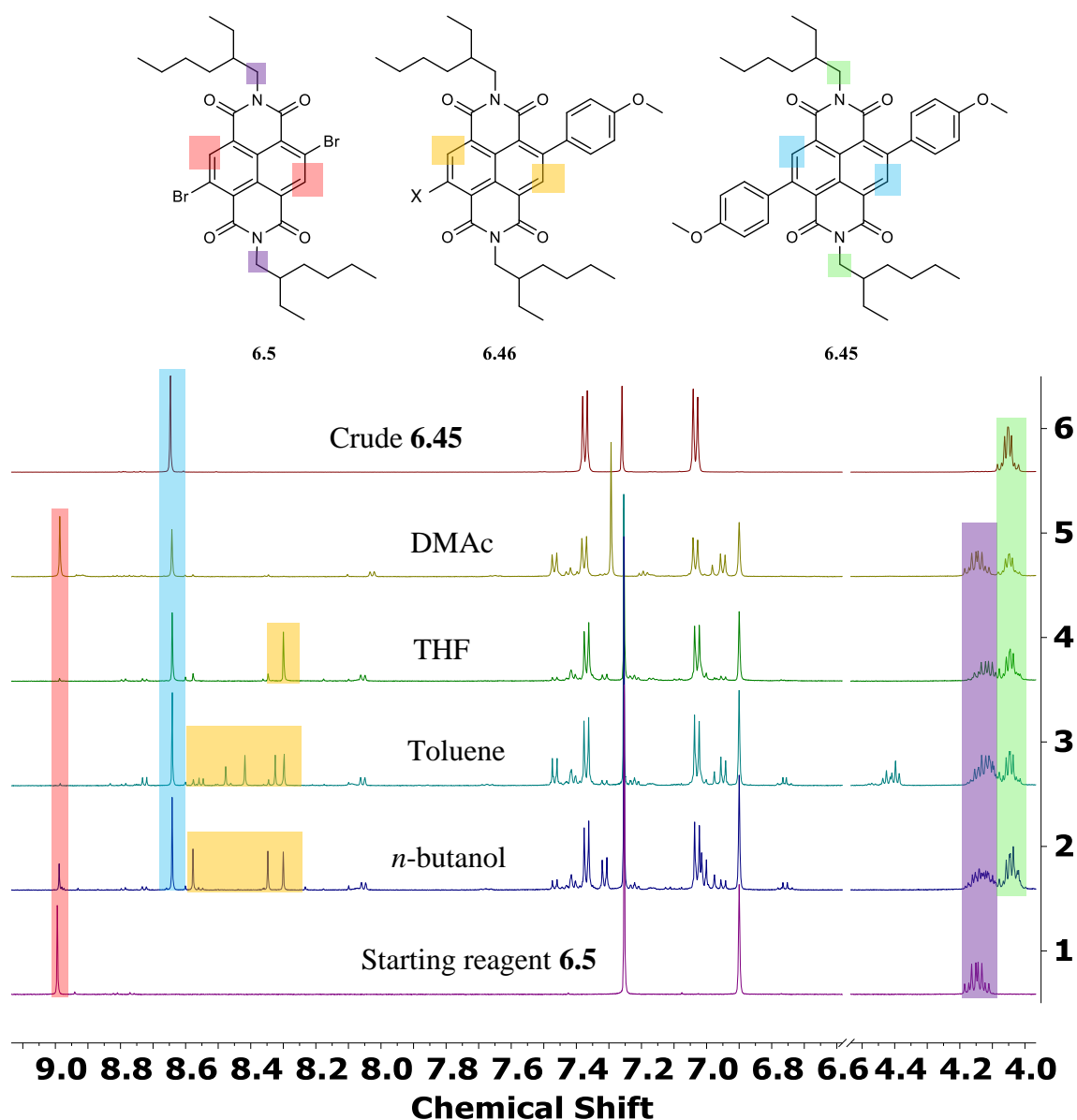


**Figure 65:** Partial  $^1\text{H}$  NMR spectra containing  $\text{K}_3\text{PO}_4$ , catalyst C1 and solvents A-D (corresponding to column 1 in Table 7 and XPhos Pd G3 is the constant catalyst)

The data for all 24 of the Kitalysis<sup>TM</sup> reactions are shown in Table 7. It can be seen that catalyst C1 is generally one of the better performing catalysts for this coupling reaction. When considering solvent, toluene is the best solvent of choice in terms of reactivity where the average highest % of loss of starting material is observed. On the other hand, toluene is one of the worst solvents with respect to selectivity of converting **6.5** to c-NDI **6.45**, as displayed in the above  $^1\text{H}$  NMR spectra with the various side products present in the spectra. THF is the worst

performing solvent, regardless of the catalyst and displays the lowest yields of **6.45** compared to the other three solvents.

Solvent	Catalyst					
	X Phos Pd G3	S Phos Pd G2	cataCXium® A Pd G2	APhos Pd G3	P (Cy3) Pd G3	Pd-PEPPSI™-IPent
	1	2	3	4	5	6
A: DMAc	57	42	53	60	0	59
B: THF	28	0	13	50	46	50
C: Toluene	53	48	48	53	55	52
D: <i>n</i> -butanol	55	30	43	36	0	27

**Table 7:** Solution state optimization results for Suzuki coupling

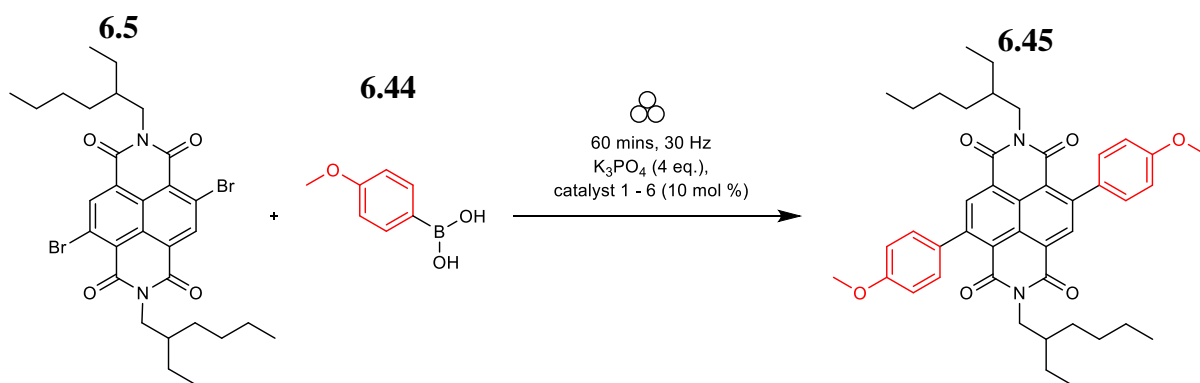
This high-throughput screening of Suzuki coupling in solution state does not show conclusively if one catalyst is better than any other when the changing variable is the solvent. None of the reactions reached full conversion to the desired product, unlike the Sonogashira coupling. The three sets of conditions that resulted in the highest % conversion of *c*-NDI **6.45** were 57 %, 60 % and 59 % in the presence of DMAc when using catalyst C1, C4 and C6 respectively. This suggests if the solution conditions were required for this reaction, it would be the solvent of choice. These yields are still however relatively low, when considering the difficulty in separation of these compounds and green sustainable synthesis ideals of reaching full Atom Economy (section 5.1 in previous chapter). Therefore, these conditions were replicated in the ball mill, albeit with the exclusion of solvent, to see if any of these catalysts, when placed with  $K_3PO_4$ , perform better or worse in the solid state. The results of this investigating are discussed below.

### 6.1.7 Suzuki solid state catalyst screening

The ball milling protocol was carried out at twice for each reaction at 30 Hz under the following conditions:  $Br_2$ -NDI (0.100 g per milling jar), 4-Methoxyphenylboronic acid (3 equivalents), catalyst C1 to C6 (10 mol %) and  $K_3PO_4$  (3 equivalents) to replicate the solution state conditions

(Scheme 40). Once the reaction was complete a crude  $^1\text{H}$  NMR was recorded in  $\text{CDCl}_3$ , and the data extracted from these spectra were used to assemble Table 9.

The raw  $^1\text{H}$  NMR spectra can be found in the supplementary information (Section S1) that accompanies this thesis. Photographs of the interior of the milling jars post reaction (Table 8) display the degree of mixing that has resulted in visible variations in colour and powder composition. Compared to starting reagents (left in Table 8), all reaction mixtures changed colour to red. Catalyst C3-C6 powder distribution can be seen to be a finely dispersed on the surface of the jar and balls, whereas C1 and C2 is dispersed in tacky clumps in the vessel.



**Scheme 40:** Solid state catalyst optimization for Suzuki coupling

Starting Reagents	Catalyst					
 <b>6.5, K<sub>3</sub>PO<sub>4</sub> and C5</b>	XPhosPd G3  <b>C1</b>	SPhosPd G2  <b>C2</b>	cataCXium® APd G2  <b>C3</b>	APhosPd G3  <b>C4</b>	P(Cy <sub>3</sub> )Pd G3  <b>C5</b>	PEPPSI™-IPent  <b>C6</b>

**Table 8:** Photograph of jars post reaction for the solid state Suzuki cross coupling catalyst screening

Compared to solution state results, higher % ratios of disubstituted c-NDI **6.45** were observed for all catalysts when combined with K<sub>3</sub>PO<sub>4</sub>. For example, XPhosPdG3 (C1) and Pd-PEPPSI<sup>TM</sup>-Ipent (C6) led to virtually complete conversion as determined by <sup>1</sup>H NMR spectroscopy. Interestingly, <sup>1</sup>H NMR spectra for all catalysts only displayed starting reagent and desired c-NDI **6.45**. This shows excellent selectivity with no unwanted side products observed, which is in contrast to that observed in the high throughput solution state Suzuki coupling (figure 76). The standard error (SE) was calculated for the results according to equation 6.1, where  $\sigma$  is the sample standard deviation and  $n$  is the number of samples. SE were observed to be between 0 – 5 % for all samples, with the majority of samples showing an SE of *ca.* 3.5 %.

Equation 6.1 
$$\text{Standard Error} = \frac{\sigma}{\sqrt{n}}$$

	Catalyst	Average % ratio of 6.5	Average % ratio of 6.45	Standard Error (%)
1	<b>C1</b>	0	100	0
2	<b>C2</b>	14	86	4.85
3	<b>C3</b>	10	90	3.41
4	<b>C4</b>	7	93	3.36
5	<b>C5</b>	3	97	3.27
6	<b>C6</b>	2	>98	3.67

The ratio of the mass of reagents to the volume of grinding jars was *ca.* 20 mg.cm<sup>-3</sup>. Reactions were carried out for 1 h at room temperature and a pre-catalyst loading of 10 mol%. Conversions were determined by <sup>1</sup>H NMR spectroscopy in CDCl<sub>3</sub> by comparing the loss of starting material vs gain of product.

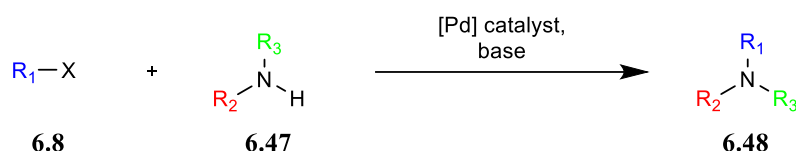
**Table 9:** Solid state optimization results for Suzuki coupling

This solid-state investigation shows that solution state results are not always comparable in a solid-state setting. Specifically, the solid-state c-NDI Suzuki coupling reactions demonstrates

better reactivity and selectivity than solution state results (Table 9). C1 is the best catalyst when combined with  $K_3PO_4$  in the solid state as complete conversion with a 0 % SE. Compared to the Sonogashira coupling reactions, variation is seen in the solution state vs. solid state results. The final section of this chapter describes using the Kitalysis<sup>TM</sup> system to screen conditions for the Buchwald-Hartwig amination reaction to form c-NDIs.

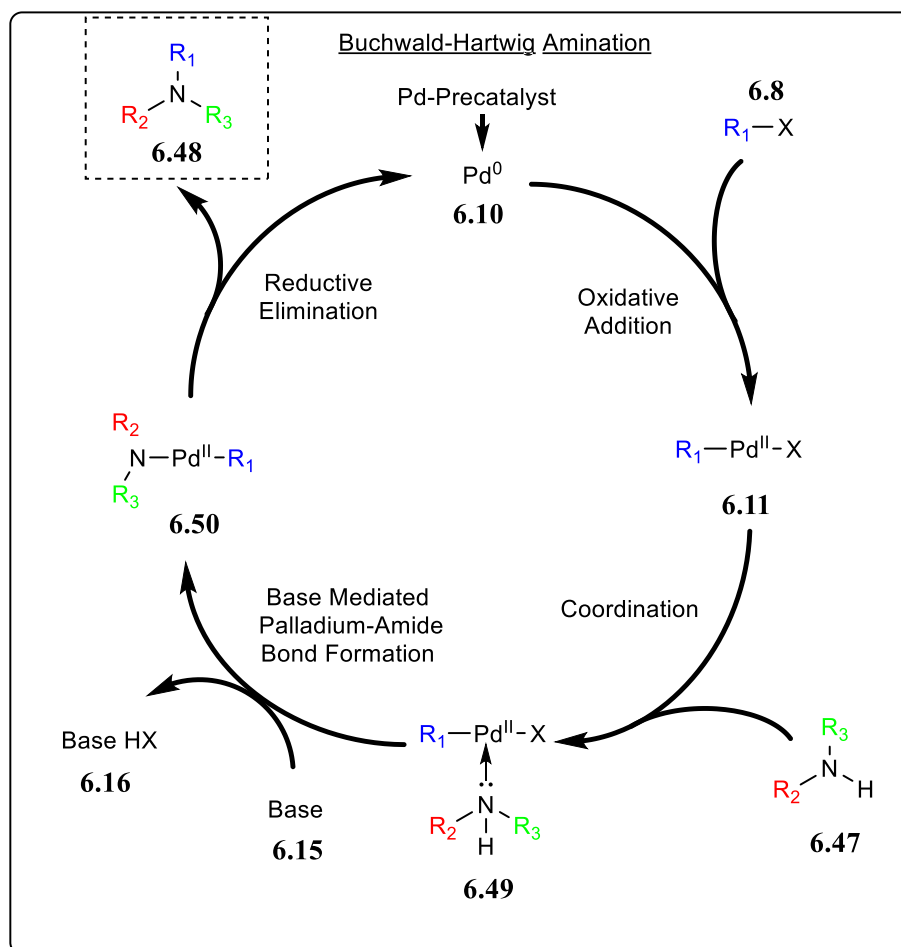
### 6.1.8 Buchwald-Hartwig Amination

Buchwald-Hartwig (B-H) aminations are an organic palladium catalysed cross-coupling reaction for the synthesis of carbon-nitrogen bonds between primary amines (**6.47**) and aryl halides (**6.8**) (Scheme 41) to produce tertiary amines (**6.48**).



**Scheme 41:** General Buchwald-Hartwig amination reaction

The general mechanism (Scheme 42) proceeds through similar steps to the previously discussed Suzuki and Sonogashira cross coupling reactions. Steps include the oxidative addition of aryl halide **6.8** to palladium (0) species to generate the palladium (II) species **6.11**. Addition of the primary amine to **6.11** then occurs *via* coordination of the primary amine species **6.47** to **6.11** followed by a base mediated palladium amine bond formation process to generate complex **6.50**. This then undergoes reductive elimination to yield the desired tertiary amine **6.48**, regenerating the palladium (0) complex simultaneously.

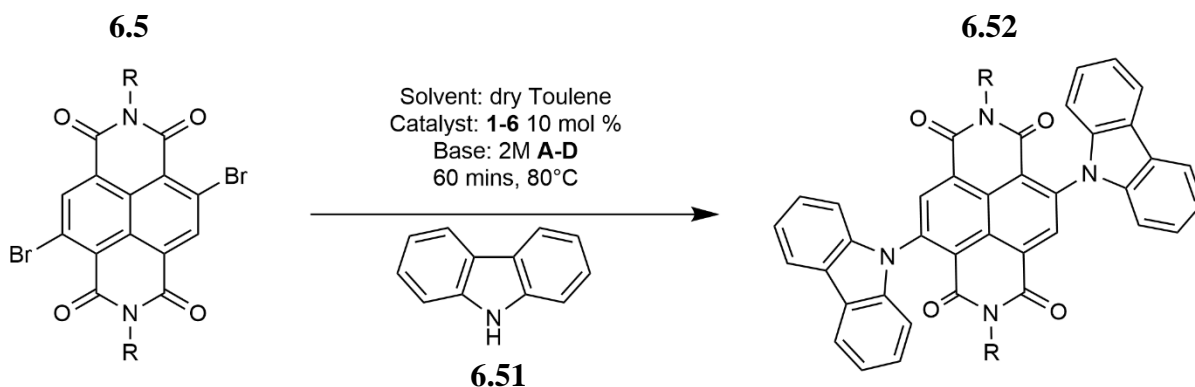


**Scheme 42:** Mechanism for a general Buchwald-Hartwig amination

### 6.1.9 Buchwald-Hartwig Amination Optimization using Kitalysis™

When exploring the literature, elevated temperature and increased loading of bases were commonplace for B-H aminations to encourage higher yielding reactions.<sup>339</sup> For this reason, the temperature was raised to 80°C and loading of the bases increased to 2M for the optimization. As varying the base rather than the solvent was more insightful in the previous couplings, this was adopted during this optimisation screen. Commonly used bases in BH-amination reactions<sup>358</sup> were selected for the reaction block (A to D) and include; NaO*t*-Bu, KO*t*-Bu, Na<sub>2</sub>CO<sub>3</sub> and hindered Cs<sub>2</sub>CO<sub>3</sub>. The Kitalysis™ apparatus was set up with the following conditions and each reaction vial contained: Br<sub>2</sub>-NDI (10 μmol), carbazole (30 μmol), catalyst C1 to C6 (10 mol %), base (2 M, 20 μL) and dry Toluene (100 μL) stirring at

300 rpm at 80°C for 1 hour (Scheme 43). The work up was identical to previous solution state high-throughput reactions and resulted in varying crude mixtures that ranged from yellow to blue in colour. The data extracted from the raw <sup>1</sup>H NMR spectra can be seen in Table 10. The raw <sup>1</sup>H NMR spectra for all 24 reactions can be found in the supplementary information (Section S1) that accompanies this thesis.



**Scheme 43:** Buchwald-Hartwig Katalysis™ optimization conditions

Base	Catalyst					
	X Phos Pd G3	S Phos Pd G2	cataCXium® A Pd G2	APhos Pd G3	P (Cy3) Pd G3	Pd-PEPPSI™-IPent
	1	2	3	4	5	6
A: NaOt-Bu	92	100	100	100	100	100
B: KOt-Bu	34	54	36	53	42	50
C: Na <sub>2</sub> CO <sub>3</sub>	0	0	7	0	0	0
D: Cs <sub>2</sub> CO <sub>3</sub>	0	0	38	0	13	18

**Table 10:** Buchwald-Hartwig high throughput solution state optimization results from <sup>1</sup>H NMR spectra.

The results shown in Table 10 conclusively show that the bases containing tert-butoxide anions resulted in higher conversions to disubstituted c-NDI **6.52** than carbonate-type bases. Sodium tert-butoxide was the best performing base, with complete conversion for 5 out of the 6 catalysts achieved and sodium carbonate performed the poorest, regardless of the catalyst (only displayed any conversion to **6.52** (7 %) with catalyst C3).

For row A in Table 10 using the base NaOt-Bu, the generally high conversion meant that differences in the efficiency of the catalyst could not be readily established. In contrast when viewing the data for bases with lower conversion (e.g. KOt-Bu) it was possible to elucidate the effects of catalyst on the system which varied from 34 to 54 % conversion to disubstituted c-NDI **6.52** – row B with catalyst C2 being the best performing. Catalyst C3 was one of the better performing catalyst for both carbonate bases (entry C3, 7 % conversion, and D3, 36 % conversion, in Table 10).

The base is known to be involved in the crucial N-C bond formation step in the catalytic cycle (Scheme 42) and is responsible for the deprotonation of the neutral palladium-amine species (**6.49** in Scheme 42) and/or the removal of the Br anion (**6.15** to **6.16** in Scheme 42).<sup>359</sup> The alkoxides have higher pKa's (19 and 17 for NaOt-Bu and KOt-Bu respectively) compared to carbonates (10 for Cs<sub>2</sub>CO<sub>3</sub> and 6.37 for Na<sub>2</sub>CO<sub>3</sub>), thus explaining the performance of bases A-D.

In order to see how these conditions transferred to the ball mill, it was decided to take one of the best performing and the worst performing conditions in the solution state (A3 and C3 in table 10) and attempt these in the solid state (Figure 66).

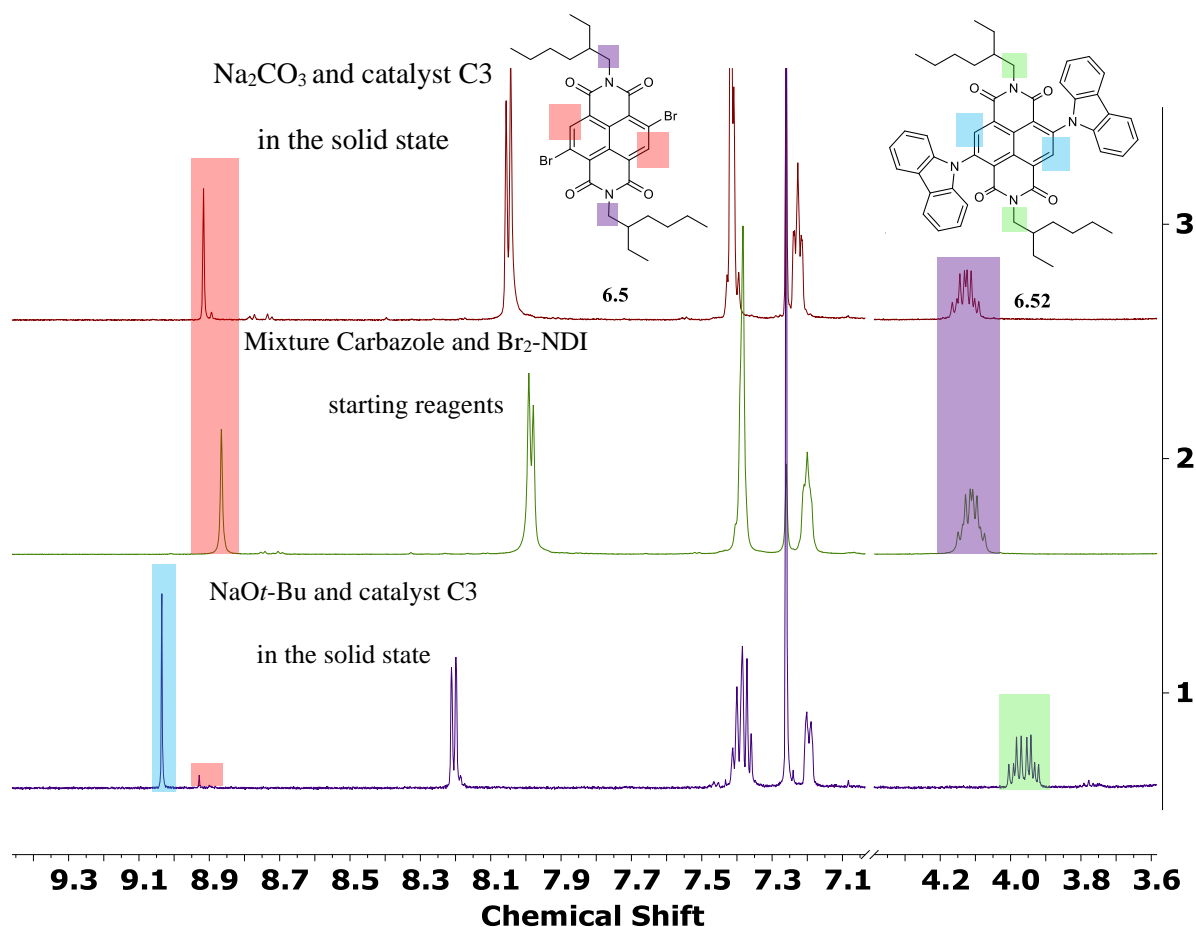


**Figure 66:** Partial  $^1\text{H}$  NMR spectra of solid-state BH reactions to compare against solution state results.

Figure 66 shows the mixture of the two unreacted starting materials (spectrum 2) stacked against the  $^1\text{H}$  NMR spectra for crude A3 (spectrum 3) and C3 (spectrum 1) reactions.

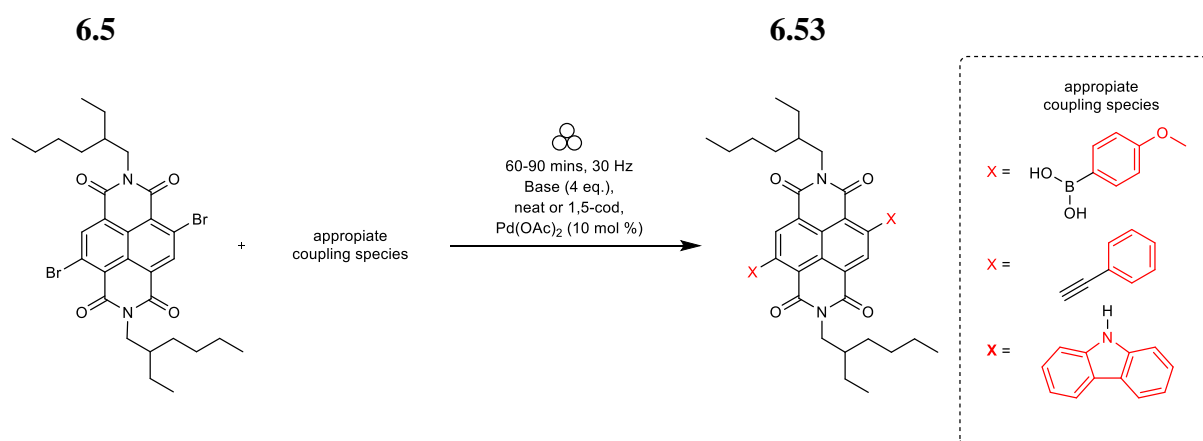
It was seen that poorly performing base in the solution state  $\text{Na}_2\text{CO}_3$  (7%) also performed poorly in the solid state (0% conversion, spectra 3), with only starting material evident in the crude spectrum after 1h milling time. However, use of  $\text{NaOt-Bu}$  in the solid state (spectra 1 in Figure 66), resulted in almost complete conversion to  $\text{c-NDI 6.52}$  (>98 %).

The success of sodium tert-butoxide in the solution state (Row A in table 10) and solid state (spectra 1 in Figure 66) would suggest that the base is one of the more influential variables in

the BH amination reaction compared to the solvent and the catalyst. Fortunately, solid state synthesis removes the need for solvent by definition. Due to the cost of specialized catalyst C1-C6 in terms of general application (e.g. C6 = £675/g), we thought it would be valuable to attempt the solid-state synthesis of all three coupling reactions with the best performing bases for each coupling in combination with a commercially available, benchtop stable and cheap palladium catalyst, palladium acetate ( $\text{Pd}(\text{OAc})_2$ , £108/g).

### 6.1.10 Solid State Coupling reactions using $\text{Pd}(\text{OAc})_2$

The ball milling jars were set up with the following conditions and each jar contained:  $\text{Br}_2$ -NDI (100 mg), appropriate coupling species **6.44**, **6.25** or **6.51** (3 equivalents),  $\text{Pd}(\text{OAc})_2$  (10 mol %), optimum base for each coupling established from previously in this chapter (4 equivalents) and neat or with 1,5-cyclooctadiene (1,5-cod) LAG agent, at 30 Hz for a duration of 60 to 90 minutes (Scheme 44).



**Scheme 44:** Solid state scheme for coupling reactions using  $\text{Pd}(\text{OAc})_2$  as the catalytic source.

The  $^1\text{H}$  NMR of each crude reaction mixture was then recorded in  $\text{CDCl}_3$  and the raw data was used to assemble the conversion Table 11. The  $^1\text{H}$  NMR of the Buchwald Hartwig amination reaction (entry 4 in Table 11) shows that essentially complete conversion was achieved with an increased milling duration of 90 minutes (Figure 67). Appropriate proton environments that correspond to the isolated product **6.52** (spectra 3 in Figure 67) compared to the starting reagent **6.5** (spectra 1 in Figure 67) are shaded and display that peaks corresponding with **6.5** are not present in the crude reaction mixture (spectra 2 in Figure 67).

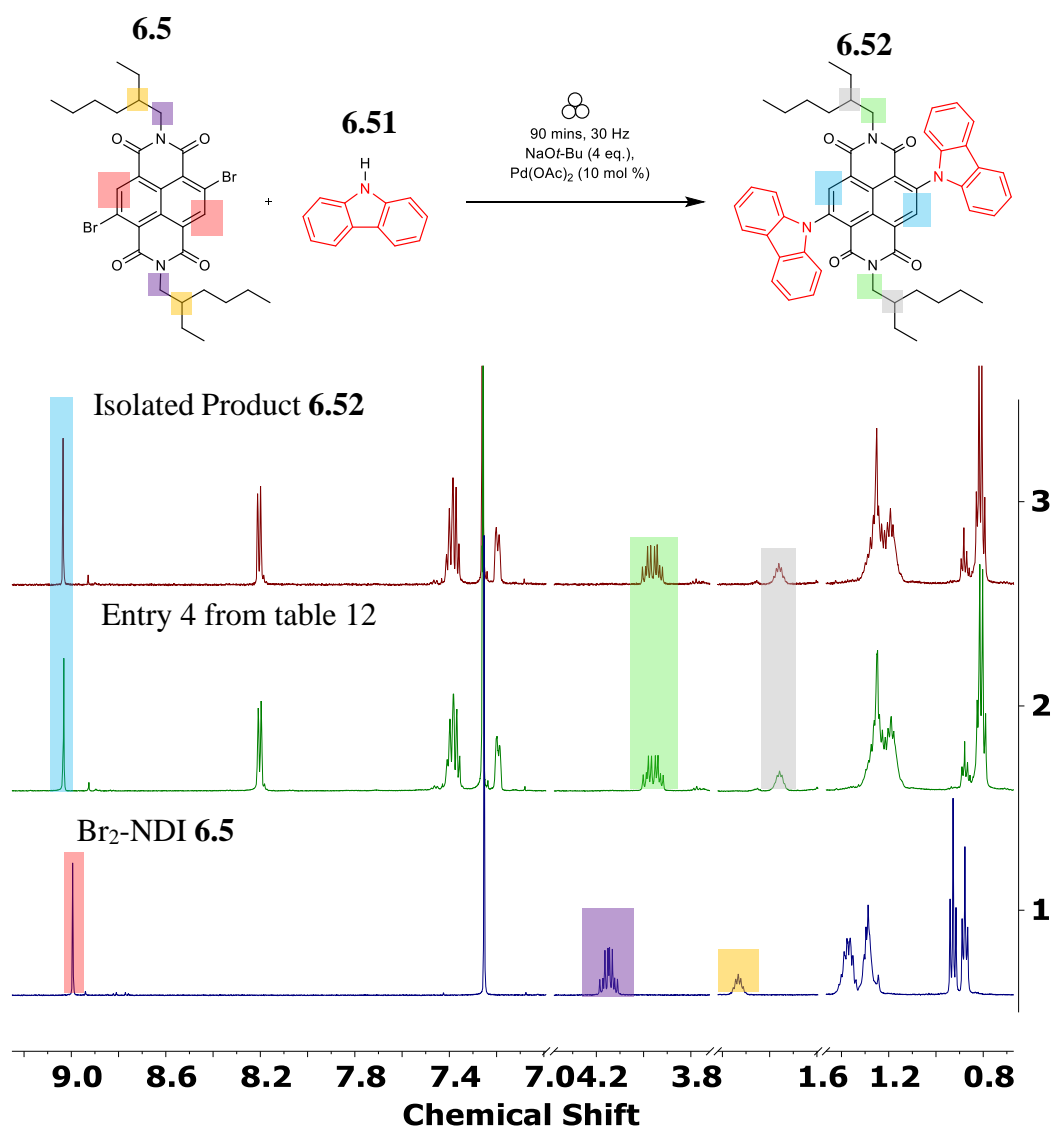


**Figure 67:** Partial  $^1\text{H}$  NMR from solid state BH reaction with palladium acetate catalyst

The complete conversion to the desired c-NDI species **6.28** (entry 1 in table 11) when combined with catalyst palladium acetate was observed. An established solid state LAG agent in cross coupling reactions<sup>274</sup> was required to achieve full conversion to desired c-NDI species **6.45** (entry 3 in table 11) in the Suzuki cross coupling reaction.

	Coupling	Coupling Species	Catalyst	Base	Time (mins)	LAG	% P
1	Sonogashira	<b>6.25</b>	Pd(OAc) <sub>2</sub>	DABCO	60	No	>98
2	Suzuki	<b>6.44</b>	Pd(OAc) <sub>2</sub>	K <sub>3</sub> PO <sub>4</sub>	60	No	86
3	Suzuki	<b>6.44</b>	Pd(OAc) <sub>2</sub>	K <sub>3</sub> PO <sub>4</sub>	60	1,5-cod	>98
4	Buchwald-Hartwig	<b>6.51</b>	Pd(OAc) <sub>2</sub>	NaOt-Bu	90	No	>98

**Table 11:** Solid state synthesis attempts of c-NDI species using a catalyst palladium acetate

## 6.2 Conclusion

The solution state high-throughput Kitalysis<sup>TM</sup> screening can be used to rapidly establish potential solid-state conditions for the cross coupling for a range of different coupling reactions: Sonogashira, Suzuki and Buchwald Hartwig. It was found to be an extremely useful technique to screen four bases simultaneously to establish the best base for the cross-coupling. High performing bases in the solution state generally performed well in the solid state as seen in Sonogashira and Buchwald-Hartwig coupling reactions. However, this was not always the case for catalysts as poorly performing catalysts performed well in the solid state for Suzuki cross-coupling (e.g. catalyst C5).

The greatest drawback of the high throughput solution technique is that it could only be used to assess six preloaded defined catalysts. Final solid-state reactions found that a commercially available, more stable, and cheaper pre-catalyst (palladium acetate) performed well in the solid state when combined with optimized bases for each coupling reaction. Overall, the solution state high-throughput technique is a useful technique that has time saving and low reagent quantity advantages however the preloaded nature of the catalysts limits the changeable variables for this technique. This led us to carry out a full solid-state optimization for each coupling reaction in the solid state in the following chapter. The scope of Sonogashira, Suzuki and BH coupling in c-NDIs with a range of coupling species was also investigated and will be discussed in the next chapter.

## Chapter 7

# **Solvent free synthesis of core-functionalised naphthalene diimides using a vibratory ball mill: Suzuki, Sonogashira and Buchwald-Hartwig reactions.**

This information in this chapter refers to our publication<sup>360</sup> whereby author contributions are listed below: B.W.G. conceived and supervised the work assisted by J.S. and M.C.B. The synthesis and photophysical studies were carried out by L.A.P. for all the reported compounds. D.G. carried out initial synthetic studies, assisted with purification and grew the single crystals for X-ray analysis. A.M., H.E., R.K.T. and A.J. conducted preliminary synthetic studies on the cross-coupling reactions of NDIs. R.G.-M. and C.A.I.G. conducted MS analysis of the samples. C.M.D. carried out ICP-MS. S.J.C and G.J.T. conducted X-ray analysis. B.W.G., L.A.P. and J.S. drafted the manuscript through discussion with all the authors who approved the final version of the manuscript.

# 7 Solvent free synthesis of core-functionalised naphthalene diimides using a vibratory ball mill: Suzuki, Sonogashira and Buchwald-Hartwig reactions.

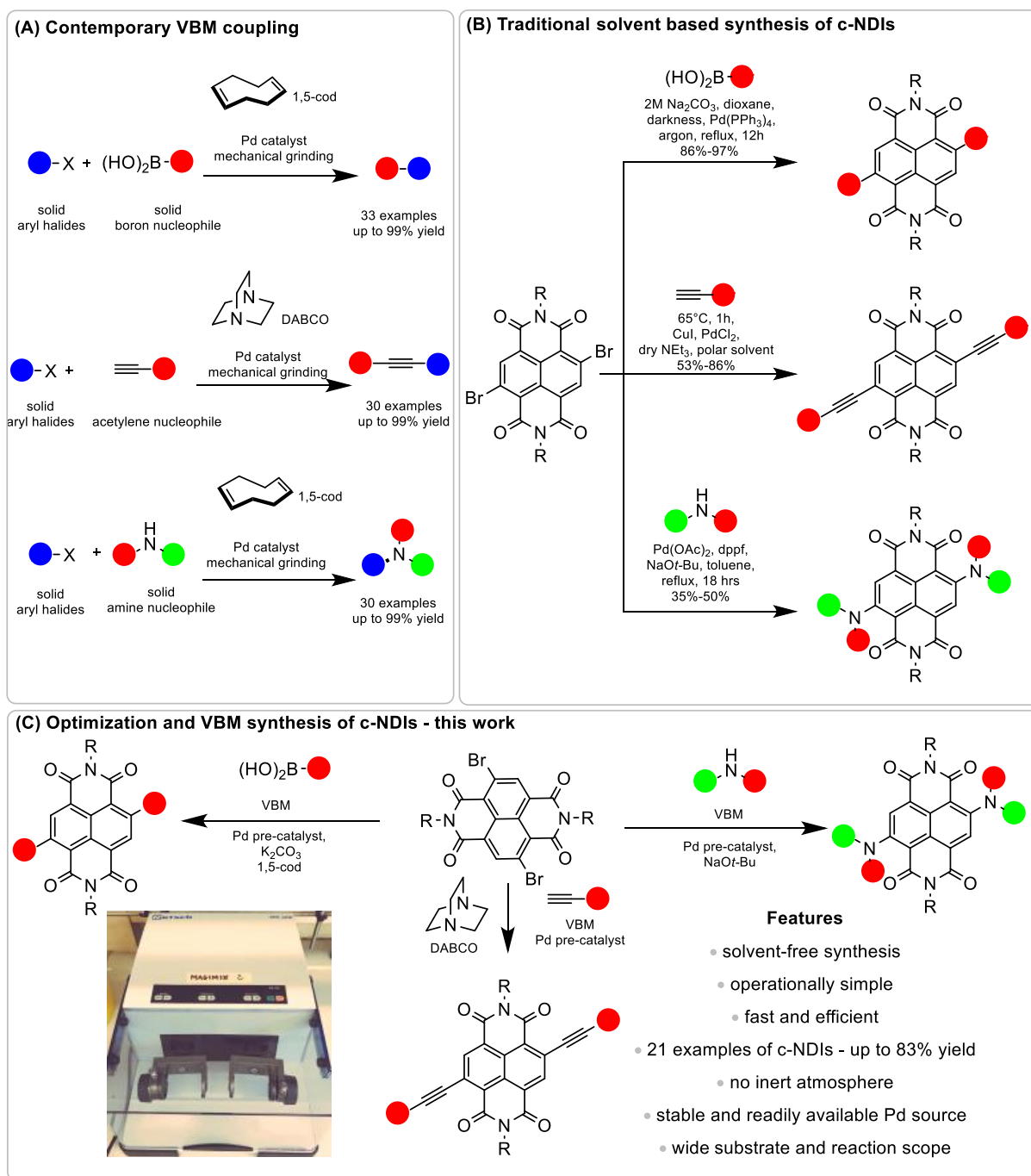
## 7.1 Introduction

As introduced in Chapter 5, metal catalysed reactions such as click chemistry,<sup>272</sup> activation of acyl azides<sup>273</sup> and couplings which include Suzuki,<sup>274,275</sup> Sonogashira (either containing copper<sup>276</sup> or copper free<sup>277,278</sup>) and Buchwald-Hartwig aminations<sup>282-284</sup> have all been successfully carried out in a ball mill ((A), Scheme 45). Ito and coworkers<sup>274,282</sup> found that addition of 1,5-cyclooctadiene (1,5-cod) as a liquid-assisted grinding (LAG) agent led to increased yields in Pd-catalysed cross coupling reactions on non-NDI derivatives, in the solid state as a consequence of decreasing the aggregation of Pd catalyst.

The synthesis of c-NDIs is reported in solution-based chemistry using Suzuki,<sup>335</sup> copper facilitated Sonogashira<sup>336-338</sup> and Buchwald-Hartwig<sup>339-341</sup> couplings ((B), Scheme 45). These processes often necessitate long reaction times (e.g. 18 hours), high temperatures (typically solvents at reflux, particularly toxic chlorinated or flammable aromatic solvents), strict anaerobic conditions, employing glove boxes and Schlenk line techniques. Sometimes, they also require light to be excluded.<sup>335</sup>

Herein, we report the solventless synthesis using VBM of c-NDIs *via* either Suzuki, copper-free Sonogashira or Buchwald-Hartwig coupling reactions ((D), Scheme 45). These require no

solvent and proceed rapidly ( $\leq 1.5$  h) using commercially available palladium sources, (frequently  $\text{Pd}(\text{OAc})_2$ ) and can be carried out under bench top conditions.



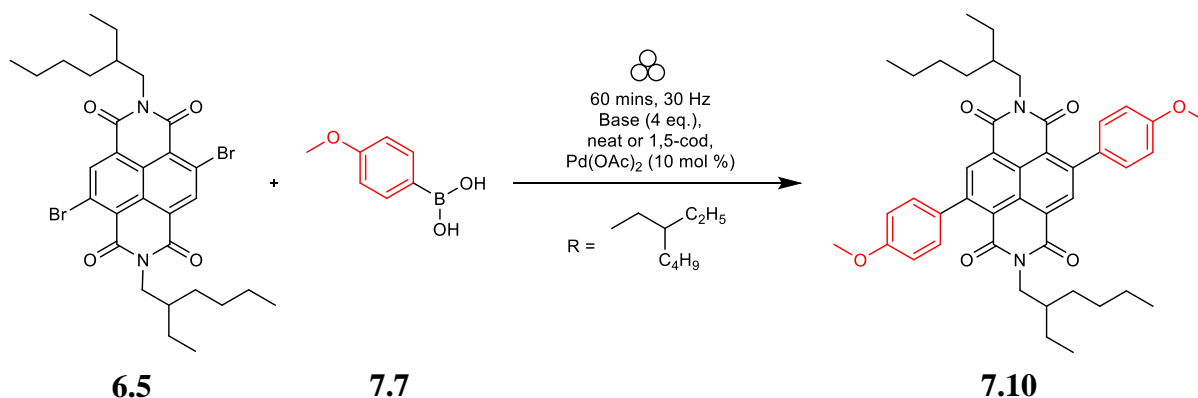
**Scheme 45:** Coupling reactions using VBM (A) and synthesis of c-NDIs (B-C). A) Contemporary VBM couplings on non-NDI derivatives; B) Traditional solvent-based synthesis of c-NDIs and C) Rapid optimization and VBM synthesis of c-NDIs. 1,5-cod = 1,5-cyclooctadiene carried out in this work.

## 7.2 Results and Discussion

### 7.2.1 Optimization of studies for Suzuki synthesis of c-NDIs

Our initial studies into the synthesis of c-NDI derivatives focused on the Suzuki coupling reaction,<sup>361</sup> a well-known solution state protocol used to produce this family of compounds.<sup>335</sup> These optimization reactions required the production of significant quantities of NDI-Br<sub>2</sub> (**6.5**), which was accessed using modified literature methods<sup>346,362</sup> in batches of up to 15 g without column chromatography.

An initial screening program using VBM conditions (zirconium oxide jars and milling balls) was carried out by varying the nature of the base, pre-catalyst and LAG additive, for the Suzuki coupling between **6.5** and (4-methoxyphenyl)boronic acid to yield **7.10** (Scheme 46). Conversion to **7.10** by <sup>1</sup>H NMR spectroscopy (%) was calculated to assemble Table 13.



**Scheme 46:** Solid state base and catalyst optimization conditions

The distribution of dispersion can be seen in the photographs of the milling jars for the base screen (Figure 68). Inorganic bases (K<sub>3</sub>PO<sub>4</sub>, KOH and NaOH) and select organic base NaOAc resulted in clumped distribution. Whereas, organic bases (Hunigs and NEt<sub>3</sub>), carbonates (Na<sub>2</sub>CO<sub>3</sub>, K<sub>2</sub>CO<sub>3</sub> and Cs<sub>2</sub>CO<sub>3</sub>) and lithium hydroxides gave finely dispersed crude material.

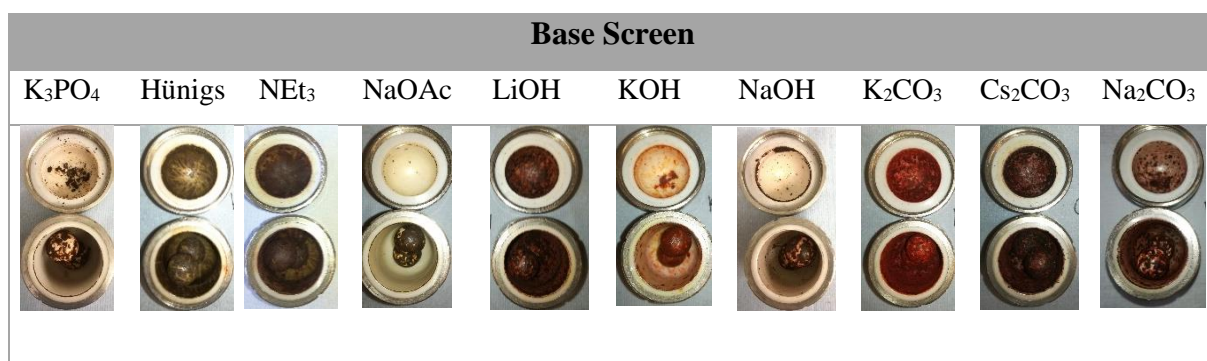


**Figure 68:** Photographs of the interior of the milling jars for the solid state base screen of Suzuki coupling reaction of *c*-NDI

Entry	[Pd]	Base [LAG]	Conversion to 7.20 by <sup>1</sup> H NMR spectroscopy (%)
1	Pd(OAc) <sub>2</sub>	Hünig's base	25
2	Pd(OAc) <sub>2</sub>	NEt <sub>3</sub>	31
3	Pd(OAc) <sub>2</sub>	LiOH	44
4	Pd(OAc) <sub>2</sub>	NaOH	>98
5	Pd(OAc) <sub>2</sub>	KOH	83
6	Pd(OAc) <sub>2</sub>	Na <sub>2</sub> CO <sub>3</sub>	54
7	Pd(OAc) <sub>2</sub>	K <sub>2</sub> CO <sub>3</sub>	>98
8	Pd(OAc) <sub>2</sub>	Cs <sub>2</sub> CO <sub>3</sub>	84
9	Pd(OAc) <sub>2</sub>	K <sub>3</sub> PO <sub>4</sub>	86
10	Pd(OAc) <sub>2</sub>	NaOAc	24
11	Pd(OAc) <sub>2</sub>	K <sub>3</sub> PO <sub>4</sub> [1,5-cod]	>98
12	XPhos Pd G3 (C1)	K <sub>3</sub> PO <sub>4</sub>	>98
13	SPhos Pd G2 (C2)	K <sub>3</sub> PO <sub>4</sub>	86
14	CataCXium®A Pd G3 (C3)	K <sub>3</sub> PO <sub>4</sub>	90
15	A Phos Pd G3 (C4)	K <sub>3</sub> PO <sub>4</sub>	93
16	P(Cy <sub>3</sub> ) Pd G3 (C5)	K <sub>3</sub> PO <sub>4</sub>	97
17	Pd-PEPPSI™-Ipent (C6)	K <sub>3</sub> PO <sub>4</sub>	>98

The ratio of the mass of reagents to the volume of grinding jars was *ca.* 20 mg.cm<sup>-3</sup>. Reactions were carried out for 1 h at room temperature and a pre-catalyst loading of 10 mol%. Conversions were determined by <sup>1</sup>H NMR spectroscopy in CDCl<sub>3</sub> by comparing the loss of starting material vs gain of product. When used, the LAG is *ca.* 10 wt% of the total reaction mass.

**Table 12:** Optimization of Suzuki coupling reactions and structures of pre-catalysts.

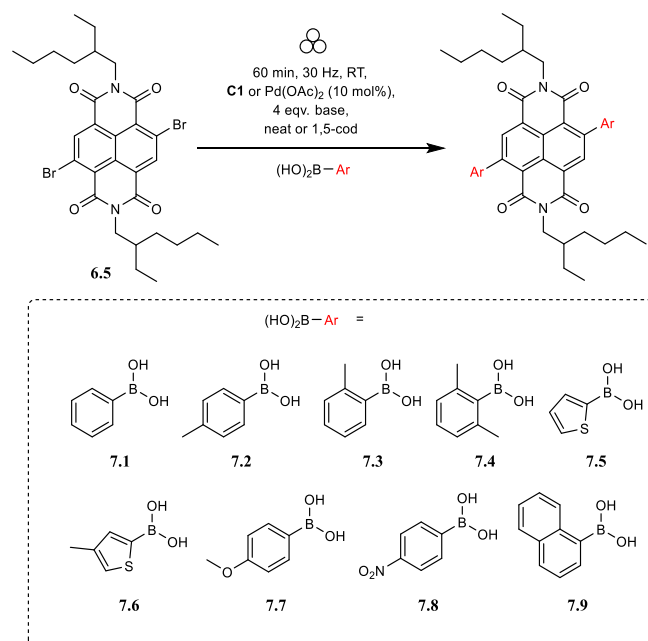
Initially, we selected Pd(OAc)<sub>2</sub> as an inexpensive and widely available pre-catalyst and screened a range of bases (Table 12). Organic bases that are liquid at room temperature performed poorly in these reactions (< 31% conversion, entries 1 and 2) compared to solid, inorganic hydroxides and carbonates (44% to >98%, entries 3-8). Notably, the use of both NaOH and K<sub>2</sub>CO<sub>3</sub> led to essentially full conversion (entries 4 and 7). Alternative inorganic bases, such as Cs<sub>2</sub>CO<sub>3</sub> and K<sub>3</sub>PO<sub>4</sub>, afforded slightly lower conversions (entries 8 (84%) and 9 (86%)).

To be able to observe the impact of other possible variables, we selected the base K<sub>3</sub>PO<sub>4</sub> that resulted in a moderate conversion (entry 9, 86%), for additive and catalyst optimization studies. As expected,<sup>274</sup> addition of the LAG, 1,5-cod, led to increased yields (entry 10, (84%) vs entry 11 (>98%)). We then screened a range of commercially available pre-catalysts containing different phosphine and NHC ligands (**C1-C6**, entries 12-17), to compare against the results for Pd(OAc)<sub>2</sub> (entries 1-11). These more active pre-catalysts led to higher yields; gratifyingly, XPhosPdG3 (**C1**) and Pd-PEPPSI<sup>TM</sup>-Ipent (**C6**) led to virtually complete conversion as determined by <sup>1</sup>H NMR spectroscopy.

## 7.2.2 Substrate scope for the synthesis of c-NDIs by Suzuki coupling

### 7.2.3 Suzuki Library Optimizations

A range of aryl and vinyl boronic acids **7.1** to **7.9** were reacted with cNDI in the presence of Pd(OAc)<sub>2</sub>, the addition of LAG and two bases (K<sub>2</sub>CO<sub>3</sub> and K<sub>3</sub>PO<sub>4</sub>) to probe the effect of the coupling species (Scheme 47). The conversion to desired disubstituted cNDI was then calculated *via* <sup>1</sup>H NMR spectroscopy and the results tabulated below (Table 13).



**Scheme 47:** Suzuki coupling of **6.5** with aryl boronic acids to produce c-NDIs

Entry	[Pd] (10 mol %)	Boronic acid	Base	LAG	<sup>1</sup> H NMR conversion (%) of c-NDI
1	Pd(OAc) <sub>2</sub>	7.1	K <sub>2</sub> CO <sub>3</sub>	-	>98
2	Pd(OAc) <sub>2</sub>	7.1	K <sub>3</sub> PO <sub>4</sub>	-	>98
3	Pd(OAc) <sub>2</sub>	7.2	K <sub>2</sub> CO <sub>3</sub>	-	>98
4	Pd(OAc) <sub>2</sub>	7.2	K <sub>3</sub> PO <sub>4</sub>	-	>98
5	Pd(OAc) <sub>2</sub>	7.3	K <sub>2</sub> CO <sub>3</sub>	-	>98
6	Pd(OAc) <sub>2</sub>	7.3	K <sub>3</sub> PO <sub>4</sub>	-	>98
7	Pd(OAc) <sub>2</sub>	7.4	K <sub>2</sub> CO <sub>3</sub>	-	0
8	Pd(OAc) <sub>2</sub>	7.4	K <sub>3</sub> PO <sub>4</sub>	-	0
9	Pd(OAc) <sub>2</sub>	7.4	K <sub>2</sub> CO <sub>3</sub>	1,5-cod	23
10	Pd(OAc) <sub>2</sub>	7.5	K <sub>2</sub> CO <sub>3</sub>	-	64
11	Pd(OAc) <sub>2</sub>	7.5	K <sub>3</sub> PO <sub>4</sub>	-	24

<b>12</b>	X Phos Pd G3 (C1)	<b>7.5</b>	K <sub>3</sub> PO <sub>4</sub>	-	21
<b>13</b>	X Phos Pd G3 (C1)	<b>7.5</b>	K <sub>2</sub> CO <sub>3</sub>	-	42
<b>14</b>	Pd(OAc) <sub>2</sub>	<b>7.5</b>	K <sub>2</sub> CO <sub>3</sub>	1,5-cod	>98
<b>15</b>	Pd(OAc) <sub>2</sub>	<b>7.6</b>	K <sub>2</sub> CO <sub>3</sub>	-	26
<b>16</b>	Pd(OAc) <sub>2</sub>	<b>7.6</b>	K <sub>2</sub> CO <sub>3</sub>	1,5-cod	>98
<b>17</b>	Pd(OAc) <sub>2</sub>	<b>7.6</b>	K <sub>3</sub> PO <sub>4</sub>	-	33
<b>18</b>	Pd(OAc) <sub>2</sub>	<b>7.7</b>	K <sub>2</sub> CO <sub>3</sub>	-	>98
<b>19</b>	Pd(OAc) <sub>2</sub>	<b>7.7</b>	K <sub>3</sub> PO <sub>4</sub>	-	86
<b>20</b>	Pd(OAc) <sub>2</sub>	<b>7.8</b>	K <sub>2</sub> CO <sub>3</sub>	-	29
<b>21</b>	Pd(OAc) <sub>2</sub>	<b>7.8</b>	K <sub>2</sub> CO <sub>3</sub>	1,5-cod	73
<b>22</b>	Pd(OAc) <sub>2</sub>	<b>7.8</b>	K <sub>3</sub> PO <sub>4</sub>	-	42
<b>23</b>	Pd(OAc) <sub>2</sub>	<b>7.9</b>	K <sub>2</sub> CO <sub>3</sub>	-	30
<b>24</b>	Pd(OAc) <sub>2</sub>	<b>7.9</b>	K <sub>2</sub> CO <sub>3</sub>	1,5-cod	66

The ratio of the mass of reagents to the volume of grinding jars was *ca.* 20 mg.cm<sup>-3</sup>. Reactions were carried out for 1 h at room temperature and a pre-catalyst loading of 10 mol%. Conversions were determined by <sup>1</sup>H NMR spectroscopy in CDCl<sub>3</sub> by comparing the loss of starting material vs gain of product. When used, the LAG is *ca.* 10 wt% of the total reaction mass.

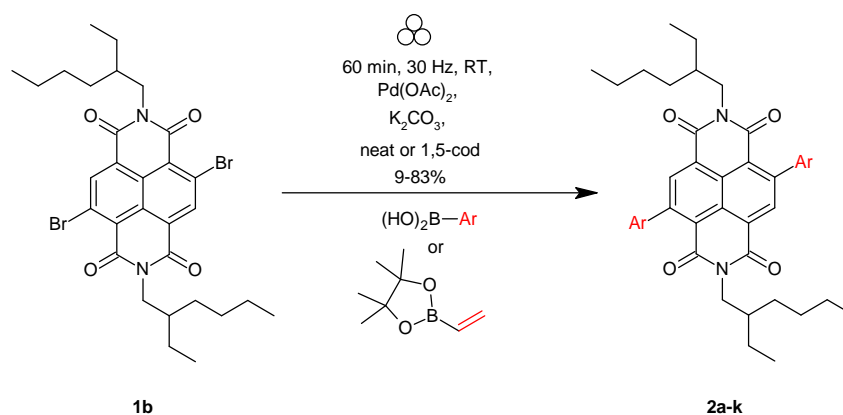
**Table 13:** Optimization of Suzuki coupling; screening choice of catalyst, boronic acids, base and addition of LAG.

As expected, based on the outcome of Table 12, K<sub>2</sub>CO<sub>3</sub> generally performed better than K<sub>3</sub>PO<sub>4</sub> for all substrates, apart from methyl substituted thiophene and para nitro substituted phenyl boronic acid (**7.6** and **7.8**, entry 17 and 22 respectively). 3 out of the selected 9 substrates achieved full conversion with K<sub>2</sub>CO<sub>3</sub> and K<sub>3</sub>PO<sub>4</sub> (**7.1**, **7.2** and **7.3**, entries 1 – 6 in Table 13), while **7.7** showed complete conversion only with K<sub>2</sub>CO<sub>3</sub> (entry 18). For **7.6**, **7.8** and substrates that experienced lower than complete conversion with K<sub>2</sub>CO<sub>3</sub>, conversion was greatly improved with the addition of known LAG 1,5-cod (**7.4**, **7.5**, **7.6**, **7.9**). The ineffectiveness of

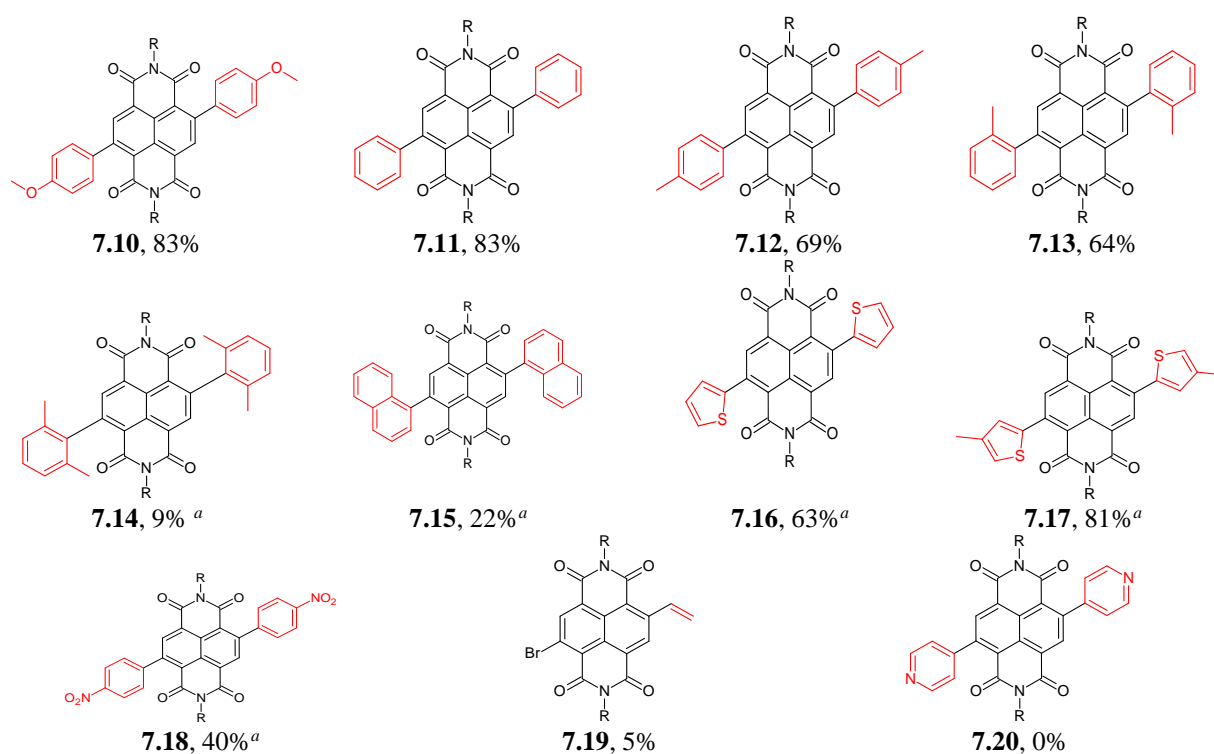
K<sub>3</sub>PO<sub>4</sub> for some substrates makes it an unsuitable base choice when aiming to investigate substrate scope.

The non-hygroscopic nature of K<sub>2</sub>CO<sub>3</sub> compared to NaOH (Table 12) made this base operationally simpler to use in a VBM. Next, the scope of the reaction was assessed using a selection of aryl and vinyl boronic acids to yield **7.10** – **7.20**, which were each isolated by flash column chromatography (Table 14). These conditions gave an excellent isolated yield for the phenyl substituted c-NDI after 60 min reaction time (**7.11**, 83%). This may be compared to reported solution state synthetic routes to phenyl substituted c-NDIs (10%; Suzuki coupling, 14 h, 100 °C, under nitrogen)<sup>341,363</sup> and 80% (CH arylation, 72 h, benzene under reflux ).<sup>364</sup>

Further expanding the substrate scope of this solid-state reaction revealed a small drop in yield when the coupling partner was substituted in either the *para* or *ortho* position, *viz.* **7.12** (69%) and **7.13** (64%). Couplings performed with the more sterically hindered 2,6-dimethylaryl-substituted boronic acid, furnished **7.14** in 9% yield. Thiophene and substituted thiophene containing c-NDIs were synthesised in yields over 80% (**7.16**, **7.17**), comparable to the reported solution state synthesis of **7.16**, *via* a Stille coupling<sup>365</sup> (80%, 5h, 90°C, N<sub>2</sub>) and CH arylation (96%, 17 h,<sup>47</sup> and 80%<sup>49</sup> in toluene at reflux, respectively). Aryl boronic acids substituted with electron donating groups were readily tolerated (**7.10** (83%)) although, as expected, a reduction in yield was observed for an electron poor aryl boronic acid derivative (**7.18** (40%)). Attempted di-addition of vinyl pinacol ester only yielded the monosubstituted vinyl c-NDI **7.19** in a low yield of 5%. Disappointingly, the di-pyridine c-NDI **7.20** could not be isolated despite closely related c-NDIs being reported by Bhosale and co-workers *via* solution state methodologies.<sup>335</sup>



### Scope of Suzuki coupled products (isolated yields)



Isolated yields. <sup>a</sup> 1,5-cyclooctadiene (10 wt%) as LAG agent. R = 2-ethylhexyl chain.

**Table 14:** Scope of c-NDI products 2a-2k synthesised via Suzuki coupling using VBM methods and isolated by flash column chromatography.

For several substituents, addition of 1,5-cod as a LAG agent markedly increased the conversion of **6.5** to the desired c-NDIs. This is exemplified in Figure 2 for the synthesis of **7.16**, which, shows the <sup>1</sup>H NMR spectrum of the starting material (**6.5**, Figure 69, spectrum 1) together with

the spectra of the crude reaction mixtures, straight after completion of ball milling. For the reaction that did not contain the LAG agent (Figure 69, spectrum 2) the conversion as measured by the ratio of the aromatic proton signals for **6.5** and **7.16** ( $\delta$ 8.99 and 8.75 ppm, respectively) was 64%, whereas essentially complete conversion was observed in the reaction that contained the LAG agent (Figure 69, spectrum 3).

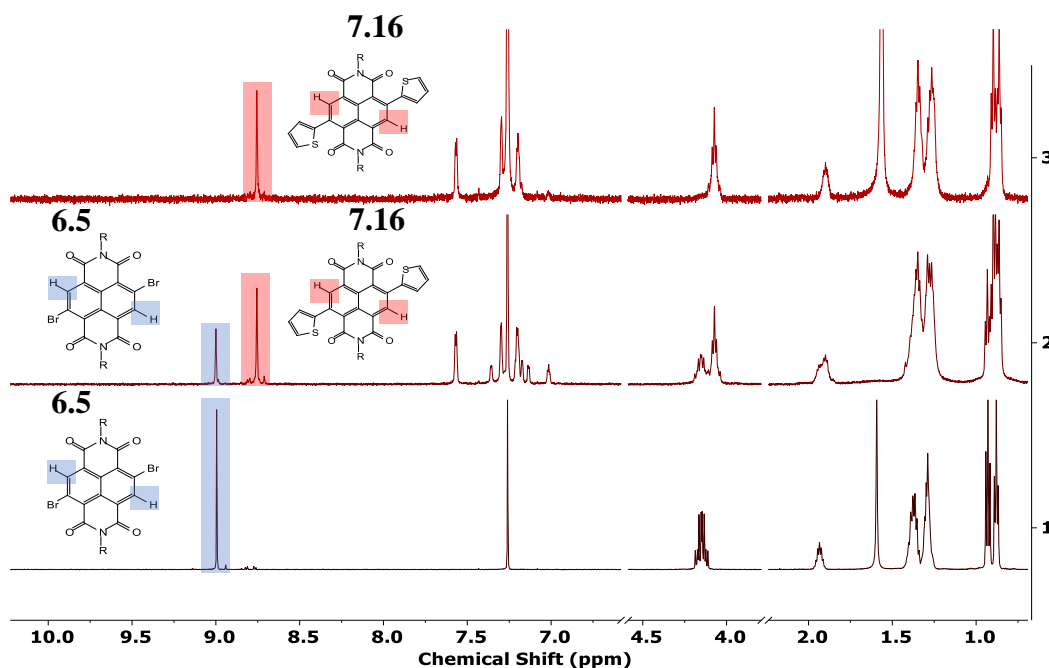
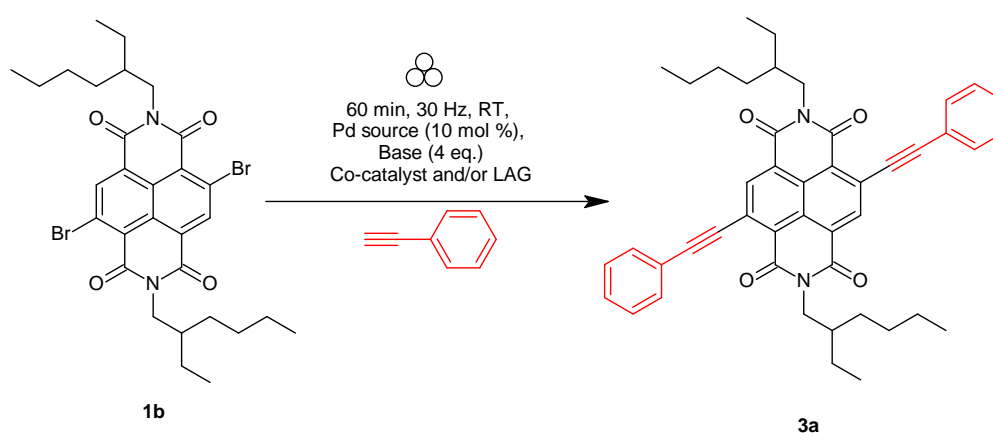


**Figure 69:** Stack of the spectra used to determine the conversion of **6.5** to **7.16** with and without the addition of LAG agent.  $^1\text{H}$  NMR spectra: (1)  $^1\text{H}$  NMR spectrum of starting material **6.5**. (2)  $^1\text{H}$  NMR spectrum of the crude reaction mix for **6.5** to **7.16** without LAG (conversion 64%). (3)  $^1\text{H}$  NMR spectrum of the crude reaction mix for **6.5** to **7.16** with LAG (conversion >98%).

## 7.2.4 Optimization studies and substrate scope for Sonogashira synthesis of c-NDIs

Sonogashira reactions to form c-NDIs are a less well studied derivatisation route compared to their Suzuki congeners.<sup>326,335</sup> Notwithstanding, diacetylene-substituted c-NDIs have suitable electronic properties for use in OLEDs<sup>338,366</sup> and n-type semiconductor materials<sup>351,367</sup> amongst

other applications.<sup>368,369</sup> Typical Sonogashira reaction conditions include the use of either an organic base such as diazabicyclooctane (DABCO)<sup>277</sup> or an inorganic base such as  $K_3PO_4$ ,<sup>370</sup> and a palladium source.<sup>350,371</sup> All reported solution state Sonogashira coupling reactions to form c-NDIs require the addition of a copper co-catalyst.<sup>336,338,372</sup> Using these precedents as guidance, a brief optimization study was carried out in order to form the diphenylacetylene substituted c-NDI **7.21** under VBM conditions (Table 15). Couplings using pre-catalyst **C2**, or  $Pd(OAc)_2$  and DABCO, resulted in essentially complete conversion to the disubstituted product **7.21** as determined by  $^1H$  NMR spectroscopy.

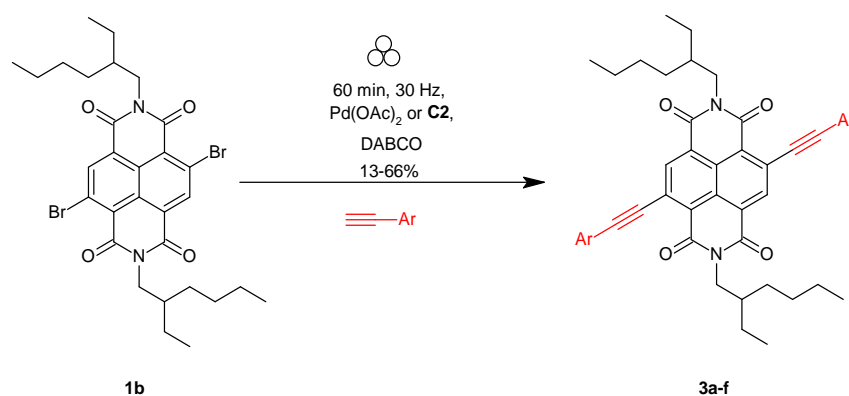


Entry	[Pd] (10 mol%)	Base	Co-catalyst	LAG	Time (min)	Conversion to <b>7.21</b> by $^1H$ NMR (%)
1	<b>C1</b>	$K_3PO_4$	CuI	None	60	32
2	<b>C1</b>	$K_3PO_4$	CuI	1,5-cod	60	45
3	<b>C2</b>	$NEt_3$	CuI	None	60	>98
4	<b>C2</b>	DABCO	None	None	60	>98
5	$Pd(OAc)_2$	DABCO	None	None	60	>98

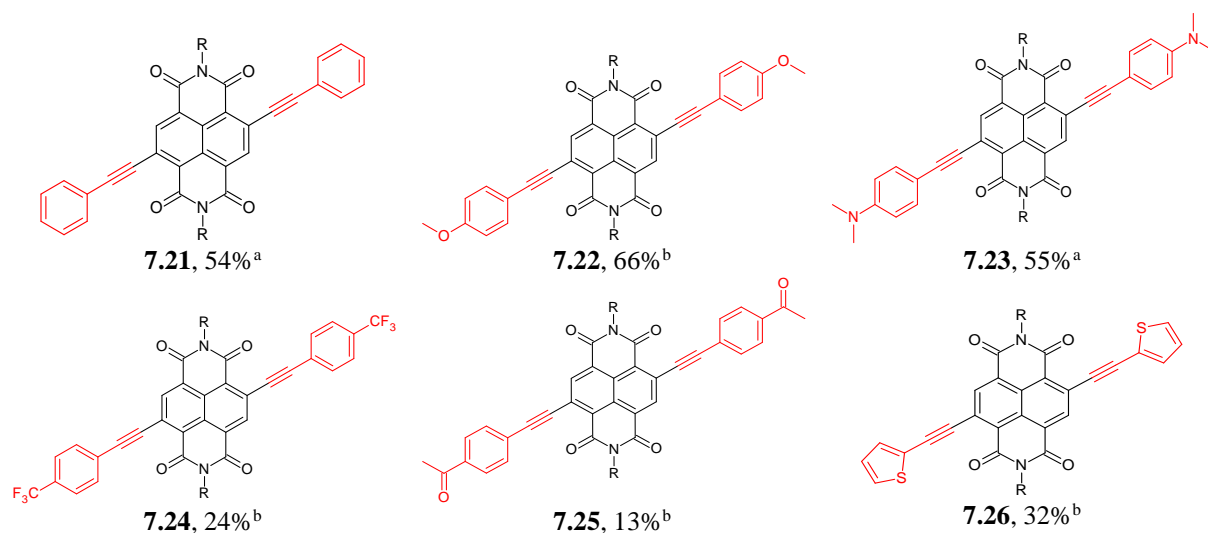
**Table 15:** Optimization of the Sonogashira coupling between phenylacetylene and **1b** in the solid state. 1,5-cyclooctadiene (10 wt%) as LAG agent.

The scope of the reaction was then assessed using a selection of aryl acetylenes to yield **7.21** – **7.26** under copper-free conditions where each product was isolated by flash column chromatography (Table 16). Double substitution of **6.5** by phenylacetylene gave **7.21** (54%

isolated yield) after only 60 min reaction time. Para-substituted electron donating aryl derivatives containing methoxy or *N,N*-dimethyl groups proceeded in similar yields (**7.22** (66%) and **7.23** (55%)). Reactions with aromatic coupling partners containing electron withdrawing groups were considerably less efficient. For example, the trifluoromethyl and keto-aryl c-NDI derivatives were isolated in 24% (**7.24**) and 13% (**7.25**) yield, respectively. Alkyne-thiophene substituted c-NDIs have been studied for use in OLEDs and n-type semiconducting materials<sup>351,367</sup> and **7.26** could be accessed under these VBM conditions (32%).



#### Scope of Sonogashira coupled products (isolated yields)



Isolated yields after flash column chromatography reported. <sup>a</sup> Using Pre-catalyst Pd(OAc)<sub>2</sub> <sup>b</sup> using pre-catalyst **C2**. R = 2-ethyl hexyl chain.

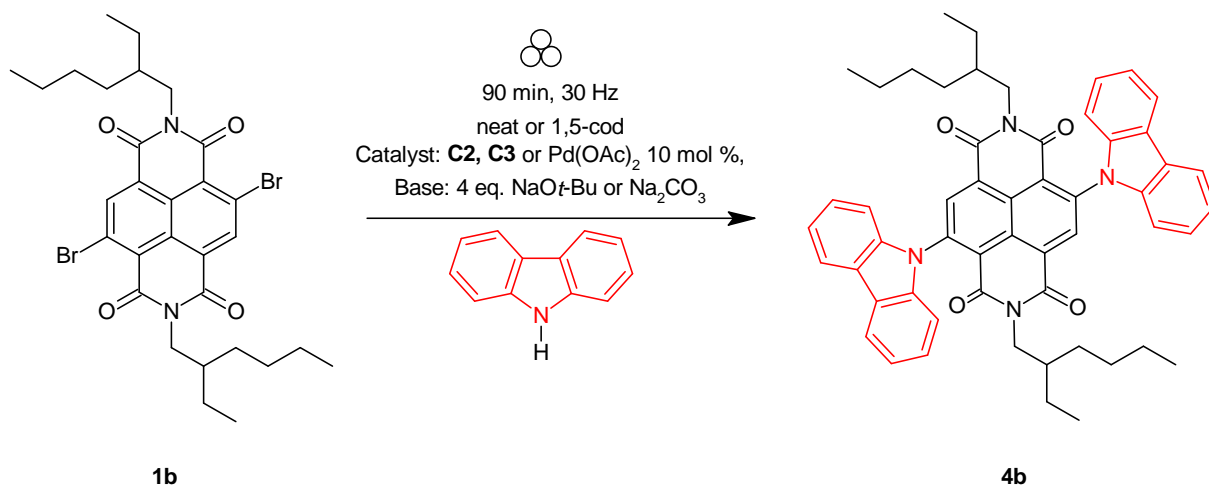
**Table 16:** Scope c-NDI synthesised via Sonogashira coupling (3a - 3f) using VBM and isolated by flash column chromatography.

## 7.2.5 Optimization studies and substrate scope for Buchwald-Hartwig amination of c-NDIs

Aminated c-NDIs have been demonstrated to behave as electron donor triads which exhibit spin-orbit charge-transfer intersystem crossing.<sup>341</sup> Compounds that have these properties are actively being studied for use in photo-dynamic therapy (PDT),<sup>373,374</sup> triplet-triplet annihilation (TTA) upconversion,<sup>375-377</sup> photocatalysis<sup>378-380</sup> and photovoltaic applications.<sup>381,382</sup>

Currently, there are three solution state studies which furnish aminated c-NDIs in modest yields (*ca.* 22-55%).<sup>339,383</sup> Each reports their synthesis using similar Buchwald-Hartwig type conditions: long reaction times (typically >12 h) with an inert solvent, a strong base such as sodium *tert*-butoxide, a palladium source, and a diaryl secondary amine as the coupling partner.

Using the solution phase optimized conditions as a starting point for our solid state studies,<sup>276</sup> we carried out an optimization study concerning the addition of carbazole to **6.5** (Table 17). Using pre-catalyst **C3**, we observed that increasing the reaction time from 60 to 90 min, led to increased conversions (entries 1 and 2 (73% to 84% respectively)). Furthermore, addition of the of the LAG agent, 1,5-cod, led to a further increase in conversion (entry 3 (>98%)). The use of either pre-catalyst **C2** or Pd(OAc)<sub>2</sub>, each with sodium *tert*-butoxide as base, also resulted in essentially complete conversion to the disubstituted product as determined by <sup>1</sup>H NMR spectroscopy (entries 4-5).

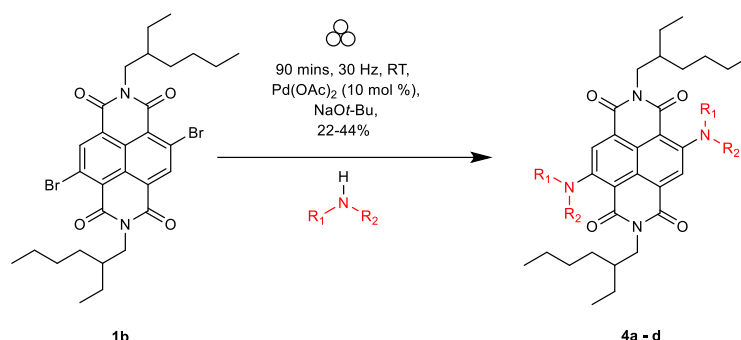


Entry	[Pd]	Base	Time (mins)	LAG	Conversion to 7.28 by <sup>1</sup> H NMR (%)
1	C3	NaOt-Bu	60	None	73
2	C3	NaOt-Bu	90	None	84
3	C3	NaOt-Bu	90	1,5-cod	>98
4	C2	NaOt-Bu	90	None	>98
5	Pd(OAc) <sub>2</sub>	NaOt-Bu	90	None	>98

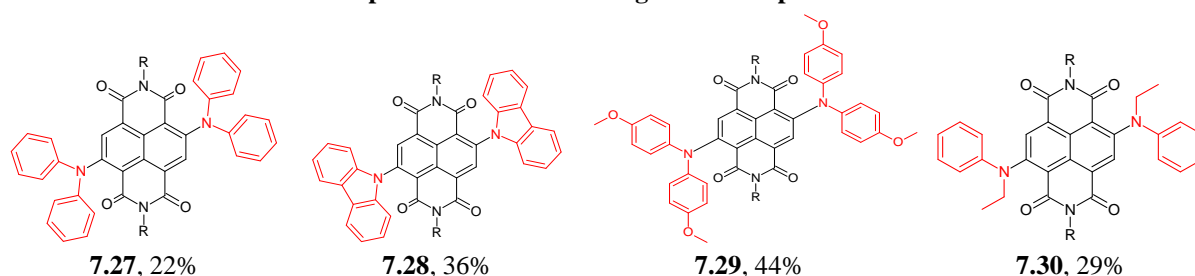
**Table 17:** Optimization of the Buchwald-Hartwig amination between carbazole and 1b under VBM conditions.

The scope of the reaction was assessed using a range of diaryl and aryl/alkyl secondary amines to yield **7.27** – **7.30** in the solid state (Table 18). These reactions proceeded in similar yields to the those reported for comparable solution state reactions (**7.27** (22%), vs. 20 - 50% in solution<sup>339,341</sup>) and carbazole (**7.28** (36%), vs. 42 - 43% in solution<sup>339-341</sup>). Electron rich groups were readily tolerated, for example *para*-methoxy substituted diphenyl amine gave **7.29** in 44% yield (*cf.* 42%<sup>339</sup> reported in the solution phase). The use of *N*-ethylaniline as a coupling partner led to the production of mono-aryl-mono-alkyl c-NDI, **7.30** (29%), which represents the first

time, to the best of our knowledge, that alkyl substituted amines (rather than diaryl substituted amines) have been coupled to NDI cores.



#### Scope of Buchwald-Hartwig amination products<sup>a</sup>



<sup>a</sup>Isolated yields after flash column chromatography. R = 2-ethylhexyl chain.

**Table 18:** Scope of c-NDI products **7.27** – **7.30** synthesised via Buchwald-Hartwig amination using VBM methods.

### 7.2.6 Impurity analysis after VBM synthesis

A problem encountered when synthesising species using cross reactions is the difficulty in removing relatively high levels of heavy metals in the products.<sup>384</sup> This could be exacerbated when using VBM synthesis by the possibility of the surface of the reaction vessel being eroded and furthering contaminating the products. Therefore, inductively coupled plasma - mass spectrometry (ICP-MS) was carried out on selected samples to see if residual Zr and Pd were present from the synthesis. **7.10** and **7.21** had Zr levels below the instrumental limit of detection

and had low residual levels of Pd (0.002 (**7.10**) and 0.003 (**7.21**) wt. %). **7.27** was found to have low but measurable levels of both of Zr (0.046 wt. %) and Pd (0.009 wt. %).

### 7.2.7 UV/vis Absorption properties of c-NDIs

A key design element of materials intended for electronic applications is an accessible and tuneable HOMO-LUMO energy gap, which is also responsible for the highly coloured nature of this class of molecule.<sup>372,385</sup> The panchromatic nature of c-NDIs produced in this work can be seen in their solution state absorption properties, where a broad range of colours is evident (Figure 70).



**Figure 70:** Photograph of 1 mM solutions of the starting material **1b** (left) and cross-coupled products **7.10** – **7.30** in chloroform under white light.

The UV-Vis spectroscopic data for all the c-NDI products are presented in Figure 84A-D. The introduction of substituents on the naphthalene core led to significant changes in the absorption spectra for the c-NDIs compared to the dibromo-NDI **6.5** (dashed black line in Figures 84A-D). All compounds, including **6.5**, exhibit a high energy absorption in the  $\lambda_{\max}$  310–380 nm (Table 19) region, which has been attributed to the NDI  $\pi$ - $\pi^*$  transition.<sup>336,337</sup> The c-NDIs (except dinitro species, **7.18**) also exhibited a lower energy band with  $\lambda_{\max}$  between 430-700 nm, which corresponds to the intramolecular charge transfer (ICT) transition.<sup>386</sup>

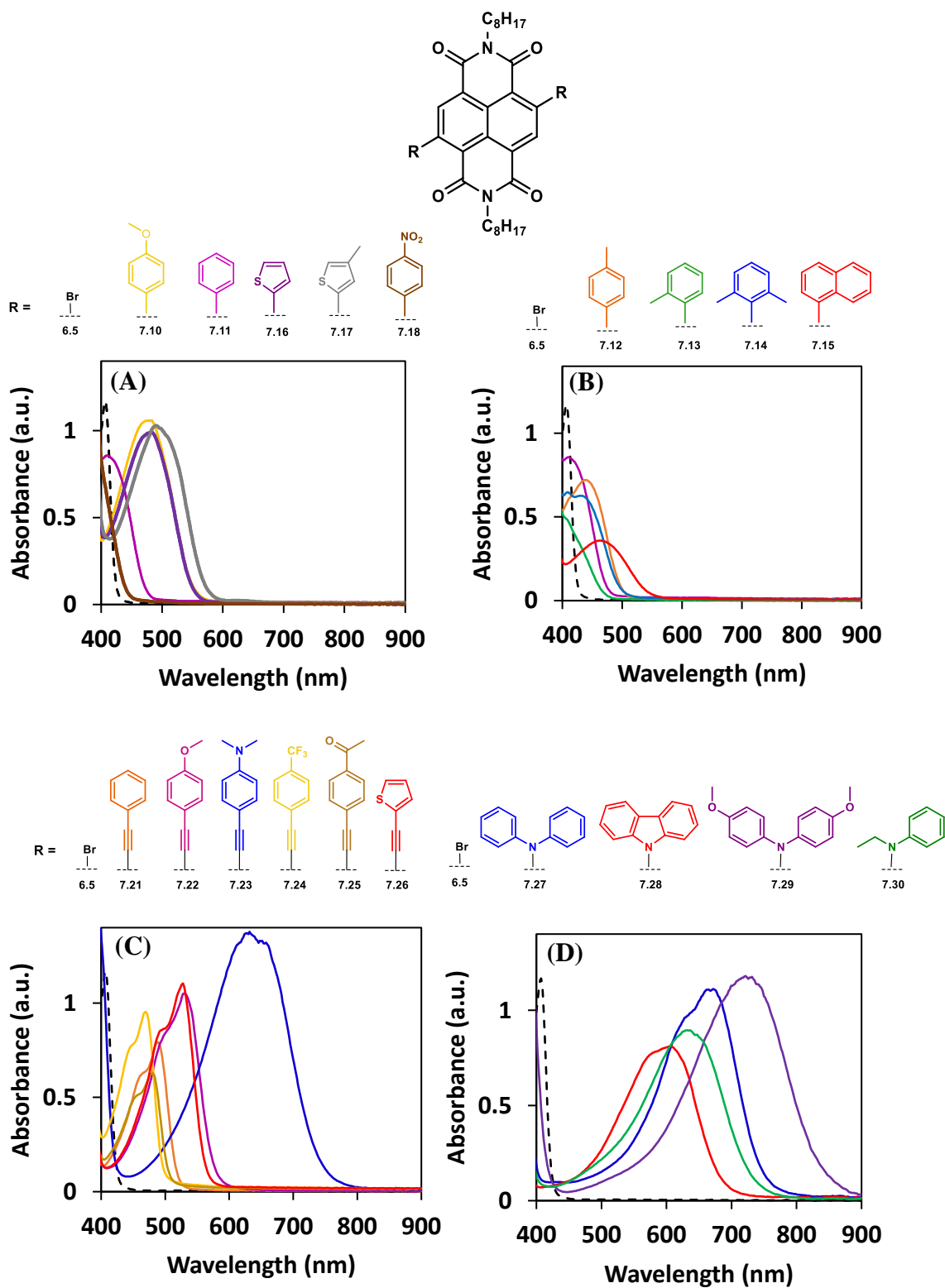


**Figure 71:** Photophysical data of c-NDIs as observed via UV/vis absorption spectroscopy (0.2 mM,  $\text{CHCl}_3$ ) for: Suzuki (A and B), Sonogashira (C) and Buchwald-Hartwig (D) coupled products.

c-NDI	$\pi$ - $\pi^*$ transition $\lambda_{\text{abs}}/\text{nm}$	ICT transition $\lambda_{\text{abs}}/\text{nm}$	c-NDI	$\pi$ - $\pi^*$ transition $\lambda_{\text{abs}}/\text{nm}$	ICT transition $\lambda_{\text{abs}}/\text{nm}$
<b>6.5</b>	357, 364	404	<b>7.21</b>	321, 370, 381	493
<b>7.10</b>	303, 359, 379	472	<b>7.22</b>	340, 374	526
<b>7.11</b>	357, 375	432	<b>7.23</b>	364, 396	646
<b>7.12</b>	359, 377	447	<b>7.24</b>	318, 374, 383	476
<b>7.13</b>	357, 375	434	<b>7.25</b>	329, 372, 381	485
<b>7.14</b>	358, 374	435	<b>7.26</b>	340, 360, 385	532
<b>7.15</b>	303, 359, 375	484	<b>7.27</b>	303, 346, 373	660
<b>7.16</b>	305, 364, 379	491	<b>7.28</b>	333, 353, 379	596
<b>7.17</b>	310, 362, 379	495	<b>7.29</b>	301, 360, 392	718
<b>7.18</b>	303, 362, 377	NS	<b>7.30</b>	336, 374	626

**Table 19:** UV-Vis absorbance values of **6.5** and c-NDIs **7.10** – **7.30** recorded at 0.2 mM in chloroform. (NS – not seen)

Comparison of the ICT transition value of the starting material **6.5** to those measured for the c-NDIs **7.10** – **7.18** shows that the addition of a phenyl ring through a carbon - carbon  $\sigma$ - $\sigma$  bond to the naphthalene core induces a bathochromic shift (from 404 nm (**6.5**) to 432 nm (**7.11**)). This is as a consequence of the extension of the  $\pi$ -conjugation region to the phenyl groups from the NDI core. Increasing  $\pi$ -conjugation further, for example by introduction of a naphthalene substituent onto the core (**7.15**), shows an even greater bathochromic shift in the ICT transition, to 484 nm.

The *para*-tolyl analogue **7.12** displayed a measurable additional bathochromic shift in the low energy transition when compared to the unsubstituted analogues (447 nm (**7.12**) compared to 432 nm (**7.11**)). However, *ortho*-mono- or dimethyl substitution of the aryl group had a negligible effect on the energy of the ICT transition (less than 3 nm difference compared to **7.11**). The presence of electron-rich substituents such as 3-methoxyaryl (**7.10**) or thiophene (**7.16**) shifts the ICT transition to significantly lower energies (472 and 491 nm respectively).

The methyl substituted more electron rich thiophene **7.17** exhibited the lowest energy absorption in the Suzuki c-NDI series, at 495 nm. Conversely, no significant electronic transitions were observed below 400 nm when a nitro substituent was on the aromatic ring attached to the NDI (**7.18**). This may be as a consequence of either a lack of an ICT transition in this species, or a hypsochromic shift in the ICT transition (to 377 nm) when compared to unsubstituted **7.11** (432 nm).

When studying the absorption characteristics of the c-NDIs produced *via* Sonogashira coupling reactions, the products generally exhibit a lower energy ICT transition (476-646 nm **7.21** – **7.26**) than those produced via the Suzuki reaction (432 to 495, **7.10** – **7.17**). This is consistent with the triple bond extending the region of conjugation compared to **7.10** – **7.17**. It also has been postulated that the steric clash between the *ortho* protons of the phenyl and the NDI core is reduced by the inclusion of the alkyne residue which, in turn allows more efficient orbital overlap in the  $\pi$ -conjugated system.<sup>385</sup> This narrowing of the HOMO–LUMO gap is evident as a red-shift of the ICT transition by 61 nm when comparing **7.21** (493 nm) to **7.11** (432 nm). The presence of electron-rich *para*-substituents such as a methoxy or NMe<sub>2</sub>-aryl, or indeed a thiophene residue on the c-NDI (**7.22**, **7.23** and **7.26**) led to a decrease in the energy of the ICT transition (526, 646, 532 nm, respectively) compared to the unsubstituted phenyl c-NDI (**7.21**, 493 nm). In contrast, electron withdrawing *para*-CF<sub>3</sub> (**7.24**, 476 nm) or acetyl substituted aryl analogues (**7.25**, 485 nm) show hypsochromic shifts compared to **7.21** (493 nm).

Finally, c-NDIs produced from the Buchwald-Hartwig reaction exhibited the largest stabilization of the HOMO-LUMO gap for a single series, with ICT transition values between 596-718 nm. Solutions of carbazole substituted NDI **7.28** were deep blue as a consequence of an ICT transition at 596 nm. This is significantly greater in wavelength than that observed for c-NDIs containing either phenyl/ethyl (**7.30**, 626 nm) or diphenyl (**7.27**, 660 nm) substituents.

Therefore, it appears that the rigidity of the carbazole as a consequence of the fused rings reduces the efficiency of the internal charge transfer process compared to the conformationally less constrained molecules in this series (e.g. **7.27** or **7.30**). The lowest energy ICT transition for the molecules studied in this work was observed for the methoxy-substituted diphenyl amine c-NDI (**7.30**) which exhibited an ICT transition of 718 nm compared to 404 nm for **6.5**.

## 7.2.8 Single crystal x-ray analysis

Single crystals for x-ray structure determination were grown by slow diffusion of heptane into a pyridine solution of **7.16** (Table 14) and **7.27** (Table 18). The resulting solid-state structures (Figure 72) revealed the correct regiochemistry of the product, and, therefore, by inference, the substitution pattern of **6.5**. Crystal packing for **7.16** is a monoclinic crystal system with  $P2_1/n$  space group whereas **7.27** displays a triclinic crystal system with  $P-1$  comprising two independent molecules with similar conformations. The branched alkane moieties **7.16** and **7.27** and the thiophene moiety of **7.16** are disordered in the crystal structures (see SI for details). There are no dominant, overarching structural features displayed in either structure. The major disorder component of **7.16** has a very weak thiophene C-H $\cdots$ O short contact (C $\cdots$ O distance 3.205(10)Å). The structure of **7.27** contains four very weak aromatic C-H $\cdots$ O short contacts (C $\cdots$ O distance 3.236(7)-3.264(6)Å).

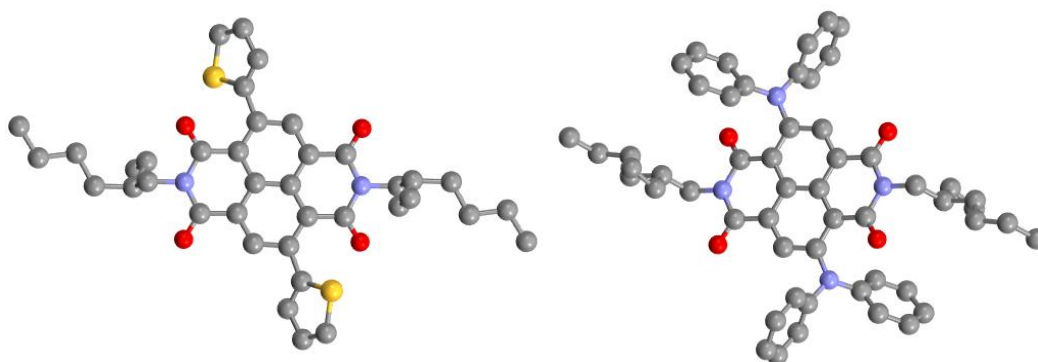
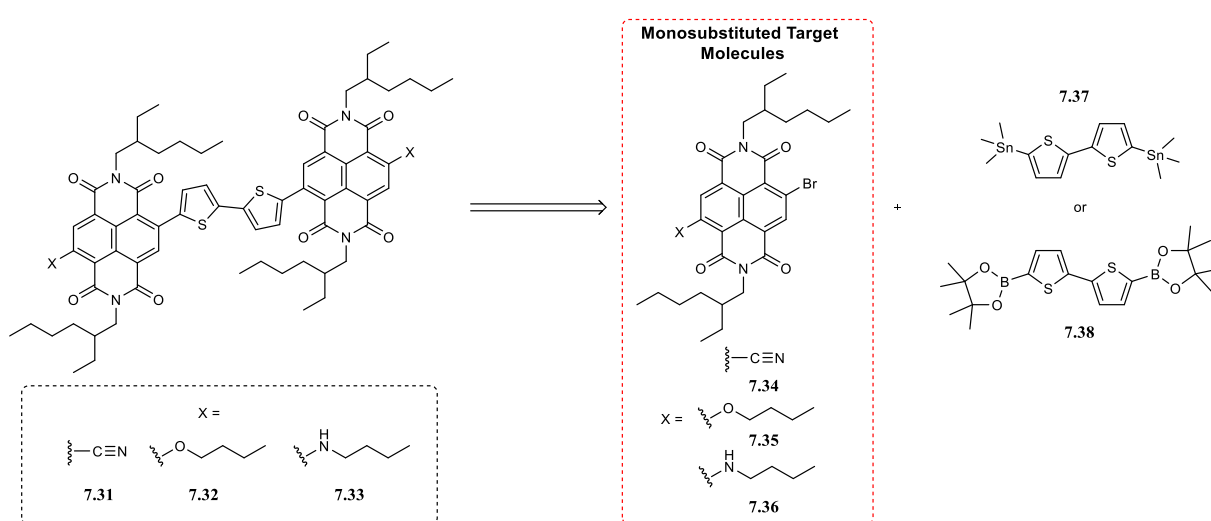


**Figure 72:** X-ray crystal structures of c-NDI **7.16** (left) and **7.27** (right). Minor disorder components and hydrogen atoms are omitted for clarity. Only one independent molecule is shown of **7.27**.

## 7.2.9 Applications: Synthesis of c-NDI dimeric systems suitable for OPVC applications

Small-molecule<sup>329,387</sup> and polymeric<sup>332,388</sup> structures containing c-NDIs have been shown to perform well as the electron accepting component in OPVCs. In particular dimer c-NDI species which sandwich an electron donating species (such as thiophene derivatives) between two NDI units capped with various end groups (**7.31**, **7.32** and **7.33**, Scheme 48)

As a final test of this VBM methodology, we wanted to synthesis one of these known c-NDI compounds used in OPVCs. The synthesis of the known monosubstituted NDI intermediates (**7.34**, **7.35** and **7.36**) was required for the synthesis of the dimer species **7.31**, **7.32** and **7.33**.



**Scheme 48:** Examples of c-NDI dimer species and synthesis pathways established by Kwon, An, Kim and McNeill groups.

Initially, the reaction to yield the monosubstituted NDI **7.34** was carried out. This involved the reaction of dibromo NDI starting reagent **6.5** with 1 equivalent of copper(I) cyanide in heated dry DMF an oxygen free environment. However, when the literature procedure was followed,<sup>387</sup> rather than the expected monosubstituted NDI **7.34**, repeated attempts kept resulting in the isolation of unwanted mono substituted NDI **7.39** and disubstituted cyanide cNDI **7.40**. Both

of these compound were isolated and fully characterised. The  $^1\text{H}$  NMR with appropriate shading of proton environments can be seen for both **7.39** and **7.40** (top and bottom spectra in Figure 73 respectively), compared to **6.5** starting reagent (middle spectrum, Figure 73) where the asymmetric aromatic protons of monosubstituted NDI are evident (shaded pink).

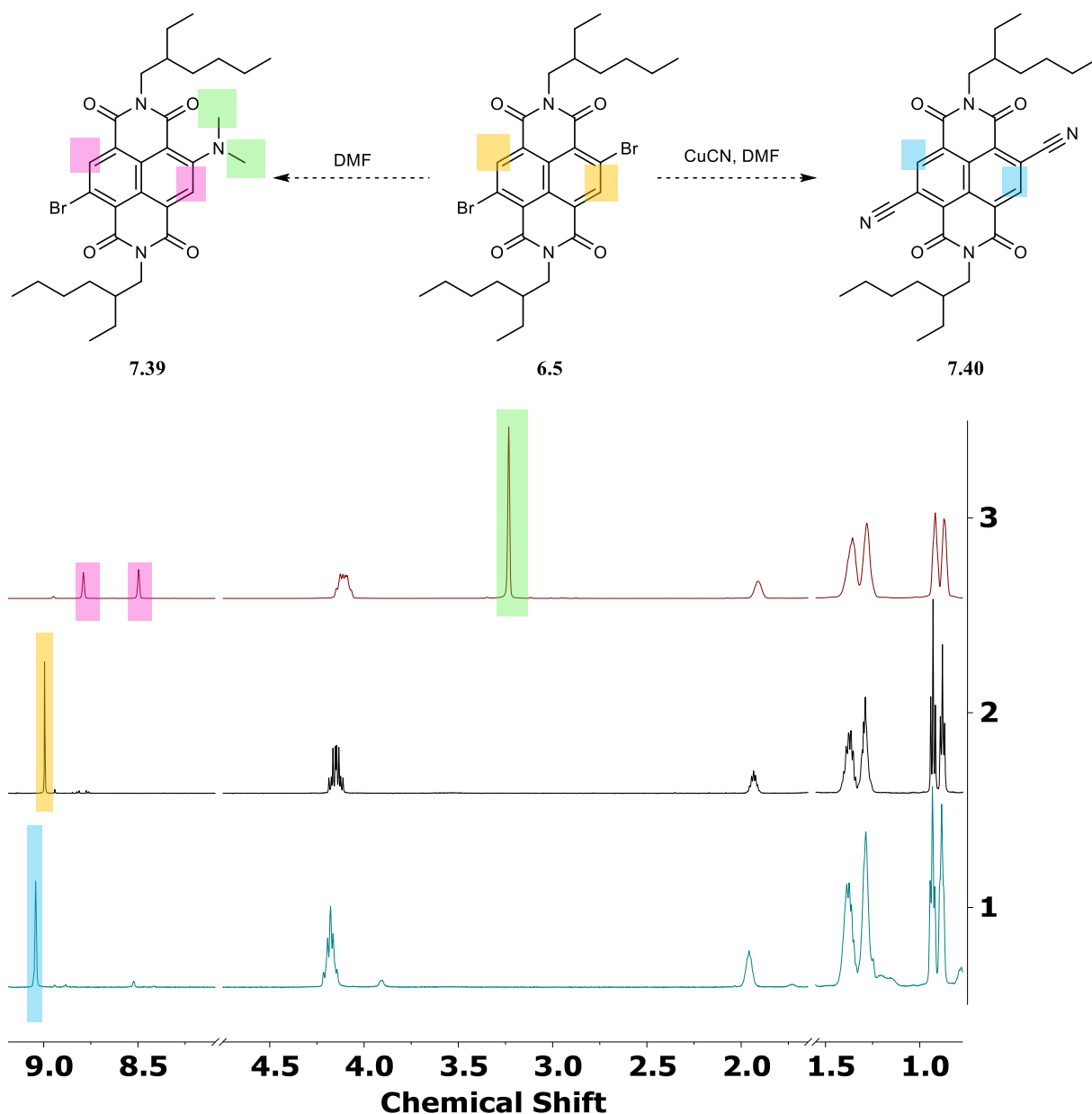
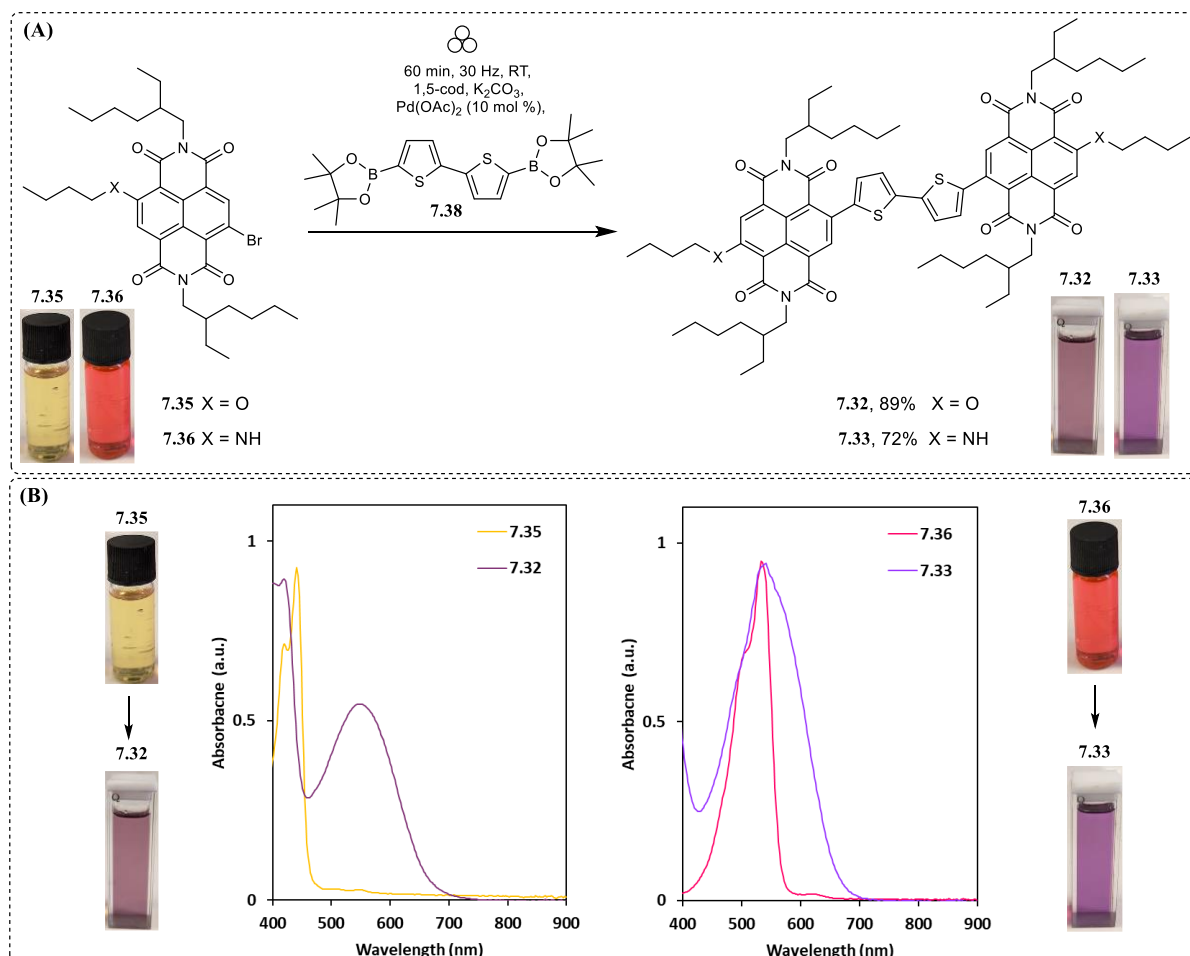


**Figure 73:** Proposed product for the mono-substitution reaction **7.34** and two isolated alternative products isolated when attempted **7.39** and **7.40**

The unsuccessful attempt to reach target **7.34** led us to attempt the synthesis of other mono-substituted cNDIs, namely those produced by the McNeil group (**7.35** and **7.36**)<sup>329</sup>. These were easily

produced following the literature procedure of either gentle heating of butyl alcohol and  $K_2CO_3$ , or addition of butyl amine at room temperature, to DCM with **6.5** to furnish desired mono cNDI, after purification *via* column chromatography. We then carried out Suzuki coupling on mono(brominated) NDIs **7.35** and **7.36** to produce two dimeric c-NDIs (**7.32** and **7.33**, A in Scheme 49). Each of these have been demonstrated to work as electron acceptor components in functioning OPVCs.<sup>329</sup> Using the conditions established above (Table 12), double addition of either **7.35** or **7.36** to the bis(pinacol ester) **7.38** gave the target species in just 1 h in air and without any exclusion of moisture (89% and 72% yield, respectively), comparable to the reported conditions for their solution state synthesis: 24 h, degassed toluene, at reflux (85% (**7.32**) and 80% (**7.33**)).<sup>329</sup> All four species exhibited a lower energy band with  $\lambda_{max}$  between 430-700 nm compared to **6.5**, corresponding to an ICT transition (B in Scheme 49).



**Scheme 49:** Synthesis of the molecular electron acceptor species **7.43** and **7.44**.

## 7.3 Conclusions

In conclusion, we have highlighted the synthesis of over 20 c-NDI structures using Suzuki, copper-free Sonogashira and Buchwald-Hartwig reactions under VBM conditions. The reactions proceed without solvent, in less than 90 min, and are tolerant of air and moisture. The purified products contained low residual levels of Pd and Zr. These VBM conditions were in contrast to those reported for the typical solution state synthesis of this class of molecule, where dry and degassed solvents, strict anaerobic conditions and longer reaction times (often 18 – 24 hours) are generally reported. In addition, the VBM conditions for the Sonogashira synthesis of c-NDIs are the first reported that do not require the addition of copper. Except for the *para*-dinitrophenyl substituted c-NDI (**7.18**) the remaining c-NDIs exhibited ICT transitions with  $I_{\max}$  in the visible region, between 432 and 718 nm. The VBM synthesis of dimeric c-NDIs (**7.32** and **7.33**) that are known to behave as electron acceptors in functioning OPVCs paves the way for a more environmentally friendly, solvent free method for production of all-polymer high value end products.

# **Chapter 8**

## **Conclusions and Future work**

# 8 Conclusions and Future Work

## 8.1 Review of Results

The work presented in this thesis has made substantial efforts towards the synthesis of  $\pi$ -poor materials which have applications in organic electronics as n-type semiconductive materials and supramolecular systems.

The Zincke reaction between a range of symmetric and asymmetric Zincke salts with aromatic amines, such as aniline or benzidine, yielded a set of oligomers that were water soluble and entirely conjugated (Chapter 2). Purification techniques such as reverse phase column chromatography were perfected to isolate dimer **2.2**, which contained 8 aromatic residues, allowing isolation of over 500 mg of clean product. A synthetic pathway for trimer **2.3** was established and the formation of **2.3** was confirmed by electrospray mass spectroscopy.

Chapter 4 reported an efficient synthesis of a range of six novel tweezer systems, each containing two,  $\pi$ -electron poor receptor sites connected by differing linker or end groups, totalling 13 distinct tweezer receptors. The binding constants and stoichiometry of the tweezer receptors with  $\pi$ -rich guest species were calculated using  $^1\text{H}$  NMR techniques on 17 binding motifs. All binding motifs were found to form  $\pi$ - $\pi$  stacked complexes with  $\pi$ -electron rich guest species in a 1:1 stoichiometry, where the guest species were found to be positioned in the cavity of the tweezer, with two face to face  $\pi$  -  $\pi$  stacking interactions. Tweezer receptors containing NDI residues generally displayed higher binding than those containing PDI or viologens, regardless of the linker or end group. There was no consistent trend between the flexibility of the linker and the strength of binding. Significant increase in binding constants were seen for tetracationic tweezer receptors in aqueous solvent systems compared to in organic solvents

(e.g. **Rigid-Vio-Ph**⊃**DHN**  $K_a = 204 \text{ M}^{-1}$  in  $\text{D}_2\text{O/TFA}$  and  $5.5 \text{ M}^{-1}$  in  $\text{MeOH/TFA}$ ). Ultimately, this study showed that the structural design cannot guarantee the binding behaviour due the subtle interplay between pre-organisation facilitating complex formation over greater flexibility enabling the complex to achieve a more energetically favourable binding geometries.

Core functionalisation of cNDIs using palladium cross coupling reactions such as Sonogashira, Suzuki and Buchwald Hartwig were achieved through solution state high-throughput Kitalysis<sup>TM</sup> screening (Chapter 6) and solid-state ball milling protocols (Chapter 7).

Solution state high-throughput screening was used as a time and reagent saving technique to find successful conditions to attempt in the ball mill. This was advantageous for base screening in Sonogashira and Buchwald Hartwig couplings however catalyst screening in the solution state for Suzuki coupling was not transferable in the ball mill. The preloaded nature of the catalysts limited the study of all the variables for this technique, and ball milling using  $\text{Pd}(\text{OAc})_2$  was found to be successful for the formation of cNDIs.

Solid state optimization of Suzuki, copper-free Sonogashira and Buchwald-Hartwig reactions using the ball mill were then followed to develop conditions which were used to synthesise 21 c-NDI structures. The ball milling reactions proceeded without solvent, in less than 90 mins, and were tolerant of air and moisture. This is in contrast to typical literature solution state synthesis of cNDIs, where dry and degassed solvents, strict anaerobic conditions and longer reaction times (often 18 – 24 hours) are often required. Visual analysis and UV-Vis studies displayed the colourful nature of these compounds. All the c-NDI compounds, bar the *para*-dinitrophenyl substituted c-NDI (**7.18**) exhibited ICT transitions with  $\lambda_{\text{max}}$  in the visible region between 432 and 718 nm. Finally, ball milling was used to synthesise dimeric cNDIs (**7.32** and **7.33**) that are known to behave as electron acceptors in functioning OPVCs. This work paves

the way for a more environmentally friendly, solvent free method for production of all-polymer high value end products

## 8.2 Future Work

The Zincke reaction was successfully employed to synthesise a set of conjugated n-type oligomers. The trimer **2.3** was shown to have been successfully synthesised but isolation was not possible. Future work could include scaling up the reaction shown in this work to yield higher quantities of trimer. With a full set of oligomers, electrochemical techniques such as cyclic voltammetry would provide insight into the effect of increasing the conjugation, gain understanding into redox processes taking place and would assess the effectiveness of these species as n-type semiconductive materials.

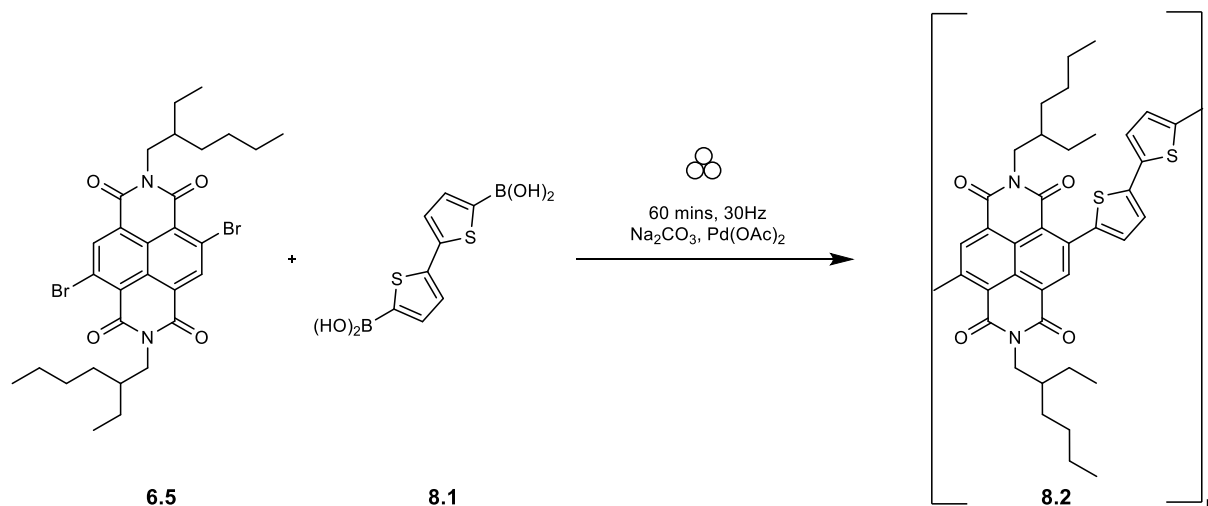
The Kitalysis<sup>TM</sup> optimization technique has shown merit in rapid assessment of variables such as base screening in palladium cross coupling. Future work could include base screens on Heck, Hiyama or Stille cross coupling reactions with cNDIs.

<sup>1</sup>H NMR spectroscopy was used to probe the ability of one of our tweezer systems, **Rigid-Vio-Ph**  $\supset$  **DHN**, to be controllably un-complexed by an external chemical stimuli, in this instance by the addition of base NEt<sub>3</sub>. This was found to be successful, but the work is still in the early stages. Refining the probing experiment and studying if the other five tweezer systems behave in this way would be interesting and open the potential to apply these tweezer systems to real world applications. Another avenue of future work for our tweezer systems would be to study the suitability of the binding motifs to separate and resolve isomers or mixtures of PAHs. This concept is inspired by Stoddart's Exbox<sup>4+</sup> PAH scavenger and by Li and co-workers work

where they exploited the favourable binding to separate and resolve two isomers (phenanthrene and anthracene).

With an established ball milling protocol for the synthesis of core functionalized NDIs using Suzuki, Sonogashira and Buchwald-Hartwig cross coupling, probing if this protocol is successful with core functionalised perylene diimides would open up this green synthesis technique to another class of rylene diimide that have known applications in organic electronics.<sup>389</sup>

We were able to develop solid state Suzuki coupling conditions to enable dithiophene addition to two c-NDI residues which produced two dimers (**7.32** and **7.33**) that are reported to be electron acceptors in functioning OPVCs. Transferring these conditions to the synthesis of thiophene-containing NDI copolymers (**8.2**) such as those reported by Durban and co-workers, which were shown to have application in OFET devices.<sup>332</sup> The proposed solid state synthesis route is shown below (Scheme 50).



**Scheme 50:** Proposed solid state conditions for the synthesis of c-NDI polymers that are known to work as n-type semiconductors in functioning OPVCs.

# **Chapter 9**

## **Experimental Details.**

# 9 Experimental Details

## 9.1 Materials

Reagents were purchased from Merck, Fisher Scientific UK Ltd, Tokyo Chemical Industry UK Ltd or Fluorochem Ltd, and used without further purification.

## 9.2 Instrumental details

### 9.2.1 General instrumental details for this thesis

UV-Vis measurements (300-900nm) were recorded at room temperature on a Perkin Elmer Lambda 25 double beam spectrometer.

$^1\text{H}$  (600 MHz) and  $^{13}\text{C}$  NMR (150 MHz) spectra were recorded on a Varian VNMRS 600 MHz spectrometer, at room temperature, using the residual protic solvent signal in the deuterated solvent for calibration ( $\text{CDCl}_3$  at 7.26 ppm,  $\text{DMSO-}d_6$  at 2.50 ppm,  $\text{D}_2\text{O}$  at 4.79 ppm,  $\text{CD}_3\text{CN}$  at 1.94 ppm or  $\text{CD}_3\text{OD}$  at 3.31 ppm). Chemical shifts are reported in ppm. Spin multiplicities are reported as a singlet (s), doublet (d), triplet (t) or multiplet (m). with coupling constants ( $J$ ) given in Hz, where applicable.

FTIR spectra were recorded over a range of 4000-500  $\text{cm}^{-1}$  on a PerkinElmer Spectrum One FT-IR fitted with a UATR polarisation accessory.

## 9.2.2 Chapter 2 instrument details

Mass spectrometry was performed by Dr. Hart using the Bruker MicroTOF QII instrument for dimer **2.2** and trimer **2.3** at the University of Reading with the following conditions - T: FTMS + p ESI Full ms [80.00-1000.00].

Purifications of dimer **2.2** and intermediate **2.17** were performed *via* reverse phase flash column chromatography on silica gel (43 g Reusable RediSep® Rf C18 Reversed Phase Columns, 40–60 microns) with varying ratios of acetonitrile and MeOH. Analytical thin layer chromatography (TLC) was performed on RP-18 W/UV254 Octadecyl-Modified HPTLC Silica.

## 9.2.3 Chapter 4 instrument details

Literature protocols followed to yield **4.18**,<sup>197</sup> **4.7** + **4.8**,<sup>226</sup> **4.12**,<sup>390</sup> **4.11**<sup>391</sup>, **4.17**<sup>236</sup> and **Flexi-NDI-Hex**.<sup>226</sup> UV-Vis sample details: all tweezers were prepared at 3mM concentration and recorded at 298K. tweezer systems **Rigid-NDI-Hex**, **Flexi-NDI-Bn**, **Rigid-PDI-Hex**, **Flexi-NDI-Hex**, **Flexi-NDI-Bn**, **flexi-NDI-Ph**, **Flexi-PDI-Bn** and **Flexi-PDI-Hex** were recorded in CHCl<sub>3</sub>:trifluoroacetic acid (9:1) and diviologen systems **Rigid-Vio-Ph** and **Flexi-Vio-Ph** in MeOH.

High Resolution Mass Spectrometry (HRMS) data for samples were obtained by Dr Iain Goodall of the University of Greenwich Mass Spectrometry Service using a Waters (Wilmslow, UK) Synapt G2 Q-ToF HRMS. Chromatographic characterisation was provided by a Waters H-class UPLC pumping module with heated column and auto-sampler, running a reversed-phase gradient. Single crystals of **4.14** and **4.15** were grown *via* slow evaporation. Crude materials were dissolved in water with 2% acetic acid and crystal of SCXRD quality formed

over 1 week. Diffraction data were obtained by Dr. Mark Roe of the University of Sussex on an Agilent Excalibur with CCD plate detector using Cu-K $\alpha$  radiation ( $\lambda = 1.54184$ ) and solved using Olex 2.0. Deposited onto the Cambridge Crystallographic Data Centre (CCDC) with Deposition Number 2193929 for compound **4.14** and 2193928 for **4.15**.

<sup>1</sup>H NMR job plots and binding study techniques: Job plots were constructed using the shifts of data points from <sup>1</sup>H NMR studies where increased molar proportions of guest species were added to host species at a fixed total concentration of host and guest. The molar fraction of host was plotted against  $\Delta\delta$  divided by the mole fraction of host. The titration studies were carried out at the highest concentration that the solubility of host would allow, and the solvent selected was governed by the solubility of the system. Increasing quantities of guest were added to aliquots of a fixed concentration of host. The binding constants were calculated from <sup>1</sup>H NMR titration studies using BindFit<sup>146,147</sup> (<http://supramolecular.org>) where 1:1 binding model and Nelder-Mead algorithm were selected for all systems.

## 9.2.4 Chapter 6 & 7 instrument details

The ball milling reactions were carried out in a Retsch MM400 vibratory ball mill (VBM) operating at 30 Hz. Milling load is defined as the sum of the mass of the reactants per free volume in the jar and unless stated otherwise was calculated to be *ca.* 20 mg.mL<sup>-1</sup>.

UV-Vis sample details: 1 mM stock solution of samples dissolved in CHCl<sub>3</sub> (Figure S3) and diluted to 0.2 mM for UV-vis measurements.

Unless stated otherwise, purifications were performed *via* flash column chromatography on silica gel (RediSep® Rf Silica Gel Disposable Flash Columns, 40–60 micron) on Teledyne

ISCO CombiFlash Lumen apparatus. Analytical thin layer chromatography (TLC) was performed on silica gel 60 F254 (Merck).

ESI mass spectra for compounds **7.14**, **7.18**, **7.19**, **7.39** and **7.40** were obtained by Dr. Ramon Gonzalez-Mendez using a Waters Xevo G2 Q-ToF HRMS (Wilmslow, UK) equipped with analytical flow ESI source. ESI experimental parameters were: capillary voltage 3.0 kV, sampling cone 35, extraction cone 4, source temperature 120 °C and desolvation gas 450°C with a desolvation gas flow of 650L/h and no cone gas. MS conditions were MS1 in resolution mode between 100-1500 Da. Accurate mass data was obtained using MassLynx software. All accurate mass data was within  $\pm 5$ ppm from its theoretical value. ICP-MS analysis for metals was done by Dr. Christopher Dadswell using an Agilent 7500ce ICP-MS instrument with collision cell (He as collision gas) for Fe and standard mode (no collision gas) for Zr and Pd, using  $^{72}\text{Ge}$  as internal standard. The following experimental parameters were used: a) plasma: RF power 1500 W, sampling depth 8.5mm, carrier gas 0.8L/min, make-up gas 0.11 L/min; b) quadrupole: mass range 1-250 amu, dwell time 100 msec, replicates 3, integration time 0.1sec/point. Calibration solutions were prepared for each element between 0 and 200ng/mL using certified reference standards (Fisher Scientific, UK)

High Resolution Mass Spectrometry (HRMS) data for all other samples in this chapter were obtained by Dr Iain Goodall of the University of Greenwich Mass Spectrometry Service using a Waters (Wilmslow, UK) Synapt G2 Q-ToF HRMS. Chromatographic characterisation was provided by a Waters H-class UPLC pumping module with heated column and auto-sampler, running a reversed-phase gradient.

Solid State Structure determination: Crystals of compound **7.16** were grown from pyridine and heptane using the slow diffusion method at room temperature. A single red rod-shaped crystal

0.10×0.03×0.03 mm<sup>3</sup> was selected and mounted on a MITIGEN holder in perfluoroether oil on a Rigaku 007HF diffractometer equipped with Arc)Sec VHF Varimax confocal mirrors and a UG2 goniometer and HyPix 6000HE detector. The crystal was kept at a steady  $T = 100(2)$  K during data collection. The structure was solved with the **ShelXT** 2018/2<sup>392</sup> structure solution program using the using dual methods solution method and by using **Olex2**<sup>393</sup> 1.5-alpha (Dolomanov *et al.*, 2009) as the graphical interface. The model was refined with **ShelXL** 2018/3<sup>243</sup> using full matrix least squares minimisation on  $F^2$  minimisation.

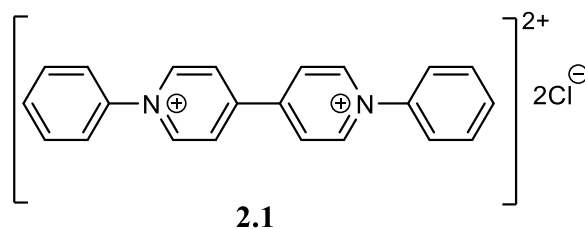
Crystals of **7.27** were grown from pyridine and heptane using the slow diffusion method at room temperature. A suitable single blue lath-shaped crystal of **7.27** with dimensions 0.20 × 0.04 × 0.01 mm<sup>3</sup> was selected and mounted on a MITIGEN holder in perfluoroether oil on a Rigaku 007HF diffractometer with HF Varimax confocal mirrors, an AFC11 goniometer and HyPix 6000HE detector diffractometer. The crystal was kept at a steady  $T = 100.00(11)$  K during data collection. The structure was solved with the **ShelXT** 2018/2<sup>392</sup> solution program using dual methods and by using **Olex2**<sup>393</sup> 1.5- $\alpha$  as the graphical interface. The model was refined with **ShelXL** 2018/3<sup>243</sup> using full matrix least squares minimisation on  $F^2$ .

Deposited onto the Cambridge Crystallographic Data Centre (CCDC) with Deposition Number 2159473 for compound **7.16** and 2159474 for **7.27**.

## 9.3 Detailed synthetic procedures

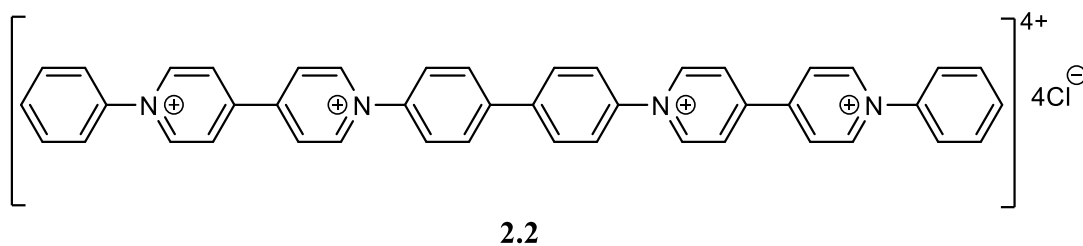
### 9.3.1 Chapter 2

#### Synthesis of unimer **2.1**



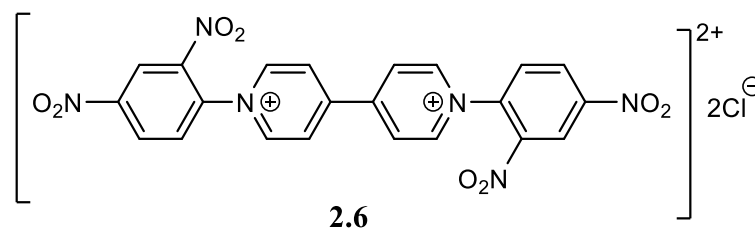
Synthetic procedure, Characterisation data Zincke salt **1** (0.902 mg, 1.59 mmol) was dissolved in a mixture of methanol (180 mL) and water (45 mL) with aniline (1.395 g, 15.00 mmol). The reaction mixture was heated to reflux and stirred vigorously under argon for 3 days. After cooling to room temperature, the solvent was evaporated, the solid was washed with THF (500 mL) and EtOAc (500 mL). The crude product was precipitated from methanol with EtOAc twice. The resulting precipitate was filtered off, washed with 100 mL of ethyl acetate, and then dried under high vacuum overnight to afford a cream solid (390 mg, 65 %).  $^1\text{H}$  NMR (600 MHz,  $\text{CD}_3\text{OD}$  with 1 % TFA)  $\delta$  9.72 (d,  $J = 9.72$  Hz, 4H), 9.10 (d,  $J = 9.10$  Hz, 5H), 8.04 – 7.94 (m, 4H), 7.81– 7.80 (m, 6H).  $^{13}\text{C}$  NMR (600 MHz,  $\text{CD}_3\text{OD}$  with 1 % TFA):  $\delta$  148.9, 146.0, 142.3, 131.6, 130.3, 126.8, 124.9; IR ( $\text{cm}^{-1}$ )  $\nu = 3000, 2347, 2085, 1628, 763$ .

## Synthesis of tetracationic dimer **2.2**



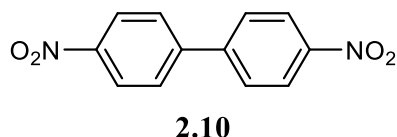
1-(phenyl)-1'-(2,4-dinitrophenyl)-[4,4'-bipyridin]-1,1'-diiumchloride (984 mg, 1.68 mmol) was dissolved in methanol (50 mL) with benzidine (155 mg, 0.84 mmol). The mixture was heated to reflux and stirred for 3 days. After cooling to room temperature, the solvent was evaporated, and the solid was washed with THF (100 mL), then precipitated twice from MeOH with ethyl acetate. The resulting precipitate was filtered off, washed with ethyl acetate (200 mL), and purified using reverse phase flash column chromatography (3:1 CH<sub>3</sub>CN : MeOH) to afford dimer **4** as a brown solid (550 mg, 86%). <sup>1</sup>H NMR (CD<sub>3</sub>OD with 1% trifluoroacetic acid (TFA); the signal of TFA is not reported; 600 MHz)  $\delta$  9.57 (d,  $J$  = 6.4 Hz, 4H), 9.49 (d,  $J$  = 6.4 Hz, 4H), 8.87 (dd,  $J$  = 13.2, 6.5 Hz, 8H), 8.14 (d,  $J$  = 8.4 Hz, 4H), 8.05 (d,  $J$  = 8.4 Hz, 4H), 7.91 – 7.81 (m, 4H), 7.73-7.72 (m, 6H). <sup>13</sup>C NMR (CD<sub>3</sub>OD with 1% TFA; the signal of TFA is not included; 150 MHz)  $\delta$  152.01, 151.84, 147.17, 144.10, 144.00, 143.75, 133.27, 131.91, 130.70, 128.54, 128.48, 126.54, 125.61. IR (cm<sup>-1</sup>)  $\nu$  = 1630 (conjugated alkene C=C) 833 (halo compound C-Cl). MS ( $m/z$ ) calc. for (C<sub>44</sub>H<sub>34</sub>N<sub>4</sub>)<sup>4+</sup>: 154.5690, found 154.5689, calc. for (C<sub>44</sub>H<sub>33</sub>N<sub>4</sub>)<sup>3+</sup>: 205.7563, found 205.7562, calc. for (C<sub>44</sub>H<sub>32</sub>N<sub>4</sub>)<sup>2+</sup>: 309.1342, found 309.1373.

## Synthesis of di-Zincke salt, **2.6**



Synthetic procedure and characterization data 4,4'-Bipyridine (1.56 g, 9.94 mmol) and 1-chloro-2,4-dinitrobenzene (7.35 g, 36.1 mmol) were dissolved in anhydrous acetonitrile (15 mL) under argon. The solvent was heated to reflux and stirred for 9 days until a large amount of pale grey precipitate was formed. A few drops of water were added to the flask and it was warmed until all the precipitate had disappeared, then ethanol was added resulting in the formation of a pale grey precipitate. The precipitate was collected by filtration, then dried in vacuo to yield 1,1'-bis(2,4-dinitrophenyl)-4,4'-bipyridilium dichloride (4.32 g, 63%) as a white powder. The crude product recrystallized in acetonitrile.  $^1\text{H}$  NMR (600 MHz,  $\text{D}_2\text{O}$ )  $\delta$  9.53 (d,  $J = 6.2$  Hz, 4H), 9.46 (d,  $J = 2.2$  Hz, 2H), 9.06 – 8.93 (m, 6H), 8.37 (d,  $J = 8.6$ , 2.0 Hz, 2H).  $^{13}\text{C}$  NMR (151 MHz,  $\text{D}_2\text{O}$ )  $\delta$  152.51, 149.71, 142.68, 138.13, 131.04, 130.61, 127.45, 127.30, 122.66. IR ( $\text{cm}^{-1}$ )  $\nu =$  3353, 2983, 1613, 1552, 1346, 838.

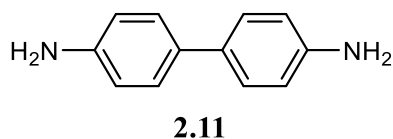
## Synthesis of 4,4'-dinitrobiphenyl, **2.10**. (known)<sup>131</sup>



A mixture of  $\text{Na}_2\text{CO}_3$  (1.696 g, 16 mmol),  $\text{Pd}(\text{OAc})_2$  (8 mg, 0.5 mol %), aryl halide (1.92 g, 8 mmol), 4-nitrophenylboronic acid (2.0 g, 12 mmol) distilled water (30 mL) and acetone (24 mL) was stirred at 35°C for 3 days. The product was precipitated in water, filtered off and

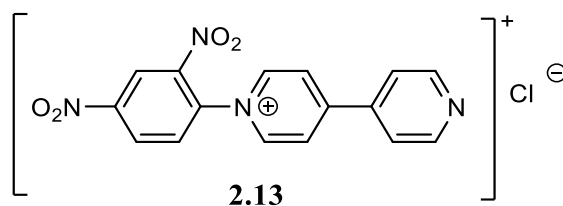
washed with methanol, water, then methanol once again before drying under vacuum for 2 h to afford the intermediate as a grey powder. Afterward, the reaction solution was extracted four times with diethyl ether (4 x10 mL) and product 1.3 was afforded (1.23 g, 55 %).  $^1\text{H}$  NMR (600 MHz,  $\text{DMSO-}d_6$ )  $\delta$  8.36 (d,  $J = 8.8$  Hz, 4H), 8.08 (d,  $J = 8.8$  Hz, 4H).  $^{13}\text{C}$  NMR (151 MHz,  $\text{DMSO-}d_6$ )  $\delta$  147.65, 144.17, 128.77, 124.30. IR ( $\text{cm}^{-1}$ )  $\nu = 1599, 1509, 1340, 839, 738$ .

Synthesis of 1,1'-biphenyl-4,4'-diamine **2.11**. (known)<sup>131</sup>



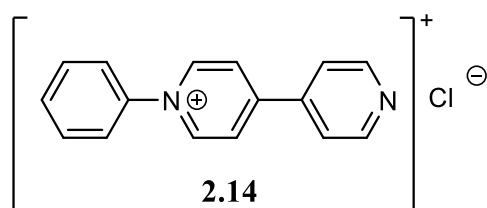
A solution of palladium (II) acetate (50 mg, 2 mmol) and 4,4'-Dinitrobiphenyl **2.10** (0.976 g, 4 mmol) in tetrahydrofuran (20 mL) was stirred until homogenous. A solution of potassium fluoride (1.0 g, 17.2 mmol) in water (8 mL) was added. Liquid polymethylhydrosiloxane (4 mL, 32 mmol) was then added dropwise. The solution was stirred for 3 h.  $\text{CHCl}_3$  (100 mL) was added to the reaction mixture and the organic phase was separated and dried over  $\text{MgSO}_4$ , then concentrated under vacuum. The resulting orange powder was easily purified by column chromatography on silica gel (ethanol: hexane 1:4, v/v) to afford the desired diamine as bright orange crystals (0.83g, 90 %).  $^1\text{H}$  NMR (600 MHz, chloroform- $d$ )  $\delta$  7.35 (d,  $J = 7.9$  Hz, 4H), 6.73 (d,  $J = 7.9$  Hz, 4H), 3.66 (s, 4H).  $^{13}\text{C}$  NMR (151 MHz, chloroform- $d$ )  $\delta$  144.85, 131.73, 127.21, 115.37. IR ( $\text{cm}^{-1}$ )  $\nu = 3320, 1602, 1498, 1264, 816$ .

Synthesis of 1-(2,4-dinitrophenyl)-4,4'-bipyridinium chloride, **2.13** (also referred to as **4.10** in chapter 4) (known)<sup>394</sup>



1-chloro-2,4'-dinitrobenzene (984 mg, 1.68 mmol) was dissolved in ethanol (200 mL) with 4,4'-bipyridine (155 mg, 0.84 mmol). The mixture was heated to reflux and stirred for 24 hours. After cooling to room temperature, the solution was added dropwise to rapidly stirring diethyl ether (1 L). The precipitate was collected and washed with ethyl acetate (100 mL) to afford 1-(2,4-dinitrophenyl)-4,4'-bipyridinium chloride (**2.13**) as a tan hygroscopic solid (550 mg, 86%).  
<sup>1</sup>H NMR (D<sub>2</sub>O, 600 MHz); δ 9.36 (d, J = 2.5 Hz, 1H), 9.21 (d, J = 7.0 Hz, 2H), 8.89 (dd, J = 8.7, 2.5 Hz, 1H), 8.80 (dd, J = 4.7, 1.6 Hz, 2H), 8.64 (d, J = 6.9 Hz, 2H), 8.23 (d, J = 8.7 Hz, 1H), 7.99 (dd, J = 4.6, 1.6 Hz, 2H).<sup>13</sup>C NMR (D<sub>2</sub>O, 150 MHz) δ 156.99, 149.92, 149.8, 145.62, 142.03, 138.18, 130.99, 130.41, 126.01, 122.60. IR (cm<sup>-1</sup>) ν = 3083, 1637, 1551, 1342, 819.

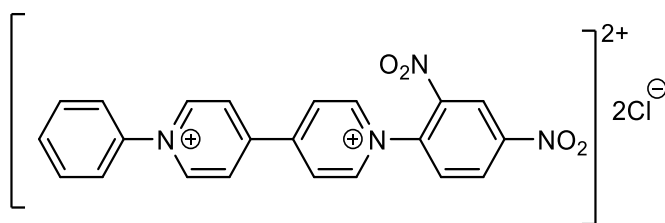
Synthesis of 1-(phenyl)-1'-(2,4-dinitrophenyl)-[4,4'-bipyridin]-1,1'-diumchloride, **2.14** (also referred to as **4.11** in chapter 4). (known)<sup>395</sup>



1-(2,4-dinitrophenyl)-4,4'-bipyridinium chloride (10.02 g, 28 mmol) was dissolved in ethanol (50 mL) with aniline (6.07 g, 80 mmol). The mixture was heated to reflux and stirred for 24 hours. After cooling to room temperature, the solvent was evaporated to ca. 5 mL, and the liquor was added dropwise into rapidly stirring THF (100 mL). The crude product was collected as a brown solid (7.0 g) which was purified by precipitating twice from MeOH (10 mL) with ethyl

acetate (500 mL). The resulting precipitate was filtered off and washed with diethyl ether (200 mL) to afford N-phenyl-4,4'-bipyridinium chloride **2.14** as a pale tan/green solid (4.2 g, 56%). <sup>1</sup>H NMR (D<sub>2</sub>O, 600 MHz) δ 9.18 (d, *J* = 6.8 Hz, 2H), 8.76 (d, *J* = 6.2 Hz, 2H), 8.53 (d, *J* = 6.8 Hz, 2H), 7.96 (d, *J* = 6.2 Hz, 2H), 7.80 – 7.66 (m, 5H). <sup>13</sup>C NMR (D<sub>2</sub>O, 150 MHz) δ 154.31, 149.67, 144.60, 142.47, 131.53, 130.39, 125.83, 123.82, 122.54. IR (cm<sup>-1</sup>) *v* = 3377, 1634, 1598, 1412, 767.

Synthesis of 1-(phenyl)-1'-(2,4-dinitrophenyl)-[4,4'bipyridin]-1,1'-diumchloride, **2.15** (also referred to as **4.12** in chapter 4). (known)<sup>395</sup>



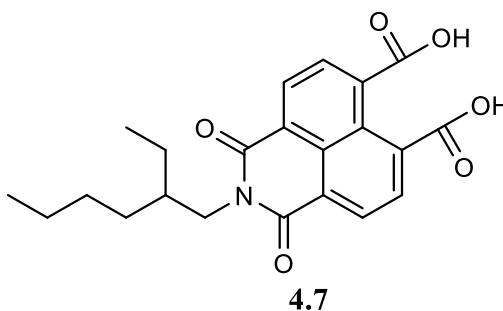
**2.15**

N-phenyl-4,4'-bipyridinium chloride, **2.14** (984 mg, 1.68 mmol) was dissolved in 1-methylpyrrolidin-2-one (50 mL) with 1-chloro-2,4-dinitrobenzene (155 mg, 0.84 mmol). The mixture was heated to 110 °C for 22 hours. After cooling to room temperature, the pale cream precipitate was separated from the dark brown liquor and washed with 1-methylpyrrolidin-2-one (80 mL) until washings were colourless. Solid washed with diethyl ether (2 x 50 mL) and dried in a vacuum oven at 50 °C for 3 hours to afford 1-(phenyl)-1'-(2,4-dinitrophenyl)-[4,4'bipyridin]-1,1'-diumchloride **2.15** as a cream hygroscopic solid (550 mg, 79%). <sup>1</sup>H NMR (D<sub>2</sub>O, 600 MHz) δ 9.43 (d, *J* = 6.2 Hz, 4H), 9.39 (d, *J* = 2.4 Hz, 1H), 8.93 (dd, *J* = 8.6, 2.4 Hz, 1H), 8.88 (d, *J* = 6.9 Hz, 2H), 8.81 (d, *J* = 6.9 Hz, 2H), 8.29 (d, *J* = 8.7 Hz, 2H), 7.82 (d, *J* = 7.0 Hz, 2H), 7.79 – 7.70 (m, 3H). <sup>13</sup>C NMR (D<sub>2</sub>O, 150 MHz) δ 152.91, 149.98, 149.67, 138.12, 131.95, 130.96, 130.53, 127.16, 123.94. IR (cm<sup>-1</sup>) *v* = 3452, 2975, 1635, 1534, 1343, 838. <sup>1</sup>H shows residual

1-methyl-pyrrolidin-2-one: 3.44 (t,  $J = 7.2$  Hz, 2H), 2.77 (s, 3H), 2.36 (t,  $J = 8.1$  Hz, 2H), 2.04 – 1.92 (m, 2H).

### 9.3.2 Chapter 4

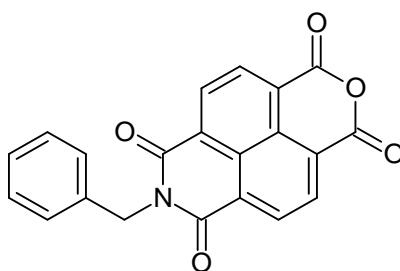
Synthesis of 2-(2-ethylhexyl)-1,3-dioxo-2,3-dihydro-1H-benzo[de]-isoquinoline-6,7-dicarboxylic acid, **4.7**. (known)<sup>226</sup>



1,4,5,8 Naphthalene tetracarboxylic dianhydride (1.99 g, 7.46 mmol) was dissolved in a solution of KOH (1.96 g) in water (350 mL) and the resulting brown solution was acidified to pH 6.3 with  $\text{H}_3\text{PO}_4$  (1 M). 2-Ethyl hexylamine (970 mg, 7.46 mmol) was added and the solution was re-acidified to pH 6.4 with  $\text{H}_3\text{PO}_4$  (1 M), then heated to 110 °C for 16 h. After cooling to room temperature, the cloudy solution was filtered and the filtrate was acidified with acetic acid (15 mL), which produced a cream precipitate. After stirring for 20 min, the solid was collected by filtration and dried under vacuum at 50 °C to give crude **4.7** as a yellow powder (1.14 g). This was dissolved in a solution of 1M KOH in water (200 mL) and washed with DCM (3 x 150 mL) to purify. The solution was then reacidified with 1M HCl in water and the precipitate collected and washed with water to afford pure **4.7** as a cream powder (2.52 g, 18 %). Mp 173–174 °C (decomp.);  $^1\text{H}$  NMR ( $\text{D}_2\text{O}/\text{KOH}$ ; 600 MHz)  $\delta$  7.55 – 7.36 (m, 4H), 3.09 – 2.95 (m, 2H), 1.39 – 1.25 (m, 1H), 1.13 – 0.97 (m, 8H), 0.59 (m, 6H).  $^{13}\text{C}$  NMR ( $\text{D}_2\text{O}/\text{KOH}$ , 150 MHz) =  $\delta$

176.65, 176.48, 176.27, 172.34, 140.73, 139.32, 138.41, 135.05, 127.97, 127.53, 126.86, 126.62, 126.41, 125.71, 42.86, 38.43, 30.21, 28.01, 23.77, 22.31, 13.35, 10.16. IR ( $\text{cm}^{-1}$ )  $\nu$  = 2926 (carboxylic acid O-H stretching), 1655, 1272 (aromatic amine C-N stretching), 766 (bending alkene C=C). MS ( $m/z$ ) calc. for  $\text{C}_{22}\text{H}_{23}\text{NO}_6[+\text{H}]^+$ : 398.1604, found 398.1598.

Synthesis of 2-(2-ethylhexyl)-1,3-dioxo-2,3-dihydro-1H-benzo[de]-isoquinoline-6,7-dicarboxylic acid, . 7-benzyl-1H-isochromeno[6,5,4-def]isoquinoline-1,3,6,8(7H)-tetraone, **4.8**.



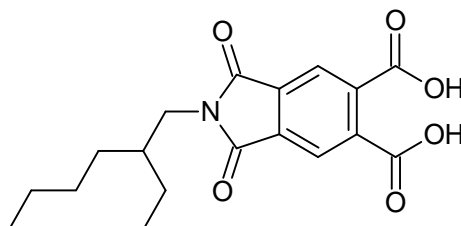
#### 4.8

1,4,5,8-Naphthalenetetracarboxylic dianhydride (4.00 g, 7.46 mmol) was dissolved in KOH solution (2.03 g, 7.2 mmol, in 400 mL water) over 30 mins to afford a dark brown solution. The solution was acidified to pH 6.3 using 1 M  $\text{H}_3\text{PO}_4$  before the addition of benzylamine (798 mg, 7.46 mmol) and subsequent stirring for 20 min. The solution was reacidified to pH 6.4 (1 M  $\text{H}_3\text{PO}_4$ ) and heated at 110 °C for 20 h. After cooling to room temperature, the precipitate was filtered off and acetic acid (10 mL) was added to the solution and the mixture was stirred for 1 hour. The isolated solid was then refluxed in acetic anhydride (25 mL) for 20 h before being filtered off and dried at 50 °C for 3 hours to afford the benzyl imide anhydride, **3**. (850 mg, 32 %).  $^1\text{H}$  NMR ( $\text{DMSO-}d_6$ , 600 MHz)  $\delta$  8.71 (s, 4H), 7.40 (d,  $J = 7.5$  Hz, 2H), 7.31 (t,  $J = 7.6$  Hz, 2H), 7.25 (t,  $J = 7.3$  Hz, 1H), 5.26 (s, 2H).  $^{13}\text{C}$  NMR ( $\text{DMSO-}d_6$ , 150 MHz)  $\delta$  162.43, 159.60, 136.70, 131.72, 130.57, 128.31, 127.54, 127.10, 126.87, 123.82, 43.37 IR ( $\text{cm}^{-1}$ )  $\nu$  = 1781

(conjugated anhydride C=O), 1667 (aromatic amine C-N stretching), 1028 (anhydride CO-O-CO stretching). MS ( $m/z$ ) calc. for  $C_{21}H_{11}NO_5[+H]^+$ : calcd 358.0715, found 358.0714.

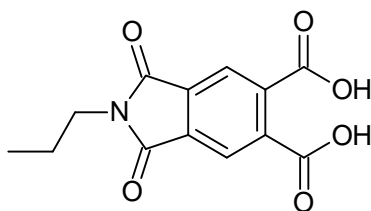
$^1H$  NMR shows residual acetic acid and acetic anhydride: 1.91 and 2.22 ppm respectively.

Synthesis of 2-(2-Ethylhexyl)-1,3-dioxoisindoline-5,6-dicarboxylic acid, **7.14**.



1,2,4,5- Benzenetetracarboxylic anhydride (10.13 g,  $4.64 \times 10^{-2}$  mol) was placed in acetic acid (100 ml) and the mixture was stirred at room temperature with slow addition of ethyl hexylamine (6 ml,  $4.64 \times 10^{-2}$  mol) over 1 h. The solution was heated at 120 °C for 48 h and then cooled to room temperature, whereby a white precipitate formed which was collected by filtration . The white precipitate (0.62 g) was crude disubstituted by-product and discarded. The remaining liquor was poured into rapidly stirring water (1 L) and then left unstirred for 3 days at room temperature where cream-coloured fluffy crystals of X-ray quality formed. The crystals were collected by filtration and dried in a vacuum oven for 12 hours at 50 °C to afford analytically pure **7.14** as fluffy cream-coloured crystals (7.05 g, 44 %);  $^1H$  NMR (600 MHz, chloroform-*d*)  $\delta$  8.23 (s, 2H), 3.61 (d,  $J = 7.5$  Hz, 2H), 1.82 (m, 1H), 1.28-1.32 (m, 8H), 0.89 (dt,  $J = 17.7, 7.1$  Hz, 6H).  $^{13}C$  NMR (151 MHz, chloroform-*d*)  $\delta$  170.96, 166.79, 136.58, 134.46, 124.09, 42.53, 38.22, 30.44, 28.39, 23.76, 22.97, 14.04, 10.33 ; IR ( $cm^{-1}$ )  $\nu = 3173, 2959, 2930, 2860, 1763, 1725, 1695, 1603, 1393, 1241, 1188, 1137, 921, 741$ ; MS ( $m/z$ ) calc. for  $C_{18}H_{21}NO_6[+H]^+$ : 348.1447, found 348.1439. triclinic, space group P-1,  $a = 5.2427(2)$   $b = 9.8758(2)$   $c = 18.0443(5)$  Å,  $a = 77.918(2)$   $b = 82.237(3)$   $\gamma = 78.295(2)$ ,  $V = 890.373$  Å<sup>3</sup>,  $T = 293$  K, R-Factor (%) 3.69.

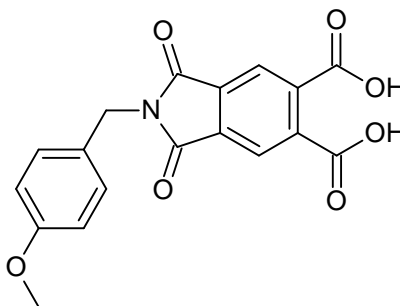
Synthesis of 1,3-Dioxo-2-propylisindoline-5,6-dicarboxylic acid, **7.15**.



1,2,4,5- Benzenetetracarboxylic anhydride (5.01 g,  $2.30 \times 10^{-2}$  mol) was placed in acetic acid (50 ml) and the mixture was stirred at room temperature with slow addition of propylamine (1.36 ml,  $2.30 \times 10^{-2}$  mol) over 30 minutes. The solution was heated at 120 °C for 24 h and then, the cooled mixture, poured into rapidly stirring water (450 mL). After 1 h, a fine white precipitate was collected by filtration and dried. The white precipitate (0.05 g) was crude disubstituted by-product and discarded. The liquor was left unstirred for 3 days at room temperature where colourless needle-like crystals of X-ray diffraction quality formed. These were collected to obtain analytically pure **7.15** as needle-like colourless crystals (4.57 g, 72 %);  $^1\text{H}$  NMR (600 MHz, chloroform-*d*)  $\delta$  8.34 (s, 2H), 3.74 (t,  $J = 7.5$  Hz, 2H), 1.73 (h,  $J = 7.5$  Hz, 2H), 0.97 (t,  $J = 7.5$  Hz, 3H).  $^{13}\text{C}$  NMR (151 MHz, chloroform-*d*)  $\delta$  171.57, 167.65, 136.74, 135.04, 125.15, 41.09, 22.06, 11.46 ; IR ( $\text{cm}^{-1}$ )  $\nu = 3116, 2980, 1743, 1696, 1599, 1351, 1277, 1106, 919, 740$ ; MS ( $m/z$ ) calc. for  $\text{C}_{13}\text{H}_{11}\text{NO}_6[+\text{H}]^+$ : 278.0665, found 278.0659.

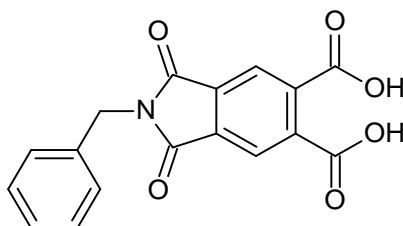
triclinic, space group P-1,  $a = 7.7949(8)$   $b = 8.5222(8)$   $c = 9.8358(11)$  Å,  $a = 89.463(8)$   $b = 84.789(9)$   $g = 64.808(9)$ ,  $V = 588.488$  Å<sup>3</sup>,  $T = 293$  K, R-Factor (%) 3.91.

Synthesis 2-(4-Methoxybenzyl)-1,3-dioxoisindoline-5,6-dicarboxylic acid, **7.16**.



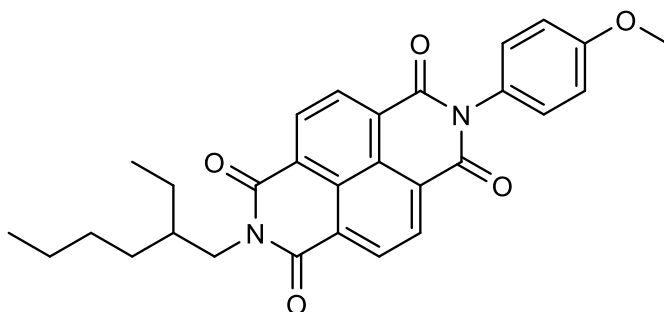
1,2,4,5- Benzenetetracarboxylic anhydride (5.01 g,  $2.30 \times 10^{-2}$  mol) was placed in acetic acid (40 ml) and the mixture was stirred at room temperature with slow addition of 4-methoxybenzylamine (3.15 g,  $2.30 \times 10^{-2}$  mol) over 30 minutes. The solution was heated at 120 °C for 48 h and then poured into rapidly stirring water (500 mL). After 2 h, a fine yellow precipitate was collected by filtration and washed with water (100 mL) before the damp solid was placed a vacuum oven heated to 50°C for 4 h to afford clean **7.16** as a pale yellow powder (6.64 g, 81 %).  $^1\text{H}$  NMR (600 MHz, chloroform-*d*)  $\delta$  8.33 (s, 2H), 7.37 (d,  $J = 8.0$  Hz, 2H), 6.91 (d,  $J = 8.0$  Hz, 2H), 4.87 (s, 2H), 3.86 (s, 3H).  $^{13}\text{C}$  NMR (151 MHz, chloroform-*d*)  $\delta$  171.03, 166.95, 136.45, 134.59, 130.35, 128.08, 124.84, 114.59, 55.73, 42.02 ; IR ( $\text{cm}^{-1}$ )  $\nu = 3103$ , 2980, 2835, 1703, 1665, 1515, 1385, 1328, 1242, 1094, 911, 763; MS ( $m/z$ ) calc. for  $\text{C}_{18}\text{H}_{13}\text{NO}_7$  [ $+\text{H}$ ] $^+$ : 356.0770, found 356.0761; calc. for  $\text{C}_{18}\text{H}_{13}\text{NO}_7$  [ $+\text{Na}$ ] $^+$ : 378.0590, found 378.0584; calc. for  $\text{C}_{18}\text{H}_{13}\text{NO}_7$  [ $+\text{NH}_4$ ] $^+$ : 373.1036, found 373.1029.

Synthesis of 2-benzyl-1,3-dioxoisindoline-5,6-dicarboxylic acid, **4.17** (known)<sup>236</sup>



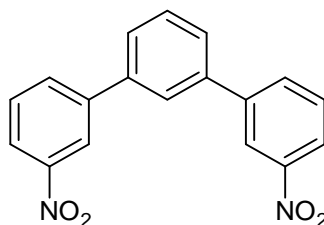
1,2,4,5-benzenetetracarboxylic anhydride (10 g, 45.8 mmol) was added to acetic acid (100 ml) and the mixture was stirred at room temperature with slow addition of benzylamine (5 ml, 45.7 mmol). The solution was heated at 120 °C for 22 h and then poured into water (1 L) and stirred at room temperature for 1 h. After filtering, the white filter cake was washed with water and dried under vacuum at 60 °C for 4 h, compound **4.17** was obtained as a white solid (9.71 g, 65%). <sup>1</sup>H NMR (DMSO-*d*<sub>6</sub>, 600 MHz) δ 8.07 (s, 2H), 7.33 (m, 5H), 4.81 (d, J = 16.1 Hz, 2H). <sup>13</sup>C NMR (DMSO-*d*<sub>6</sub>, 150 MHz) δ 167.46, 166.64, 138.48, 136.48, 133.54, 128.76, 127.65, 127.59, 123.07, 41.39. <sup>13</sup>C NMR in agreement with literature. IR (cm<sup>-1</sup>) ν = 3502 (carboxylic acid O-H), 3040 (alkane stretching C-H), 1695 (conjugated acid C=O), 1386 (aromatic amine C-N stretching), 744 (alkene bending C=C). MS (*m/z*) calc. for C<sub>21</sub>H<sub>11</sub>NO<sub>5</sub> [H]<sup>+</sup>: 358.0715, found 358.0714.

Synthesis of **4.19**



The mono-imide diacid intermediate **4.7** (0.250 g,  $6.29 \times 10^{-4}$  mol) and 4-methoxyaniline (0.078 g,  $6.29 \times 10^{-4}$  mol) were dissolved in DMAc (2.5 mL) and toluene (0.5 mL) under argon and the solution was heated to 135°C for 23 h. The reaction was cooled to room temperature, where a pale yellow solid precipitated. The yellow solid was collected under vacuum and washed with diethyl ether (20 mL) and chloroform (10 mL) before the damp solid was placed a vacuum oven heated to 50°C for 4 h to afford clean **4.19** as a pale yellow powder (0.143 g, 47%);  $^1\text{H}$  NMR (600 MHz, chloroform-*d*)  $\delta$  8.91 – 8.71 (m, 4H), 7.24 (d,  $J = 8.5$  Hz, 2H), 7.08 (d,  $J = 8.5$  Hz, 2H), 4.16 (qd,  $J = 12.9, 7.3$  Hz, 2H), 3.89 (s, 3H), 1.95 (p,  $J = 6.6$  Hz, 1H), 1.48 – 1.26 (m, 8H), 0.92 (dt,  $J = 36.6, 7.1$  Hz, 6H).  $^{13}\text{C}$  NMR (151 MHz, chloroform-*d*)  $\delta$  163.60, 163.52, 131.72, 131.44, 129.74, 127.30, 127.19, 127.06, 115.24, 55.87, 45.00, 38.26, 31.02, 28.97, 24.37, 23.39, 14.45, 10.95. IR ( $\text{cm}^{-1}$ )  $\nu = 2939, 1661, 1654, 1240, 772$ .

Synthesis of 3,3''-dinitro-1,1':3',1''-terphenyl, **4.18a**. (known)<sup>197</sup>

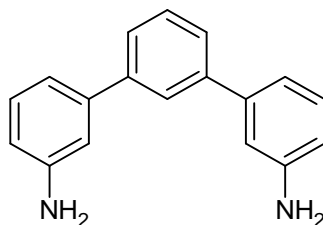


**4.18a**

modified experimental procedure.<sup>197</sup> : 1,3-dibromobenzene (1.55 g, 6.36 mmol), 3-nitrophenyl boronic acid (2.27 g, 13.3 mmol),  $\text{Na}_2\text{CO}_3$  (2.7 g, 25.4 mmol) and  $\text{Pd}(\text{OAc})_2$  ( $\sim 20$  mg) were stirred in a mixture of water (30 mL) and DMF (55 mL) at 70 °C overnight. The product was precipitated in water, filtered off and washed with methanol, water, then methanol once again before drying under vacuum for 4 h to afford the intermediate **4.19** as a grey powder (1.67 g, 72%).  $^1\text{H}$  NMR (600 MHz, DMSO-*d*<sub>6</sub>)  $\delta$  8.58 (t,  $J = 2.1$  Hz, 2H), 8.29 (dd,  $J = 7.8, 1.8$  Hz, 2H), 8.28 – 8.23 (m, 2H), 8.15 (t,  $J = 1.9$  Hz, 1H), 7.86 (dd,  $J = 7.8, 1.8$  Hz, 2H), 7.79 (t,  $J = 8.0$  Hz,

2H), 7.67 (t,  $J = 7.7$  Hz, 1H).  $^{13}\text{C}$  NMR (151 MHz,  $\text{DMSO-}d_6$ )  $\delta$  148.50, 141.47, 138.87, 133.81, 130.52, 130.13, 127.33, 126.00, 122.50, 121.61. IR ( $\text{cm}^{-1}$ )  $\nu = 1528, 1344, 733$ .

Synthesis of 3,3''-dinitro-1,1':3',1''-terphenyl, **4.18**. (known)<sup>197</sup>

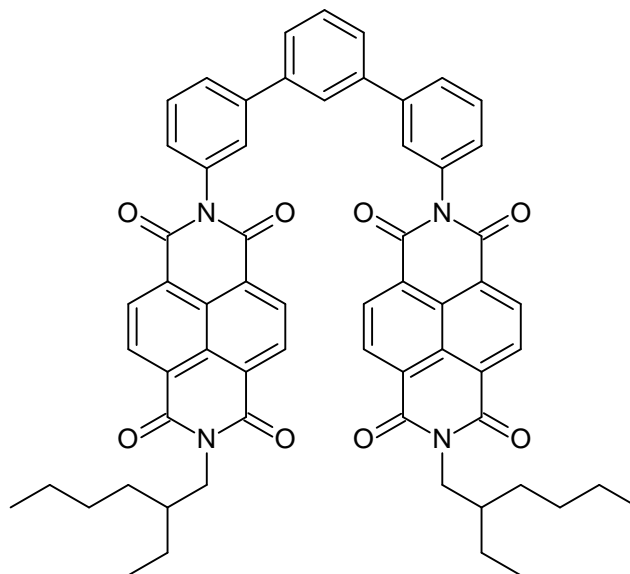


**4.20**

modified experimental procedure.<sup>197</sup>

A solution of palladium(II) acetate (46 mg, 2 mmol) and intermediate **4.19** (1.33 g, 4 mmol) in tetrahydrofuran (20 mL) was stirred until homogenous. A solution of potassium fluoride (1.0 g, 17.2 mmol) in water (8 mL) was added. Liquid polymethylhydrosiloxane (4 mL, 32 mmol) was then added dropwise. The solution was stirred for 3 h.  $\text{CHCl}_3$  (100 mL) was added to the reaction mixture and the organic phase was separated and dried over  $\text{MgSO}_4$ , then concentrated under vacuum. The resulting oil was purified by column chromatography on silica gel (ethanol: hexane 1:4, v/v) to afford the desired diamine **4.20** as yellow oil (0.75g, 95%).  $^1\text{H}$  NMR (600 MHz, chloroform- $d$ )  $\delta$  7.78 – 7.74 (m, 1H), 7.53 (dd,  $J = 7.6, 1.9$  Hz, 2H), 7.47 (dd,  $J = 8.4, 6.9$  Hz, 1H), 7.25 (d,  $J = 15.2$  Hz, 1H), 7.04 (dt,  $J = 7.7, 1.3$  Hz, 2H), 6.96 (t,  $J = 2.0$  Hz, 2H), 6.74 – 6.68 (m, 2H), 3.76 (s, 4H).  $^{13}\text{C}$  NMR (151 MHz, chloroform- $d$ )  $\delta$  147.08, 142.76, 142.11, 130.05, 129.29, 126.39, 126.36, 118.08, 114.51, 114.29. IR ( $\text{cm}^{-1}$ )  $\nu = 3340, 1594, 1474, 774$ .

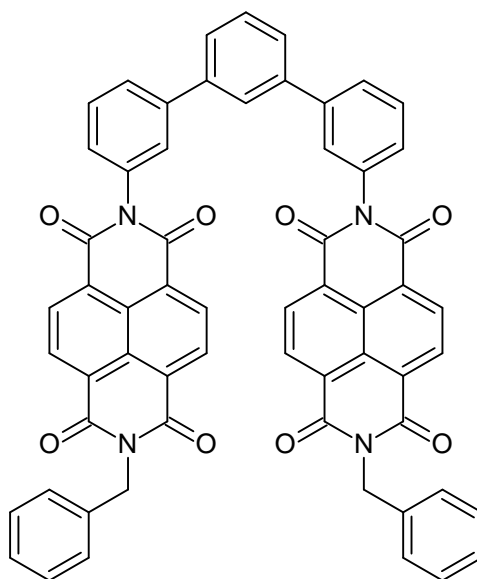
Synthesis of 7,7'-([1,1':3',1''-Terphenyl]-3,3''-diyl)bis(2-(2-ethylhexyl)benzo[*lmn*][3,8]phenanthroline-1,3,6,8(2H,7H)-tetraone), **Rigid-NDI-Hex**.



The mono-imide diacid intermediate **4.7** (0.277 g,  $6.99 \times 10^{-4}$  mol) and terphenyl diamine **4.20** (0.09 g,  $3.49 \times 10^{-4}$  mol) were dissolved in DMAc (2.5 mL) and toluene (0.5 mL) under argon. The stoichiometry was confirmed, by  $^1\text{H}$  NMR spectroscopy, and then the solution was heated to  $135^\circ\text{C}$  for 22 h. Upon completion, observed by  $^1\text{H}$  NMR monitoring, the reaction was cooled to room temperature, where a pale yellow solid precipitated. The yellow solid was collected *invacuo* and washed with diethyl ether (20 mL) and chloroform (10 mL) before the damp solid was placed a vacuum oven heated to  $50^\circ\text{C}$  for 4 h to afford analytically pure **Rigid-NDI-Hex** as a pale yellow powder (0.291 g, 85%);  $^1\text{H}$  NMR (600 MHz, chloroform-*d*)  $\delta$  8.87 (d,  $J = 5$  Hz, 8H), 7.80 (d,  $J = 10.5$  Hz, 3H), 7.67 (s, 2H), 7.60 (d,  $J = 2.0$  Hz, 2H), 7.57 (s, 2H), 7.54 (s, 1H), 7.32 (d,  $J = 2.0$  Hz, 2H), 4.17-4.20 (m, 4H), 1.95 (m, 2H), 1.47 – 1.24 (m, 16H), 0.92 (m, 12H).  $^{13}\text{C}$  NMR (151 MHz, chloroform-*d*)  $\delta$  163.51, 163.42, 143.00, 141.04, 135.45, 131.78, 131.47, 130.35, 129.71, 128.39, 127.75, 127.72, 127.42, 127.31, 127.22, 127.10, 126.98, 126.60, 45.04, 38.28, 31.03, 28.98, 24.38, 23.41, 14.46, 10.95; IR ( $\text{cm}^{-1}$ )  $\nu = 2959, 2926, 2854,$

1706, 1664, 1657, 1581, 1451, 1343, 1245, 1193, 770; MS ( $m/z$ ) calc. for  $C_{62}H_{54}N_4O_8[+H]^+$ : 983.4020, found 983.4011. calc. for  $C_{62}H_{54}N_4O_8[+Na]^+$ : 1005.3839, found 1005.3826. calc. for  $C_{62}H_{54}N_4O_8[+NH_4]^+$ : 1000.4285, found 1000.4283.

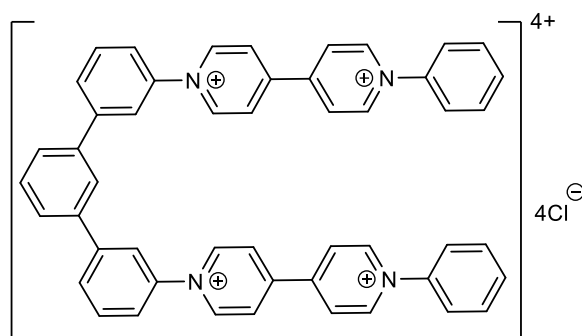
Synthesis of 7,7'-([1,1':3',1''-Terphenyl]-3,3''-diyl)bis(2-benzylbenzo[*lmn*][3,8]phenanthroline-1,3,6,8(2H,7H)-tetraone), **Flexi-NDI-Bn**.



The mono-imide mono-anhydride intermediate **4.8** (0.336 g,  $9.40 \times 10^{-4}$  mol) and terphenyl diamine **4.20** (0.122 g,  $4.70 \times 10^{-4}$  mol) were dissolved in DMAc (2.5 mL) and toluene (0.4 mL) under argon. The stoichiometry was confirmed, by  $^1H$  NMR spectroscopy, and then the solution was heated to 135°C for 24 h. During this time, the solution lightened in colour from dark brown to rich yellow and a brown solid precipitated. After reaction and whilst hot, the brown precipitate was collected by filtration on a low porosity sinter and washed with diethyl ether (200 mL) and chloroform (10 mL) before the damp solid was placed in the vacuum oven heated to 50°C for 16 h to afford analytically pure **Flexi-NDI-Bn** as a brown solid (0.329 g, 79%);  $^1H$  NMR (600 MHz, chloroform-*d*)  $\delta$  8.86 (s, 8H), 7.83 – 7.75 (m, 3H), 7.65 (t,  $J = 7.5$  Hz, 2H), 7.59 (d,  $J = 7.5$  Hz, 2H), 7.57 – 7.50 (m, 7H), 7.36 (t,  $J = 7.5$  Hz, 4H), 7.31 (t,  $J = 7.5$

Hz, 4H), 5.44 (s, 4H).  $^{13}\text{C}$  NMR (151 MHz, chloroform-*d*)  $\delta$  164.16, 163.49, 143.23, 140.23, 135.59, 134.02, 132.37, 131.94, 130.45, 129.54, 128.92, 128.74, 128.71, 128.21, 127.03, 127.00, 126.97, 126.95, 126.83, 126.73, 126.28, 126.03, 44.58 ; IR ( $\text{cm}^{-1}$ )  $\nu$  = 3034, 2887, 1707, 1663, 1579, 1449, 1336, 1243, 1190, 766; MS ( $m/z$ ) calc. for  $\text{C}_{60}\text{H}_{34}\text{N}_4\text{O}_8[+\text{H}]^+$ : 939.2455, found 939.2452. calc. for  $\text{C}_{60}\text{H}_{34}\text{N}_4\text{O}_8[+\text{Na}]^+$ : 961.2274, found 961.2256. calc. for  $\text{C}_{60}\text{H}_{34}\text{N}_4\text{O}_8[+\text{NH}_4]^+$ : 956.2720, found 956.2708.

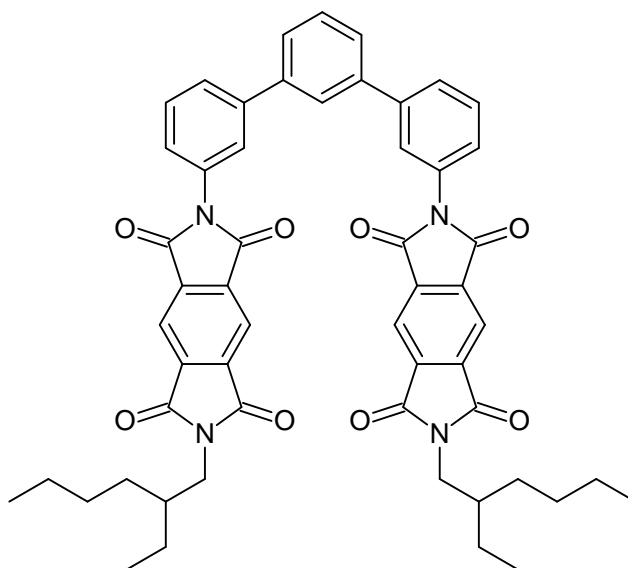
Synthesis of 1',1'''-([1,1':3',1''-Terphenyl]-3,3''-diyl)bis(1-phenyl-[4,4'-bipyridine]-1,1'-dium) chloride, **Rigid-Vio-Ph**.



1-(phenyl)-1'-(2,4-dinitrophenyl)-[4,4'bipyridin]-1,1'-diumchloride **4.12** ( $0.458\text{ g}, 9.74 \times 10^{-4}$  mol) and terphenyl amine **4.20** ( $0.127\text{ g}, 4.84 \times 10^{-4}$  mol) were dissolved in warmed MeOH (35 mL) separately. The solutions were combined under argon whilst stirring and refluxed for 48 hours. During this time, colour change from yellow to brown observed. The reaction mixture was cooled to ambient temperature and the solvent was reduced to ca. 5 mL then added to rapidly stirring THF (300 mL). The precipitate was collected and washed with EtOAc (2 x 100 mL) and dried in a vacuum oven for 12 hours at  $50\text{ }^\circ\text{C}$  to afford pure tweezer, **Rigid-Vio-Ph**, as a pale brown powder ( $0.50\text{ g}, 85\%$ ) M.p.  $> 400\text{ }^\circ\text{C}$ .  $^1\text{H}$  NMR (600 MHz, methanol-*d*<sub>4</sub>)  $\delta$  9.74 – 9.69 (m, 4H), 9.59 – 9.52 (m, 4H), 8.94 (dd,  $J = 7.0, 5.5\text{ Hz}$ , 8H), 8.46 (t,  $J = 2.0\text{ Hz}$ , 2H), 8.35 (d,  $J = 2\text{ Hz}$ , 1H), 8.21 (dd,  $J = 7.5, 2.0\text{ Hz}$ , 2H), 7.98 – 7.87 (m, 10H), 7.83 – 7.76 (m,

6H), 7.71 (t,  $J = 8.0$  Hz, 1H).  $^{13}\text{C}$  NMR (151 MHz, methanol- $d_4$ )  $\delta$  151.89, 151.88, 147.82, 147.37, 147.25, 147.15, 144.73, 144.70, 144.10, 141.01, 133.26, 132.45, 131.90, 131.68, 131.32, 128.63, 128.48, 127.52, 125.61, 124.52 ; IR ( $\text{cm}^{-1}$ )  $\nu = 3332, 2999, 1665, 1630, 1435, 771$ . MS ( $m/z$ ) calc. for  $(\text{C}_{50}\text{H}_{38}\text{N}_4)^{4+}$ : 173.5769, found 173.5761, calc. for  $(\text{C}_{50}\text{H}_{38}\text{N}_4)^{3+}$ : 231.436, found 231.4337, calc. for  $(\text{C}_{50}\text{H}_{38}\text{N}_4)^{2+}$ : 347.1543, found 347.1509,  $(\text{C}_{50}\text{H}_{38}\text{N}_4)^{1+}$ : 694.3091, found 694.3068

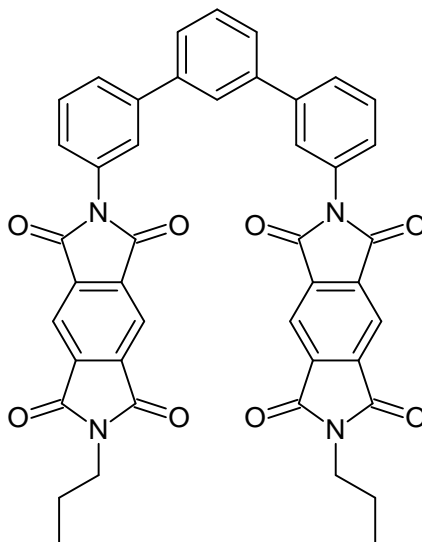
Synthesis of 6,6'-([1,1':3',1''-Terphenyl]-3,3''-diyl)bis(2-(2-ethylhexyl)pyrrolo[3,4-f]isoindole-1,3,5,7(2H,6H)-tetraone), **Rigid-PDI-Hex**.



The mono-imide diacid intermediate **7.14** (0.184 g,  $5.30 \times 10^{-4}$  mol) and terphenyl diamine **4.20** (0.069 g,  $2.65 \times 10^{-4}$  mol) were dissolved in DMAc (3 mL) under argon. The stoichiometry was confirmed, by  $^1\text{H}$  NMR spectroscopy, and then the solution was heated to  $135^\circ\text{C}$  for 20 h. During this time, the solution lightened in colour from orange to yellow and an off-white solid precipitated. The mixture was cooled to room temperature and the off-white solid was collected *invacuo* and washed with diethyl ether (20 mL) before the damp solid was placed a vacuum oven heated to  $50^\circ\text{C}$  for 2 h to afford analytically pure **Rigid-PDI-Hex** as an off-white powder

(0.152 g, 65%);  $^1\text{H}$  NMR (600 MHz, chloroform-*d*)  $\delta$  8.38 (s, 4H), 7.81 (s, 1H), 7.72 (d,  $J = 7.5$  Hz, 4H), 7.63 (s, 4H), 7.55 (s, 1H), 7.48 – 7.44 (m, 2H), 3.66 (d,  $J = 7.5$  Hz, 4H), 1.87 (s, 2H), 1.23-1.34 (m, 16H), 0.83-0.99 (m, 12H).  $^{13}\text{C}$  NMR (151 MHz, chloroform-*d*)  $\delta$  166.79, 165.62, 142.72, 141.08, 137.92, 137.10, 131.85, 130.13, 129.86, 127.93, 127.22, 126.61, 125.67, 125.64, 42.98, 38.58, 30.83, 28.79, 24.19, 23.32, 14.41, 10.73; IR ( $\text{cm}^{-1}$ )  $\nu = 2936, 2931, 2860, 1771, 1704, 1353, 1074, 774, 724$ ; MS ( $m/z$ ) calc. for  $\text{C}_{54}\text{H}_{50}\text{N}_4\text{O}_8[+\text{H}]^+$ : 883.3707, found 883.3700. calc. for  $\text{C}_{54}\text{H}_{50}\text{N}_4\text{O}_8[+\text{Na}]^+$ : 905.3526, found 905.3527. calc. for  $\text{C}_{54}\text{H}_{50}\text{N}_4\text{O}_8[+\text{NH}_4]^+$ : 900.3972, found 900.3966.

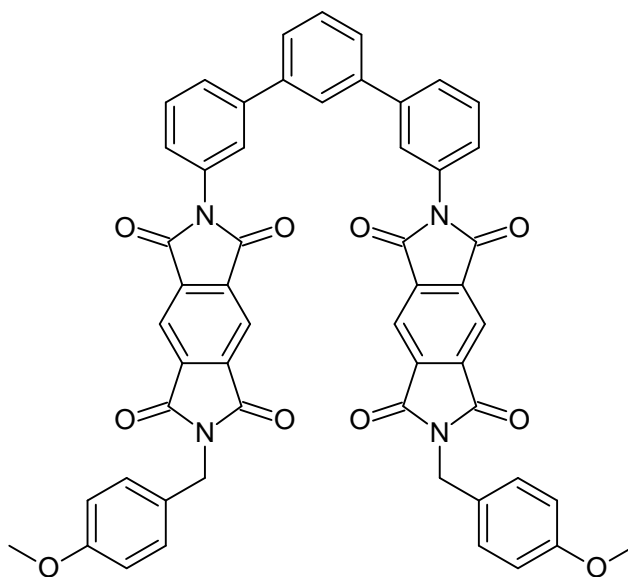
Synthesis of 6,6'-([1,1':3',1''-Terphenyl]-3,3''-diyl)bis(2-propylpyrrolo[3,4-f]isoindole-1,3,5,7(2H,6H)-tetraone), **Rigid-PDI-Pr**.



The mono-imide diacid intermediate **4.15** (0.413 g,  $1.49 \times 10^{-3}$  mol) and terphenyl diamine **4.20** (0.195 g,  $7.47 \times 10^{-4}$  mol) were each dissolved in DMAc (3 mL and 5 mL respectively) under argon. The solutions were combined, and the stoichiometry confirmed by  $^1\text{H}$  NMR spectroscopy, before the mixture was heated to  $135^\circ\text{C}$  for 22 h. Upon completion, observed by  $^1\text{H}$  NMR monitoring, the reaction was cooled to room temperature, where a white solid precipitated. The white solid was collected *invacuo* on a low porosity sinter and washed with

diethyl ether (40 mL) before the damp solid was placed in a vacuum oven heated to 50°C for 10 h to afford analytically pure **Rigid-PDI-Pr** as a fine white powder (0.304 g, 55%); <sup>1</sup>H NMR (600 MHz, chloroform-*d*/TFA 6:1 v/v, the signal of TFA is not reported) δ 8.44 (d, *J* = 2.0 Hz, 4H), 7.80 (s, 1H), 7.77 (d, *J* = 7.5 Hz, 2H), 7.69 – 7.60 (m, 6H), 7.57 (t, *J* = 7.5 Hz, 1H), 7.42 (d, *J* = 7.5 Hz, 2H), 3.77 (t, *J* = 7.5 Hz, 4H), 1.76 (h, *J* = 7.5 Hz, 4H), 0.99 (t, *J* = 7.5 Hz, 6H). <sup>13</sup>C NMR (151 MHz, chloroform-*d*/TFA 6:1 v/v, the signal of TFA is not reported) δ 167.30, 166.31, 142.90, 140.69, 137.70, 137.03, 130.93, 130.22, 129.81, 128.44, 127.14, 126.37, 125.69, 125.63, 119.52, 40.94, 21.86, 11.28; IR (cm<sup>-1</sup>) ν = 3098, 3035, 2971, 1733, 1706, 1583, 1468, 1366, 1077, 723; MS (*m/z*) calc. for C<sub>44</sub>H<sub>30</sub>N<sub>4</sub>O<sub>8</sub>[+Na]<sup>+</sup>: 765.1961, found 765.1947.

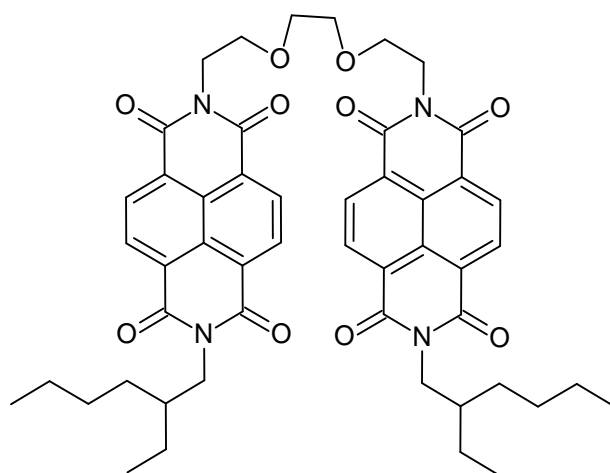
Synthesis of 6,6'-([1,1':3',1''-Terphenyl]-3,3''-diyl)bis(2-(4-methoxybenzyl)pyrrolo[3,4-*f*]isoindole-1,3,5,7(2H,6H)-tetraone), **Rigid-PDI-MBn**.



The mono-imide diacid intermediate **7.16** (0.404 g,  $1.14 \times 10^{-3}$  mol) and terphenyl diamine **4.20** (0.149 g,  $5.68 \times 10^{-4}$  mol) were dissolved in DMAc (5 mL) and toluene (1 mL) under argon. The stoichiometry was confirmed, by <sup>1</sup>H NMR spectroscopy, and then the solution was heated to 135°C for 18 h. During this time, the solution changed colour from dark yellow to

pale yellow and a bright yellow solid precipitated. After reaction and whilst hot, the yellow precipitate was collected by filtration on a low porosity sinter and washed with diethyl ether (200 mL) and chloroform (5 mL) before the damp solid was placed in the vacuum oven heated to 50°C for 5 h to afford analytically pure **Rigid-PDI-MBn** as a bright yellow solid (0.194 g, 38%);  $^1\text{H}$  NMR (600 MHz, chloroform-*d* /TFA 6:1 v/v, the signal of TFA is not reported)  $\delta$  8.45 (s, 4H), 7.78 (d,  $J = 7.5$  Hz, 2H), 7.72 – 7.60 (m, 7H), 7.56 (d,  $J = 8.5$  Hz, 1H), 7.46 – 7.35 (m, 6H), 6.95 (d,  $J = 8.5$  Hz, 4H), 4.91 (s, 4H), 3.89 (s, 6H).  $^{13}\text{C}$  NMR (151 MHz, chloroform-*d* /TFA 6:1 v/v, the signal of TFA is not reported)  $\delta$  167.29, 166.85, 158.64, 143.18, 140.69, 137.84, 137.16, 130.73, 130.70, 130.40, 129.92, 128.83, 128.53, 127.25, 126.39, 125.85, 125.78, 119.86, 114.98, 56.07, 42.41 ; IR ( $\text{cm}^{-1}$ )  $\nu = 3066, 2990, 2831, 1763, 1702, 1514, 1468, 1396, 1353, 1248, 1102, 1031, 917, 723$  ; MS ( $m/z$ ) calc. for  $\text{C}_{54}\text{H}_{34}\text{N}_4\text{O}_{10}[\text{Na}]^+$ : 921.2173, found 921.2153.

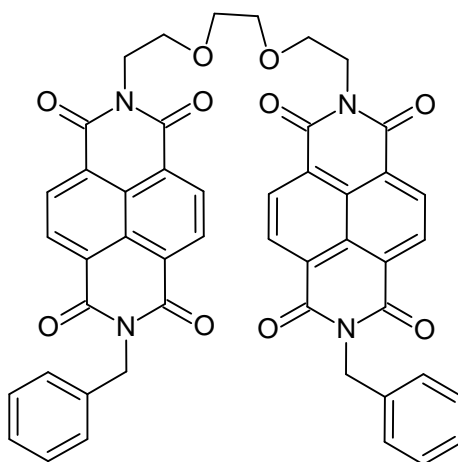
Synthesis of 7,7'-((ethane-1,2-diylbis(oxy))bis(ethane-2,1-diyl))bis(2-(2-ethylhexyl)benzo[*lmn*][3,8]phenanthroline-1,3,6,8(2H,7H)-tetraone), **Flexi-NDI-Hex**. (known)<sup>226</sup>



Flexi-NDI-Hex was synthesised and provided by a masters student in our group, Monika Stankunaite, following literature procedures.<sup>226</sup> Characterisation data recorded by myself for this thesis.  $^1\text{H}$  NMR (chloroform-*d* /TFA 6:1 v/v, the signal of TFA is not reported; 600 MHz)

$\delta$  8.71 (d,  $J = 5.3$  Hz, 8H), 4.36 (t,  $J = 6.0$  Hz, 4H), 4.12 (qd,  $J = 13.0, 7.2$  Hz, 4H), 3.76 (t,  $J = 6.0$  Hz, 4H), 3.65 (s, 4H), 1.99 – 1.85 (m, 3H), 1.46 – 1.16 (m, 19H), 0.90 (dt,  $J = 33.3, 7.2$  Hz, 14H).  $^{13}\text{C}$  NMR (chloroform-*d* /TFA 6:1 v/v, the signal of TFA is not reported; 150 MHz)  $\delta$  163.51, 163.20, 131.35, 131.32, 127.04, 127.00, 126.78, 70.54, 68.06, 44.95, 39.86, 38.27, 31.01, 28.96, 24.34, 23.39, 14.44, 10.93; IR ( $\text{cm}^{-1}$ )  $\nu = 2951, 2912, 2869, 1706, 1672, 1581, 1453, 1375, 1333, 1238$ ; MS ( $m/z$ ) calc. for  $\text{C}_{50}\text{H}_{54}\text{O}_4\text{N}_{10}[\text{+H}]^+$ , 871.3918; found: 871.3935

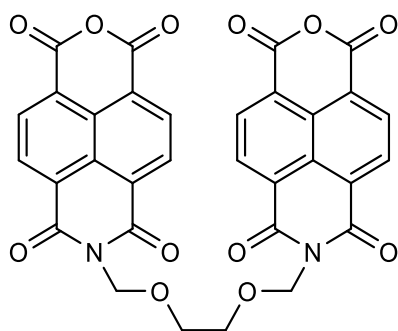
Synthesis of 7,7'-((Ethane-1,2-diylbis(oxy))bis(ethane-2,1-diyl))bis(2-benzylbenzo[*lmn*][3,8]phenanthroline-1,3,6,8(2H,7H)-tetraone), **Flexi-NDI-Bn**.



The mono-imide mono-anhydride intermediate **4.8** (0.253 g,  $7.08 \times 10^{-4}$  mol) and 2,2'-(ethylenedioxy) bis(ethylamine) **4.21** (0.0524 g,  $3.54 \times 10^{-4}$  mol) were dissolved in DMAc (5 mL) under argon and heated to 150°C for 18 h. During this time, a pink solid precipitated. The mixture was cooled to room temperature and filtered on a low porosity sinter. The filtrand was washed with cold DMAc (5mL) and diethyl ether (220 mL) and then dried to afford pure **Flexi-NDI-Bn** as a pale pink powder (0.266 g, 91%);  $^1\text{H}$  NMR (600 MHz, chloroform-*d*)  $\delta$  8.82 (d,  $J = 7.5$  Hz, 4H), 8.77 (d,  $J = 7.5$  Hz, 4H), 7.48 (d,  $J = 7.5$  Hz, 4H), 7.35 – 7.24 (m, 6H), 5.42 (s, 4H), 4.46 (t,  $J = 5.5$  Hz, 4H), 3.93 (t,  $J = 5.5$  Hz, 4H), 3.84 (s, 4H).  $^{13}\text{C}$  NMR (151 MHz, chloroform-*d*)  $\delta$  163.87, 163.79, 135.46, 132.00, 131.87, 128.74, 128.72, 128.19, 126.65,

126.52, 126.25, 69.63, 67.98, 44.63, 39.61 ; IR (cm<sup>-1</sup>)  $\nu$  = 2928, 2922, 2858, 1705, 1661, 1580, 1454, 1326, 1243, 767 ; MS (m/z) calc. for C<sub>48</sub>H<sub>34</sub>O<sub>4</sub>N<sub>10</sub>[+Na]<sup>+</sup>, 849.2173; found: 849.2160.

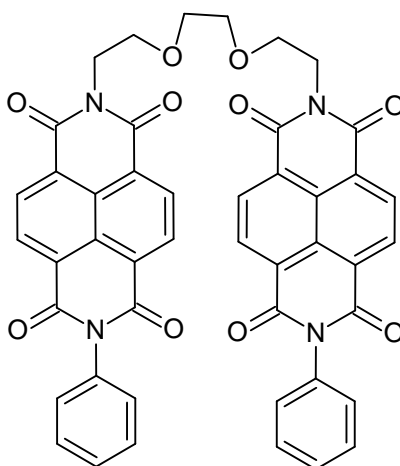
Synthesis of 7,7'-((ethane-1,2-diylbis(oxy))bis(ethane-2,1-diyl))bis(1H-isochromeno[6,5,4-def]isoquinoline-1,3,6,8(7H)-tetraone), **Flexi-NDI dianhydride** (known)<sup>396</sup>



1,4,5,8-Naphthalenetetracarboxylic dianhydride (2.00 g, 7.46 mmol) was dissolved in KOH solution (2.20 g, 7.5 mmol, in 400 mL water) over 40 mins to afford a dark brown solution. The solution was acidified to pH 6.3 using 1 M H<sub>3</sub>PO<sub>4</sub> before the addition of 2,2'-(ethylenedioxy)bis(ethylamine) (564 mg, 7.46 mmol) and subsequent stirring for 20 min. The solution was reacidified to pH 6.4 (1 M H<sub>3</sub>PO<sub>4</sub>) and heated at 110 °C for 20 h. After cooling to room temperature, acetic acid (10 mL) was added and the mixture was stirred for 30 min. The isolated solid was then refluxed in acetic anhydride (30 mL) for 20 h before being filtered off and dried at 50 °C overnight to afford the bis-diimide dianhydride (0.789 g, 17 %). Mpt = 304–307 °C. <sup>1</sup>H NMR (chloroform-*d* /TFA 6:1 v/v, the signal of TFA is not reported; 600 MHz):  $\delta$  8.96 – 8.76 (m, 8H), 4.46 (t, J = 5.5 Hz, 4H), 3.94 (t, J = 5.5 Hz, 4H), 3.86 (s, 4H). <sup>13</sup>C NMR (chloroform-*d* /TFA 6:1 v/v, the signal of TFA is not reported; 150 MHz):  $\delta$  163.67, 162.25, 161.96, 161.68, 159.85, 134.05, 132.33, 129.24, 127.72, 127.22, 123.35, 68.35, 40.02. IR (cm<sup>-1</sup>)  $\nu$  = 3058 (stretching alkene C-H), 2869 (stretching alkane C-H), 1789 (conjugated

anhydride C=O), 1670, 1238 (aromatic amine C-N stretching), 1029 (stretching anhydride CO-O-CO), 759 (bending alkene C=C). Residual acetic anhydride shown in  $^1\text{H}$  NMR @ 2.21 ppm.

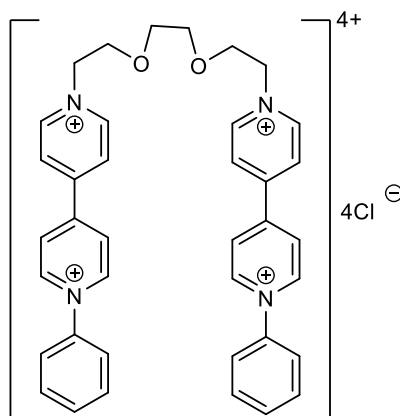
Synthesis of 7,7'-((ethane-1,2-diylbis(oxy))bis(ethane-2,1-diyl))bis(2-phenylbenzo[*lmn*][3,8]phenanthroline-1,3,6,8(2H,7H)-tetraone), **Flexi-NDI-Ph**. (known)<sup>396</sup>



The intermediate **Flexi-NDI dianhydride** (0.886 g,  $3.54 \times 10^{-4}$  mol) and aniline (0.2567 g,  $7.08 \times 10^{-4}$  mol) were dissolved in DMAc (5 mL) under argon and heated to 135°C for 23 h. During this time, a pink solid precipitated. The mixture was cooled to room temperature and filtered on a low porosity sinter. The filtrand was washed with cold DMAc (5mL) and diethyl ether (220 mL) and then dried to afford pure **Flexi-NDI-Ph** as a pale pink powder (0.266 g, 67%);  $^1\text{H}$  NMR (600 MHz, chloroform-*d* /TFA 6:1 v/v, the signal of TFA is not reported)  $\delta$  9.00 – 8.77 (m, 8H), 7.59 (d,  $J = 6.7$  Hz, 6H), 7.38 – 7.28 (m, 4H), 4.50 (t,  $J = 5.5$  Hz, 4H), 3.98 (t,  $J = 5.6$  Hz, 4H), 3.88 (s, 4H).  $^{13}\text{C}$  NMR (151 MHz, chloroform-*d* /TFA 6:1 v/v, the signal of TFA is not reported)  $\delta$  164.64, 164.02, 133.51, 132.73, 132.13, 130.43 (d,  $J = 9.3$  Hz),

128.35, 127.27, 126.97, 126.54, 69.86, 68.23, 39.89. IR ( $\text{cm}^{-1}$ )  $\nu = 2878, 1700, 1657, 1337, 1242, 766$ . MS ( $m/z$ ) calc. for  $\text{C}_{46}\text{H}_{30}\text{N}_4\text{O}_{10}[\text{Na}]^+$ : 821.1860, found 821.1850.

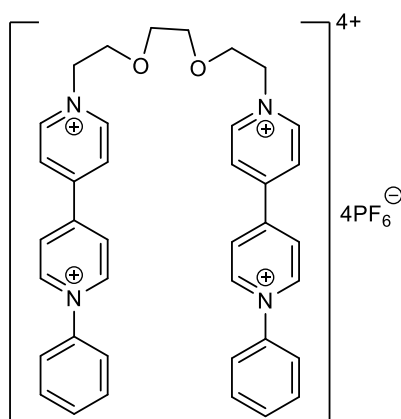
Synthesis of 1,1'''-((Ethane-1,2-diylbis(oxy))bis(ethane-2,1-diyl))bis(1-phenyl-[4,4'-bipyridine]-1,1'-dium) chloride, **Flexi-Vio-Ph**.



1-phenyl-[4,4'-bipyridin]-1-ium chloride **4.11** (0.722 g,  $2.69 \times 10^{-3}$  mol) was dissolved in warmed EtOH (10 mL) and combined with 1,2-bis(2-chloroethoxy)ethane **4.22** (0.252 g,  $1.35 \times 10^{-3}$  mol) and KI (0.45 g,  $2.7 \times 10^{-3}$  mol). The mixture was refluxed under argon for 72 h. Upon completion, monitored by  $^1\text{H}$  NMR spectroscopy, the solution was cooled to room temperature, where a red solid precipitated and was collected by filtration and washed with EtOAc (20 mL). The red solid was dissolved in the minimum amount of water (5 mL) and added dropwise to rapidly stirring solution of  $\text{NH}_4\text{PF}_6$  (12.4 g) in water (100 mL). After stirring at room temperature for 2 h, the  $\text{PF}_6$  salt derivative **Flexi-Vio-Ph** was collected as a light grey solid (0.76 g, 48%).  $\text{PF}_6$  derivative **Flexi-Vio-Ph** (277 mg,  $2.38 \times 10^{-4}$  mol) was converted to the Cl salt **Flexi-Vio-Ph** by dissolving in nitromethane (3 mL) and adding dropwise to rapidly stirring solution of tert-butylammonium chloride (1 g) in nitromethane (20 mL), whereby a dark grey solid precipitated. After 1h, the grey solid was collected by filtration and washed with nitromethane (5 mL) and acetonitrile (3 mL) and then dried in a vacuum oven heated to  $50^\circ\text{C}$

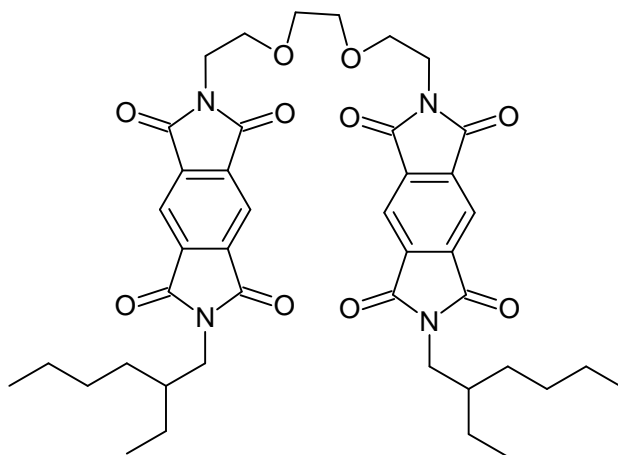
for 4 h to afford clean **Flexi-Vio-Ph** as a dark grey solid (0.129 g, 75 %);  $^1\text{H}$  NMR (600 MHz,  $\text{D}_2\text{O}$ )  $\delta$  9.45 – 9.26 (m, 4H), 9.13 (d,  $J = 6.5$  Hz, 4H), 8.72 – 8.65 (m, 4H), 8.61 (d,  $J = 6.5$  Hz, 4H), 7.83 – 7.69 (m, 10H), 4.92 (t,  $J = 5.0$  Hz, 4H), 4.08 (t,  $J = 5.0$  Hz, 4H), 3.68 (s, 4H).  $^{13}\text{C}$  NMR (151 MHz,  $\text{D}_2\text{O}$ )  $\delta$  150.48, 150.19, 145.88, 145.36, 142.08, 131.89, 130.50, 126.85, 126.83, 123.92, 69.70, 68.62, 61.16 ; IR ( $\text{cm}^{-1}$ )  $\nu$  3338, 3009, 2926, 2868, 1706, 1628, 1434, 1341, 1111, 845, 773, 554; MS ( $m/z$ ) calc. for  $\text{C}_{38}\text{H}_{38}\text{N}_4\text{O}_2$  [ $+\text{H}$ ] $^+$ :583.3073, found 583.3034.

Synthesis of 1',1''-((ethane-1,2-diylbis(oxy))bis(ethane-2,1-diyl))bis(1-phenyl-[4,4'-bipyridine]-1,1'-dium) hexafluorophosphate(V), **Flexi-Vio-Ph** ( $\text{PF}_6^-$ ).



$^1\text{H}$  NMR (600 MHz, acetonitrile- $d_3$ )  $\delta$  9.17 (d,  $J = 6.4$  Hz, 4H), 8.96 (d,  $J = 6.3$  Hz, 4H), 8.59 (d,  $J = 6.3$  Hz, 4H), 8.50 (d,  $J = 6.2$  Hz, 4H), 7.88 – 7.68 (m, 10H), 4.81 (t,  $J = 4.8$  Hz, 4H), 3.98 (t,  $J = 4.8$  Hz, 4H).  $^{13}\text{C}$  NMR (151 MHz, acetonitrile- $d_3$ )  $\delta$  151.54, 150.82, 147.10, 146.51, 143.24, 133.05, 131.56, 128.12, 127.83, 125.38, 71.05, 69.54, 62.64.

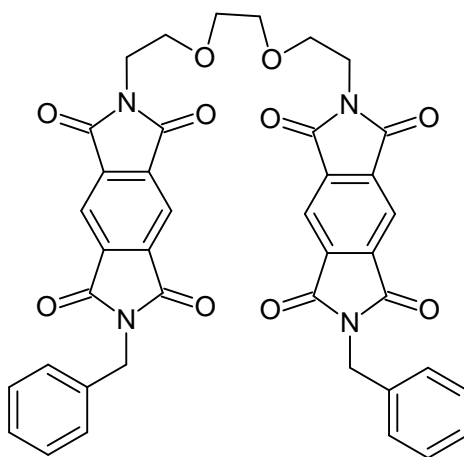
Synthesis of 7,7'-([1,1':3',1''-Terphenyl]-3,3''-diyl) bis(2-(2-ethylhexyl)benzo[*lmn*][3,8]phenanthroline-1,3,6,8(2H,7H)-tetraone), **Flexi-PDI-Hex**.



The mono-imide diacid intermediate **4.14** (0.541 g,  $1.55 \times 10^{-3}$  mol) and 2,2'-(ethylenedioxy)bis(ethylamine) **4.21** (0.115 g,  $7.7 \times 10^{-4}$  mol) were dissolved in DMAc (4 mL) and toluene (1 mL) under argon and heated to 135°C for 24 h. During this time, the solution changed colour from colourless to rich orange. The solution was cooled to room temperature and added dropwise to rapidly water (100 mL) where an emulsion formed. This mixture was then washed with chloroform (3 x 100 mL) until the washings ran clear. The combined organic phases were then dried over MgSO<sub>4</sub>, filtered, and the pale-yellow liquor was concentrated to a volume where a cream precipitate formed (ca. 10 mL). The cream solid was collected by filtration on a low porosity sinter and washed with diethyl ether (10 mL) before the damp solid was placed in the vacuum oven heated to 50°C for 2 h to afford analytically pure **Flexi-PDI-Hex** as a cream solid (0.512 g, 85%); <sup>1</sup>H NMR (600 MHz, chloroform-*d*) δ 8.25 (s, 4H), 3.90 (t, *J* = 5.5 Hz, 4H), 3.69 (t, *J* = 5.5 Hz, 4H), 3.64 (d, *J* = 7.5 Hz, 4H), 3.58 (s, 4H), 1.85 (p, *J* = 6.5 Hz, 2H), 1.41 – 1.21 (m, 16H), 0.92-0.88 (m, 12H). <sup>13</sup>C NMR (151 MHz, chloroform-*d*) δ 166.58, 166.16, 137.21, 137.15, 118.19, 70.03, 67.60, 42.53, 38.24, 37.83, 30.47, 28.43, 23.81,

22.96, 14.04, 10.36 ; IR ( $\text{cm}^{-1}$ )  $\nu$  2985, 2931, 2868, 1768, 1704, 1667, 1391, 1354, 1098, 1055, 845, 728; MS ( $m/z$ ) calc. for  $\text{C}_{42}\text{H}_{50}\text{N}_4\text{O}_{10}$   $[\text{+H}]^+$ : 771.3605, found 771.3597. calc. for  $\text{C}_{42}\text{H}_{50}\text{N}_4\text{O}_{10}[\text{+NH}_4]^+$ :788.3871, found 788.3875.

Synthesis of 7,7'-([1,1':3',1''-Terphenyl]-3,3''-diyl)bis(2-benzylbenzo[*lmn*][3,8]phenanthroline-1,3,6,8(2H,7H)-tetraone), Flexi-PDI-Bn.

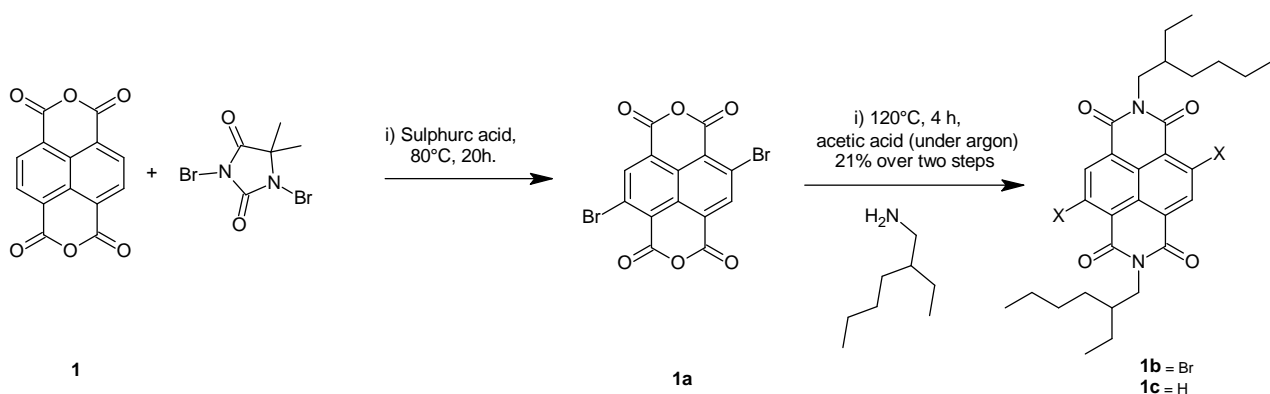


The mono-imide diacid intermediate **4.17** (0.463 g,  $1.42 \times 10^{-3}$  mol) and 2,2'-(Ethylenedioxy)bis(ethylamine) **4.21** (0.105 g,  $7.10 \times 10^{-4}$  mol) were dissolved in DMAc (4 mL) and toluene (1 mL) under argon and heated to  $135^\circ\text{C}$  for 24 h. During this time, the solution darkened in colour from straw yellow to dark orange. The solution was cooled to room temperature, whereby a pale pink solid precipitated. The pink precipitate was collected by filtration on a low porosity sinter and washed with cold DMAc (15 mL) and diethyl ether (140 mL) before the damp solid was placed in the vacuum oven heated to  $50^\circ\text{C}$  for 4 h to afford clean **Flexi-PDI-Bn** as a pale pink solid (0.407 g, 79%);  $^1\text{H}$  NMR (600 MHz, chloroform-*d*)  $\delta$  8.25 (s, 4H), 7.45 (d,  $J = 7.5$  Hz, 4H), 7.33 (t,  $J = 7.5$  Hz, 4H), 7.29 (d,  $J = 7.5$  Hz, 2H), 4.89 (d,  $J = 7.0$  Hz, 4H), 3.88 (q,  $J = 6.0$  Hz, 4H), 3.68 (q,  $J = 6.0$  Hz, 4H), 3.57 (d,  $J = 7.0$  Hz, 4H).  $^{13}\text{C}$  NMR (151 MHz, chloroform-*d*)  $\delta$  166.42, 166.27, 137.57, 129.20, 129.18, 129.14, 128.57, 118.70, 70.38, 67.93, 42.64, 38.20 ; IR ( $\text{cm}^{-1}$ )  $\nu$  2936, 2861, 1701, 1665, 1396, 1351, 1112,

727; MS ( $m/z$ ) calc. for  $C_{40}H_{30}N_4O_{10}$   $[+H]^+$ : 727.2040, found 727.2036. calc. for  $C_{40}H_{30}N_4O_{10}$   $[+Na]^+$ : 749.1860, found 749.1854. calc. for  $C_{40}H_{30}N_4O_{10}[+NH_4]^+$ : 744.2306, found 744.2303.

### 8.3.3 Chapter 6

Synthesis of N,N'-bis(2-ethylhexyl)-2,6-dibromo-1,4,5,8-naphthalenetetracarboxylic acid, **6.5** (known)<sup>346,347</sup>.



**Scheme S2:** Synthesis of **6.5**.

Modified literature procedure by T. Govindaraju and co-workers was followed, details outlined below:

#### Synthesis of 2,6-dibromo-1,4,5,8-naphthalene tetracarboxylic acid **6.4**:

Into a 500 mL round bottomed flask, naphthalenetetracarboxylic acid **6.3** (30.02 g, 0.11 mol) was added to stirring conc. sulphuric acid (18 M, 300 mL) at room temperature (CAUTION, strong acid). 1.25 equivalents of 5,5-dimethyl-1,3-dibromohydantoin (40.02 g, 0.14 mol) were added in four portions over 1 hr. The reaction was stoppered and heated to 80°C for 20 h, where the mixture turned from beige to bright yellow with a red gas produced. The hot mixture was then poured directly onto 3L of crushed ice which melted to give a volume of approximately 1.5L of water whereupon the resulting yellow precipitate was collected *in-vacuo* on a low

porosity sinter. The solid was washed with MeOH (300 mL) followed by water (300 mL) and dried in an oven at 40 °C under vacuum for 72 h to yield a mixture (47.4 g) of 2,6-dibromo-1,4,5,8-naphthalenetetracarboxylic acid (NDA) **6.4** and NDA starting material **6.3**. 32:68 ratio of dibrominated NDA:NDA starting material was calculated from <sup>1</sup>H NMR data by integration of the signals at  $\delta = 8.79 \text{ ppm} : 8.71 \text{ ppm}$ . The crude product was used in the next step of synthesis without purification due to its poor solubility.

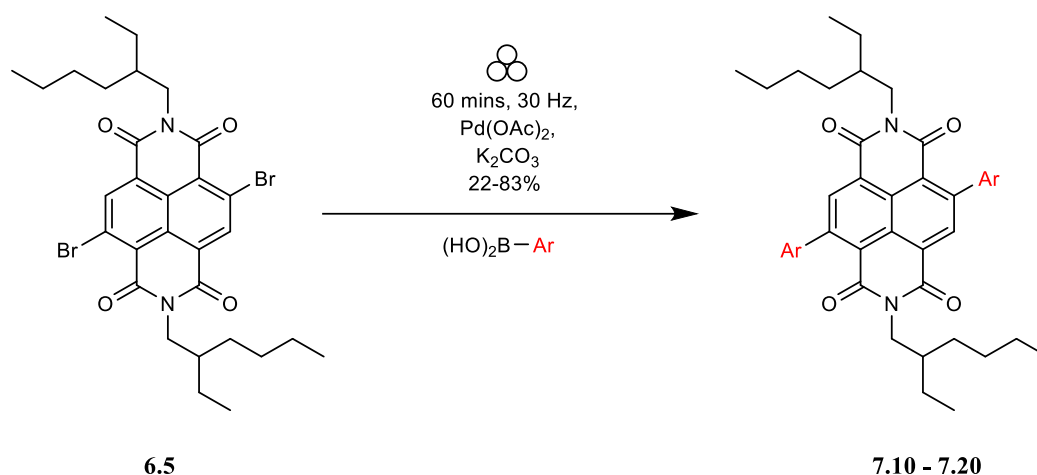
Imidization of **6.4** to N,N'-bis(2-ethylhexyl)-2,6-dibromo-1,4,5,8-naphthalenetetracarboxylic acid, **6.5**:

Crude product **6.4** (44.2 g) was added to acetic acid (300 mL) and stirred. 2-Ethylhexylamine (47.0 g, 0.41 mol) was added in four portions over 30 min at room temperature. The reaction was then heated to 120°C for 4 hr, where a colour change in solution from yellow to dark red was observed. Once the reaction was complete, confirmed by TLC (DCM:hexane v:v 70:30  $R_f^{\text{SM}} = 0.00$ ,  $R_f^{\text{Prod}} = 0.45$ ), it was cooled and poured onto ice (2 L). The resulting bright orange precipitate was collected *in vacuo* on a low porosity sinter and washed with water (300 mL), MeOH (500 mL) where red washings were observed, and finally hexane (1 L) where orange washings were observed. The crude orange solid (44.32 g, 33:67 ratio of **6.5**:**6.6** by <sup>1</sup>H NMR) was then dissolved in a minimum amount of boiling CHCl<sub>3</sub> (*ca.* 500 mL) and was poured, while hot, into rapidly stirring cold hexane (2 L) to remove non-brominated diimide impurities and the pale orange crude solid was collected *in vacuo*. The precipitation procedure was repeated to yield yellow solid (25 g, 90:10 ratio of **6.5**:**6.6** by <sup>1</sup>H NMR). **6.5** was isolated by a recrystallization over two weeks in DCM, where it was transferred to the fridge after one week, to yield analytically pure product as a yellow fluffy needle-like crystalline solid (15.2 g, 21% over two steps). <sup>1</sup>H NMR (600 MHz, chloroform-*d*)  $\delta$  8.99 (s, 2H), 4.15 (m, 4H), 1.93 (m, 2H), 1.43 – 1.33 (m, 8H), 1.22-1.32 (m, 8H), 0.93 (m, 6H), 0.88 (m, 6H). <sup>13</sup>C NMR (151 MHz,

chloroform-*d*)  $\delta$  161.6, 161.4, 139.5, 128.7, 128.1, 125.6, 124.4, 45.5, 38.1, 30.9, 28.9, 24.3, 23.4, 14.5, 10.9. HRMS-ESI: calcd for  $C_{30}H_{37}Br_2N_2O_4$   $[M+H]^+$  647.1042 found 647.1120. Characterization data in agreement with the literature.<sup>362</sup>

### 8.3.4 Chapter 7

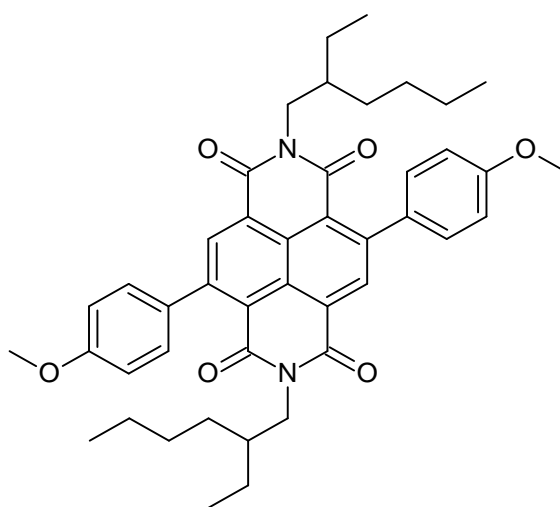
#### General synthesis 1: Suzuki-Miyaura coupling



**General protocol 1.** Into a 25mL ZrO<sub>2</sub> grinding jar were placed N,N'-bis(2-ethylhexyl)-2,6-dibromo-1,4,5,8-naphthalenetetracarboxylic acid **6.5** (100 mg, 0.15 mmol), 3 equivalents of the requisite aryl boronic acid (0.46 mmol), 10 mol% palladium acetate (3.5 mg, 1.54 x 10<sup>-2</sup> mmol), K<sub>2</sub>CO<sub>3</sub> (85 mg, 0.62 mmol) and two 15 mm ZrO<sub>2</sub> balls. The total mass of the reagents was calculated so that milling load equals *ca.* 20 mg.mL<sup>-1</sup>. The jar was then closed and subjected to grinding for 60 minutes in the VBM operated at 30 Hz. The jars were left to cool to room temperature and the resulting solid was dissolved in dichloromethane (25 mL) and passed through Celite, which was then washed with dichloromethane until the washings ran clear. Unless stated otherwise, the combined organic phases were washed with water (3 x 50 mL), dried over MgSO<sub>4</sub>, filtered and the solvent was removed *in vacuo*. The crude material was then

subjected to flash column chromatography (DCM:hexane) using a solvent gradient starting from 40% DCM up to 100% to obtain the c-NDI products.

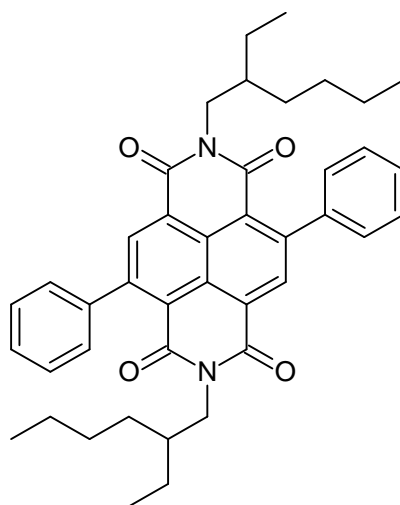
Synthesis of (2,7-bis(2-ethylhexyl)-4,9-bis(4-methoxyphenyl)benzo[lmn][3,8]phenanthroline-1,3,6,8(2H,7H)-tetraone) **7.10** (also referred to as **6.45** in chapter 6)



**7.10**

The title compound was synthesized by following general protocol 1 using *p*-methoxybenzene boronic acid (70 mg, 0.46 mmol), **6.5** (100 mg, 0.15 mmol), K<sub>2</sub>CO<sub>3</sub> (85 mg, 0.62 mmol) and Pd(OAc)<sub>2</sub> (3.5 mg, 1.54 x10<sup>-2</sup> mmol). **7.10** was isolated as a bright red solid after column chromatography (59 mg, 83%). (DCM:hexane2:1 (v/v) R<sub>f</sub> = 0.45). <sup>1</sup>H NMR (600 MHz, chloroform-*d*) δ 8.79 (s, 2H), 7.67 (d, *J* = 8.4 Hz, 4H), 6.95 (d, *J* = 8.4 Hz, 4H), 4.13 - 4.18 (m, 4H), 3.87 (s, 6H), 1.98 - 1.95 (m, 2H), 1.36 (m, 16H), 1.03 - 0.85 (m, 12H). <sup>13</sup>C NMR (151 MHz, chloroform-*d*) δ 163.0, 162.9, 159.8, 147.3, 136.2, 132.5, 129.8, 127.2, 125.4, 122.6, 113.9, 55.3, 44.4, 37.6, 30.5, 28.5, 23.8, 23.1, 14.1, 10.6. IR(ATR); ν<sub>max</sub> (cm<sup>-1</sup>) 2933, 2859, 1704, 1664, 1438, 1246, 1035, 797. HRMS-ESI: calcd for C<sub>44</sub>H<sub>51</sub>N<sub>2</sub>O<sub>6</sub> [M+H]<sup>+</sup> 703.3747; found 703.3740.

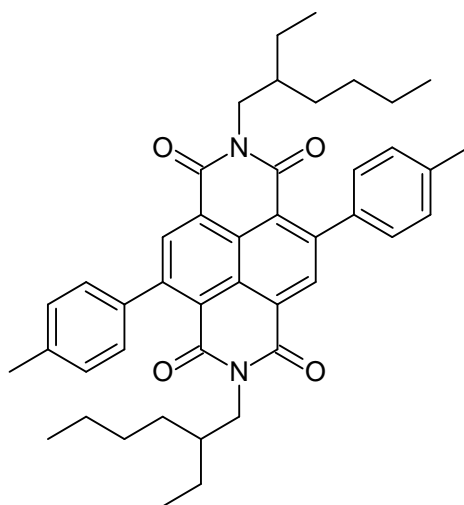
Synthesis of (2,7-bis(2-ethylhexyl)-4,9-diphenylbenzo[*lmn*][3,8]phenanthroline-1,3,6,8(2H,7H)-tetraone) **7.11** (known)<sup>341,363</sup>



**7.11**

The title compound was synthesized by following general protocol 1 using phenylboronic acid (56 mg, 0.46 mmol), **6.5** (100 mg, 0.15 mmol),  $K_2CO_3$  (85 mg, 0.62 mmol) and  $Pd(OAc)_2$  (3.5 mg,  $1.54 \times 10^{-2}$  mmol). **7.11** was isolated as a bright yellow solid by column chromatography (85 mg, 83%). (DCM: hexane 60:40 (v/v)  $R_f = 0.4$ ).  $^1H$  NMR (600 MHz, chloroform-*d*)  $\delta$  8.66 (s, 2H), 7.51 (d,  $J = 7.0$  Hz, 6H), 7.41 (d,  $J = 7.0$  Hz, 4H), 4.11 – 3.96 (m, 4H), 1.87 (h,  $J = 6.6$  Hz, 2H), 1.29 (m, 16H), 0.87 (m, 12H).  $^{13}C$  NMR (151 MHz, chloroform-*d*)  $\delta$  163.3, 163.0, 148.0, 140.9, 136.2, 128.8, 128.6, 128.4, 127.6, 125.9, 123.3, 44.7, 38.0, 30.9, 28.8, 24.2, 23.4, 14.4, 10.9. IR(ATR);  $\nu_{max}$  ( $cm^{-1}$ ) 2957, 2854, 1706, 1667, 1573 1436, 1305, 1198, 696. HRMS-ESI: calcd for  $C_{42}H_{47}N_2O_4$   $[M+H]^+$  643.3536; found 643.3538.

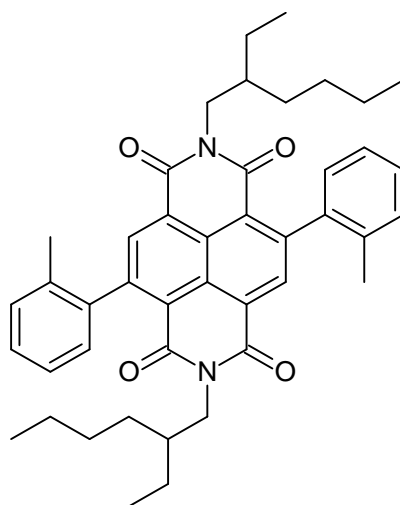
Synthesis of (2,7-bis(2-ethylhexyl)-4,9-di-*p*-tolylbenzo[*lmn*][3,8]phenanthroline-1,3,6,8(2H,7H)-tetraone) **7.12**



**7.12**

The title compound was synthesized by following general protocol 1 using *p*-tolylboronic acid (64 mg, 0.46 mmol), **6.5** (100 mg, 0.15 mmol), K<sub>2</sub>CO<sub>3</sub> (85 mg, 0.62 mmol) and Pd(OAc)<sub>2</sub> (3.5 mg, 1.54 × 10<sup>-2</sup> mmol). **7.12** isolated as a bright yellow solid by column chromatography (73 mg, 69%). (DCM: hexane 70:30 (v/v) R<sub>f</sub> = 0.5). <sup>1</sup>H NMR (600 MHz, chloroform-*d*) δ 8.64 (s, 2H), 7.32 (s, 8H), 4.09 – 3.98 (m, 4H), 2.47 (s, 6H), 1.92 – 1.84 (m, 2H), 1.29 (m, 16H), 0.87 (m, 12H). <sup>13</sup>C NMR (151 MHz, chloroform-*d*) δ 163.0, 162.8, 147.7, 138.2, 137.5, 136.0, 129.2, 128.1, 127.2, 125.4, 122.8, 44.4, 37.6, 30.5, 28.5, 23.8, 23.1, 21.5, 14.1, 10.6. IR(ATR); ν<sub>max</sub> (cm<sup>-1</sup>) 2958, 2858, 1704, 1667, 1439, 1305, 1201, 796. HRMS-ESI: calcd for C<sub>44</sub>H<sub>51</sub>N<sub>2</sub>O<sub>4</sub> [M+H]<sup>+</sup> 671.3849; found 671.3859.

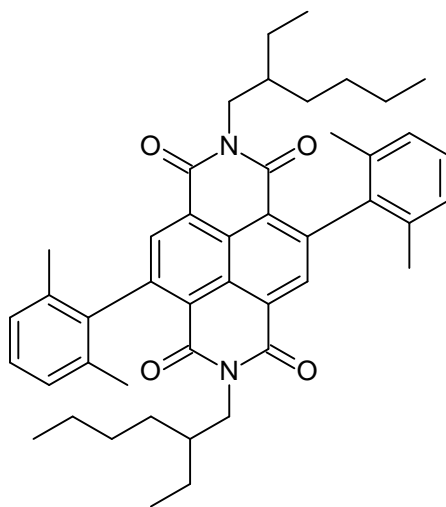
Synthesis of (2,7-bis(2-ethylhexyl)-4,9-di-*o*-tolylbenzo[*lmn*][3,8]phenanthroline-1,3,6,8(2H,7H)-tetraone) **7.13**



**7.13**

The title compound was synthesized by following general protocol 1 using *o*-tolylboronic acid (63 mg, 0.46 mmol), **6.5** (100 mg, 0.15 mmol), K<sub>2</sub>CO<sub>3</sub> (85 mg, 0.62 mmol) and Pd(OAc)<sub>2</sub> (3.5 mg, 1.54 x10<sup>-2</sup> mmol). **7.13** was isolated as a pale-yellow solid by column chromatography (67 mg, 64%). (DCM:hexane70:30 (v/v) R<sub>f</sub> = 0.5). <sup>1</sup>H NMR (600 MHz, chloroform-*d*) δ 8.58 (s, 2H), 7.47 – 7.29 (m, 6H), 7.13 (dt, J = 12.7, 6.5 Hz, 2H), 4.03 (s, 4H), 2.12 (s, 3H), 2.09 (s, 3H), 1.91- 1.83 (m, 2H), 1.35 – 1.16 (m, 16H), 0.90 – 0.80 (m, 12H). <sup>13</sup>C NMR (151 MHz, chloroform-*d*) δ 162.9, 162.4, 147.2, 140.5, 135.5, 134.2, 130.0, 128.2, 127.1, 127.0, 126.0, 125.7, 123.5, 44.4, 37.5, 30.5, 28.5, 23.8, 23.1, 20.0, 14.1, 10.6. IR(ATR); ν<sub>max</sub> (cm<sup>-1</sup>) 2956, 1705, 1665, 1435, 1308, 1203, 798. HRMS-ESI: C<sub>44</sub>H<sub>51</sub>N<sub>2</sub>O<sub>4</sub> [M+H]<sup>+</sup> 671.3849; found 671.3853.

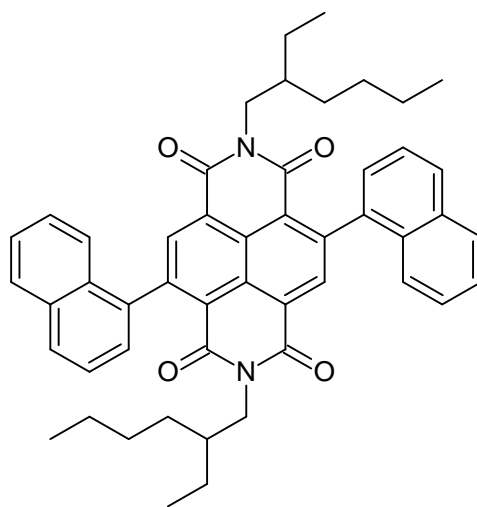
Synthesis of (4,9-bis(2,6-dimethylphenyl)-2,7-bis(2-ethylhexyl)benzo[*lmn*][3,8]phenanthroline-1,3,6,8(2H,7H)-tetraone) **7.14**



**7.14**

The title compound was synthesized by following general protocol 1 using 2,6-dimethylphenylboronic acid (69 mg, 0.46 mmol), **6.5** (100 mg, 0.15 mmol),  $K_2CO_3$  (85 mg, 0.62 mmol) and  $Pd(OAc)_2$  (3.5 mg,  $1.54 \times 10^{-2}$  mmol). **7.14** was isolated as a yellow solid by column chromatography (8 mg, 9%). (DCM:hexane70:30 (v/v)  $R_f = 0.6$ ).  $^1H$  NMR (600 MHz, chloroform-*d*)  $\delta$  8.50 (s, 2H), 7.30 (t,  $J = 8.7, 6.3$  Hz, 2H), 7.21 (d,  $J = 7.6$  Hz, 4H), 4.03 (m, 4H), 1.98 (s, 12H), 1.85 (m, 2H), 1.35 – 1.13 (m, 16H), 0.92 – 0.76 (m, 12H).  $^{13}C$  NMR (151 MHz, chloroform-*d*)  $\delta$  162.8, 162.3, 146.9, 140.1, 135.2, 133.5, 133.5, 127.8, 127.7, 127.1, 126.4, 123.6, 44.3, 37.5, 30.4, 28.4, 23.8, 23.1, 20.8, 20.7, 14.0, 10.6. HRMS-ESI:  $C_{46}H_{55}N_2O_4$   $[M+H]^+$  699.4162; found 699.4177.

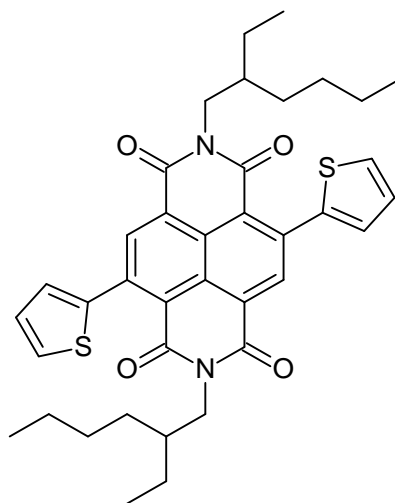
Synthesis of (2,7-bis(2-ethylhexyl)-4,9-di(naphthalen-1-yl)benzo[*lmn*][3,8]phenanthroline-1,3,6,8(2H,7H)-tetraone) **7.15**



**7.15**

The title compound was synthesized by following general protocol 1 using naphthalene-1-boronic acid pinacol ester (117 mg, 0.46 mmol), **6.5** (100 mg, 0.15 mmol),  $K_2CO_3$  (85 mg, 0.62 mmol) and  $Pd(OAc)_2$  (3.5 mg,  $1.54 \times 10^{-2}$  mmol). **7.15** was isolated as an orangey yellow solid by column chromatography (25 mg, 22%). (EtOAc:hexane 60:40 (v/v)  $R_f = 0.45$ ).  $^1H$  NMR (600 MHz, chloroform-*d*)  $\delta$  8.75 (s, 2H), 8.00 (dd,  $J = 15.4, 8.2$  Hz, 4H), 7.65 (dd,  $J = 7.2$  Hz, 2H), 7.52 (dd,  $J = 7.2$  Hz, 2H), 7.48 – 7.30 (m, 6H), 4.04 – 3.78 (m, 4H), 1.74 (tt,  $J = 13.1, 6.3$  Hz, 2H), 1.47 – 1.01 (m, 16H), 0.79 (m, 12H).  $^{13}C$  NMR (151 MHz, chloroform-*d*)  $\delta$  162.8, 162.1, 146.1, 146.0, 138.7, 136.3, 133.4, 130.9, 128.8, 128.6, 127.3, 126.4, 126.0, 125.9, 125.5, 125.0, 124.6, 44.2, 44.2, 37.5, 37.4, 30.4, 30.3, 28.4, 28.3, 23.8, 23.7, 22.9, 22.9, 14.1, 14.0, 10.6. IR(ATR);  $\nu_{max}$  ( $cm^{-1}$ ) 2958, 2859, 1703, 1662, 1439, 1307, 772. HRMS-ESI: calcd for  $C_{50}H_{51}N_2O_4$   $[M+H]^+$  743.3849; found 743.3852.

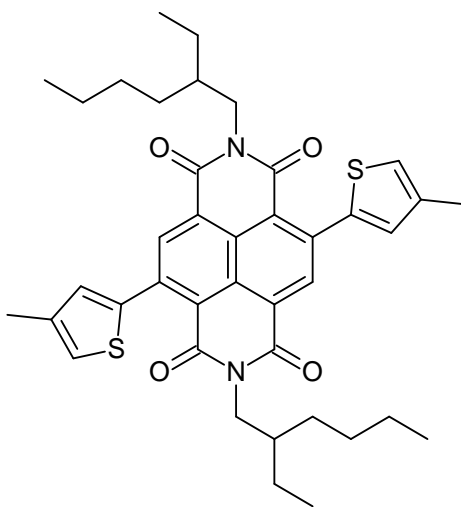
Synthesis of (2,7-bis(2-ethylhexyl)-4,9-di(thiophen-2-yl)benzo[*lmn*][3,8]phenanthroline-1,3,6,8(2H,7H)-tetraone) **7.16** (known)<sup>365</sup>



**7.16**

The title compound was synthesized by following general protocol 1 using 2-Thienylboronic acid (64 mg, 0.46 mmol), **6.5** (100 mg, 0.15 mmol), K<sub>2</sub>CO<sub>3</sub> (85 mg, 0.62 mmol) and Pd(OAc)<sub>2</sub> (3.5 mg, 1.54 x 10<sup>-2</sup> mmol). **7.16** was isolated as a bright red solid by column chromatography (68 mg, 67%). (DCM:hexane 80:20 (v/v) R<sub>f</sub> = 0.6). <sup>1</sup>H NMR (600 MHz, chloroform-*d*) δ 8.75 (s, 2H), 7.57 (d, *J* = 5.1 Hz, 2H), 7.30 (d, *J* = 3.6 Hz, 2H), 7.20 (dd, *J* = 5.1, 3.6 Hz, 2H), 4.14 – 4.02 (m, 4H), 1.88-1.92 (m, 2H), 1.41 – 1.19 (m, 16H), 0.84-0.92 (m, 12H). <sup>13</sup>C NMR (151 MHz, chloroform-*d*) δ 162.6, 162.4, 140.8, 140.2, 136.7, 128.3, 128.1, 127.5, 127.4, 125.4, 123.4, 44.6, 37.7, 30.6, 28.6, 23.9, 23.1, 14.1, 10.6. IR(ATR); ν<sub>max</sub> (cm<sup>-1</sup>) 2959, 2859, 1706, 1660, 1574, 1441, 1307, 1195, 696. HRMS-ESI: calcd for C<sub>38</sub>H<sub>43</sub>N<sub>2</sub>O<sub>4</sub>S<sub>2</sub> [M+H]<sup>+</sup> 655.2664; found 655.2654.

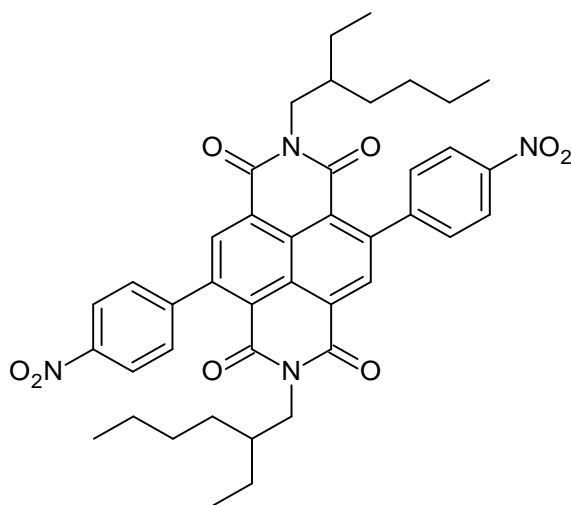
Synthesis of (2,7-bis(2-ethylhexyl)-4,9-bis(4-methylthiophen-2-yl)benzo[*lmn*][3,8]phenanthroline-1,3,6,8(2H,7H)-tetraone) **7.17**



**7.17**

The title compound was synthesized by following general protocol 1 using 3-methylthiophene-2-boronic acid (66 mg, 0.46 mmol), **6.5** (100 mg, 0.15 mmol), K<sub>2</sub>CO<sub>3</sub> (85 mg, 0.62 mmol) and Pd(OAc)<sub>2</sub> (3.5 mg, 1.54 x10<sup>-2</sup> mmol). **7.17** was isolated as a dark red solid by column chromatography (87 mg, 83%). (DCM:hexane 80:20 (v/v) R<sub>f</sub> = 0.65). <sup>1</sup>H NMR (600 MHz, chloroform-*d*) δ 8.73 (s, 2H), 7.13 (d, *J* = 15.8 Hz, 4H), 4.09 (q, *J* = 9.7, 7.2 Hz, 4H), 2.37 (s, 6H), 1.91 (d, *J* = 10.3 Hz, 2H), 1.47 – 1.20 (m, 16H), 1.02 – 0.74 (m, 12H). <sup>13</sup>C NMR (151 MHz, chloroform-*d*) δ 163.0, 162.8, 141.0, 140.7, 138.4, 136.9, 130.9, 127.7, 125.7, 124.1, 123.4, 44.9, 38.0, 30.9, 28.9, 24.2, 23.4, 16.2, 14.4, 10.9. IR(ATR); ν<sub>max</sub> (cm<sup>-1</sup>) 2958, 2859, 1671, 1662, 1445, 1307, 1193, 795. HRMS-ESI: calcd for C<sub>40</sub>H<sub>47</sub>N<sub>2</sub>O<sub>4</sub>S<sub>2</sub> [M+H]<sup>+</sup> 683.2977; found 683.2972.

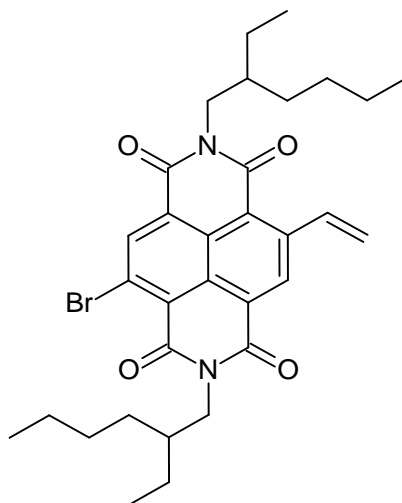
Synthesis of (2,7-bis(2-ethylhexyl)-4,9-bis(4-nitrophenyl)benzo[*lmn*][3,8]phenanthroline-1,3,6,8(2H,7H)-tetraone) **7.18**



**7.18**

The title compound was synthesized by following general protocol 1 using *p*-nitrobenzene boronic acid (77 mg, 0.46 mmol), **6.5** (100 mg, 0.15 mmol), K<sub>2</sub>CO<sub>3</sub> (85 mg, 0.62 mmol) and Pd(OAc)<sub>2</sub> (3.5 mg, 1.54 x10<sup>-2</sup> mmol). **7.18** was isolated as a sandy yellow solid by column chromatography (49 mg, 43%).(DCM:hexane2:1 (v/v) R<sub>f</sub> = 0.35). <sup>1</sup>H NMR (600 MHz, chloroform-*d*) δ 8.62 (s, 2H), 8.39 (d, J = 8.5 Hz, 4H), 7.55 (d, J = 8.5 Hz, 4H), 4.08 – 3.94 (m, 4H), 1.83 (hept, J = 6.4 Hz, 2H), 1.40 – 1.14 (m, 16H), 1.03-0.75 (m, 12H). <sup>13</sup>C NMR (151 MHz, chloroform-*d*) δ 162.3, 162.3, 147.7, 147.0, 145.5, 134.9, 129.0, 127.4, 126.0, 123.8, 123.3, 44.7, 37.7, 30.5, 28.4, 23.8, 23.1, 14.1, 10.6. IR(ATR); ν<sub>max</sub> (cm<sup>-1</sup>) 2958, 2859, 1708, 1662, 1511, 1340, 1198, 848. HRMS-ESI: calcd for C<sub>42</sub>H<sub>45</sub>N<sub>4</sub>O<sub>8</sub> [M+H]<sup>+</sup> 733.3237; found 733.3243.

Synthesis of (4-bromo-2,7-bis(2-ethylhexyl)-9-vinylbenzo[*lmn*][3,8]phenanthroline-1,3,6,8(2H,7H)-tetraone) **7.19**

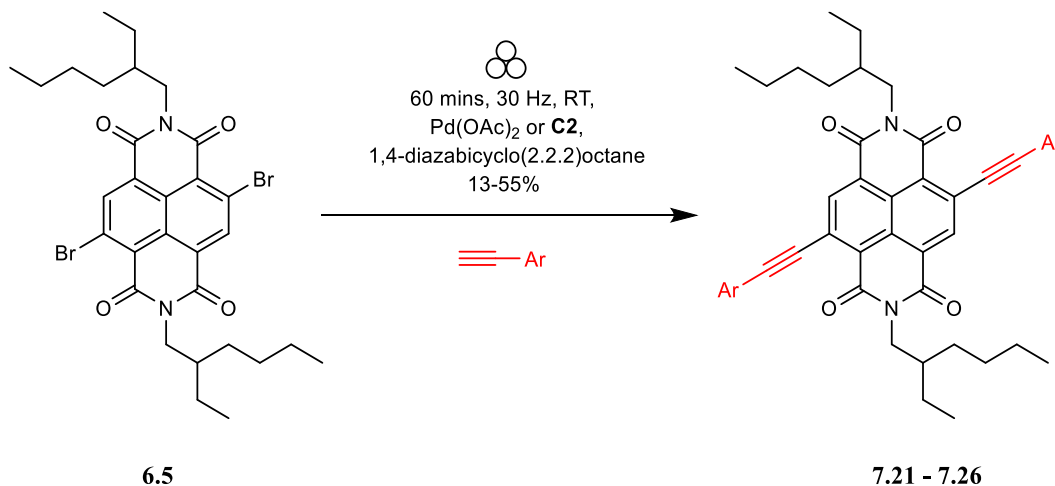


**7.19**

The title compound was synthesized by following general protocol 1 using vinyl boronic pinacol ester (71 mg, 0.46 mmol), **6.5** (100 mg, 0.15 mmol),  $K_2CO_3$  (85 mg, 0.62 mmol) and  $Pd(OAc)_2$  (3.5 mg,  $1.54 \times 10^{-2}$  mmol). **7.19** was isolated as a red solid product (16 mg, 5.2%) and isolated using the procedure below: Upon completion of ball milling, the vessels were cooled to room temperature before the contents were dissolved in a mixture of dichloromethane and methanol (18 ml, 2:1). This suspension was filtered through a celite plug and the resulting filtrate was concentrated to yield a deep red, viscous semi solid. The red solid was dissolved in ethyl acetate (40 ml) and stirred for 10 minutes leading to the formation of an insoluble brown precipitate which was removed by filtration. The filtrate was concentrated and purified by column chromatography (16 mg, 5.2 %.)  $^1H$  NMR (600 MHz, chloroform-*d*)  $\delta$  8.84 (s, 1H), 8.32 (s, 1H), 8.08 (dd,  $J = 17.5, 11.0$  Hz, 1H), 5.98 (d,  $J = 17.5$  Hz, 1H), 5.72 (d,  $J = 11.0$  Hz, 1H), 4.19 – 4.01 (m, 4H), 1.92 (m, 2H), 1.48 – 1.13 (m, 16H), 0.95 – 0.84 (m, 12H).  $^{13}C$  NMR (151 MHz, chloroform-*d*)  $\delta$  163.7, 163.7, 162.9, 162.4, 141.1, 135.9, 132.7, 129.2, 127.1, 124.7,

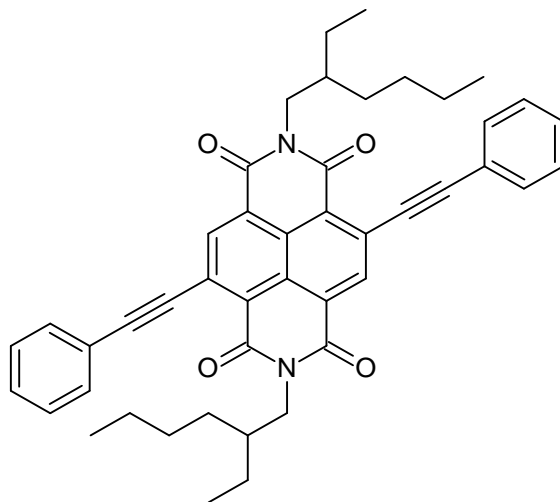
123.9, 122.0, 121.8, 120.6, 105.4, 44.7, 44.1, 37.8, 37.8, 30.7, 30.6, 28.6, 28.5, 23.99, 23.97, 23.07, 23.02, 14.07, 10.59, 10.56. IR(ATR);  $\nu_{\max}$  ( $\text{cm}^{-1}$ ) 2925, 2858, 1700, 1643, 1279, 799, 762, 729, 529. HRMS-ESI: calcd for  $\text{C}_{32}\text{H}_{39}\text{BrN}_2\text{O}_4$   $[\text{M}+\text{Na}]^+$ , 617.1991 [ $^{79}\text{Br}$ ] and 619.1970 [ $^{81}\text{Br}$ ]; found, 617.2279 and 619.2303.

### General synthesis 2: Sonogashira coupling



**General Protocol 2.** Into a 25mL  $\text{ZrO}_2$  grinding jar were placed N,N'-bis(2-ethylhexyl)-2,6-dibromo-1,4,5,8-naphthalenetetracarboxylic acid **6.5** (100 mg, 0.15 mmol), 3 equivalents of the requisite aryl acetylene (0.46 mmol), 10 mol% palladium source ( $1.54 \times 10^{-2}$  mmol), 4 equivalents of fresh 1,4-diazabicyclo[2.2.2]octane (69 mg, 0.62 mmol) and two 15 mm  $\text{ZrO}_2$  balls. The total mass of the reagents was calculated so that milling load equals *ca.* 20 mg.mL $^{-1}$ . The jar was then closed and subjected to grinding for 60 minutes in the VBM operated at 30 Hz. The jars were left to cool to room temperature and the resulting solid was dissolved in dichloromethane (25 mL) and passed through Celite, which was then washed with dichloromethane until the washings ran colourless. The combined organic layers were dried *in vacuo* and the crude material was then subjected to flash column chromatography (DCM:hexane) using a solvent gradient starting from 30% DCM up to 100% to obtain the c-NDI products.

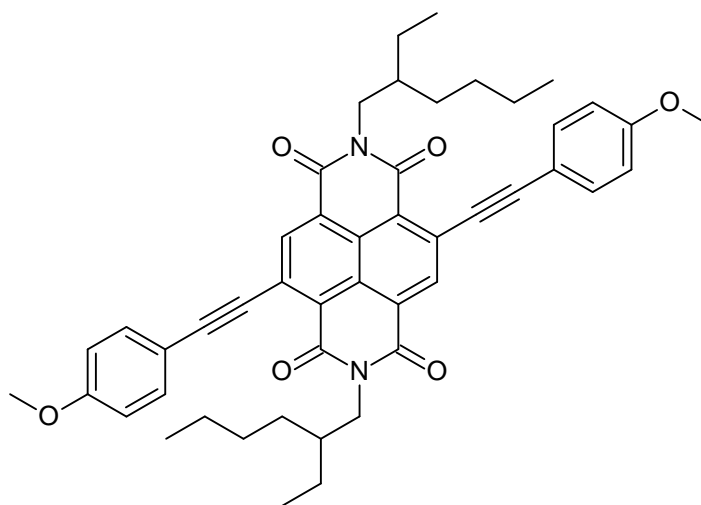
Synthesis of (2,7-bis(2-ethylhexyl)-4,9-bis(phenylethynyl)benzo[*lmn*][3,8]phenanthroline-1,3,6,8(2H,7H)-tetraone) **7.21** (also referred to as **6.28** in Chapter 6)



**7.21**

The title compound was synthesized by following general protocol 2 using phenyl acetylene (47 mg, 0.46 mmol), **6.5** (100 mg, 0.15 mmol), 1,4-diazabicyclo[2.2.2]octane (85 mg, 0.62 mmol) and Pd(OAc)<sub>2</sub> (3.5 mg, 1.54 x 10<sup>-2</sup> mmol). **7.21** was isolated as a bright orange solid by column chromatography (51 mg, 48%). (DCM:hexane2:1 (v/v) R<sub>f</sub> = 0.5). <sup>1</sup>H NMR (600 MHz, chloroform-*d*) δ 8.88 (s, 2H), 7.76 (dd, *J* = 6.7, 2.9 Hz, 4H), 7.44-7.46 (m, 6H), 4.18 (qd, *J* = 13.0, 7.3 Hz, 4H), 1.97-2.03 (m, 2H), 1.45 – 1.30 (m, 16H), 0.84-0.96 (m, 12H). <sup>13</sup>C NMR (151 MHz, chloroform-*d*) δ 162.5, 161.8, 137.3, 132.6, 129.9, 128.6, 127.2, 126.5, 125.3, 125.1, 122.5, 102.9, 89.6, 44.6, 37.7, 30.6, 28.5, 24.0, 23.1, 14.2, 10.6. IR(ATR); ν<sub>max</sub> (cm<sup>-1</sup>) 2928, 2859, 2198 (C≡C), 1702, 1659, 1443, 1220, 768. HRMS-ESI: calcd for C<sub>46</sub>H<sub>47</sub>N<sub>2</sub>O<sub>4</sub> [M+H]<sup>+</sup> 691.3536; found 691.3542.

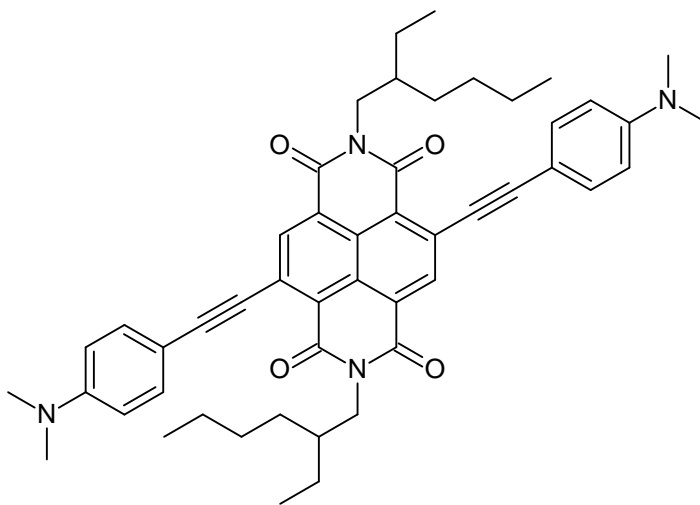
Synthesis of (2,7-bis(2-ethylhexyl)-4,9-bis((4-methoxyphenyl)ethynyl)benzo[*lmn*][3,8]phenanthroline-1,3,6,8(2H,7H)-tetraone) **7.22**



**7.22**

The title compound was synthesized by following general protocol 2 using 1-ethynyl-4-methoxybenzene (70 mg, 0.46 mmol), **6.5** (100 mg, 0.15 mmol), 1,4-diazabicyclo[2.2.2]octane (85 mg, 0.62 mmol) and **C2** (11 mg,  $1.54 \times 10^{-2}$  mmol). **7.22** was isolated as a rich purple solid by column chromatography (76 mg, 66%). (DCM: hexane 80:20 (v/v)  $R_f = 0.4$ ).  $^1\text{H}$  NMR (600 MHz, chloroform-*d*)  $\delta$  8.79 (s, 2H), 7.67 (d,  $J = 8.4$  Hz, 4H), 6.95 (d,  $J = 8.4$  Hz, 4H), 4.16 (qd,  $J = 13.0, 7.4$  Hz, 4H), 3.87 (s, 6H), 1.98 (s, 2H), 1.29-1.45 (m, 16H), 1.03 – 0.85 (m, 12H).  $^{13}\text{C}$  NMR (151 MHz, chloroform-*d*)  $\delta$  162.5, 161.9, 161.0, 137.1, 134.44, 127.2, 126.3, 124.8, 124.6, 114.6, 114.3, 103.6, 89.4, 55.4, 44.5, 37.7, 30.6, 28.5, 24.0, 23.1, 14.2, 10.6. IR(ATR);  $\nu_{\text{max}}$  ( $\text{cm}^{-1}$ ) 2958, 2859, 2188 ( $\text{C}\equiv\text{C}$ ), 1702, 1660, 1510, 1248, 831. HRMS-ESI: calcd for  $\text{C}_{48}\text{H}_{51}\text{N}_2\text{O}_6$   $[\text{M}+\text{H}]^+$  751.3747; found 751.3740.

Synthesis of (4,9-bis((4-(dimethylamino)phenyl)ethynyl)-2,7-bis(2-ethylhexyl)benzo[*lmn*][3,8]phenanthroline-1,3,6,8(2H,7H)-tetraone) **7.23**

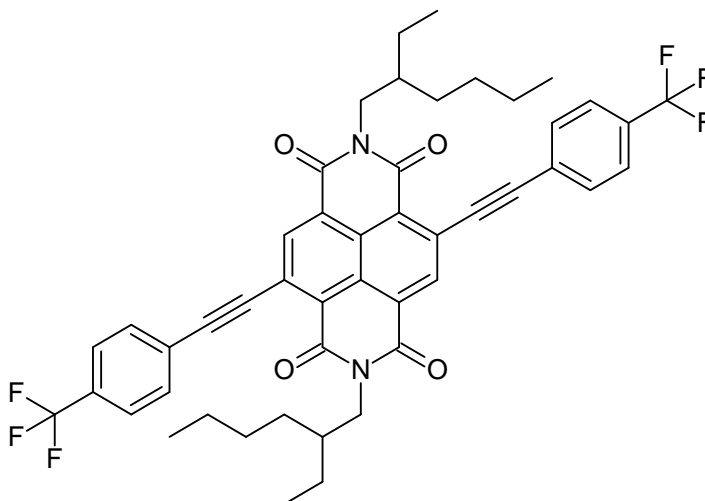


**7.23**

The title compound was synthesized by following general protocol 2 using 4-ethynyl-N,N-dimethylaniline (71 mg, 0.46 mmol), **6.5** (100 mg, 0.15 mmol), 1,4-diazabicyclo[2.2.2]octane (85 mg, 0.62 mmol) and Pd(OAc)<sub>2</sub> (3.5 mg, 1.54 × 10<sup>-2</sup> mmol). **7.23** was isolated as a dark blue solid by column chromatography (68 mg, 55%). (DCM:hexane70:30 (v/v) R<sub>f</sub> = 0.2). <sup>1</sup>H NMR (600 MHz, chloroform-*d*) δ 8.75 (s, 2H), 7.56 (d, *J* = 9.0 Hz, 4H), 6.66 (d, *J* = 9.0 Hz, 4H), 4.17 (qd, *J* = 13.0, 7.3 Hz, 4H), 3.05 (s, 12H), 2.01 (dq, *J* = 13.2, 6.7, 5.4 Hz, 2H), 1.49 – 1.21 (m, 16H), 0.86 – 0.97 (m, 12H). <sup>13</sup>C NMR (151 MHz, chloroform-*d*) δ 162.8, 162.0, 150.8, 136.9, 134.0, 127.0, 126.1, 124.4, 123.5, 111.4, 108.8, 105.5, 90.6, 44.31, 40.0, 37.7, 30.7, 29.7, 28.6, 24.0, 23.1, 14.2, 10.6. IR(ATR); ν<sub>max</sub> (cm<sup>-1</sup>) 2934, 2853, 2173 (C≡C), 1694, 1656, 1568, 1445, 1367, 1187, 813. HRMS-ESI: calcd for C<sub>50</sub>H<sub>57</sub>N<sub>4</sub>O<sub>4</sub> [M+H]<sup>+</sup> 777.4380; found 777.4385.

Synthesis of (2,7-bis(2-ethylhexyl)-4,9-bis((4-(trifluoromethyl)phenyl)ethynyl)benzo[lmn][3,8] phenanthroline-1,3,6,8(2H,7H)-tetraone)

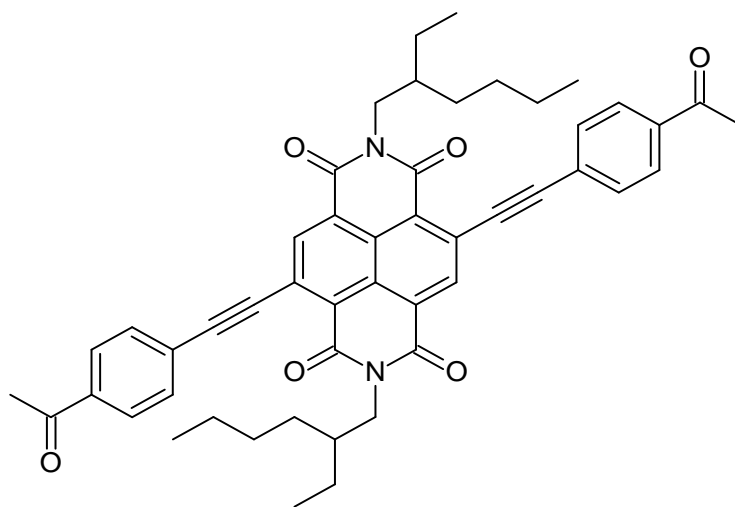
**7.24**



**7.24**

The title compound was synthesized by following general protocol 2 using 4-ethynyl- $\alpha,\alpha,\alpha$ -trifluorotoluene (78 mg, 0.46 mmol), **6.5** (100 mg, 0.15 mmol), 1,4-diazabicyclo[2.2.2]octane (85 mg, 0.62 mmol) and **C2** (11 mg,  $1.54 \times 10^{-2}$  mmol). **7.24** was isolated as a sandy yellow solid by column chromatography (30 mg, 24%). (DCM:hexane50:50 (v/v)  $R_f = 0.6$ ). <sup>1</sup>H NMR (600 MHz, chloroform-*d*)  $\delta$  8.79 (s, 2H), 7.83 (d,  $J = 8.0$  Hz, 4H), 7.69 (d,  $J = 8.0$  Hz, 4H), 4.14 (qd,  $J = 13.1, 7.3$  Hz, 4H), 1.96 (hept,  $J = 6.9$  Hz, 2H), 1.25 – 1.44 (m, 16H), 0.74 – 0.96 (m, 12H). <sup>13</sup>C NMR (151 MHz, chloroform-*d*)  $\delta$  162.1, 161.6, 137.2, 132.8, 132.5, 126.6, 125.2, 91.0, 44.6, 37.7, 30.6, 28.5, 24.0, 23.1, 14.1, 10.6. IR(ATR);  $\nu_{\max}$  (cm<sup>-1</sup>) 2932, 2853, 2204 (C≡C), 1704, 1661, 1447, 1315, 1122, 845. HRMS-ESI: calcd for C<sub>48</sub>H<sub>45</sub>F<sub>6</sub>N<sub>2</sub>O<sub>4</sub> [M+H]<sup>+</sup> 827.3284; found 827.3256. Low solubility and C-F coupling meant not all signals in the <sup>13</sup>C NMR spectrum could be resolved.

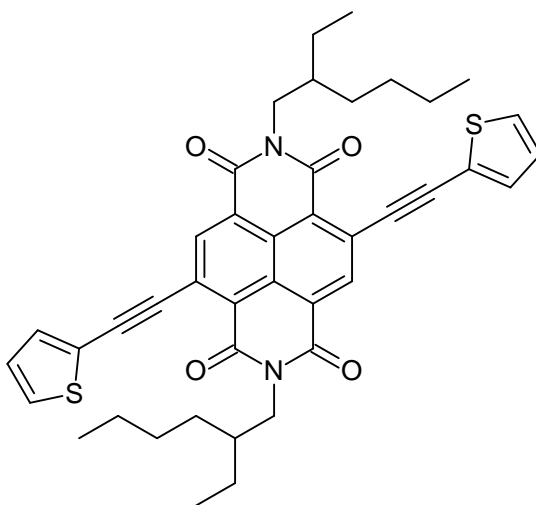
Synthesis of (4,9-bis((4-acetylphenyl)ethynyl)-2,7-bis(2-ethylhexyl)benzo[*lmn*][3,8]phenanthroline-1,3,6,8(2H,7H)-tetraone) **7.25**



**7.25**

The title compound was synthesized by following general protocol 2 using 4'-ethynylacetophenone (70 mg, 0.46 mmol), **6.5** (100 mg, 0.15 mmol), 1,4-diazabicyclo[2.2.2]octane (85 mg, 0.62 mmol) and Pd(OAc)<sub>2</sub> (3.5 mg, 1.54 x 10<sup>-2</sup> mmol). **7.25** was isolated as a dark orange solid by column chromatography (21 mg, 13%). (DCM 100% (v/v) R<sub>f</sub> = 0.1). <sup>1</sup>H NMR (600 MHz, chloroform-*d*) δ 8.79 (s, 2H), 7.99 (d, *J* = 8.3 Hz, 4H), 7.78 (d, *J* = 8.3 Hz, 4H), 4.15 (qd, *J* = 13.1, 7.4 Hz, 4H), 2.63 (s, 6H), 1.97 (h, *J* = 6.5 Hz, 2H), 1.22–1.44 (m, 16H), 0.84–0.96 (m, 12H). <sup>13</sup>C NMR (151 MHz, chloroform-*d*) δ 197.2, 162.1, 161.5, 137.3, 137.1, 132.7, 128.4, 127.0, 126.6, 126.54, 125.7, 125.2, 101.3, 91.9, 44.6, 37.7, 30.6, 28.5, 26.7, 24.0, 23.1, 14.1, 10.6. IR(ATR); ν<sub>max</sub> (cm<sup>-1</sup>) 2930, 2858, 2202 (C≡C), 1686, 1665, 1573, 1261, 791. HRMS-ESI: calcd for C<sub>50</sub>H<sub>51</sub>N<sub>2</sub>O<sub>6</sub> [M+H]<sup>+</sup> 775.3747; found 775.3732.

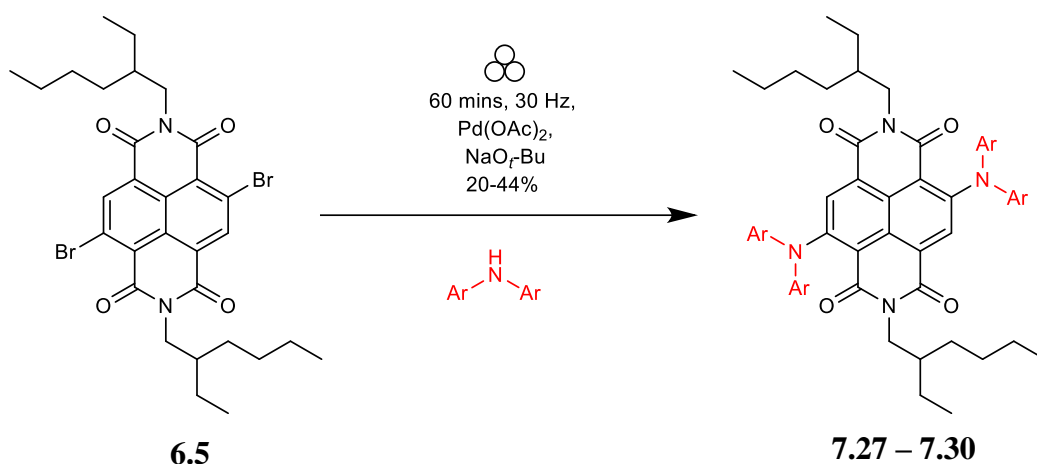
Synthesis of (2,7-bis(2-ethylhexyl)-4,9-bis(thiophen-2-ylethynyl)benzo[lmn][3,8]phenanthroline-1,3,6,8(2H,7H)-tetraone) **7.26**



**7.26**

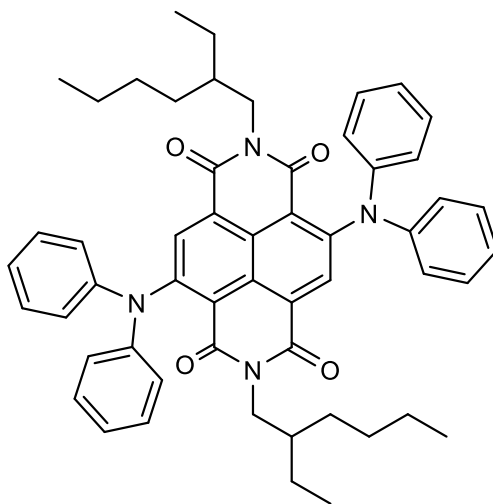
The title compound was synthesized by following general protocol 2 using 2-ethynylthiophene (50 mg, 0.46 mmol), **6.5** (100 mg, 0.15 mmol), 1,4-diazabicyclo[2.2.2]octane (85 mg, 0.62 mmol) and **C2** (11 mg,  $1.54 \times 10^{-2}$  mmol). **7.26** was isolated as a bright red solid by column chromatography (70 mg, 32%). (DCM:hexane 70:30 (v/v)  $R_f = 0.3$ ).  $^1\text{H}$  NMR (600 MHz, chloroform-*d*)  $\delta$  8.80 (s, 2H), 7.56 (d,  $J = 5.1$  Hz, 2H), 7.50 (d,  $J = 5.1$  Hz, 2H), 7.12 (t,  $J = 4.4$  Hz, 2H), 4.16 (m, 4H), 1.98 (m, 2H), 1.46 – 1.27 (m, 16H), 0.89 – 0.96 (m, 12H).  $^{13}\text{C}$  NMR (151 MHz, chloroform-*d*)  $\delta$  162.4, 161.8, 136.8, 134.8, 130.5, 127.7, 126.7, 126.4, 125.0, 124.7, 122.5, 96.5, 94.1, 44.6, 37.7, 30.6, 28.5, 24.0, 23.1, 14.2, 10.6. IR(ATR);  $\nu_{\text{max}}$  ( $\text{cm}^{-1}$ ) 2957, 2852, 2186 ( $\text{C}\equiv\text{C}$ ), 1701, 1652, 1445, 1195, 724. HRMS-ESI: calcd for  $\text{C}_{42}\text{H}_{43}\text{N}_2\text{O}_4\text{S}_2$   $[\text{M}+\text{H}]^+$  703.2664; found 703.2667.

### General synthesis 3: Buchwald-Hartwig Aminations



**General Protocol 3.** Into a 25mL ZrO<sub>2</sub> grinding jar were placed N,N'-bis(2-ethylhexyl)-2,6-dibromo-1,4,5,8-naphthalenetetracarboxylic acid **6.5** (100 mg, 0.15 mmol), 3 equivalents of the requisite aryl amine (0.46 mmol), 10 mol% palladium acetate (3.5 mg, 1.54 x10<sup>-2</sup> mmol), 4 equivalents of fresh sodium *tert*-butoxide (60 mg, 0.62 mmol) and two 15 mm ZrO<sub>2</sub> balls. The total mass of the reagents was calculated so that milling load equals *ca.* 20 mg.mL<sup>-1</sup>. The jar was then closed and subjected to grinding for 60 minutes in the VBM operated at 30 Hz. The jars were left to cool to room temperature and the resulting solid was dissolved in dichloromethane (25 mL) and passed through Celite, which was then washed with dichloromethane until the washings ran colourless. The combined organic layers were dried *in vacuo* and the crude material was then subjected to flash column chromatography (DCM:hexane) using a solvent gradient starting from 40% DCM up to 100% to obtain the c-NDI products.

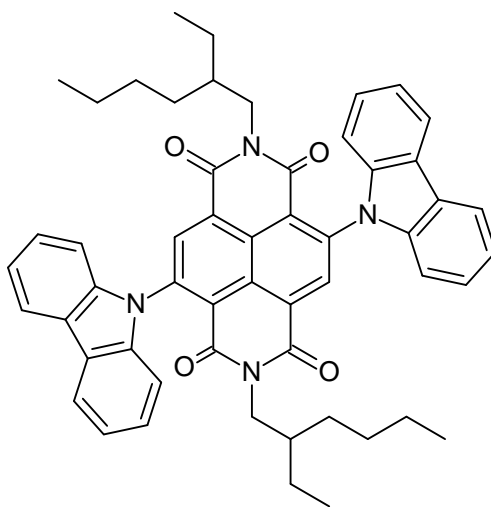
Synthesis of (4,9-bis(diphenylamino)-2,7-bis(2-ethylhexyl)benzo[lmn][3,8]phenanthroline-1,3,6,8(2H,7H)-tetraone) **7.27** (known)<sup>341</sup>



**7.27**

The title compound was synthesized by following general protocol 3 using diphenylamine (79 mg, 0.46 mmol), **6.5** (100 mg, 0.15 mmol), sodium tert-butoxide (59 mg, 0.62 mmol) and Pd(OAc)<sub>2</sub> (3.5 mg, 1.54 x10<sup>-2</sup> mmol). **7.27** was isolated as a dark turquoise solid by column chromatography (39 mg, 22%). (DCM:hexane 55:45 (v/v) R<sub>f</sub> = 0.3). <sup>1</sup>H NMR (600 MHz chloroform-*d*) δ 8.43 (s, 2H), 7.24 (d, *J* = 7.6 Hz, 8H), 7.07 (d, 7.6z Hz, 12H), 3.77-3.90 (m, 4H), 1.15-1.18 (m 12H), 0.99-1.01 (m, 2H), 0.93 – 0.63 (m, 16H). <sup>13</sup>C NMR (151 MHz, chloroform-*d*) δ 162.9, 160.3, 148.9, 147.1, 133.8, 129.4, 126.3, 126.1, 124.4, 123.9, 116.7, 43.9, 37.3, 30.4, 28.6, 23.5, 23.0, 14.1, 10.4. IR(ATR); ν<sub>max</sub> (cm<sup>-1</sup>) 2958, 2853, 1695, 1662, 1491, 1442, 1196, 691. HRMS-ESI: calcd for C<sub>54</sub>H<sub>57</sub>N<sub>4</sub>O<sub>4</sub> [M+H]<sup>+</sup> 825.4380; found 825.4390. C<sub>54</sub>H<sub>56</sub>N<sub>4</sub>O<sub>4</sub>, *M<sub>r</sub>* = 825.02, triclinic, *P*-1 (No. 2), *a* = 11.5685(9) Å, *b* = 14.3736(9) Å, *c* = 15.5702(10) Å, *a* = 115.595(6)°, *b* = 99.722(7)°, *g* = 97.130(6)°, *V* = 2244.2(3) Å<sup>3</sup>, *T* = 100.00(11) K, *Z* = 2, *Z'* = 1, *m*(Cu K<sub>α</sub>) = 0.606, 28811 reflections measured, 4997 unique (*R*<sub>int</sub> = 0.0926) which were used in all calculations. The final *wR*<sub>2</sub> was 0.2433 (all data) and *R*<sub>I</sub> was 0.0775 (*I* ≥ 2 *s*(*I*)).

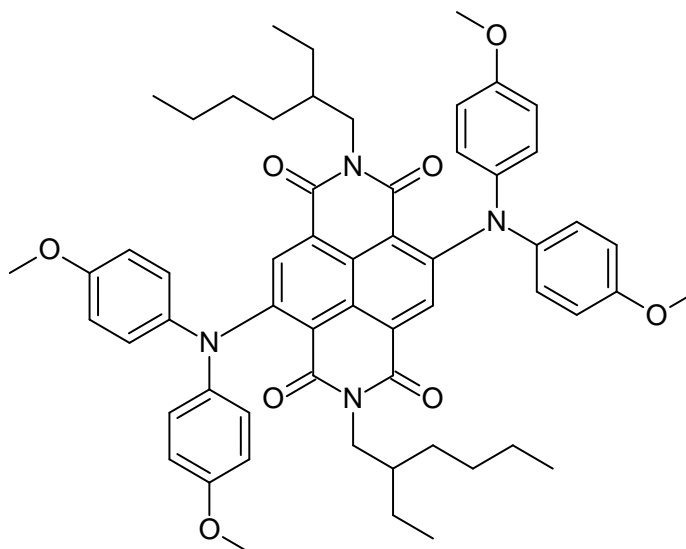
Synthesis of (4,9-di(9H-carbazol-9-yl)-2,7-bis(2-ethylhexyl)benzo[*lmn*][3,8]phenanthroline-1,3,6,8(2H,7H)-tetraone) **7.28** (also referred to as **6.52** in Chapter 6) (known)<sup>341</sup>



**7.28**

The title compound was synthesized by following general protocol 3 using carbazole (78 mg, 0.46 mmol), **6.5** (100 mg, 0.15 mmol), sodium tert-butoxide (59 mg, 0.62 mmol) and Pd(OAc)<sub>2</sub> (3.5 mg, 1.54 × 10<sup>-2</sup> mmol). **7.28** was isolated as a royal blue solid by column chromatography (44 mg, 36%). (DCM:hexane2:1 (v/v) R<sub>f</sub> = 0.6). <sup>1</sup>H NMR (600 MHz, chloroform-*d*) δ 9.03 (s, 2H), 8.20 (d, *J* = 7.5 Hz, 4H), 7.46 – 7.34 (m, 8H), 7.19 (d, *J* = 7.5, 4H), 4.05 – 3.87 (m, 4H), 1.82 – 1.69 (m, 2H), 1.36 – 1.11 (m, 16H), 0.96 – 0.73 (m, 12H). <sup>13</sup>C NMR (151 MHz, chloroform-*d*) δ 162.0, 160.1, 140.5, 139.9, 134.3, 127.9, 127.8, 126.4, 126.3, 124.7, 121.5, 120.9, 109.6, 44.5, 37.5, 30.4, 28.5, 23.7, 23.0, 14.1, 10.5. IR(ATR); ν<sub>max</sub> (cm<sup>-1</sup>) 2928, 2853, 1706, 1659, 1445, 1301, 743. HRMS-ESI: calcd for C<sub>54</sub>H<sub>53</sub>N<sub>4</sub>O<sub>4</sub> [M+H]<sup>+</sup> 821.4067; found 821.4063.

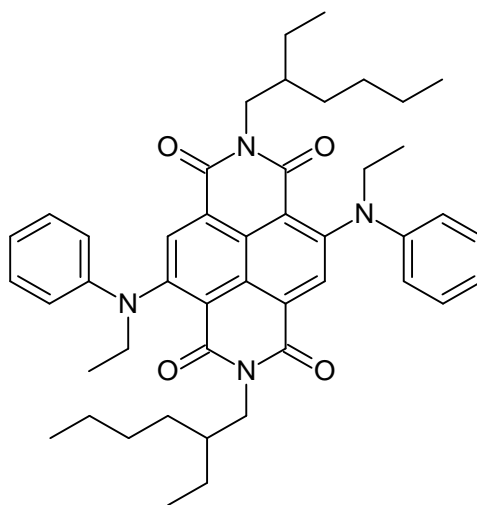
Synthesis of (4,9-bis(bis(4-methoxyphenyl)amino)-2,7-bis(2-ethylhexyl)benzo[*lmn*][3,8]phenanthroline-1,3,6,8(2H,7H)-tetraone) **7.29**



**7.29**

The title compound was synthesized by following general protocol 3 using 4,4'-dimethoxydiphenylamine (106 mg, 0.46 mmol), **6.5** (100 mg, 0.15 mmol), sodium tert-butoxide (59 mg, 0.62 mmol) and Pd(OAc)<sub>2</sub> (3.5 mg, 1.54 x 10<sup>-2</sup> mmol). **7.29** was isolated as a dark blue solid by column chromatography (129 mg, 44%). (DCM:hexane 60:40 (v/v) R<sub>f</sub> = 0.25). <sup>1</sup>H NMR (600 MHz, chloroform-*d*) δ 8.35 (s, 2H), 6.98 (d, *J* = 8.4 Hz, 8H), 6.78 (d, *J* = 8.4 Hz, 8H), 3.90-3.78 (m, 4H), 3.78 (s, 12H), 1.72 – 1.56 (m, 2H), 1.25 – 1.20 (m, 16H), 0.96 – 0.71 (m, 12H). <sup>13</sup>C NMR (151 MHz, chloroform-*d*) δ 163.1, 160.2, 156.5, 148.7, 140.8, 132.7, 125.8, 125.5, 125.2, 114.6, 55.3, 43.7, 37.3, 30.4, 28.5, 23.4, 22.9, 14.0, 10.1. IR(ATR); ν<sub>max</sub> (cm<sup>-1</sup>) 2925, 2839, 1689, 1654, 1502, 1241, 833. HRMS-ESI: calcd for C<sub>58</sub>H<sub>65</sub>N<sub>4</sub>O<sub>8</sub> [M+H]<sup>+</sup> 945.4802; found 945.4802.

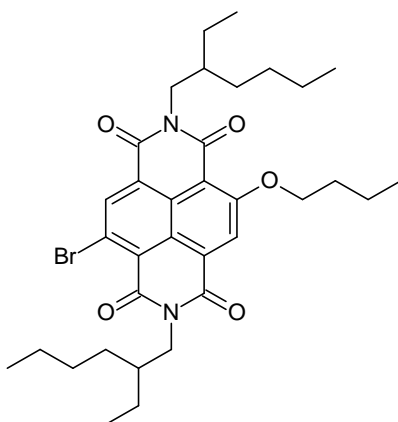
Synthesis of (4,9-bis(ethyl(phenyl)amino)-2,7-bis(2-ethylhexyl)benzo[lmn][3,8]phenanthroline-1,3,6,8(2H,7H)-tetraone) **7.30**



**7.30**

The title compound was synthesized by following general protocol 3 using N-ethylaniline (60 mg, 0.46 mmol), **6.5** (100 mg, 0.15 mmol), sodium tert-butoxide (59 mg, 0.62 mmol) and Pd(OAc)<sub>2</sub> (3.5 mg, 1.54 x10<sup>-2</sup> mmol). **7.30** was isolated as a dark blue solid by column chromatography (67 mg, 29%). (DCM:hexane 60:40 (v/v) R<sub>f</sub> = 0.3). <sup>1</sup>H NMR (600 MHz, chloroform-*d*) δ 8.55 (s, 2H), 7.21 (t, *J* = 7.8 Hz, 4H), 6.93 (d, *J* = 7.8 Hz, 6H), 4.04 (q, *J* = 7.3 Hz, 4H), 3.95 (m, 4H), 1.57 (s, 6H), 1.52 (s, 2H), 1.34 – 1.12 (m, 16H), 0.84 (m, 12H). <sup>13</sup>C NMR (151 MHz, chloroform-*d*) δ 163.1, 161.0, 149.1, 147.5, 131.9, 129.4, 126.1, 126.0, 122.0, 119.2, 48.2, 44.1, 37.4, 30.5, 28.6, 23.7, 23.1, 14.1, 13.8, 10.5. IR(ATR); ν<sub>max</sub> (cm<sup>-1</sup>) 2958, 2857, 1692, 1652, 1445, 1255, 691. HRMS-ESI: calcd for C<sub>46</sub>H<sub>57</sub>N<sub>4</sub>O<sub>4</sub> [M+H]<sup>+</sup> 729.4380; found 729.4368.

Synthesis of 4-bromo-9-butoxy-2,7-bis(2-ethylhexyl)benzo[*lmn*][3,8]phenanthroline-1,3,6,8(2H,7H)-tetraone **7.35** (known)<sup>329</sup>

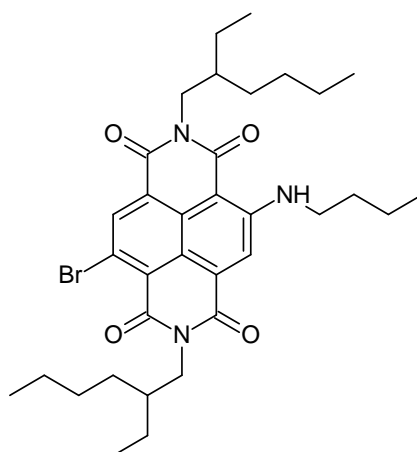


**7.35**

Into a 250 mL round bottomed flask, **6.5** (0.50 g, 7.71 mmol) was dissolved in dry DMF (125 mL). Pestle and mortar ground  $K_2CO_3$  (1.07 g, 0.771 mmol) followed by *n*-butanol (0.29 mL, 0.385 mmol) were added to the vessel which was then heated to 80°C for 28 h. The mixture was cooled to room temperature and DCM (100 mL) was added to the reaction mixture. The organic phase was washed with water (3 x 75 mL) and the combined aqueous phases were washed with DCM (3 x 20 mL) washings were colourless. The organic phases were combined and dried with  $MgSO_4$  before the solvent was removed *invacuo*. **7.35** was isolated as a deep yellow solid by flash column chromatography (253 mg, 51%). (DCM:hexane 70:30 (v/v)  $R_f = 0.25$ ).  $^1H$  NMR (600 MHz, chloroform-*d*)  $\delta$  8.94 (d,  $J = 3.2$  Hz, 1H), 8.51 (d,  $J = 3.2$  Hz, 1H), 4.47 (q,  $J = 5.0, 3.8$  Hz, 2H), 4.13 (m, 5H), 2.02 (t,  $J = 7.6$  Hz, 2H), 1.94 (s, 2H), 1.62 (q,  $J = 7.7$  Hz, 2H), 1.45 – 1.21 (m, 16H), 1.08 – 0.99 (m, 3H), 0.97 – 0.84 (m, 12H).  $^{13}C$  NMR (151 MHz, chloroform-*d*)  $\delta$  162.32, 162.21, 161.96, 161.63, 161.13, 139.14, 128.45, 127.56, 125.07, 123.56, 123.47, 119.99, 111.23, 70.79, 53.58, 45.19, 44.51, 37.95, 37.78, 31.18, 30.79, 30.72, 28.71, 28.68, 24.12, 24.07, 23.23, 19.21, 14.25, 13.93, 10.75, 10.73. IR(ATR);  $\nu_{max}$  (cm<sup>-1</sup>) 2921,

1670, 1658, 1565, 1442, 1260, 789. HRMS-ESI: calcd for  $C_{34}H_{46}BrN_2O_5[M+H]^+$  642.2590; found 642.2595.

Synthesis of (4-bromo-9-(butylamino)-2,7-bis(2-ethylhexyl)benzo[*lmn*][3,8]phenanthroline-1,3,6,8(2H,7H)-tetraone **7.36** (known)<sup>329</sup>

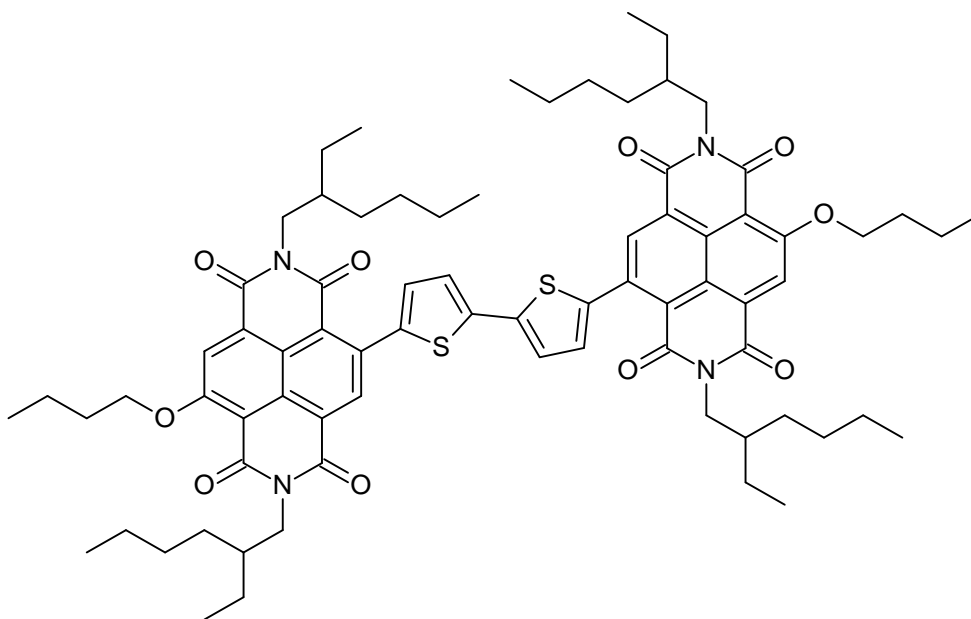


**7.36**

Into a 500 mL round bottomed flask, **6.5** (310 mg, 0.48 mmol) was dissolved  $CHCl_3$  (240 mL) at room temperature. Butylamine (24 mL, excess) was added to the reaction mixture and an instantaneous colour change from yellow to bright pink was observed. The reaction was complete after 5 minutes, confirmed by TLC (DCM:hexane v:v 70:30  $R_f^{SM} = 0.45$ ,  $R_f^{Prod} = 0.60$ ). DCM (200 mL) was added and the mixture was then washed with water (3 x 150 mL) and the organic layer was dried using  $MgSO_4$ . The solvent was removed *invacuo* and **7.36** was isolated as a pink solid by flash column chromatography (293 mg, 96%). (DCM:hexane 90:10 (v/v)  $R_f = 0.65$ ).  $^1H$  NMR (600 MHz, chloroform-*d*)  $\delta$  10.10 (s, 1H), 8.86 (d,  $J = 2.6$  Hz, 1H), 8.28 (d,  $J = 2.9$  Hz, 1H), 4.12 (tq,  $J = 13.5, 7.2$  Hz, 3H), 3.58 (q,  $J = 6.9$  Hz, 2H), 1.93 (s, 2H), 1.81 (q,  $J = 7.7$  Hz, 2H), 1.54 (dd,  $J = 14.4, 7.0$  Hz, 2H), 1.45 – 1.23 (m, 12H), 1.02 (t,  $J = 7.5$  Hz, 2H), 0.91 (dt,  $J = 31.7, 7.4$  Hz, 9H).  $^{13}C$  NMR (151 MHz, chloroform-*d*)  $\delta$  166.29, 162.54,

162.31, 161.80, 151.86, 138.39, 128.75, 123.44, 123.37, 121.51, 120.64, 120.28, 99.90, 44.95, 44.13, 43.06, 37.78, 37.75, 31.46, 30.64, 28.58, 23.98, 23.09, 20.22, 14.10, 13.78, 10.65, 10.60; IR(ATR);  $\nu_{\text{max}}$  ( $\text{cm}^{-1}$ ) 3250, 2932, 1635, 1584, 1438, 1258, 788. HRMS-ESI: calcd for  $\text{C}_{34}\text{H}_{47}\text{BrN}_3\text{O}_4$   $[\text{M}+\text{H}]^+$  640.2750; found 640.2747

Synthesis of 9,9'-([2,2'-bithiophene]-5,5'-diyl)bis(4-butoxy-2,7-bis(2-ethylhexyl)benzo[*lmn*][3,8]phenanthroline-1,3,6,8(2H,7H)-tetraone) **7.32**. (known)<sup>329</sup>

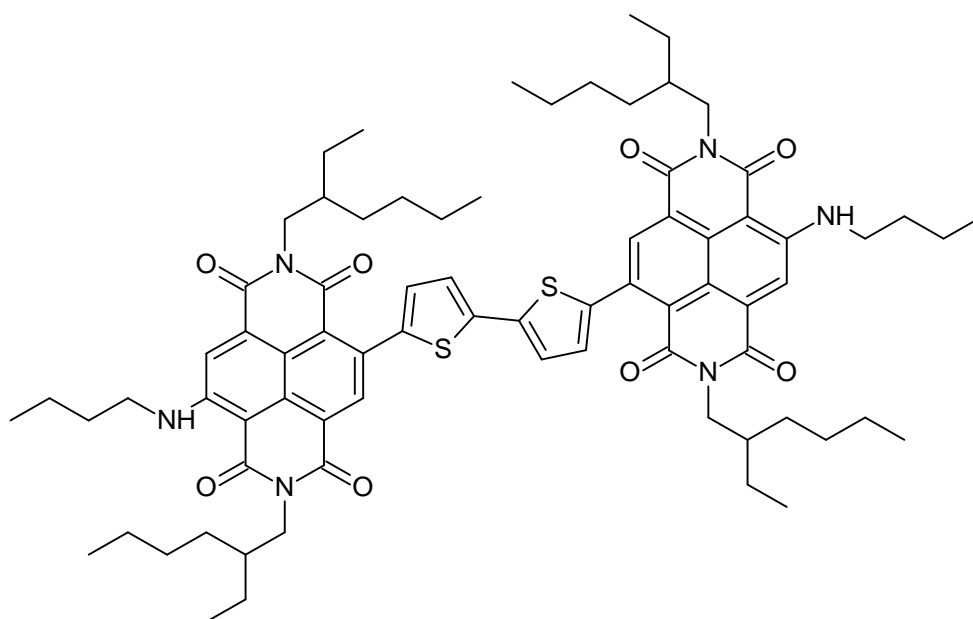


**7.32**

Into a 25mL  $\text{ZrO}_2$  grinding jar were placed 4-bromo-9-butoxy-2,7-bis(2-ethylhexyl)benzo[*lmn*][3,8]phenanthroline-1,3,6,8(2H,7H)-tetraone **7.35** (59.61 mg, 0.093 mmol), 5,5'-bis(4,4,5,5-tetramethyl-1,3,2-dioxaborolan-2-yl)-2,2'-bithiophene **7.38** (19.61 mg, 0.047 mmol), 10 mol% palladium acetate (2.4 mg,  $0.93 \times 10^{-2}$  mmol),  $\text{K}_2\text{CO}_3$  (63 mg, 0.37 mmol), 1,5-cod (27  $\mu\text{L}$ ) and two 15 mm  $\text{ZrO}_2$  balls. The jar was then closed and subjected to grinding for 60 minutes in the VBM operated at 30 Hz. The jar was left to cool to room temperature and the resulting solid was dissolved in dichloromethane (25 mL) and passed

through Celite, which was then washed with dichloromethane until the washings ran clear. The combined organic phases were washed with water (3 x 50 mL), dried over MgSO<sub>4</sub>, filtered and the solvent was removed *in vacuo*. **7.32** was isolated as a green brown solid by flash column chromatography (53 mg, 89%). (DCM 100% R<sub>f</sub> = 0.20). <sup>1</sup>H NMR (600 MHz, chloroform-*d*) δ 8.74 (s, 2H), 8.51 (s, 2H), 7.28 (s, 2H), 7.22 (d, *J* = 3.1 Hz, 2H), 4.49 (t, *J* = 6.9 Hz, 5H), 4.11 (tdd, *J* = 21.4, 13.1, 7.2 Hz, 10H), 2.04 (p, *J* = 7.3 Hz, 5H), 1.94 (dp, *J* = 19.6, 6.8 Hz, 6H), 1.64 (h, *J* = 7.6 Hz, 6H), 1.44 – 1.23 (m, 42H), 1.05 (t, *J* = 7.4 Hz, 8H), 0.90 (dt, *J* = 32.5, 7.1 Hz, 31H). <sup>13</sup>C NMR (151 MHz, chloroform-*d*) δ 162.82, 162.71, 162.51, 161.90, 161.27, 140.37, 139.41, 136.73, 129.17, 128.78, 128.20, 124.48, 124.38, 122.96, 122.56, 119.62, 110.85, 70.59, 44.67, 44.27, 37.80, 37.66, 31.08, 30.65, 30.61, 28.58, 23.95, 23.92, 23.12, 23.10, 19.08, 14.12, 13.82, 10.64, 10.62; IR(ATR); ν<sub>max</sub> (cm<sup>-1</sup>) 2930, 1701, 1661, 1454, 1200, 793; HRMS-ESI: calcd for C<sub>76</sub>H<sub>94</sub>N<sub>4</sub>O<sub>10</sub>S<sub>2</sub> [M+H]<sup>+</sup> 1287.6490; found 1287.6521 Characterization data in agreement with the literature.

Synthesis of 9,9'-([2,2'-bithiophene]-5,5'-diyl)bis(4-(butylamino)-2,7-bis(2-ethylhexyl)benzo[lmn] [3,8]phenanthroline-1,3,6,8(2H,7H)-tetraone) **7.33**. (known)<sup>329</sup>

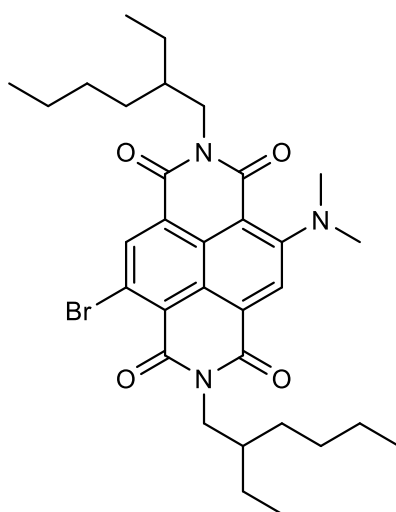


### 7.33

Into a 25mL ZrO<sub>2</sub> grinding jar were placed (4-bromo-9-(butylamino)-2,7-bis(2-ethylhexyl)benzo[*lmn*][3,8]phenanthroline-1,3,6,8(2H,7H)-tetraone **7.36** (100 mg, 0.15 mmol), 5,5'-bis(4,4,5,5-tetramethyl-1,3,2-dioxaborolan-2-yl)-2,2'-bithiophene **7.38** (32.45 mg, 0.075 mmol), 10 mol% palladium acetate (3.5 mg, 1.54 x 10<sup>-2</sup> mmol), K<sub>2</sub>CO<sub>3</sub> (85 mg, 0.62 mmol), 1,5-cod (27 μL) and two 15 mm ZrO<sub>2</sub> balls. The total mass of the reagents was calculated so that milling load equals *ca.* 20 mg.mL<sup>-1</sup>. The jar was then closed and subjected to grinding for 60 minutes in the VBM operated at 30 Hz. The jars were left to cool to room temperature and the resulting solid was dissolved in dichloromethane (25 mL) and passed through Celite and the solvent removed. The crude material was purified and **7.33** was isolated as a deep purple solid by flash column chromatography (73 mg, 72%). (DCM:hexane 95:5 (v/v) R<sub>f</sub> = 0.40). <sup>1</sup>H NMR (600 MHz, chloroform-*d*) δ 10.10 (d, *J* = 5.9 Hz, 2H), 8.61 (s, 2H), 8.27 (s, 2H), 7.22 (s, 2H), 7.11 (s, 2H), 4.10 (ddd, *J* = 32.9, 16.1, 9.1 Hz, 9H), 3.61 (q, *J* = 6.8 Hz, 4H), 2.00 – 1.88 (m, 5H), 1.84 (p, *J* = 7.6 Hz, 5H), 1.68 – 1.49 (m, 9H), 1.46 – 1.20 (m, 38H), 1.04 (t, *J* = 7.4 Hz, 7H), 0.98 – 0.70 (m, 29H). <sup>13</sup>C NMR (151 MHz, chloroform-*d*) δ 166.46,

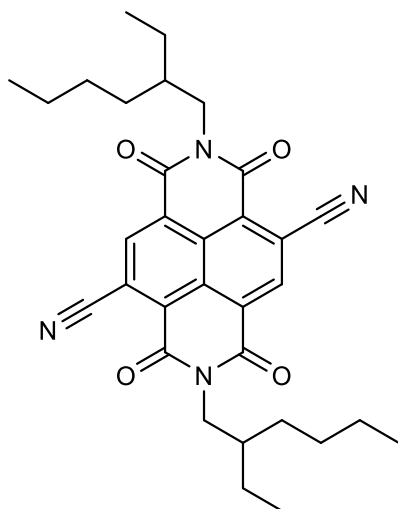
163.08, 163.03, 162.76, 151.99, 140.85, 138.83, 136.24, 133.13, 129.24, 128.24, 128.12, 123.93, 123.54, 122.32, 120.47, 120.31, 99.79, 44.55, 44.00, 43.06, 37.77, 31.53, 30.68, 30.65, 28.61, 24.00, 23.92, 23.14, 23.11, 20.26, 14.12, 13.81, 10.69, 10.64; IR(ATR);  $\nu_{\max}$  ( $\text{cm}^{-1}$ ) 3258, 2931, 1635, 1455, 1204, 792; HRMS-ESI: calcd for  $\text{C}_{76}\text{H}_{96}\text{N}_6\text{O}_8\text{S}_2[\text{M}+\text{H}]^+$  1285.6809; found 1285.6862. Characterization data in agreement with the literature.

Characterization data for **7.39**.



Characterization data:  $^1\text{H}$  NMR (600 MHz, chloroform-*d*)  $\delta$  8.79 (s, 1H), 8.50 (s, 1H), 4.11 (dt,  $J = 19.3, 12.1$  Hz, 4H), 3.23 (s, 6H), 2.01 – 1.79 (m, 2H), 1.46 – 1.18 (m, 16H), 0.99 – 0.79 (m, 12H).  $^{13}\text{C}$  NMR (151 MHz, chloroform-*d*)  $\delta$  163.00, 162.93, 162.18, 161.90, 161.50, 153.49, 139.44, 137.97, 129.90, 125.64, 125.28, 124.83, 123.21, 122.74, 121.38, 104.90, 45.24, 44.83, 44.46, 38.29, 38.11, 31.09, 30.97, 29.05, 28.91, 24.32, 24.30, 23.44, 23.41, 14.45, 10.96, 10.94; IR(ATR);  $\nu_{\max}$  ( $\text{cm}^{-1}$ ) 2959, 2853, 1646, 1566, 1406, 1238, 785; MS ( $m/z$ ) calc. for  $\text{C}_{32}\text{H}_{42}\text{BrN}_3\text{O}_4[\text{M}+\text{H}]^+$  612.2563; found 612.2470.

Characterization data for **7.40**.



Characterization data:  $^1\text{H}$  NMR (600 MHz, chloroform-*d*)  $\delta$  9.04 (d,  $J = 2.4$  Hz, 2H), 4.27 – 4.08 (m, 4H), 1.96 (p,  $J = 6.6$  Hz, 2H), 1.49 – 1.22 (m, 16H), 0.91 (dt,  $J = 28.7, 7.2$  Hz, 12H).  $^{13}\text{C}$  NMR (151 MHz, chloroform-*d*)  $\delta$  160.45, 160.03, 136.06, 128.56, 127.51, 127.11, 116.84, 115.81, 45.47, 37.71, 30.51, 28.44, 23.88, 23.04, 14.07, 10.48.; IR(ATR);  $\nu_{\text{max}}$  ( $\text{cm}^{-1}$ ) 3064, 2932, 2862, 1669, 1658, 1451, 1314, 1207, 794; MS ( $m/z$ ) calc. for  $\text{C}_{32}\text{H}_{36}\text{N}_4\text{O}_4$  [ $+\text{H}$ ] $^+$ : 541.2815, found 541.2805. calc. for  $\text{C}_{32}\text{H}_{36}\text{N}_4\text{O}_0$  [ $+\text{Na}$ ] $^+$ : 563.2634, found 563.2640.

# 10 References

- 1 Consumer Electronics Market (By Product: Smartphones, Desktops, Tablets, Laptops & Notebooks, Digital Cameras, Air Conditioners, Others; By Distribution Channel: Online, Offline; By Application: Personal, Professional; By Technology: NFC, MST, AI, VR Tech, <https://www.precedenceresearch.com/consumer-electronics-market>.
- 2 M. Fuechsle, J. A. Miwa, S. Mahapatra, H. Ryu, S. Lee, O. Warschkow, L. C. L. Hollenberg, G. Klimeck and M. Y. Simmons, *Nat. Nanotechnol.*, 2012, **7**, 242–246.
- 3 X. Yao, J. Wang, S. Yuan, X. Zhang, G. Wu, X. Wang and S. W. Yang, *Nanoscale*, 2015, **7**, 15277–15283.
- 4 Ansori, *Pap. Knowl. . Towar. a Media Hist. Doc.*, 2015, **3**, 49–58.
- 5 L. Chen, *PhD Thesis*, A general synthesis of  $\pi$ -conjugated materials, University of Reading, 2016.
- 6 S. Bhandari, in *Polyaniline Blends, Composites, and Nanocomposites*, Elsevier, 2018, pp. 23–60.
- 7 H. Kallmann and M. Pope, *Nature*, 1960, **186**, 31–33.
- 8 H. Kallmann and M. Pope, *J. Chem. Phys.*, 1960, **32**, 300–301.
- 9 H. Shirakawa, E. J. Louis, A. G. MacDiarmid, C. K. Chiang and A. J. Heeger, *J. Chem. Soc. Chem. Commun.*, 1977, 578.
- 10 C. K. Chiang, M. A. Drury, S. C. Gau, A. J. Heeger, E. J. Louis, A. G. MacDiarmid, Y. W. Park and H. Shirakawa, *J. Am. Chem. Soc.*, 1978, **100**, 1013–1015.
- 11 C. K. Chiang, C. R. Fincher, Y. W. Park, A. J. Heeger, H. Shirakawa, E. J. Louis, S. C. Gau and A. G. MacDiarmid, *Phys. Rev. Lett.*, 1977, **39**, 1098–1101.
- 12 A. J. Heeger, *Rev. Mod. Phys.*, 2001, **73**, 681–700.
- 13 A. K. Chauhan, P. Jha, D. K. Aswal and J. V. Yakhmi, *J. Electron. Mater.*, 2022, **51**, 447–485.
- 14 X. Wu, W. Fu and H. Chen, *ACS Appl. Polym. Mater.*, 2022, **4**, 4609–4623.
- 15 Web of science ‘n-type semiconductor’ keyword search, <https://www.webofscience.com/wos/woscc/summary/a6dec91b-9e46-4eb4-bb5c-05723ac1abf7-48c7f6ca/relevance/1>. Accessed: August 2022
- 16 R. A. Street and A. Salleo, *Appl. Phys. Lett.*, 2002, **81**, 2887–2889.
- 17 S. C. Lim, Y. S. Yang, S. H. Kim, Z.-S. Kim, D.-H. Youn, T. Zyung, J. Y. Kwon, D.-H. Hwang and D. J. Kim, *ETRI J.*, 2009, **31**, 647–652.
- 18 L. Kinder, J. Kanicki and P. Petroff, *Synth. Met.*, 2004, **146**, 181–185.
- 19 M. M. Mandoc, W. Veurman, L. J. A. Koster, B. de Boer and P. W. M. Blom, *Adv. Funct. Mater.*, 2007, **17**, 2167–2173.
- 20 A. J. Wise, T. P. Martin, J. Gao, K. VanDerGeest and J. K. Grey, *J. Chem. Phys.*, 2010, **133**, 174901.
- 21 M. Onoda, Y. Manda, T. Iwasa, S. Morita, T. Kawai and K. Yoshino, *Synth. Met.*, 1991, **41**, 1349–1352.
- 22 T. W. Kelley, D. V. Muires, P. F. Baude, T. P. Smith and T. D. Jones, *MRS Proc.*, 2003, **771**, L6.5.
- 23 Yen-Yi Lin, D. I. Gundlach, S. F. Nelson and T. N. Jackson, *IEEE Trans. Electron Devices*, 1997, **44**, 1325–1331.
- 24 T. Hasegawa and J. Takeya, *Sci. Technol. Adv. Mater.*, 2009, **10**, 024314.
- 25 Z. Bao, A. Dodabalapur and A. J. Lovinger, *Appl. Phys. Lett.*, 1996, **69**, 4108–4110.
- 26 J.-F. Chang, B. Sun, D. W. Breiby, M. M. Nielsen, T. I. Sölling, M. Giles, I. McCulloch and H. Sirringhaus, *Chem. Mater.*, 2004, **16**, 4772–4776.

- 27 T. Bjørnholm, T. Hassenkam, D. R. Greve, R. D. McCullough, M. Jayaraman, S. M. Savoy, C. E. Jones and J. T. McDevitt, *Adv. Mater.*, 1999, **11**, 1218–1221.
- 28 K.-Y. Jen, M. Maxfield, L. W. Shacklette and R. L. Elsenbaumer, *J. Chem. Soc. Chem. Commun.*, 1987, 309.
- 29 F. Banishoeib, A. Henckens, S. Fourier, G. Vanhooyland, M. Breselge, J. Manca, T. J. Cleij, L. Lutsen, D. Vanderzande, L. H. Nguyen, H. Neugebauer and N. S. Sariciftci, *Thin Solid Films*, 2008, **516**, 3978–3988.
- 30 G. Horowitz, D. Fichou, X. Peng, Z. Xu and F. Garnier, *Solid State Commun.*, 1989, **72**, 381–384.
- 31 F. Garnier, *Pure Appl. Chem.*, 1996, **68**, 1455–1462.
- 32 L. Torsi, A. Dodabalapur, L. J. Rothberg, A. W. P. Fung and H. E. Katz, *Science (80-. )*, 1996, **272**, 1462–1464.
- 33 H. E. Katz, *J. Mater. Chem.*, 1997, **7**, 369–376.
- 34 C. D. Dimitrakopoulos, B. K. Furman, T. Graham, S. Hegde and S. Purushothaman, *Synth. Met.*, 1998, **92**, 47–52.
- 35 M. Halik, H. Klauk, U. Zschieschang, G. Schmid, S. Ponomarenko, S. Kirchmeyer and W. Weber, *Adv. Mater.*, 2003, **15**, 917–922.
- 36 C. Bulumulla, R. Gunawardhana, P. L. Gamage, J. T. Miller, R. N. Kularatne, M. C. Biewer and M. C. Stefan, *ACS Appl. Mater. Interfaces*, 2020, **12**, 32209–32232.
- 37 M. Fujii, T. Nishinaga and M. Iyoda, *Tetrahedron Lett.*, 2009, **50**, 555–558.
- 38 F. A. Larik, M. Faisal, A. Saeed, Q. Abbas, M. A. Kazi, N. Abbas, A. A. Thebo, D. M. Khan and P. A. Channar, *J. Mater. Sci. Mater. Electron.*, 2018, **29**, 17975–18010.
- 39 S. Khalifeh, in *Polymers in Organic Electronics*, Elsevier, 2020, pp. 251–339.
- 40 Z. Bao, A. J. Lovinger and A. Dodabalapur, *Appl. Phys. Lett.*, 1996, **69**, 3066–3068.
- 41 Z. Bao, A. J. Lovinger and A. Dodabalapur, *Adv. Mater.*, 1997, **9**, 42–44.
- 42 R. Rella, A. Serra, P. Siciliano, A. Tepore, L. Valli and A. Zocco, *Langmuir*, 1997, **13**, 6562–6567.
- 43 Z. Bao, A. J. Lovinger and J. Brown, *J. Am. Chem. Soc.*, 1998, **120**, 207–208.
- 44 H.-Y. Lin, G.-S. Liou, W.-Y. Lee and W.-C. Chen, *J. Polym. Sci. Part A Polym. Chem.*, 2007, **45**, 1727–1736.
- 45 A. Angeli and A. Pieroni, *Qazz. Chim. Ital.*, 1919, **49**, 146.
- 46 A. G. MacDiarmid, *Angew. Chemie Int. Ed.*, 2001, **40**, 2581–2590.
- 47 Y. Okamoto and W. Brenner, in *Polymers*, Reinhold, 1964, pp. 125–158.
- 48 J.-F. Morin, M. Leclerc, D. Adès and A. Siove, *Macromol. Rapid Commun.*, 2005, **26**, 761–778.
- 49 J.-F. Morin, N. Drolet, Y. Tao and M. Leclerc, *Chem. Mater.*, 2004, **16**, 4619–4626.
- 50 C. Reese, M. Roberts, M. Ling and Z. Bao, *Mater. Today*, 2004, **7**, 20–27.
- 51 T. B. Singh and N. S. Sariciftci, *Annu. Rev. Mater. Res.*, 2006, **36**, 199–230.
- 52 X. Gao and Y. Hu, *J. Mater. Chem. C*, 2014, **2**, 3099–3117.
- 53 J. G. Laquindanum, H. E. Katz, A. Dodabalapur and A. J. Lovinger, *J. Am. Chem. Soc.*, 1996, **118**, 11331–11332.
- 54 H. E. Katz, J. Johnson, A. J. Lovinger and W. Li, *J. Am. Chem. Soc.*, 2000, **122**, 7787–7792.
- 55 B. J. Jung, K. Lee, J. Sun, A. G. Andreou and H. E. Katz, *Adv. Funct. Mater.*, 2010, **20**, 2930–2944.
- 56 K. C. See, C. Landis, A. Sarjeant and H. E. Katz, *Chem. Mater.*, 2008, **20**, 3609–3616.
- 57 A. Babel and S. A. Jenekhe, *J. Am. Chem. Soc.*, 2003, **125**, 13656–13657.
- 58 P. R. L. Malenfant, C. D. Dimitrakopoulos, J. D. Gelorme, L. L. Kosbar, T. O. Graham, A. Curioni and W. Andreoni, *Appl. Phys. Lett.*, 2002, **80**, 2517–2519.

- 59 R. J. Chesterfield, J. C. McKeen, C. R. Newman, P. C. Ewbank, D. A. da Silva Filho, J.-L. Brédas, L. L. Miller, K. R. Mann and C. D. Frisbie, *J. Phys. Chem. B*, 2004, **108**, 19281–19292.
- 60 J. H. Oh, S. Liu, Z. Bao, R. Schmidt and F. Würthner, *Appl. Phys. Lett.*, 2007, **91**, 212107.
- 61 G. Horowitz, F. Kouki, P. Spearman, D. Fichou, C. Nogués, X. Pan and F. Garnier, *Adv. Mater.*, 1996, **8**, 242–245.
- 62 Y.-C. Chang, M.-Y. Kuo, C.-P. Chen, H.-F. Lu and I. Chao, *J. Phys. Chem. C*, 2010, **114**, 11595–11601.
- 63 S. Chen, Q. Zhang, Q. Zheng, C. Tang and C.-Z. Lu, *Chem. Commun.*, 2012, **48**, 1254–1256.
- 64 S.-C. Chen, D. Ganeshan, D. Cai, Q. Zheng, Z. Yin and F. Wang, *Org. Electron.*, 2013, **14**, 2859–2865.
- 65 C. Di, J. Li, G. Yu, Y. Xiao, Y. Guo, Y. Liu, X. Qian and D. Zhu, *Org. Lett.*, 2008, **10**, 3025–3028.
- 66 Y. Ie, M. Ueta, M. Nitani, N. Tohnai, M. Miyata, H. Tada and Y. Aso, *Chem. Mater.*, 2012, **24**, 3285–3293.
- 67 Y.-I. Park, J. S. Lee, B. J. Kim, B. Kim, J. Lee, D. H. Kim, S.-Y. Oh, J. H. Cho and J.-W. Park, *Chem. Mater.*, 2011, **23**, 4038–4044.
- 68 H. E. Katz, A. J. Lovinger, J. Johnson, C. Kloc, T. Siegrist, W. Li, Y.-Y. Lin and A. Dodabalapur, *Nature*, 2000, **404**, 478–481.
- 69 A. R. Brown, D. M. de Leeuw, E. J. Lous and E. E. Havinga, *Synth. Met.*, 1994, **66**, 257–261.
- 70 J. B. Torrance, *Acc. Chem. Res.*, 1979, **12**, 79–86.
- 71 Z. Peng, Y. Gao and G. Xie, *Molecules*, 2021, **26**, 1670.
- 72 R. J. Chesterfield, C. R. Newman, T. M. Pappenfus, P. C. Ewbank, M. H. Haukaas, K. R. Mann, L. L. Miller and C. D. Frisbie, *Adv. Mater.*, 2003, **15**, 1278–1282.
- 73 T. M. Pappenfus, R. J. Chesterfield, C. D. Frisbie, K. R. Mann, J. Casado, J. D. Raff and L. L. Miller, *J. Am. Chem. Soc.*, 2002, **124**, 4184–4185.
- 74 R. C. Haddon, A. S. Perel, R. C. Morris, T. T. M. Palstra, A. F. Hebard and R. M. Fleming, *Appl. Phys. Lett.*, 1995, **67**, 121–123.
- 75 S. Kobayashi, T. Takenobu, S. Mori, A. Fujiwara and Y. Iwasa, *Appl. Phys. Lett.*, 2003, **82**, 4581–4583.
- 76 F. Zhang, O. Inganäs, Y. Zhou and K. Vandewal, *Natl. Sci. Rev.*, 2016, **3**, 222–239.
- 77 H. Sun, X. Guo and A. Facchetti, *Chem*, 2020, **6**, 1310–1326.
- 78 Y. Takeda, T. L. Andrew, J. M. Lobe, A. J. Mork and T. M. Swager, *Angew. Chemie Int. Ed.*, 2012, **51**, 9042–9046.
- 79 D. Izuhara and T. M. Swager, *J. Am. Chem. Soc.*, 2009, **131**, 17724–17725.
- 80 D. Izuhara and T. M. Swager, *Macromolecules*, 2011, **44**, 2678–2684.
- 81 H. M. Colquhoun, B. W. Greenland, Z. Zhu, J. S. Shaw, C. J. Cardin, S. Burattini, J. M. Elliott, S. Basu, T. B. Gasa and J. F. Stoddart, *Org. Lett.*, 2009, **11**, 5238–5241.
- 82 L. Chen, H. Willcock, C. J. Wedge, F. Hartl, H. M. Colquhoun and B. W. Greenland, *Org. Biomol. Chem.*, 2016, **14**, 980–988.
- 83 T.-G. Zhan, T.-Y. Zhou, F. Lin, L. Zhang, C. Zhou, Q.-Y. Qi, Z.-T. Li and X. Zhao, *Org. Chem. Front.*, 2016, **3**, 1635–1645.
- 84 L. Chen, E. Vivier, C. J. Eling, T. S. Babra, J. S. G. Bouillard, A. M. Adawi, D. M. Benoit, F. Hartl, H. M. Colquhoun, O. A. Efremova and B. W. Greenland, *Synth. Met.*, 2018, **241**, 31–38.
- 85 H. Kamogawa and S. Sato, *Bull. Chem. Soc. Jpn.*, 1991, **64**, 321–323.

- 86 A. C. Fahrenbach, S. Sampath, D. J. Late, J. C. Barnes, S. L. Kleinman, N. Valley, K. J. Hartlieb, Z. Liu, V. P. Dravid, G. C. Schatz, R. P. Van Duyne and J. F. Stoddart, *ACS Nano*, 2012, **6**, 9964–9971.
- 87 W. Geuder, S. Hünig and A. Suchy, *Tetrahedron*, 1986, **42**, 1665–1677.
- 88 D. Izuhara and T. M. Swager, *J. Am. Chem. Soc.*, 2009, **131**, 17724–17725.
- 89 T. Liu, X. Wei, Z. Nie, V. Sprenkle and W. Wang, *Adv. Energy Mater.*, 2016, **6**, 15011449
- 90 J. Luo, B. Hu, C. Debruler and T. L. Liu, *Angew. Chemie - Int. Ed.*, 2018, **57**, 231–235.
- 91 M. Kathiresan, B. Ambrose, N. Angulakshmi, D. E. Mathew, D. Sujatha and A. M. Stephan, *J. Mater. Chem. A*, 2021, **9**, 27215–27233.
- 92 L. Liu, Y. Ren, J. Pan, Z. Liu, B. Wu and F. Yan, *ACS Appl. Mater. Interfaces*, 2020, **12**, 1495–1503.
- 93 K. W. Shah, S. X. Wang, D. X. Y. Soo and J. Xu, *Polymers*, 2019, 11.
- 94 Y. Lin, Y. Firdaus, M. I. Nugraha, F. Liu, S. Karuthedath, A. H. Emwas, W. Zhang, A. Seitkhan, M. Neophytou, H. Faber, E. Yengel, I. McCulloch, L. Tsetseris, F. Laquai and T. D. Anthopoulos, *Adv. Sci.*, , 2020, **7**, 1903419.
- 95 M. E. Ghica and C. M. A. Brett, *Anal. Chim. Acta*, 2005, **532**, 145–151.
- 96 D. D. Dashitsyrenova, S. A. Adonin, I. D. Gorokh, O. A. Kraevaya, A. V. Pavlova, P. A. Abramov, L. A. Frolova, M. N. Sokolov, V. P. Fedin and P. A. Troshin, *Chem. Commun.*, 2020, **56**, 9162–9165.
- 97 K. Madasamy, D. Velayutham, V. Suryanarayanan, M. Kathiresan and K.-C. Ho, *J. Mater. Chem. C*, 2019, **7**, 4622–4637.
- 98 J. Palenzuela, A. Viñuales, I. Odriozola, G. Cabañero, H. J. Grande and V. Ruiz, *ACS Appl. Mater. Interfaces*, 2014, **6**, 14562–14567.
- 99 J. H. Ross and R. I. Krieger, *J. Agric. Food Chem.*, 1980, **28**, 1026–1031.
- 100 K. Ageishi, T. Endo and M. Okawara, *J. Polym. Sci. A1.*, 1981, **19**, 1085–1090.
- 101 T. G. Zhan, T. Y. Zhou, F. Lin, L. Zhang, C. Zhou, Q. Y. Qi, Z. T. Li and X. Zhao, *Org. Chem. Front.*, 2016, **3**, 1635–1645.
- 102 Y. Zheng and A. E. Kaifer, *J. Org. Chem.*, 2020, **85**, 10240–10244.
- 103 X. H. Zhou, Y. Fan, W. X. Li, X. Zhang, R. R. Liang, F. Lin, T. G. Zhan, J. Cui, L. J. Liu, X. Zhao and K. Da Zhang, *Chinese Chem. Lett.*, 2020, **31**, 1757–1767.
- 104 M. Kato, H. Sano, T. Kiyobayashi and M. Yao, *ChemSusChem*, 2020, **13**, 2379–2385.
- 105 A. Factor and G. E. Heinsohn, *J. Polym. Sci. Part B Polym. Lett.*, 1971, **9**, 289–295.
- 106 N. Menshutkin, *Zeitschrift für Phys. Chemie*, 1890, **5U**, 589–600.
- 107 M. Shimomura, K. Utsugi, J. Horikoshi, K. Okuyama, O. Hatozaki and N. Oyama, *Langmuir*, 1991, **7**, 760–765.
- 108 E. V. Kuznetsov, I. V. Shcherbakova and A. T. Balaban, 1990, pp. 157–254.
- 109 W. Dilthey, *J. für Prakt. Chemie*, 1916, **94**, 53–76.
- 110 M. Valášek, J. Pecka, Jindřich, G. Calleja, P. R. Craig and J. Michl, *J. Org. Chem.*, 2005, **70**, 405–412.
- 111 A. K. Nedeltchev, H. Han and P. K. Bhowmik, *Polym. Chem.*, 2010, **1**, 908.
- 112 V. Kolivoška, M. Valášek, M. Gál, R. Sokolová, J. Bulíčková, L. Pospíšil, G. Mészáros and M. Hromadová, *J. Phys. Chem. Lett.*, 2013, **4**, 589–595.
- 113 M. Hromadová, V. Kolivoška, M. Gál, L. Pospíšil, R. Sokolová and M. Valášek, *J. Incl. Phenom. Macrocycl. Chem.*, 2011, **70**, 461–469.
- 114 S. A. X. Huang, K. C. Chuang, S. Z. D. Cheng and F. W. Harris, *Polymer (Guildf.)*, 2000, **41**, 5001–5009.
- 115 W. C. Cheng and M. J. Kurth, *Org. Prep. Proced. Int.*, 2002, **34**, 585–608.
- 116 T. Zincke, G. Heuser and W. Möller, *Justus Liebig's Ann. der Chemie*, 1904, **333**, 296–

- 345.
- 117 W. König, *J. für Prakt. Chemie*, 1904, **69**, 105–137.
- 118 L. Striepe and T. Baumgartner, *Chem. - A Eur. J.*, 2017, **23**, 16924–16940.
- 119 L. Chen, F. Hartl, H. M. Colquhoun and B. W. Greenland, *Tetrahedron Lett.*, 2017, **58**, 1859–1862.
- 120 Y. Song, X. Huang, H. Hua and Q. Wang, *Dye. Pigment.*, 2017, **137**, 229–235.
- 121 Suman, A. Siddiqui, M. L. Keshtov, G. D. Sharma and S. P. Singh, *J. Mater. Chem. C*, 2019, **7**, 543–552.
- 122 J. C. Barnes, M. Juríček, N. L. Strutt, M. Frascioni, S. Sampath, M. A. Giesener, P. L. McGrier, C. J. Bruns, C. L. Stern, A. A. Sarjeant and J. F. Stoddart, *J. Am. Chem. Soc.*, 2013, **135**, 183–192.
- 123 T. Gong, X. Yang, Q. Sui, Y. Qi, F.-G. Xi and E.-Q. Gao, *Inorg. Chem.*, 2016, **55**, 96–103.
- 124 H. Kamogawa and S. Sato, *Bull. Chem. Soc. Jpn.*, 1991, **64**, 321–323.
- 125 R.-T. Wang, G.-H. Lee and C. K. Lai, *J. Mater. Chem. C*, 2018, **6**, 9430–9444.
- 126 M. Nanasawa, M. Miwa, M. Hirai and T. Kuwabara, *J. Org. Chem.*, 2000, **65**, 593–595.
- 127 H. Kamogawa and T. Suzuki, *J. Chem. Soc. Chem. Commun.*, 1985, 525–526.
- 128 J. E. Anthony, A. Facchetti, M. Heeney, S. R. Marder and X. Zhan, *Adv. Mater.*, 2010, **22**, 3876–3892.
- 129 W. W. Porter and T. P. Vaid, *J. Org. Chem.*, 2005, **70**, 5028–5035.
- 130 N. Miyaura, K. Yamada and A. Suzuki, *Tetrahedron Lett.*, 1979, **20**, 3437–3440.
- 131 L. Liu, Y. Zhang and B. Xin, *J. Org. Chem.*, 2006, **71**, 3994–3997.
- 132 R. J. Rahaim and R. E. Maleczka, *Org. Lett.*, 2005, **7**, 5087–5090.
- 133 S. K. Nimkar, A. H. Anderson, J. M. Rimoldi, M. Stanton, K. P. Castagnoli, S. Mabic, Y.-X. Wang and N. Castagnoli, *Chem. Res. Toxicol.*, 1996, **9**, 1013–1022.
- 134 L. Chen, H. Willcock, C. J. Wedge, F. Hartl, H. M. Colquhoun and B. W. Greenland, *Org. Biomol. Chem.*, 2016, **14**, 980–988.
- 135 T. Skorjanc, D. Shetty, S. K. Sharma, J. Raya, H. Traboulsi, D. S. Han, J. Lalla, R. Newlon, R. Jagannathan, S. Kirmizialtin, J. C. Olsen and A. Trabolsi, *Chem. - A Eur. J.*, 2018, **24**, 8648–8655.
- 136 J. L. A. Jonathan W. Steed, *Supramolecular Chemistry*, John Wiley & Sons Ltd., 3rd Editio., 2022.
- 137 J. Lehn, *Supramolecular Chemistry*, Wiley, 1995, vol. 107.
- 138 Web of science ‘supramolecular’ keyword search, <https://www.webofscience.com/wos/woscc/summary/2de924f4-9d91-48bd-bfee-c4970e8db3f7-53e45af5/relevance/1>. Accessed August 2022.
- 139 H. Schneider, *J. Phys. Org. Chem.*, 2022, **35**, e4340 1-11.
- 140 J.-M. Lehn, *Angew. Chemie Int. Ed. English*, 1988, **27**, 89–112.
- 141 J.-M. Lehn, *Angew. Chemie Int. Ed. English*, 1990, **29**, 1304–1319.
- 142 F. J. M. Hoeben, P. Jonkheijm, E. W. Meijer and A. P. H. J. Schenning, *Chem. Rev.*, 2005, **105**, 1491–1546.
- 143 P. D. Beer, P. A. Gale and Smith D. K., *Supramolecular Chemistry*, Oxford University Press, Oxford, 1999.
- 144 C. F. J. Faul and M. Antonietti, *Adv. Mater.*, 2003, **15**, 673–683.
- 145 P. Thordarson, in *Supramolecular Chemistry*, John Wiley & Sons, Ltd, Chichester, UK, 2012.
- 146 D. Brynn Hibbert and P. Thordarson, *Chem. Commun.*, 2016, **52**, 12792–12805.
- 147 P. Thordarson, *Chem. Soc. Rev.*, 2011, **40**, 1305–1323.
- 148 T. Ackermann, *Berichte der Bunsengesellschaft für Phys. Chemie*, 1987, **91**, 1398–1398.

- 149 B. König, *Angew. Chemie*, 1997, **109**, 1055–1056.
- 150 S. Sivakova and S. J. Rowan, *Chem. Soc. Rev.*, 2005, **34**, 9–21.
- 151 J. Pranata, S. G. Wierschke and W. L. Jorgensen, *J. Am. Chem. Soc.*, 1991, **113**, 2810–2819.
- 152 W. L. Jorgensen and J. Pranata, *J. Am. Chem. Soc.*, 1990, **112**, 2008–2010.
- 153 R. P. Sijbesma, F. H. Beijer, L. Brunsveld, B. J. B. Folmer, J. H. K. K. Hirschberg, R. F. M. Lange, J. K. L. Lowe and E. W. Meijer, *Science*, 1997, **278**, 1601–1604.
- 154 S. Wang, L. Wu, L. Zhang and C. Tung, *Chinese Sci. Bull.*, 2006, **51**, 129–138.
- 155 Z. Zhang, C. Liu, X. Cao, L. Gao and Q. Chen, *Macromolecules*, 2016, **49**, 9192–9202.
- 156 H. Rupp, R. Bhandary, A. Kulkarni and W. Binder, *Adv. Mater. Technol.*, 2022, **7**, 2200088.
- 157 G. Zhang, Z. Sun and M. Li, *E3S Web Conf.*, 2021, **290**, 01037.
- 158 R. Suriano, L. Brambilla, M. Tommasini and S. Turri, *Polym. Adv. Technol.*, 2018, **29**, 2899–2908.
- 159 C. J. Pedersen, *J. Am. Chem. Soc.*, 1967, **89**, 2495–2496.
- 160 C. J. Pedersen, *Science*, 1988, **241**, 536–540.
- 161 G. Crini, *Chem. Rev.*, 2014, **114**, 10940–10975.
- 162 F. Cramer and H. Hettler, *Naturwissenschaften*, 1967, **54**, 625–632.
- 163 R. Zadmand, F. Hokmabadi, M. R. Jalali and A. Akbarzadeh, *RSC Adv.*, 2020, **10**, 32690–32722.
- 164 D.-S. Guo and Y. Liu, *Chem. Soc. Rev.*, 2012, **41**, 5907.
- 165 H. D. Correia, S. Chowdhury, A. P. Ramos, L. Guy, G. J. Demets and C. Bucher, *Polym. Int.*, 2019, **68**, 572–588.
- 166 E. H. Wanderlind, D. G. Liz, A. P. Gerola, R. F. Affeldt, V. Nascimento, L. C. Bretanha, R. Montecinos, L. Garcia-Rio, H. D. Fiedler and F. Nome, *ACS Catal.*, 2018, **8**, 3343–3347.
- 167 S. Dong, J. Yuan and F. Huang, *Chem. Sci.*, 2014, **5**, 247–252.
- 168 M. Li, B. Hua and F. Huang, *Org. Chem. Front.*, 2021, **8**, 3675–3680.
- 169 Y. Han, G.-F. Huo, J. Sun, J. Xie, C.-G. Yan, Y. Zhao, X. Wu, C. Lin and L. Wang, *Sci. Rep.*, 2016, **6**, 28748.
- 170 T. Aida, E. W. Meijer and S. I. Stupp, *Science*, 2012, **335**, 813–817.
- 171 V. Balzani, A. Credi, F. M. Raymo and J. F. Stoddart, *Angew. Chemie*, 2000, **39**, 3348–3391.
- 172 E. R. Kay, D. A. Leigh and F. Zerbetto, *Angew. Chemie Int. Ed.*, 2007, **46**, 72–191.
- 173 D. Philp and J. F. Stoddart, *Angew. Chemie Int. Ed. English*, 1996, **35**, 1154–1196.
- 174 J. Leblond and A. Petitjean, *ChemPhysChem*, 2011, **12**, 1043–1051.
- 175 C. R. Martinez and B. L. Iverson, *Chem. Sci.*, 2012, **3**, 2191–2201.
- 176 J. F. Stoddart, *Angew. Chemie - Int. Ed.*, 2017, **56**, 11094–11125.
- 177 S. Hünig, *Pure Appl. Chem.*, 1967, **15**, 109–122.
- 178 S. Hünig and M. Kiessel, *J. für Prakt. Chemie*, 1958, **5**, 224–232.
- 179 M. Horner and S. Hünig, *Angew. Chemie Int. Ed. English*, 1977, **16**, 410–411.
- 180 S. Hünig and H. Berneth, in *Organic Chemistry*, Springer-Verlag, Berlin/Heidelberg, pp. 1–44.
- 181 K. Deuchert and S. Hünig, *Angew. Chemie Int. Ed. English*, 1978, **17**, 875–886.
- 182 B. Odell, M. V. Reddington, A. M. Z. Slawin, N. Spencer, J. F. Stoddart and D. J. Williams, *Angew. Chemie Int. Ed. English*, 1988, **27**, 1547–1550.
- 183 P. R. Ashton, B. Odell, M. V. Reddington, A. M. Z. Slawin, J. F. Stoddart and D. J. Williams, *Angew. Chemie Int. Ed. English*, 1988, **27**, 1550–1553.
- 184 D. A. Leigh, *Angew. Chemie - Int. Ed.*, 2016, **55**, 14506–14508.

- 185 N. H. Evans and P. D. Beer, *Chem. Soc. Rev.*, 2014, **43**, 4658–4683.
- 186 G. Gil-Ramírez, D. A. Leigh and A. J. Stephens, *Angew. Chemie Int. Ed.*, 2015, **54**, 6110–6150.
- 187 G. F. Swiegers, in *Comprehensive Coordination Chemistry II*, Elsevier, 2003, pp. 747–759.
- 188 M. Xue, Y. Yang, X. Chi, X. Yan and F. Huang, *Chem. Rev.*, 2015, **115**, 7398–7501.
- 189 J. D. Badjić, S. Stojanović and Y. Ruan, *Adv. Phys. Org. Chem.*, 2011, **45**, 1–37.
- 190 A. Trabolsi, N. Khashab, A. C. Fahrenbach, D. C. Friedman, M. T. Colvin, K. K. Cotí, D. Benítez, E. Tkatchouk, J. C. Olsen, M. E. Belowich, R. Carmielli, H. A. Khatib, W. A. Goddard, M. R. Wasielewski and J. F. Stoddart, *Nat. Chem.*, 2010, **2**, 42–49.
- 191 D. K. James and J. M. Tour, *Top. Curr. Chem.*, 2005, **257**, 33–62.
- 192 A. Credi, V. Balzani, S. J. Langford and J. F. Stoddart, *J. Am. Chem. Soc.*, 1997, **119**, 2679–2681.
- 193 J. E. Green, J. Wook Choi, A. Boukai, Y. Bunimovich, E. Johnston-Halperin, E. Deionno, Y. Luo, B. A. Sheriff, K. Xu, Y. Shik Shin, H. R. Tseng, J. F. Stoddart and J. R. Heath, *Nature*, 2007, **445**, 414–417.
- 194 M. Juriček, J. C. Barnes, N. L. Strutt, N. A. Vermeulen, K. C. Ghooray, E. J. Dale, P. R. McGonigal, A. K. Blackburn, A.-J. Avestro and J. F. Stoddart, *Chem. Sci.*, 2014, **5**, 2724.
- 195 Y. Wang, M. Frasconi and J. F. Stoddart, *ACS Cent. Sci.*, 2017, **3**, 927–935.
- 196 L. Tong, D. Zhu, B. Chen, Y. Chen, G. Wu, F. Zeng and H. Li, *Org. Lett.*, 2021, **23**, 9343–9347.
- 197 L. Chen, K. J. C. Lim, T. S. Babra, J. O. Taylor, M. Pižl, R. Evans, A. M. Chippindale, F. Hartl, H. M. Colquhoun and B. W. Greenland, *Org. Biomol. Chem.*, 2018, **16**, 5006–5015.
- 198 C. Gong and H. W. Gibson, *Macromol. Chem. Phys.*, 1997, **198**, 2321–2332.
- 199 C. Gong and H. W. Gibson, *Macromolecules*, 1996, **29**, 7029–7033.
- 200 C. Gong and H. W. Gibson, *J. Am. Chem. Soc.*, 1997, **119**, 8585–8589.
- 201 H. W. Gibson, S. Liu, C. Gong, Q. Ji and E. Joseph, *Macromolecules*, 1997, **30**, 3711–3727.
- 202 M. Arunachalam and H. W. Gibson, *Prog. Polym. Sci.*, 2014, **39**, 1043–1073.
- 203 S. Burattini, B. W. Greenland, D. H. Merino, W. Weng, J. Seppala, H. M. Colquhoun, W. Hayes, M. E. Mackay, I. W. Hamley and S. J. Rowan, *J. Am. Chem. Soc.*, 2010, **132**, 12051–12058.
- 204 S. Burattini, H. M. Colquhoun, J. D. Fox, D. Friedmann, B. W. Greenland, P. J. F. Harris, W. Hayes, M. E. Mackay and S. J. Rowan, *Chem. Commun.*, 2009, 6717–6719.
- 205 R. Vaiyapuri, B. W. Greenland, H. M. Colquhoun, J. M. Elliott and W. Hayes, *Polym. Int.*, 2014, **63**, 933–942.
- 206 L. R. Hart, J. L. Harries, B. W. Greenland, H. M. Colquhoun and W. Hayes, *Polym. Chem.*, 2013, **4**, 4860–4870.
- 207 J. S. Shaw, R. Vaiyapuri, M. P. Parker, C. A. Murray, K. J. C. Lim, C. Pan, M. Knappert, C. J. Cardin, B. W. Greenland, R. Grau-Crespo and H. M. Colquhoun, *Chem. Sci.*, 2018, **9**, 4052–4061.
- 208 J. Han, H. Gong, S. Jiang, Y. Gao, J. Nie and F. Sun, *Macromol. Chem. Phys.*, 2019, **220**, 1900362–1900372.
- 209 L. R. Hart, J. L. Harries, B. W. Greenland, H. M. Colquhoun and W. Hayes, *Polym. Chem.*, 2015, **6**, 7342–7352.
- 210 D. Sluysmans, L. Zhang, X. Li, A. Garci, J. F. Stoddart and A.-S. Duwez, *J. Am. Chem. Soc.*, 2020, **142**, 21153–21159.
- 211 J. Q. Nguyen and B. L. Iverson, *J. Am. Chem. Soc.*, 1999, **121**, 2639–2640.

- 212 M. S. Cubberley and B. L. Iverson, *J. Am. Chem. Soc.*, 2001, **123**, 7560–7563.
- 213 J. J. Reczek and B. L. Iverson, *Macromolecules*, 2006, **39**, 5601–5603.
- 214 P. M. Alvey, R. J. Ono, C. W. Bielawski and B. L. Iverson, *Macromolecules*, 2013, **46**, 718–726.
- 215 R. Watari, M. Nishihara, H. Tajiri, H. Otsuka and A. Takahara, *Polym. J.*, 2013, **45**, 839–844.
- 216 C. W. Chen and H. W. Whitlock, *J. Am. Chem. Soc.*, 1978, **100**, 4921–4922.
- 217 X. Xing and Y. Zhao, *Org. Biomol. Chem.*, 2018, **16**, 3885–3888.
- 218 S. C. Zimmerman, C. M. VanZyl and G. S. Hamilton, *J. Am. Chem. Soc.*, 1989, **111**, 1373–1381.
- 219 S. C. Zimmerman, W. Wu and Z. Zeng, *J. Am. Chem. Soc.*, 1991, **113**, 196–201.
- 220 X. Peng, L. Wang and S. Chen, *J. Incl. Phenom. Macrocycl. Chem.*, 2021, **99**, 131–154.
- 221 S. Takenaka, *Polym. J.*, 2021, **53**, 415–427.
- 222 A. Diac, M. Matache, I. Grosu and N. D. Hädade, *Adv. Synth. Catal.*, 2018, **360**, 817–845.
- 223 Q.-H. Ling, J.-L. Zhu, Y. Qin and L. Xu, *Mater. Chem. Front.*, 2020, **4**, 3176–3189.
- 224 P. Spenst and F. Würthner, *J. Photochem. Photobiol. C Photochem. Rev.*, 2017, **31**, 114–138.
- 225 F. Würthner, *Chem. Commun.*, 2004, **14**, 1564–1579.
- 226 B. W. Greenland, S. Burattini, W. Hayes and H. M. Colquhoun, *Tetrahedron*, 2008, **64**, 8346–8354.
- 227 M. B. Nielsen, J. O. Jeppesen, J. Lau, C. Lomholt, D. Damgaard, J. P. Jacobsen, J. Becher and J. F. Stoddart, *J. Org. Chem.*, 2001, **66**, 3559–3563.
- 228 Z. Zhu, C. J. Cardin, Y. Gan and H. M. Colquhoun, *Nat. Chem.*, 2010, **2**, 653–660.
- 229 G. J. Gabriel and B. L. Iverson, *J. Am. Chem. Soc.*, 2002, **124**, 15174–15175.
- 230 A. R. Smith and B. Iverson, 2017, pp. 37–71.
- 231 B. A. Ikkanda, S. A. Samuel and B. L. Iverson, *J. Org. Chem.*, 2014, **79**, 2029–2037.
- 232 A. J. Zych and B. L. Iverson, *J. Am. Chem. Soc.*, 2000, **122**, 8898–8909.
- 233 R. Scott Lokey and B. L. Iverson, *Nature*, 1995, **375**, 303–305.
- 234 L. Panther, M. Stankunaite, M. Sharma, J. Spencer and B. W. Greenland, *Euro. J. Org. Chem.*, 2023, e202201321.
- 235 E. Buncel, N. L. Mailloux, R. S. Brown, P. M. Kazmaier and J. Dust, *Tetrahedron Lett.*, 2001, **42**, 3559–3562.
- 236 D. Song, S. Sun, Y. Tian, S. Huang, Y. Ding, Y. Yuan and A. Hu, *J. Mater. Chem. B*, 2015, **3**, 3195–3200.
- 237 F. Biedermann, V. D. Uzunova, O. A. Scherman, W. M. Nau and A. De Simone, *J. Am. Chem. Soc.*, 2012, **134**, 15318–15323.
- 238 C. A. Murray, Z. Zhu, C. J. Cardin, H. M. Colquhoun and B. W. Greenland, *Supramol. Chem.*, 2018, **30**, 751–757.
- 239 P. T. Anastas and J. C. Warner, *Green chemistry : theory and practice*, Oxford University Press, Oxford [England]; New York, 1998.
- 240 O. V. Kharissova, B. I. Kharisov, C. M. Oliva González, Y. P. Méndez and I. López, *R. Soc. Open Sci.*, 2019, **6**, 191378.
- 241 D. J. C. Constable, *iScience*, 2021, **24**, 103489.
- 242 P. Anastas and N. Eghbali, *Chem. Soc. Rev.*, 2010, **39**, 301–312.
- 243 G. M. Sheldrick, *Acta Crystallogr. Sect. A Found. Adv.*, 2015, **71**, 3–8.
- 244 J. L. Howard, Q. Cao and D. L. Browne, *Chem. Sci.*, 2018, **9**, 3080–3094.
- 245 R. R. A. Bolt, J. A. Leitch, A. C. Jones, W. I. Nicholson and D. L. Browne, *Chem. Soc. Rev.*, 2022, **51**, 4243–4260.

- 246 F. Gomollón-Bel, *Chem. Int.*, 2020, **42**, 3–9.
- 247 Q. Cao, D. E. Crawford, C. Shi and S. L. James, *Angew. Chemie - Int. Ed.*, 2020, **59**, 4478–4483.
- 248 L. Takacs and J. S. McHenry, in *Journal of Materials Science*, Springer US, 2006, vol. 41, pp. 5246–5249.
- 249 Y. S. Kwon, K. B. Gerasimov and S. K. Yoon, *J. Alloys Compd.*, 2002, **346**, 276–281.
- 250 D. E. Crawford, C. K. G. Miskimmin, A. B. Albadarin, G. Walker and S. L. James, *Green Chem.*, 2017, **19**, 1507–1518.
- 251 H. A. Garekani, A. Nokhodchi, M. A. Rayeni and F. Sadeghi, *Drug Dev. Ind. Pharm.*, 2013, **39**, 1238–1246.
- 252 D. K. Tan, M. Maniruzzaman and A. Nokhodchi, *Pharmaceutics*, 2018, **10**, 203–208.
- 253 M. Maniruzzaman and A. Nokhodchi, *Drug Discov. Today*, 2017, **22**, 340–351.
- 254 H. G. Moradiya, A. Nokhodchi, M. S. A. Bradley, R. Farnish and D. Douroumis, *Pharm. Dev. Technol.*, 2016, **21**, 445–452.
- 255 M. Meier, E. John, D. Wieckhusen, W. Wirth and W. Peukert, *Powder Technol.*, 2009, **188**, 301–313.
- 256 R. Roufail and B. Klein, *J. Miner. Mater. Charact. Eng.*, 2021, **09**, 528–543.
- 257 M. Ferguson, M. S. Moyano, G. A. Tribello, D. E. Crawford, E. M. Bringa, S. L. James, J. Kohanoff and M. G. Del Pópolo, *Chem. Sci.*, 2019, **10**, 2924–2929.
- 258 B. P. Hutchings, D. E. Crawford, L. Gao, P. Hu and S. L. James, *Angew. Chemie - Int. Ed.*, 2017, **56**, 15252–15256.
- 259 X. Ma, W. Yuan, S. E. J. Bell and S. L. James, *Chem. Commun.*, 2014, **50**, 1585–1587.
- 260 J. G. Hernández and C. Bolm, *J. Org. Chem.*, 2017, **82**, 4007–4019.
- 261 A. R. Katritzky, S. Ledoux, R. M. Witek and S. K. Nair, *J. Org. Chem.*, 2004, **69**, 2976–2982.
- 262 A. R. Katritzky, R. M. Witek, V. Rodriguez-Garcia, P. P. Mohapatra, J. W. Rogers, J. Cusido, A. A. A. Abdel-Fattah and P. J. Steel, *J. Org. Chem.*, 2005, **70**, 7866–7881.
- 263 V. Štrukil, D. Gracin, O. V. Magdysyuk, R. E. Dinnebier and T. Friščić, *Angew. Chemie Int. Ed.*, 2015, **54**, 8440–8443.
- 264 Y.-T. Su and G.-W. Wang, *Org. Lett.*, 2013, **15**, 3408–3411.
- 265 W. I. Nicholson, F. Barreteau, J. A. Leitch, R. Payne, I. Priestley, E. Godineau, C. Battilocchio and D. L. Browne, *Angew. Chemie Int. Ed.*, 2021, **60**, 21868–21874.
- 266 P. Nun, V. Pérez, M. Calmès, J. Martinez and F. Lamaty, *Chem. - A Eur. J.*, 2012, **18**, 3773–3779.
- 267 A. Baron, J. Martinez and F. Lamaty, *Tetrahedron Lett.*, 2010, **51**, 6246–6249.
- 268 P. F. M. Oliveira, M. Baron, A. Chamayou, C. André-Barrès, B. Guidetti and M. Baltas, *RSC Adv.*, 2014, **4**, 56736–56742.
- 269 V. Declerck, P. Nun, J. Martinez and F. Lamaty, *Angew. Chemie - Int. Ed.*, 2009, **48**, 9318–9321.
- 270 E. Colacino, P. Nun, F. M. Colacino, J. Martinez and F. Lamaty, *Tetrahedron*, 2008, **64**, 5569–5576.
- 271 H. C. Kolb, M. G. Finn and K. B. Sharpless, *Angew. Chemie Int. Ed.*, 2001, **40**, 2004–2021.
- 272 V. Štrukil, M. D. Igrc, M. Eckert-Maksić and T. Friščić, *Chem. - A Eur. J.*, 2012, **18**, 8464–8473.
- 273 K. Yoo, E. J. Hong, T. Q. Huynh, B. S. Kim and J. G. Kim, *ACS Sustain. Chem. Eng.*, 2021, **9**, 8679–8685.
- 274 T. Seo, T. Ishiyama, K. Kubota and H. Ito, *Chem. Sci.*, 2019, **10**, 8202–8210.
- 275 A. F. Asachenko, K. R. Sorochkina, P. B. Dzhevakov, M. A. Topchiy and M. S. Nechaev,

- Adv. Synth. Catal.*, 2013, **355**, 3553–3557.
- 276 D. A. Fulmer, W. C. Shearouse, S. T. Medonza and J. Mack, *Green Chem.*, 2009, **11**, 1821–1825.
- 277 R. Luque and D. J. MacQuarrie, *Org. Biomol. Chem.*, 2009, **7**, 1627–1632.
- 278 R. Thorwirth, A. Stolle and B. Ondruschka, *Green Chem.*, 2010, **12**, 985–99.
- 279 Q. Cao, J. L. Howard, E. Wheatley and D. L. Browne, *Angew. Chemie*, 2018, **130**, 11509–11513.
- 280 E. Tullberg, D. Peters and T. Frejd, *J. Organomet. Chem.*, 2004, **689**, 3778–3781.
- 281 G. N. Hermann, P. Becker and C. Bolm, *Angew. Chemie Int. Ed.*, 2015, **54**, 7414–7417.
- 282 K. Kubota, T. Seo, K. Koide, Y. Hasegawa and H. Ito, *Nat. Commun.*, 2019, **10**, 1–11.
- 283 Q. L. Shao, Z. J. Jiang and W. K. Su, *Tetrahedron Lett.*, 2018, **59**, 2277–2280.
- 284 K. Kubota, T. Endo, M. Uesugi, Y. Hayashi and H. Ito, *ChemSusChem*, 2022, **15**, e202102132 (1-6).
- 285 C. C. C. Johansson Seechurn, M. O. Kitching, T. J. Colacot and V. Snieckus, *Angew. Chemie Int. Ed.*, 2012, **51**, 5062–5085.
- 286 P. Devendar, R.-Y. Qu, W.-M. Kang, B. He and G.-F. Yang, *J. Agric. Food Chem.*, 2018, **66**, 8914–8934.
- 287 P. Ruiz-Castillo and S. L. Buchwald, *Chem. Rev.*, 2016, **116**, 12564–12649.
- 288 M. J. Buskes and M.-J. Blanco, *Molecules*, 2020, **25**, 3493.
- 289 V. V. Boldyrev, *J. Mater. Sci.*, 2004, **39**, 5117–5120.
- 290 D. Tan, L. Loots and T. Friščić, *Chem. Commun.*, 2016, **52**, 7760–7781.
- 291 G. M. R. Plastics Europe and Conversio Market & Strategy GmbH, 2019, 14, 35.
- 292 O. Guinea, A. Espés, *International EU27 pharmaceutical production, trade, dependencies and vulnerabilities: a factual analysis*, European Centre for International Political Economy (ECIPE), European Federation of Pharmaceutical Industries and Associations (EFPIA), 2021 .
- 293 J. Gong, X.-J. Cui, Z.-W. Xie, S.-G. Wang and L.-Y. Qu, *Synth. Met.*, 2002, **129**, 187–192.
- 294 T. Abdiryim, R. Jamal and I. Nurulla, *J. Appl. Polym. Sci.*, 2007, **105**, 576–584.
- 295 J. Huang, J. A. Moore, J. H. Acquaye and R. B. Kaner, *Macromolecules*, 2005, **38**, 317–321.
- 296 T. Hirai, Y. Nagae, K. L. White, K. Kamitani, M. Kido, T. Uchiyama, M. Nishibori, Y. Konishi, K. Yokomachi, R. Sugimoto, K. Saigo, T. Ohishi, Y. Higaki, K. Kojio and A. Takahara, *RSC Adv.*, 2016, **6**, 111993–111996.
- 297 T. Abdiryim, R. Jamal, C. Zhao, T. Awut and I. Nurulla, *Synth. Met.*, 2010, **160**, 325–332.
- 298 A. Kumar, R. Singh, S. P. Gopinathan and A. Kumar, *Chem. Commun.*, 2012, **48**, 4905.
- 299 M. S. Zoromba and M. H. Abdel-Aziz, *Polymer (Guildf.)*, 2017, **120**, 20–29.
- 300 K. A. Houton, G. M. Burslem and A. J. Wilson, *Chem. Sci.*, 2015, **6**, 2382–2388.
- 301 J. B. Ravnsbæk and T. M. Swager, *ACS Macro Lett.*, 2014, **3**, 305–309.
- 302 C. G. Vogt, S. Grätz, S. Lukin, I. Halasz, M. Etter, J. D. Evans and L. Borchardt, *Angew. Chemie - Int. Ed.*, 2019, **58**, 18942–18947.
- 303 A. Insuasty, S. Maniam and S. J. Langford, *Chem. – A Eur. J.*, 2019, **25**, 7058–7073.
- 304 R. Taylor, J. P. Hare, A. K. Abdul-Sada and H. W. Kroto, *J. Chem. Soc. Chem. Commun.*, 1990, **17**, 1423–1425.
- 305 B. Schwarzschild, *Phys. Today*, 1996, **49**, 19–21.
- 306 J. C. Hummelen, B. W. Knight, F. Lepeq, F. Wudl, J. Yao and C. L. Wilkins, *J. Org. Chem.*, 1995, **60**, 532–538.
- 307 M. M. Wienk, J. M. Kroon, W. J. H. Verhees, J. Knol, J. C. Hummelen, P. A. Van Hal

- and R. A. J. Janssen, *Angew. Chemie - Int. Ed.*, 2003, **42**, 3371–3375.
- 308 M. Ueda, N. Imai, S. Yoshida, H. Yasuda, T. Fukuyama and I. Ryu, *European J. Org. Chem.*, 2017, **2017**, 6483–6485.
- 309 R. Ganesamoorthy, G. Sathiyam and P. Sakthivel, *Sol. Energy Mater. Sol. Cells*, 2017, **161**, 102–148.
- 310 H. Y. Chen, J. Hou, S. Zhang, Y. Liang, G. Yang, Y. Yang, L. Yu, Y. Wu and G. Li, *Nat. Photonics*, 2009, **3**, 649–653.
- 311 Y. Liang, Y. Wu, D. Feng, S. T. Tsai, H. J. Son, G. Li and L. Yu, *J. Am. Chem. Soc.*, 2009, **131**, 56–57.
- 312 Y. Liang and L. Yu, *Acc. Chem. Res.*, 2010, **43**, 1227–1236.
- 313 Y. Li, *Acc. Chem. Res.*, 2012, **45**, 723–733.
- 314 S. H. Liao, H. J. Jhuo, Y. S. Cheng and S. A. Chen, *Adv. Mater.*, 2013, **25**, 4766–4771.
- 315 J. Zhao, Y. Li, G. Yang, K. Jiang, H. Lin, H. Ade, W. Ma and H. Yan, *Nat. Energy*, 2016, **1**, 15027–15029.
- 316 M. Li, K. Gao, X. Wan, Q. Zhang, B. Kan, R. Xia, F. Liu, X. Yang, H. Feng, W. Ni, Y. Wang, J. Peng, H. Zhang, Z. Liang, H. L. Yip, X. Peng, Y. Cao and Y. Chen, *Nat. Photonics*, 2017, **11**, 85–90.
- 317 Y. Chen, X. Wan and G. Long, *Acc. Chem. Res.*, 2013, **46**, 2645–2655.
- 318 Y. He, H. Y. Chen, J. Hou and Y. Li, *J. Am. Chem. Soc.*, 2010, **132**, 1377–1382.
- 319 Y. He and Y. Li, *Phys. Chem. Chem. Phys.*, 2011, **13**, 1970–1983.
- 320 P. Cheng and X. Zhan, *Chem. Soc. Rev.*, 2016, **45**, 2544–2582.
- 321 X. Wang, J. Huang, Z. Niu, X. Zhang, Y. Sun and C. Zhan, *Tetrahedron*, 2014, **70**, 4726–4731.
- 322 K. D. Deshmukh, T. Qin, J. K. Gallaher, A. C. Y. Liu, E. Gann, K. O'Donnell, L. Thomsen, J. M. Hodgkiss, S. E. Watkins and C. R. McNeill, *Energy Environ. Sci.*, 2015, **8**, 332–342.
- 323 A. Facchetti, *Mater. Today*, 2013, **16**, 123–132.
- 324 C. Yan, S. Barlow, Z. Wang, H. Yan, A. K. Y. Jen, S. R. Marder and X. Zhan, *Nat. Rev. Mater.*, 2018, **3**, 18003–18021.
- 325 Y. Lin and X. Zhan, *Adv. Energy Mater.*, 2015, **5**, 1–9.
- 326 J. Shukla and P. Mukhopadhyay, *European J. Org. Chem.*, 2019, **2019**, 7770–7786.
- 327 X. Zhan, A. Facchetti, S. Barlow, T. J. Marks, M. A. Ratner, M. R. Wasielewski and S. R. Marder, *Adv. Mater.*, 2011, **23**, 268–284.
- 328 L. Ye, X. Jiao, H. Zhang, S. Li, H. Yao, H. Ade and J. Hou, *Macromolecules*, 2015, **48**, 7156–7163.
- 329 K. Rundel, S. Maniam, K. Deshmukh, E. Gann, S. K. K. Prasad, J. M. Hodgkiss, S. J. Langford and C. R. McNeill, *J. Mater. Chem. A*, 2017, **5**, 12266–12277.
- 330 E.-F. Huo, Y. Zou, H.-Q. Sun, J.-L. Bai, Y. Huang, Z.-Y. Lu, Y. Liu, Q. Jiang and S.-L. Zhao, *Polym. Bull.*, 2011, **67**, 843–857.
- 331 F. Liu, Y. Wu, C. Wang, J. Ma, F. Wu, Y. Zhang and X. Ba, *Polymers*, 2018, **10**, 790.
- 332 M. M. Durban, P. D. Kazarinoff and C. K. Luscombe, *Macromolecules*, 2010, **43**, 6348–6352.
- 333 X. Guo, D. Tu and X. Liu, *J. Energy Chem.*, 2015, **24**, 675–685.
- 334 S. Kumar and P. Mukhopadhyay, *Green Chem.*, 2018, **20**, 4620–4628.
- 335 S. V. Bhosale, M. B. Kalyankar, S. V. Bhosale, S. J. Langford, E. F. Reid and C. F. Hogan, *New J. Chem.*, 2009, **33**, 2409–2413.
- 336 S. Chopin, F. Chaignon, E. Blart and F. Odobel, *J. Mater. Chem.*, 2007, **17**, 4139–4146.
- 337 D. Bansal and P. Mukhopadhyay, *J. Mater. Chem. C*, 2021, **9**, 3948–3956.
- 338 M. Korzec, S. Kotowicz, K. Łaba, M. Łapkowski, J. G. Małecki, K. Smolarek, S.

- Maćkowski and E. Schab-Balcerzak, *Euro. J. Org. Chem.*, 2018, **2018**, 1756–1760.
- 339 J. Shukla, M. R. Ajayakumar and P. Mukhopadhyay, *Org. Lett.*, 2018, **20**, 7864–7868.
- 340 S. Kuila, A. Ghorai, P. K. Samanta, R. B. K. Siram, S. K. Pati, K. S. Narayan and S. J. George, *Chem. - A Eur. J.*, 2019, **25**, 16007–16011.
- 341 M. Hussain, A. M. El-Zohry, Y. Hou, A. Toffoletti, J. Zhao, A. Barbon and O. F. Mohammed, *J. Phys. Chem. B*, 2021, **125**, 10813–10831.
- 342 D. Chen, A. Avestro, Z. Chen, J. Sun, S. Wang, M. Xiao, Z. Erno, M. M. Algaradah, M. S. Nassar, K. Amine, Y. Meng and J. F. Stoddart, *Adv. Mater.*, 2015, **27**, 2907–2912.
- 343 N. Zhou and A. Facchetti, *Mater. Today*, 2018, **21**, 377–390.
- 344 J. L. Sessler, C. T. Brown, D. O'Connor, S. L. Springs, R. Wang, M. Sathiosatham and T. Hirose, *J. Org. Chem.*, 1998, **63**, 7370–7374.
- 345 M. Nakano, D. Hashizume and K. Takimiya, *Molecules*, 2016, **21**, 1–12.
- 346 M. Sasikumar, Y. V. Suseela and T. Govindaraju, *Asian J. Org. Chem.*, 2013, **2**, 779–785.
- 347 Y. V. Suseela, M. Sasikumar and T. Govindaraju, *Tetrahedron Lett.*, 2013, **54**, 6314–6318.
- 348 R. Chinchilla and C. Nájera, *Chem. Soc. Rev.*, 2011, **40**, 5084.
- 349 M. Gazvoda, M. Virant, B. Pinter and J. Košmrlj, *Nat. Commun.*, 2018, **9**, 4814.
- 350 X. Wang, Y. Song, J. Qu and Y. Luo, *Organometallics*, 2017, **36**, 1042–1048.
- 351 Y. Li, G. Zhang, W. Zhang, J. Wang, X. Chen, Z. Liu, Y. Yan, Y. Zhao and D. Zhang, *Chem. - An Asian J.*, 2014, **9**, 3207–3214.
- 352 R. Chinchilla and C. Nájera, *Chem. Rev.*, 2007, **107**, 874–922.
- 353 J. Huang, M. Isaac, R. Watt, J. Becica, E. Dennis, M. I. Saidaminov, W. A. Sabbers and D. C. Leitch, *ACS Catal.*, 2021, **11**, 5636–5646.
- 354 N. Miyaura and A. Suzuki, *J. Chem. Soc. Chem. Commun.*, 1979, 866.
- 355 A. L. Casado and P. Espinet, *Organometallics*, 1998, **17**, 954–959.
- 356 R. W. Holman, *J. Chem. Educ.*, 2005, **82**, 1780.
- 357 C. Amatore, A. Jutand and G. Le Duc, *Chem. - A Eur. J.*, 2011, **17**, 2492–2503.
- 358 R. Dorel, C. P. Grugel and A. M. Haydl, *Angew. Chemie Int. Ed.*, 2019, **58**, 17118–17129.
- 359 Y. Sunesson, E. Limé, S. O. Nilsson Lill, R. E. Meadows and P.-O. Norrby, *J. Org. Chem.*, 2014, **79**, 11961–11969.
- 360 L. A. Panther, D. P. Guest, A. McGown, H. Emerit, R. K. Tareque, A. Jose, C. M. Dadswell, S. J. Coles, G. J. Tizzard, R. González-Méndez, C. A. I. Goodall, M. C. Bagley, J. Spencer and B. W. Greenland, *Chem. - A Eur. J.*, 2022, **28**, e202201444 (1–13).
- 361 N. Miyaura, T. Yanagi and A. Suzuki, *Synth. Commun.*, 1981, **11**, 513–519.
- 362 X. Guo and M. D. Watson, *Org. Lett.*, 2008, **10**, 5333–5336.
- 363 K. Chen, J. Zhao, X. Li and G. G. Gurzadyan, *J. Phys. Chem. A*, 2019, **123**, 2503–2516.
- 364 S. B. Schmidt, T. Biskup, X. Jiao, C. R. McNeill and M. Sommer, *J. Mater. Chem. C*, 2019, **7**, 4466–4474.
- 365 Z. Wu, C. Sun, S. Dong, X. F. Jiang, S. Wu, H. Wu, H. L. Yip, F. Huang and Y. Cao, *J. Am. Chem. Soc.*, 2016, **138**, 2004–2013.
- 366 F. Silvestri and A. Marrocchi, *Int. J. Mol. Sci.*, 2010, **11**, 1471–1508.
- 367 Y. Li, G. Zhang, G. Yang, Y. Guo, C. Di, X. Chen, Z. Liu, H. Liu, Z. Xu, W. Xu, H. Fu and D. Zhang, *J. Org. Chem.*, 2013, **78**, 2926–2934.
- 368 W. Yue, Y. Zhen, Y. Li, W. Jiang, A. Lv and Z. Wang, *Org. Lett.*, 2010, **12**, 3460–3463.
- 369 P. M. Alvey and B. L. Iverson, *Org. Lett.*, 2012, **14**, 2706–2709.
- 370 C. Liu, F. Bao and Q. Ni, *Arkivoc*, 2011, **2011**, 60–68.

- 371 K. Sonogashira, *J. Organomet. Chem.*, 2002, **653**, 46–49.
- 372 F. Doria, C. M. Gallati and M. Freccero, *Org. Biomol. Chem.*, 2013, **11**, 7838–7842.
- 373 S. G. Awuah and Y. You, *RSC Adv.*, 2012, **2**, 11169–11183.
- 374 P. Majumdar, R. Nomula and J. Zhao, *J. Mater. Chem. C*, 2014, **2**, 5982–5997.
- 375 Z. Mahmood, A. Toffoletti, J. Zhao and A. Barbon, *J. Lumin.*, 2017, **183**, 507–512.
- 376 C. Ye, L. Zhou, X. Wang and Z. Liang, *Phys. Chem. Chem. Phys.*, 2016, **18**, 10818–10835.
- 377 T. N. Singh-Rachford and F. N. Castellano, *Coord. Chem. Rev.*, 2010, **254**, 2560–2573.
- 378 D. P. Hari and B. König, *Angew. Chemie - Int. Ed.*, 2013, **52**, 4734–4743.
- 379 D. Ravelli, M. Fagnoni and A. Albini, *Chem. Soc. Rev.*, 2013, **42**, 97–113.
- 380 M. Freitag, N. Möller, A. Rühling, C. A. Strassert, B. J. Ravoo and F. Glorius, *ChemPhotoChem*, 2019, **3**, 24–27.
- 381 Z. Ning and H. Tian, *Chem. Commun.*, 2009, 5483–5495.
- 382 Y. Wu and W. Zhu, *Chem. Soc. Rev.*, 2013, **42**, 2039–2058.
- 383 N. Sivendran, N. Pirkl, Z. Hu, A. Doppiu and L. J. Goossen, *Angew. Chemie - Int. Ed.*, 2021, **60**, 25151–25160.
- 384 M. Chatzopoulou, K. S. Madden, L. J. Bromhead, C. Greaves, T. J. Cogswell, S. Da Silva Pinto, S. R. G. Galan, I. Georgiou, M. S. Kennedy, A. Kennett, G. Apps, A. J. Russell and G. M. Wynne, *ACS Med. Chem. Lett.*, 2022, **13**, 262–270.
- 385 C. Gu, Y. Li, L. Xiao, H. Fu, D. Wang, L. Cheng and L. Liu, *J. Org. Chem.*, 2017, **82**, 12806–12812.
- 386 C. Thalacker, C. Röger and F. Würthner, *J. Org. Chem.*, 2006, **71**, 8098–8105.
- 387 J. Hong, Y. H. Ha, H. Cha, R. Kim, Y. J. Kim, C. E. Park, J. R. Durrant, S. K. Kwon, T. K. An and Y. H. Kim, *ACS Appl. Mater. Interfaces*, 2017, **9**, 44667–44677.
- 388 J. Yang, B. Xiao, S. W. Heo, K. Tajima, F. Chen and E. Zhou, *ACS Appl. Mater. Interfaces*, 2017, **9**, 44070–44078.
- 389 J. Cao and S. Yang, *RSC Adv.*, 2022, **12**, 6966–6973.
- 390 Momentive Performance Materials GmbH, EP1950255, 2008.
- 391 F. Lin, T.-Y. Zhou, T.-G. Zhan and X. Zhao, *Tetrahedron*, 2014, **70**, 2251–2256.
- 392 G. M. Sheldrick, *Acta Crystallogr. Sect. C Struct. Chem.*, 2015, **71**, 3–8.
- 393 O. V. Dolomanov, L. J. Bourhis, R. J. Gildea, J. A. K. Howard and H. Puschmann, *J. Appl. Crystallogr.*, 2009, **42**, 339–341.
- 394 M. Hanke and C. Jutz, *Synthesis (Stuttg.)*, 1980, **01**, 31–32.
- 395 Fujifilm Corporation, EP20060823252 20061109, 2008.
- 396 M. P. Parker, C. A. Murray, L. R. Hart, B. W. Greenland, W. Hayes, C. J. Cardin and H. M. Colquhoun, *Cryst. Growth Des.*, 2018, **18**, 386–392.

